MODULATION TECHNIQUES FOR DATA SUPERPOSITION ON AMPLITUDE-MODULATED SIGNALS

by

YAZAN OTHMAN AHMAD AL-JALILI, B.Sc., M.Sc.

Submitted in fulfilment of the requirements
for the Degree of Doctor of Philosophy

The University of Leeds
Department of Electrical and Electronic Engineering

January 1983

ABSTRACT

Double-sideband amplitude-modulation is widely used because of its simplicity in transmission and reception, but in a number of applications the inclusion of a data channel has become an additional requirement. An additional data signal, transmitted with a normal AM broadcast signal, can be used by a specially-equipped receiver to provide for display and control functions. The data signals should not impair the main broadcast signals, and should be imperceptible to listeners with ordinary radio receivers.

The principles of a new modulation scheme, which permits an additional data channel to be superimposed on conventional DSB-AM signals without any bandwidth increase or envelope distortion, are described in this thesis. The proposed system uses combined amplitude/frequency modulation to provide for the additional data channel. It is shown that bandlimitation may be preserved by frequency modulating the carrier with frequency-modulating functions related to the complex zeros of the amplitude-modulating signal.

The performance of the new modulation technique is assessed by computer simulation. The cross-talk between the two channels due to multipath propagation is considered to be a limiting factor. A novel complex filtering technique to detect complex zeros of real

signals is introduced and discussed. The distribution of the complex zeros of positive bandlimited signals is assessed experimentally, and the possible data rates of the proposed system are discussed.

ABBREVIATIONS

AM	Amplitude modulation
DBS-AM	Double-sideband amplitude modulation
FM	Frequency modulation
PM	Phase modulation
PA	Power amplification
CNR	Carrier-to-noise power ratio
SNR	Signal-to-noise power ratio
S/D	Signal-to-distortion power ratio
ZSFM	Zero synchronous frequency modulation

ACKNOWLEDGEMENTS

The author would like to thank God, without His help this work could never have been achieved.

The author is very grateful to Dr. G.B. Lockhart for his advice and supervision throughout the period of the research and during the preparation of this thesis.

The author would also like to thank Professor P.J. Lawrenson for permission to undertake the research in the Department of Electrical and Electronic Engineering at the University of Leeds and for the use of the departmental facilities.

Finally the author thanks Mrs. M. Hall for her efficient typing.

TO MY PARENTS

CONTENTS

CHAPTER 1

INTRODUCTION

1.1 Preliminary

Although the problem of radio frequency spectrum utilisation has existed since electromagnetic waves were discovered, the spectrum remains one of the most under-utilised natural resources. Radio communication of all kinds are expanding on a very large scale at the present time, and radio spectrum requirements are increasing consequently. The efficiency of spectrum utilisation depends on such parameters as radiated power, bandwidth, antenna pattern, ... etc. (1).

The use of spectrally efficient modulation systems is becoming very important. Such systems will maximise the bandwidth efficiency. Conventional double-sideband amplitude-modulated (DSB-AM) systems are wasteful of spectrum and power, but they are widely used because of the simple detection using envelope detectors.

The idea of using multi-parameter modulation to improve the characteristics of communication systems is not a new one, but only recently has work on this problem been intensified. This may lead to more rational use of the radio spectrum, and hence may improve the efficiency of spectrum utilisation.

For public-service broadcasting, there has not always been much opportunity to make the most efficient

use of the radio frequency spectrum. This has been because in broadcast systems the emphasis is mainly on making simple and cheap "domestic" receivers. Hence, it would be efficient if additional services could be incorporated while maintaining compatibility with existing channels. In the past, additional services have been introduced such as colour signals into television broadcasting, and also teletext which exploit the remaining under-utilised parts of the television signal (2). In radio broadcast (AM and FM) services, the inclusion of additional data signals has become of significant importance (3).

These additional "radio-data" signals, transmitted along with the normal sound-programme signals, can be used in many different ways at the receiver to provide for display and control functions. For example, a display of the network name (e.g. BBC R2) and programme type (e.g. NEWS, MUSIC, SPORTS, etc.) can be provided. Provision and display of motoring information, weather conditions, time checks is also possible. The data signals can also be used to control a programme search in automatic tuning which is highly important for motorists. Other possible applications of the additional data signals will emerge as radio-data systems develop.

However, the additional data signals should not be allowed to impair the main programme, and should be

imperceptible to listeners with existing ordinary receivers. Suitably equipped future domestic radio-receivers could detect the data messages, and then use them for display or control purposes.

In this thesis, a novel modulation technique is studied which permits data signals to be transmitted with amplitude-modulated radio broadcast signals.

1.2 Radio-Data Systems

During the last years the BBC and other European broadcasters have been investigating systems for broadcasting radio-data signals from v.h.f./f.m. radio broadcast transmitters (4, 5). The problem for the broadcaster has been to devise a method of adding the radio-data signals so that they cause negligible impairment to normal programme reception on existing receivers. The cross-talk between the data signal and the main programme signal should be imperceptible even under difficult reception conditions.

For v.h.f./f.m. transmitters the preferred method for broadcasting radio-data signals uses a subcarrier added to the stereo multiplex signal. Figure 1.1 shows the spectrum of a stereo multiplex signal.

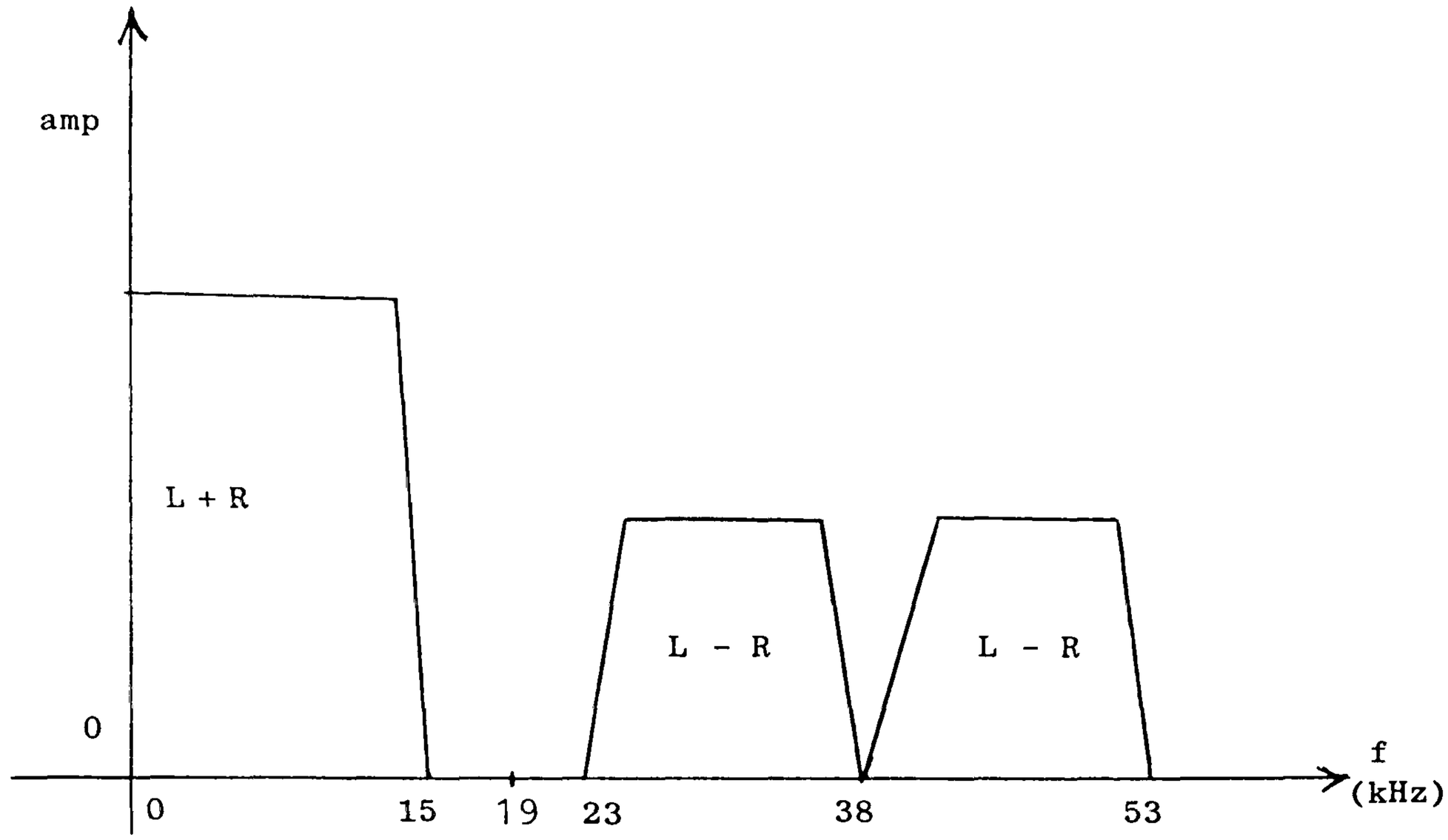

L + R = sum (mono) signal
L - R = difference signal

Spectrum of stereo multiplex signal.

Fig. 1.1

It may be seen that there are two regions in the spectrum of a stereo multiplex signal where a subcarrier could be, in theory, located without causing perceptible impairment to the normal programme. The first region is in the vicinity of the 19 kHz pilot tone, between the upper frequencies of the sum signal and the lower frequencies of the difference signal. The second region is above the upper frequencies of the difference signal, and subcarrier frequencies around 57 kHz are preferred (4). Some European broadcasters use subcarriers in the region of 19 kHz, while others use subcarriers in the region of 57 kHz. These subcarriers are amplitude-modulated by the data signals and added to the multiplex signal at the transmitter modulation input terminal. The BBC radio-data system for v.h.f./f.m. has the highest data

rate of 1187.5 bit/sec among all the other European systems (4).

The above techniques relate to v.h.f./f.m. signals that have adequately wide bandwidth to accommodate the additional data signals. The situation is quite different when superimposing additional data signals on amplitude-modulated broadcast signals. Development of radio-data systems is considerably less advanced for low and medium frequency (l.f. and m.f.) broadcasting where AM predominates and the inherent redundancy of the double-sideband amplitude-modulated (DSB-AM) signal is more difficult to exploit. The data signal can be provided for by using combined amplitude/phase modulation so that the data phase or frequency modulates the carrier of a conventional DSB-AM signal, while amplitude modulation is achieved in the usual way. A combined AM/PM signal can be expressed as:

$$x(t) = s(t) \cos[\omega_o t + \theta(t)]$$

where $s(t)$ = envelope, $\theta(t)$ = phase, and ω_o is the carrier frequency. Figure 1.2 shows such a hybrid AM/PM modulator.

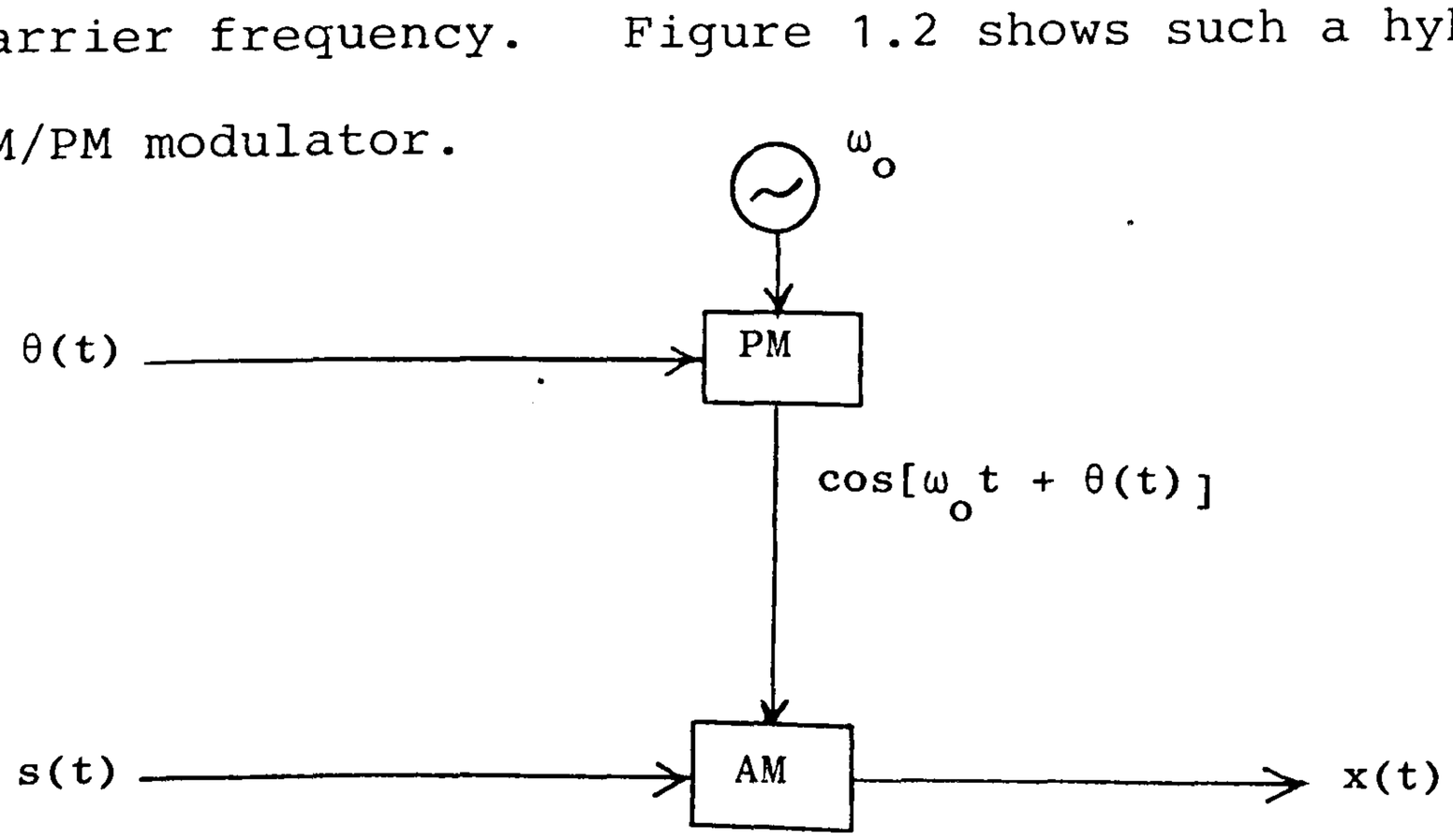

Fig. 1.2

However, combined AM/PM will generate, in general, non-bandlimited signals for all but very low data rates (6). The limited bandwidth available for AM broadcast imposes severe limits on the choice of a modulation system for an additional data signal. Three requirements must be satisfied:

i) bandwidth must not increase due to the additional data signals so that no co-channel interference is incurred.

ii) the envelope of the AM signal should not be distorted so that the main programme signal is not impaired.

iii) the cross-talk between the two channels should be negligible even under the worst reception conditions. Cross-talk causes unwanted a.m./p.m. and p.m./a.m. conversions rendering the data signals to be audible. This is mainly due to two mechanisms, (a) the non-ideal IF tuned circuits of receivers, and (b) multipath fading causing the received signal to be the sum of different versions of the transmitted signal which have travelled by different paths.

The BBC have proposed a system for adding data signals to amplitude-modulated broadcast signals, at l.f. and m.f., in which the carrier is phase-modulated with shaped data signals (5, 7). The maximum available signalling rate is mainly limited by unwanted p.m./a.m.

conversion in receivers causing the data signal to be audible. In the absence of fading or co-channel interference, preliminary laboratory tests of the BBC system showed that signalling rates up to 100 bit/sec using a peak phase deviation of ± 50° would cause imperceptible impairment to the majority of receivers (5). Biphase coding of the data is used so that there is no long-term change to the carrier frequency. The condition of multipath-fading interference has been found to limit the BBC system's data rate to about 25 bit/sec and peak phase deviation to ± 22.5° (5, 7). This data rate is too low to be compared with the data rate of 1187.5 bit/sec that is provided for v.h.f./f.m. signals. Consequently the BBC have suggested that radio-data system for l.f. and m.f. broadcast cannot be expected to be used in similar applications as those for v.h.f./f.m. A recent BBC Research Department report (8) has revealed that for data signalling at l.f./m.f. sound broadcasts, the dominant mechanism likely to cause cross-talk from the PM data channel to the AM sound channel is that of sky-wave interference. It also showed that if the impairment due to data signalling is to be imperceptible when sky-wave fading interference causes a fading depth of 10 dB, then, for a relative delay of up to 1 msec between the ground-wave and sky-wave signals, the data rate must not exceed 50 bit/sec for a phase deviation of ± 11.25°. For a phase deviation of ± 22.5° the data

rate is 25 bit/sec under the same conditions. A fading depth of 10 dB corresponds to the nominal, maximum acceptable value (8), and it also implies that the sky-wave signal is half the ground-wave signal in magnitude.

1.3 A Novel Modulation Technique for Radio-Data Application

A new modulation technique, permitting additional data signals to be superimposed on conventional double-sideband amplitude-modulated (DSB-AM) signals, is introduced briefly in this section. The detailed theoretical background and the bulk of the results will be presented later in this thesis.

In principle the new system uses combined amplitude/frequency modulation to provide for the additional data channel. A special class of frequency-modulating functions must be used so that there is no bandwidth increase or envelope distortion in the DSB-AM signal. This frequency-modulating function is related to temporal variations of the amplitude-modulating signal. The principles of this modulation technique are derived from the concept of the "common envelope set" (9), whose members have the same envelope and bandwidth but different phase functions. As the zeros of bandlimited signals can be regarded as fundamental informational attributes (10), then amplitude-modulating signals can be characterised as a succession of zeros obtained by factorisation of their Fourier series. A process of

zero manipulation can lead to the generation of other members of the "common envelope set" having the same envelope and bandwidth. The binary data signal is imposed by frequency-modulating the carrier with a frequency-modulating function related to the complex zeros of the amplitude-modulating signal. It is also required that frequency modulation must be applied in synchronism with the time of occurrence of the complex zeros of amplitude-modulating signal. Therefore the proposed system is named Zero Synchronous Frequency Modulation (ZSFM).

Additional signal processing is required at the AM transmitter in order to detect complex zeros before frequency modulation takes place, as well as provision for combined AM/FM of the carrier.

On reception, the usual arrangements for envelope detection apply, while a simple frequency demodulator can be used to recover the additional data signals, which can then be used for different purposes as mentioned in Section 1.1.

It will be shown that data transmission at rates up to 5 kbit/sec is theoretically possible over a 10 kHz broadcast channel.

1.4 Scope of the Thesis

This thesis is concerned with the study and development of a novel modulation technique, permitting

additional data signals to be transmitted with conventional AM broadcast signals without any bandwidth increase or envelope distortion.

Chapter 2 presents a mathematical study of the zeros of bandlimited signals. The zero pattern of DSB-AM signals is discussed due to its significance in the understanding of the proposed ZSFM system.

The basic theory of the ZSFM system is studied in Chapter 3. It is shown that the carrier of a DSB-AM signal can be frequency or phase modulated without increasing the bandwidth of the transmitted signal. An aperiodic model for zeros has been developed whereby the zeros of a signal are viewed individually. Data rates of ZSFM are derived, and a prototype ZSFM transmitter is proposed.

The problem of detecting the complex zeros of a real signal, using complex filters, is studied in Chapter 4. Practical realisations of a complex filter are proposed comprising:

a) delay line approximation

b) cascaded differentiators

c) computer implementation

The performance of ZSFM has been assessed by computer simulation and the results are presented in Chapter 5. Characteristics of the ZSFM signal such as bandlimitation and envelope distortion were studied. Both envelope and frequency detectors were simulated to

obtain the demodulated envelope and data signals respectively. The problem of IF cross-talk between the two channels was studied by simulating an IF filter consisting of coupled-tuned circuits. It is considered that the cross-talk due to IF non-linearities is negligible. The problem of multipath fading was studied to estimate its effects on cross-talk. Multipath propagation of ZSFM has been simulated using a 2-path fading model, and it has been shown that PM/AM conversion, as a result of multipath propagation conditions, is expected to be a major limiting factor. Computer implementation of the complex filter was also studied. Finally a simple phase-locked loop was used as a frequency detector to demonstrate recovery of the data signal.

Chapter 6 introduces theoretical and experimental studies of the complex zero distributions of positive, bandlimited, real signals. A computer simulation has been used to find the probability-density function (p.d.f.) of the complex zeros of a positive bandlimited random signal. The achievable bit rate of ZSFM has been estimated.

The performance of ZSFM is compared with the BBC radio-data system for l.f./m.f. broadcast in Chapter 7.

CHAPTER 2

MATHEMATICAL ANALYSIS

2.1 Introduction

Mathematical information relevant to the problem of interest is presented in this chapter.

The most general form of bandlimited modulated signals exhibit simultaneous envelope and phase fluctuations. The general relations, which govern these attributes, are derived in this chapter. The zeros of bandlimited signals are shown to have major informational contribution. The idea of a "common envelope set" is introduced, and the generation of the different members of such a set is discussed. It is possible to classify signals according to their characteristic zero patterns.

2.2 Hilbert Transform

Let s(t) be a real signal of the real time variable (t). If s(t) is Fourier-transformable, then its Hilbert transform is defined by:

$$H\ [s(t)] = \hat{s}(t) = \frac{1}{\pi} P \int_{-\infty}^{\infty} \frac{s(\tau)}{t - \tau}\, d\tau$$

$$= P \int_{-\infty}^{\infty} \frac{s(\tau)}{\pi(t - \tau)}\, d\tau$$

$$= s(t) * \frac{1}{\pi t} = s(t) * h(t) \qquad (2.1)$$

where P denotes Cauchy principal value, * denotes convolution and $h(t) = \frac{1}{\pi t}$ is the impulse response of the Hilbert transformer.

If S(f) and H(f) are the Fourier transforms of s(t) and h(t) respectively then the Fourier transform of $\hat{s}(t)$ is:

$$F[\hat{s}(t)] = S(f) \,.\, H(f) \tag{2.2}$$

where F[ ] denotes Fourier transform. It is shown in Appendix (1) that H(f) is given by:

$$H(f) = -j \ \text{sgn}\,(f) \tag{2.3}$$

$$\text{where } \text{sgn}(f) = \begin{cases} 1, & f > 0 \\ 0, & f = 0 \\ -1, & f < 0 \end{cases}$$

Substituting eqn. (2.3) into eqn. (2.2) gives:

$$F\,[\hat{s}(t)] = \begin{cases} -j\ S(f), & f > 0 \\ 0 \qquad , & f = 0 \\ +j\ S(f), & f < 0 \end{cases} \tag{2.4}$$

It is apparent that H(f), the transfer function of the Hilbert transformer, represents a 90° phase shifting network.

2.3 Analytic Signal

Let m(x) be a complex function of the complex variable $x = t + j\sigma$, where t and σ are real. m(x) can be written as

$$m(x) = u(t,\sigma) + jv(t,\sigma) \tag{2.5}$$

where $u(t,\sigma)$ and $v(t,\sigma)$ are real functions. If m(x) is

regular (i.e. continuous and free from singularities) in the region (R) in the x-plane, then a unique derivative of m(x) exists (11) and any function obeying the above is called analytic in the region (R).

A function m(x) which is analytic in the open upper-half x-plane will be named "Analytic"(9).

If s(t) is a real signal which is Fourier transformable and usually bandlimited, its Analytic signal is defined (12) as:

$$m(t) = s(t) + j\,\hat{s}(t)$$

$$= |m(t)|\, e^{j\phi(t)} \qquad (2.6)$$

where $|m(t)| = \sqrt{s^2(t) + \hat{s}^2(t)}$ = envelope of m(t),

$$\phi(t) = \arctan\left[\frac{\hat{s}(t)}{s(t)}\right] = \text{phase of } m(t),$$

and $\hat{s}(t)$ is the Hilbert transform of s(t). To find the spectrum of the Analytic signal, M(f), we can use eqns. (2.6) and (2.4):

$$M(f) = S(f) + j\,F[\hat{s}(t)]$$

$$= \begin{cases} 2\,S(f), & f > 0 \\ 0, & f < 0 \end{cases} \qquad (2.7)$$

Hence M(f) is single-sided and has zero content at negative frequencies. If s(t) is bandlimited to ± W Hz, then m(t) is bandlimited to W Hz. It is this single-sided property that makes the Analytic signal very useful. The Analytic signal concept can be used to represent different modulation methods (12). For example a real modulated signal can be illustrated by

using the Analytic signal representation as shown:

$$f_{\omega_o}(t) = \mathrm{Re}\ [m(t)\ e^{j\omega_o t}]$$

$$= \mathrm{Re}\ [|m(t)|\ e^{j\phi(t)}\ e^{j\omega_o t}]$$

$$= |m(t)|\ \cos[\omega_o t + \phi(t)] \qquad (2.8)$$

where Re denotes the real part and ω_o is the carrier radian frequency.

It is apparent that the magnitude of m(t) gives the envelope of the modulated signal $f_{\omega_o}(t)$. It is clear that eqn. (2.8) represents a conventional amplitude-modulated signal when $\phi(t) = 0$ in which case eqn. (2.8) becomes:

$$f_{\omega_o}(t)\big|_{AM} = s(t)\ \cos(\omega_o t) \qquad (2.9)$$

Using inverse Fourier transform, the Analytic signal m(t) can be expressed as:

$$m(t) = \int_{-\infty}^{\infty} M(f)\ e^{j2\pi ft}\ df$$

$$= \int_{o}^{\infty} M(f)\ e^{j2\pi ft}\ df \qquad (2.10)$$

Replacing t by $x = t + j\sigma$ gives:

$$m(x) = \int_{o}^{\infty} M(f)\ e^{-2\pi f\sigma}\ e^{j2\pi ft}\ df \qquad (2.11)$$

It is clear that the existence of the above Fourier transform requires the integrability and convergence of eqn. (2.11), and therefore it must converge for any

$\sigma \geq 0$, i.e. no singularities in the open upper-half x-plane. The properties of an Analytic signal can be summarised as follows:

i) it is a complex-valued signal.

ii) it has no singularities in the open upper-half x-plane (UHP)

iii) its spectrum vanishes for negative frequencies

iv) its complex conjugate will have conjugate

Analytic properties

$$m^*(t) = s(t) - j\,\hat{s}(t)$$

$$= |m(t)|\, e^{-j\phi(t)} \qquad (2.12)$$

$m^*(t)$ is called Image-Analytic (6) and its spectrum vanishes for positive frequencies. $m^*(t)$ has no singularities in the open lower-half x-plane (LHP).

Considering the integral given by eqn. (2.11):

$$m(x) = \int_o^\infty M(f)\, e^{-2\pi f\sigma}\, e^{j2\pi ft}\, df$$

Assuming that m(f) is bandlimited to W Hz, then the above becomes (9):

$$m(x) = \int_o^W M(f)\, e^{-2\pi f\sigma}\, e^{j2\pi ft}\, df$$

$$\therefore |m(x)|^2 = \left| \int_o^W M(f)\, e^{-2\pi f\sigma}\, e^{j2\pi ft}\, df \right|^2 \qquad (2.13)$$

and by Schwarz inequality,

$$|m(x)|^2 \leq \int_o^W |M(f)|^2\, df \int_o^W e^{-4\pi f\sigma}\, df$$

$$\leq \int_o^W |M(f)|^2\, df \left[\frac{1 - e^{-4\pi W\sigma}}{4\pi\sigma}\right] \qquad (2.14)$$

The finite energy of the bandlimited Analytic signal m(t) is given, by Parseval's Theorem, as:

$$E_m = \int_{-\infty}^{\infty} |m(t)|^2 \, dt = \int_{0}^{W} |M(f)|^2 \, df \qquad (2.15)$$

$\therefore$ eqn. (2.14) becomes:

$$|m(x)|^2 \leq E_m \left[\frac{1 - e^{-4\pi W\sigma}}{4\pi\sigma} \right] \qquad (2.16)$$

This shows that m(x) is bounded (has finite value) in the finite lower-half x-plane, and hence m(x) is finite and analytic in the finite x-plane. Thus m(x) is an entire (integral) function if it is bandlimited. For bandlimited m(x), the singularities at the lower-half x-plane are at infinity. It is worthy to note that Analyticity follows from the single-sided property of M(f) and does not depend on bandlimitation.

2.4 Phase-Envelope Relationships

The Analytic signal is called a minimum-phase (MP) signal if its envelope and phase satisfy a specific condition as will be shown.

Consider the integral

$$I = \oint_C \frac{g(x)}{x - t_1} dx$$

where C is a closed contour comprising a real axis t, excluding a point at $x = t_1$, and infinite semi-circle Γ in the upper-half x-plane as shown in Figure 2.1.

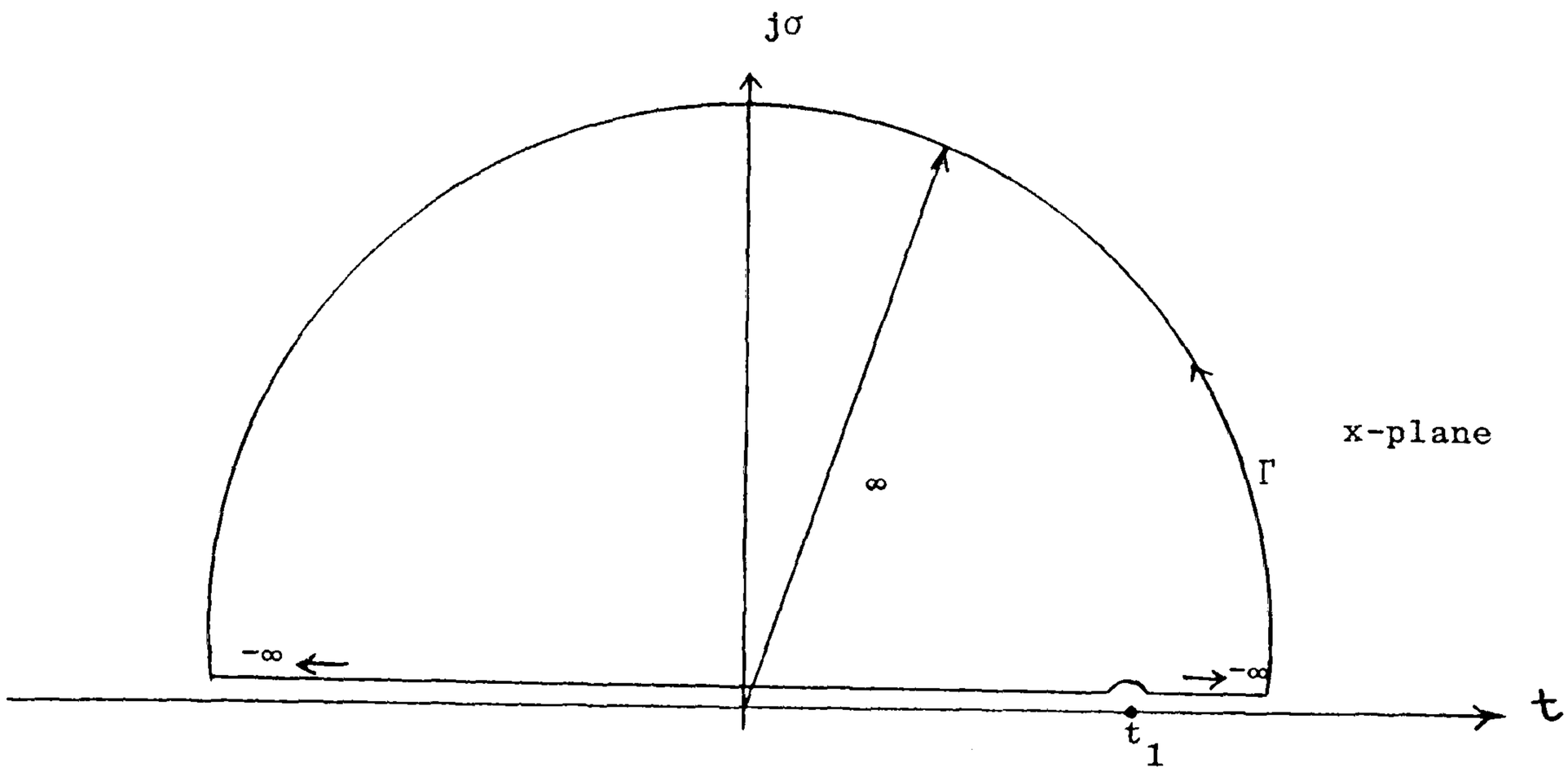

Fig. 2.1

Closed Contour C

It is shown in Appendix (2) that if g(x) is analytic in the upper-half x-plane and on C, then:

$$\text{Im}[g(t)] = H\{\text{Re}[g(t)]\}$$

$$\text{Re}[g(t)] = -H\{\text{Im}[g(t)]\} \qquad (2.17)$$

where Im denotes imaginary part, Re denotes real part, and H { } the Hilbert transform.

Applying this result to the logarithm of the Analytic signal (9) given by eqn. (2.6) renders:

$$m(x) = |m(x)|\, e^{j\phi(x)}$$

$$\therefore \quad \ln m(x) = \ln |m(x)| + j\phi(x) \qquad (2.18)$$

Taking the derivative of the above gives:

$$\ln' m(x) = \ln' |m(x)| + j\phi'(x)$$

$$= \frac{m'(x)}{m(x)} \qquad (2.19)$$

The assumption, that m(x) is Analytic, does not guarantee that ln'm(x) will be Analytic as ln'|m(x)| can have upper-half plane singularities at the upper-half plane zeros of m(x). However, if m(x) is zero-free in

the upper-half x-plane, then ln'm(x) is Analytic. If it can further be assumed that ln'm(x) is square - integrable then eqn. (2.17) applies with g(t) = ln'm(x).

$$\therefore \quad \phi'(t) = H\,[\ln'|m(t)|]$$

$$\ln'|m(t)| = -H\,[\phi'(t)] \tag{2.20}$$

Any Analytic signal m(t) satisfying eqn. (2.20) is called a minimum-phase (MP) signal (9) and is zero-free in the upper-half x-plane. Alternatively, if m(t) has zeros in the upper-half x-plane then ln'm(x) is not Analytic in general and m(t) is called a non-minimum phase (NMP) signal. An Analytic signal m(t) with zeros only in the upper-half x-plane is called maximum-phase.

2.5 Zeros of Bandlimited Signals

The real and complex zeros of bandlimited signals can be regarded as fundamental informational attributes. This follows from the sufficiency of the zero-based representations of signals (10).

For a periodic signal, the zeros are obtained by the factorisation of its Fourier series representation. If s(t) is a real signal and bandlimited then it can be written as:

$$s(t) = \sum_{n=-N}^{N} a_n\, e^{jn\Omega t} \tag{2.21}$$

where the a_n's are the coefficients, $\Omega = \frac{2\pi}{T}$ is the fundamental frequency (rad/sec), T is the period and s(t) has a bandwidth of $\pm \frac{N\Omega}{2\pi}$ Hz.

From the definition of Hilbert transform as given in (2.4):

$$\hat{s}(t) = H[s(t)] = j \sum_{n=-N}^{-1} a_n e^{jn\Omega t} - j \sum_{n=1}^{N} a_n e^{jn\Omega t} \qquad (2.22)$$

The Analytic signal of s(t) is:

$$m(t) = s(t) + j\,\hat{s}(t)$$
$$= a_o + 2 \sum_{n=1}^{N} a_n e^{jn\Omega t} \qquad (2.23)$$

putting:

$$c_o = a_o,\ c_n = 2\,a_n$$
$$\therefore\ m(t) = \sum_{n=o}^{N} c_n e^{jn\Omega t} \qquad (2.24)$$

The above represents an Analytic signal and it is expressed as a trigonometric polynomial. This trigonometric polynomial behaves within a period, much like an algebraic polynomial behaves over the whole x-plane.

$$m(x) = \sum_{n=o}^{N} c_n e^{jn\Omega x}$$
$$= \sum_{n=o}^{N} c_n e^{-n\sigma\Omega} e^{jn\Omega t},\ x = t + j\sigma \qquad (2.25)$$

The Analytic signal m(x) expressed in (2.25) has:

i) N zeros per period

ii) spectral width of $\frac{N\Omega}{2\pi}$ Hz

iii) fundamental frequency of $\frac{\Omega}{2\pi}$ Hz

iv) its bandwidth is proportional to the number of zeros per period

Using the conformal transformation $z = e^{j\Omega x}$ gives a direct mapping from the complex x-plane to the complex z-plane, as shown in Figure 2.2.

$\therefore$ eqn. (2.25) becomes :

$$m(z) = \sum_{n=o}^{N} c_n z^n \qquad (2.26)$$

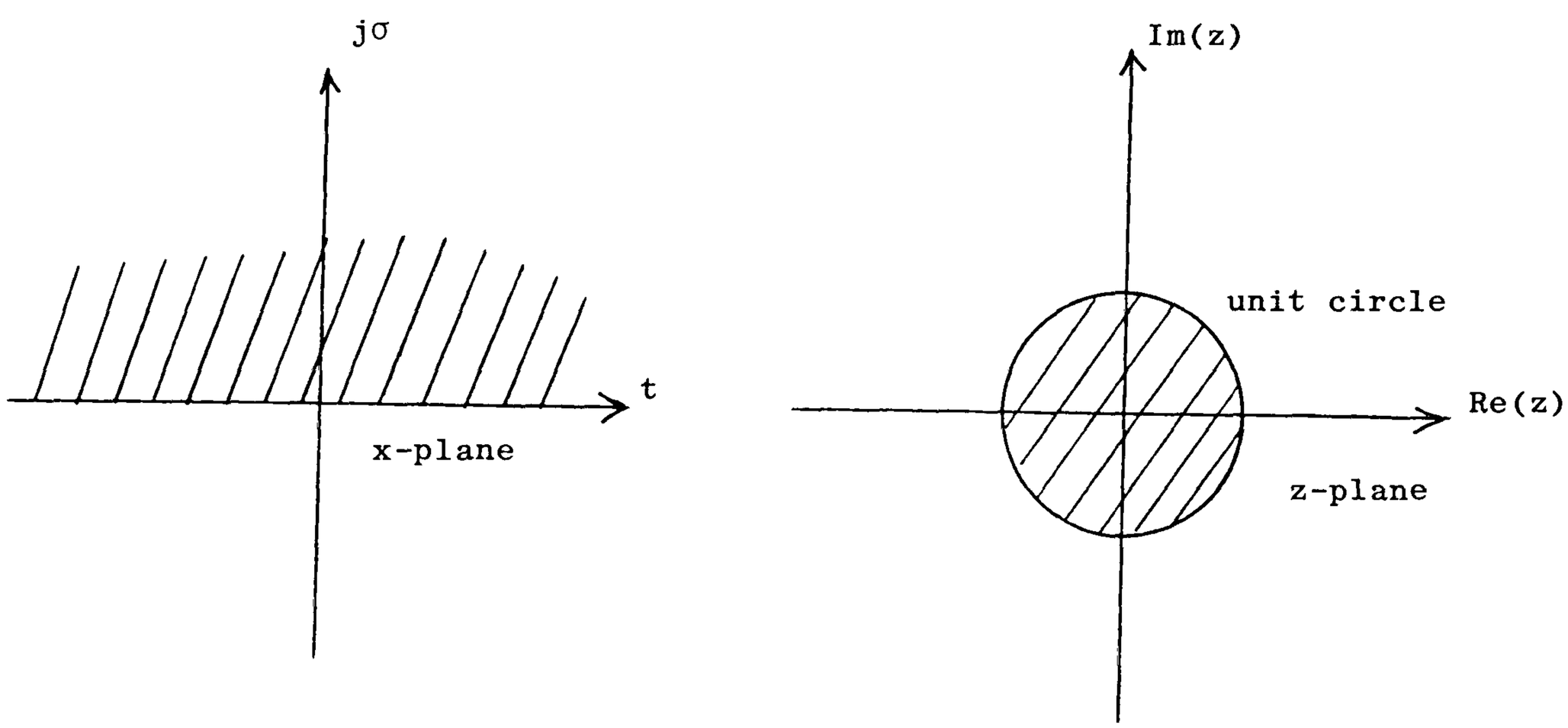

Fig. 2.2

This maps the UHP (x-plane) into the interior of the unit circle in the z-plane and the LHP (x-plane) into the exterior of the unit circle. The periphery of the unit circle corresponds to the real time axis. Eqn. (2.26) shows that m(z) is analytic inside the unit circle, i.e. it is Analytic. Eqn.(2.26) represents an algebraic polynomial in z of degree N.
m(z) has:

i) N zeros which are not periodic (z-plane zeros).

ii) (N + 1) coefficients.

Hence m(z) can be represented as multiplicative factors, each representing a zero in the z-plane, i.e.

$$m(z) = a_k \prod_{n=1}^{N} (z - z_n) \qquad (2.27)$$

Example

As an example of the zeros of bandlimited signal consider:

$$m(t) = 1 + a\, e^{j\Omega t} \qquad (2.28)$$

where a is a real constant. The function m(x) of the complex variable $x = t + j\sigma$ is:

$$m(x) = 1 + a\, e^{j\Omega x}$$

Putting $z = e^{j\Omega x}$ gives:

$m(z) = 1 + az$, which has a simple zero at $z = -\frac{1}{a}$.

Clearly m(z) is Analytic as it does not have singularities inside the unit circle in the z-plane.

To find the corresponding zeros in the complex x-plane:

$$z = e^{j\Omega x} = -\frac{1}{a} = \frac{1}{a}\, e^{j(\pi + 2k\pi)} \qquad (2.29)$$

$$k = 0, \pm 1, \pm 2, \ldots$$

Taking natural logarithm of both sides of eqn.(2.29) gives:

$$j\Omega x = \ln(\frac{1}{a}) + j(\pi + 2k\pi)$$

$$\therefore\ x = \frac{(\pi + 2k\pi)}{\Omega} + j\,\frac{\ln a}{\Omega} \qquad (2.30)$$

Eqn.(2.30) gives the position of the zeros of m(t) in the x-plane.

Note that the zeros in the x-plane are periodic repetition, while there is only single zero in the z-plane.

For $a < 1$, the zeros are shown in Figure 2.3.

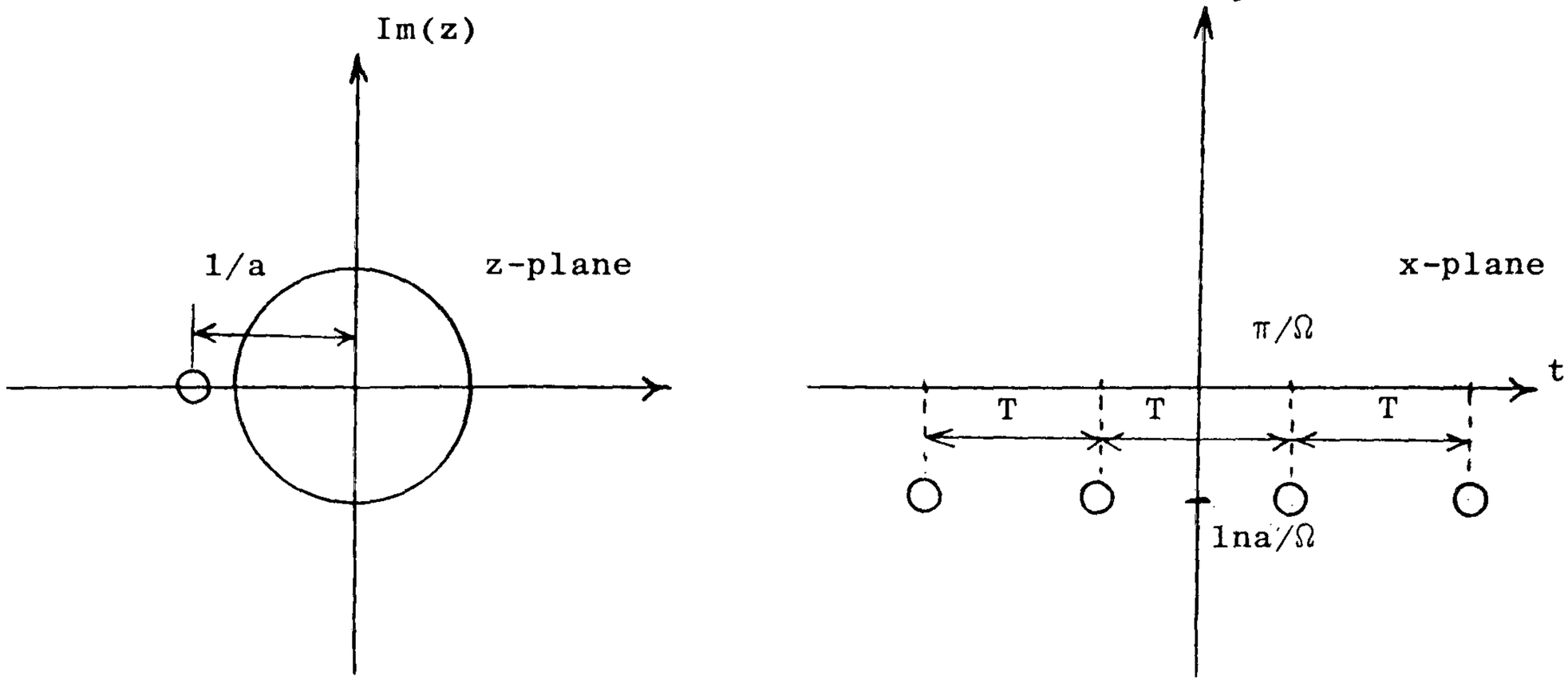

z-plane and x-plane zeros of m(t) for a < 1

Fig. 2.3

As all the zeros lie in the LHP (x-plane), m(t) represents a minimum-phase signal. For a > 1, the zeros are shown in Figure 2.4

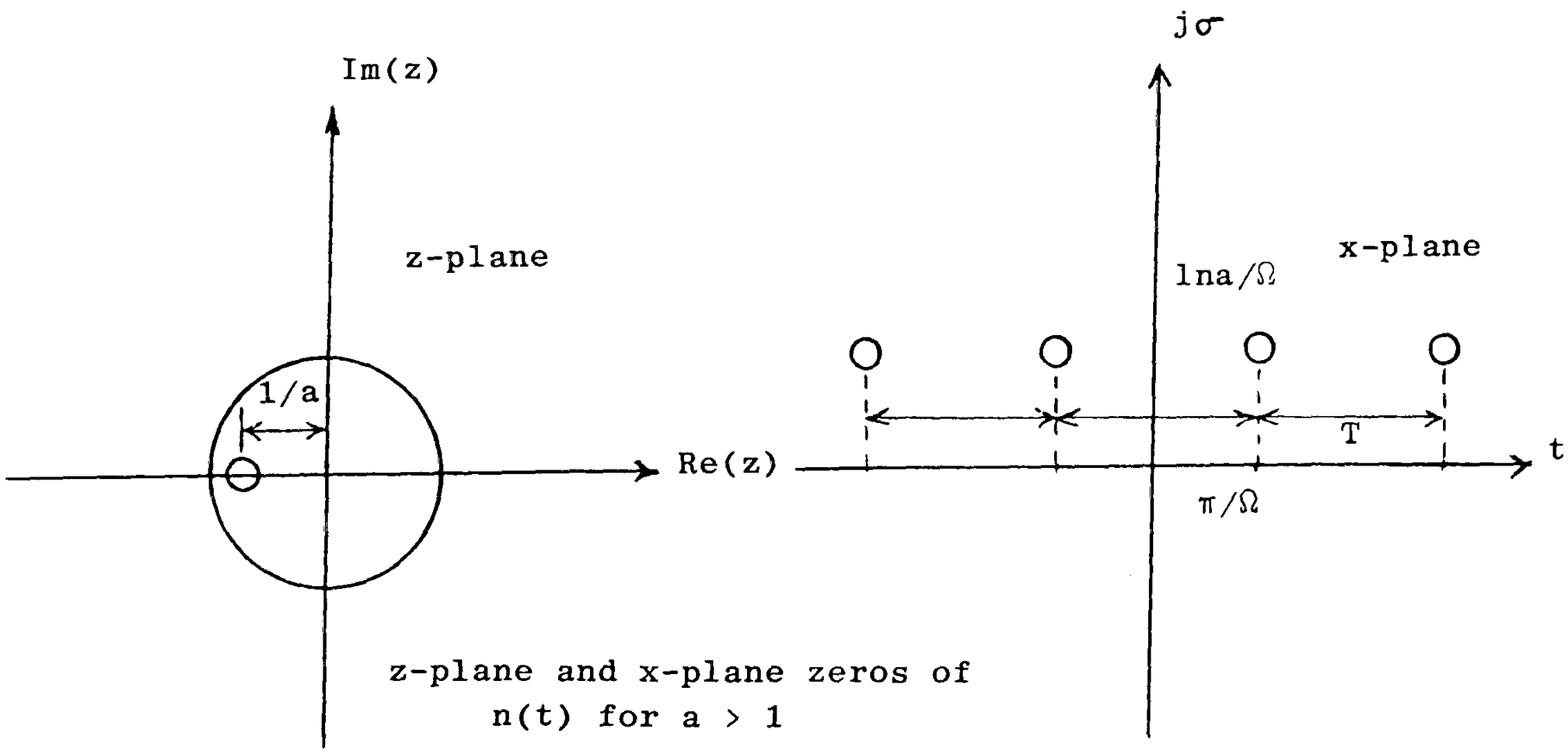

z-plane and x-plane zeros of
n(t) for a > 1

Fig. 2.4

m(t) represents a maximum-phase signal as all the zeros lie in the UHP (x-plane).

$m(t) = 1 + a\, e^{j\Omega t}$ can be represented by phasor diagram as shown in Figure 2.5

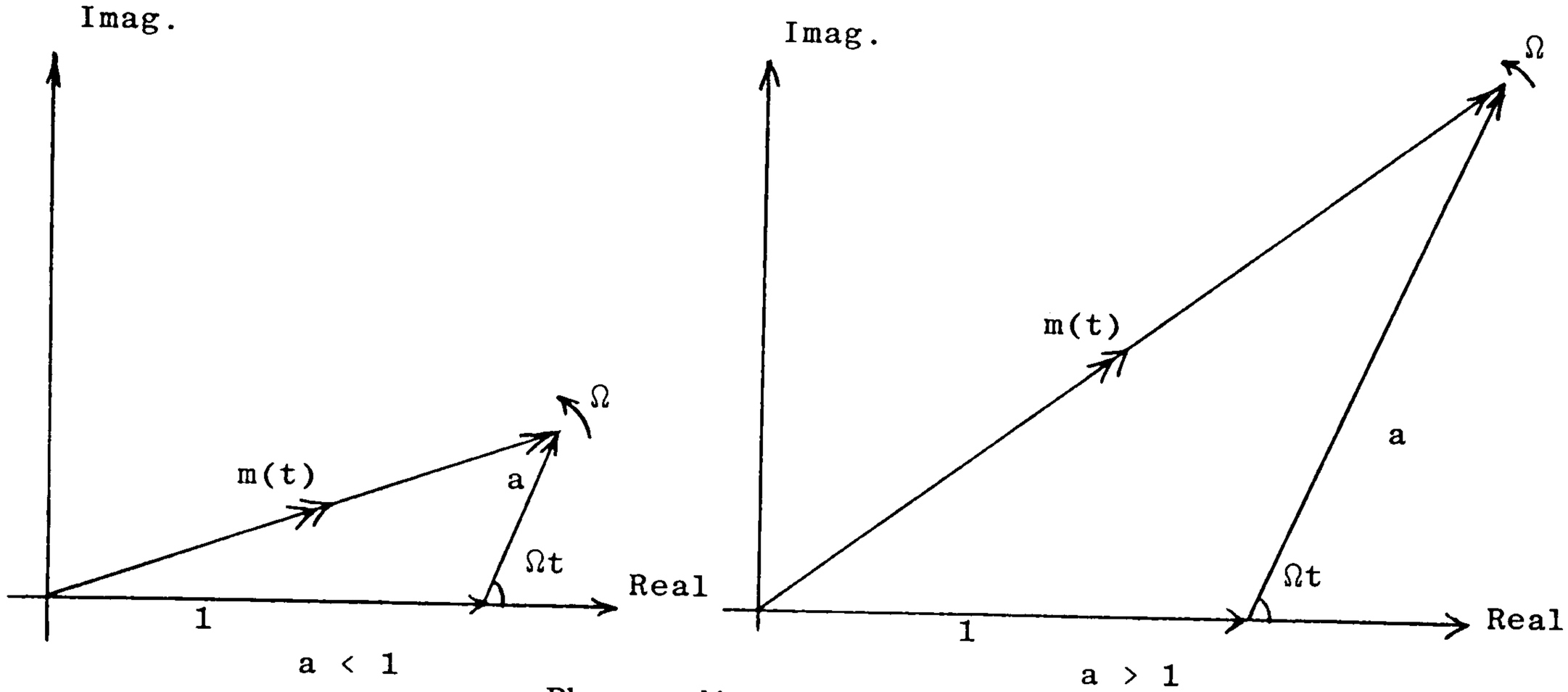

Phasor diagram of m(t)

Fig. 2.5

For $a < 1$ the average speed of rotation of the vector $(1 + a\, e^{j\Omega t})$ is zero, i.e. it is a minimum-phase.

For $a > 1$ the average speed of the rotation of the vector $(1 + a\, e^{j\Omega t})$ is Ω(rad/sec), i.e. it is maximum-phase. The above is valid for Analytic signals, while for Image-Analytic signals minimum-phaseness is related to non-zero average speed of rotation of the vector and maximum-phaseness is related to zero average speed of rotation of the vector.

For the Image-Analytic signal:

$$m(t) = 1 + a\, e^{-j\Omega t}$$

$m(t)$ is a minimum-phase for $a > 1$ and a maximum-phase for $a < 1$.

2.6 Characteristic Zero Pattern for DSB-AM Signals

The zeros of bandlimited signals are regarded as major informational attributes and therefore it is possible to express these signals in terms of their zero patterns.

The zero pattern of a conventional double-sideband amplitude-modulated (DSB-AM) signal is worthwhile to be considered at this stage as it gives an idea about the zero pattern symmetry of DSB-AM about the real axis. An AM signal is conventionally defined as given by eqn. (2.9):

$$f_{\omega_o}(t)\big|_{AM} = s(t)\cos(\omega_o t)$$

where $s(t)$ is a real modulating signal of bandwidth $\pm$ W Hz, and $\omega_o > 2\pi W$ is the carrier frequency.

In DSB-AM the signal must be positive, i.e. it contains an additive constant that prevents overmodulation from happening. The Analytic form of the AM signal $f_{\omega_o}(t)\big|_{AM}$ can be written as:

$$\begin{aligned} m_{AM}(t) &= f_{\omega_o}(t)\big|_{AM} + j\,\hat{f}_{\omega_0}(t)\big|_{AM} \\ &= s(t)\, e^{j\omega_o t} \end{aligned} \qquad (2.31)$$

For example, if the real baseband signal $s(t)$ is a single-tone with a constant, i.e.

$$s(t) = 1 + a\cos\Omega t,\ a < 1$$

then the Analytic AM signal becomes:

$$m_{AM}(t) = (1 + a\cos\Omega t)\, e^{j\omega_o t} \qquad (2.32)$$

In terms of the complex time variable $x = t + j\sigma$ the Analytic AM signal becomes:

$$m_{AM}(x) = (1 + a\cos\Omega x)\, e^{j\omega_o x}$$

Putting $z = e^{j\Omega x}$ and $\beta = \frac{\omega_o}{\Omega}$

$$m_{AM}(z) = (1 + \frac{a}{2}z + \frac{a}{2} z^{-1})\, e^{j\beta\Omega x}$$

$$= (1 + \frac{a}{2} z + \frac{a}{2} z^{-1})\, z^{\beta}$$

$$= \frac{a}{2} (1 + \frac{2}{a} z + z^2)\, z^{\beta}\, z^{-1}$$

$$= \frac{a}{2} (1 + \frac{2}{a} z + z^2)\, z^{(\beta-1)}$$

Ignoring $z^{(\beta-1)}$ for the time being, the Analytic AM signal becomes:

$$m_{AM}(z) = \frac{a}{2} (z^2 + \frac{2}{a} z + 1) \qquad (2.33)$$

The zeros of $m_{AM}(z)$ are obtained by solving for:

$$(z^2 + \frac{2}{a} z + 1) = 0 \text{ , i.e.}$$

$$z = \frac{-2/a \pm \sqrt{4/a^2 - 4}}{2} = \frac{-1 \pm \sqrt{1 - a^2}}{a}$$

$$\therefore \quad m_{AM}(z) = \frac{a}{2} (z + r)(z + \frac{1}{r}) \qquad (2.34)$$

where $r = \frac{1 - \sqrt{1 - a^2}}{a}$, $\frac{1}{r} = \frac{1 + \sqrt{1 - a^2}}{a}$ and the z-plane zeros of $m_{AM}(z)$ are shown in Figure 2.6

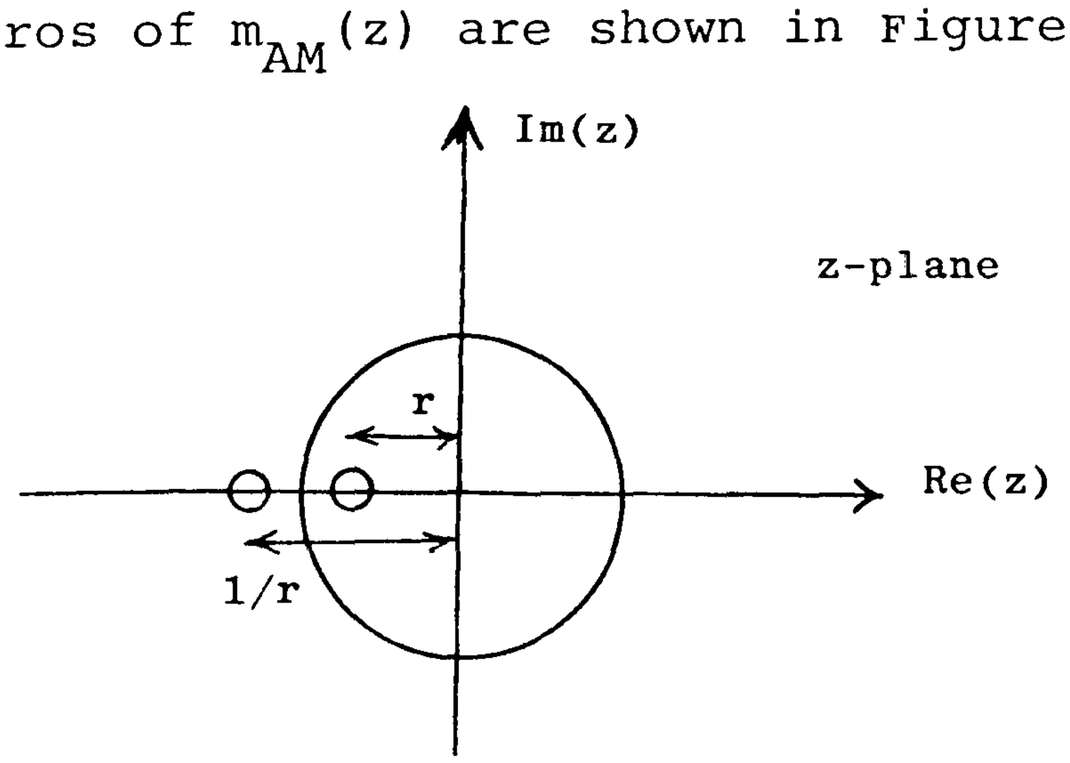

Fig. 2.6

The corresponding x-plane zeros can be found by substituting $z = e^{j\Omega x}$ and solving for x to give:

$$x = \frac{(2k\pi + \pi)}{\Omega} \pm j\frac{\ln r}{\Omega} \quad , \; k = 0, \pm 1, \pm 2, \ldots$$

These complex conjugate x-plane zero pairs are shown in Figure 2.7

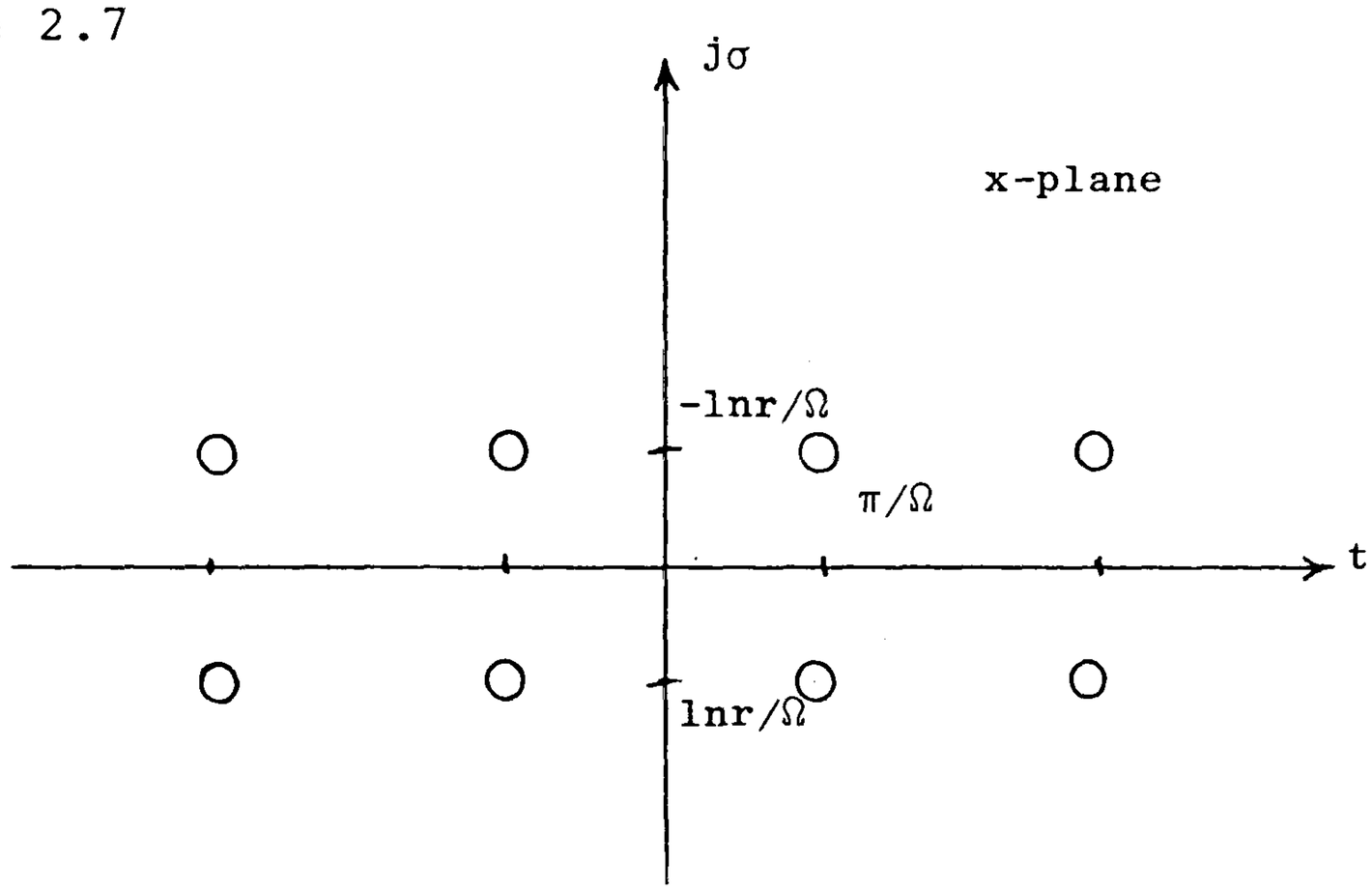

Fig. 2.7

It is apparent that the DSB-AM signal is characterised by zero pattern symmetry about the real axis of the complex x-plane. When the modulation depth a approaches 1 then r approaches 1 also and the complex zeros move closer to the real axis till they become real zeros when a becomes 1, i.e. 100% modulation.

It is this zero pattern symmetry of DSB-AM signal that will be exploited in order to superimpose additional data channels on conventional broadcast channels.

2.7 Common Envelope Set

This is a term (9) defining a complete group of signals whose members differ only in phase functions, but not in envelope or bandwidth.

In equation (2.27) m(t) has N zeros and these can be conjugated and yet the envelope $|m(t)|$ is invariant. Conjugation means that a complex zero in the x-plane is replaced by its complex conjugate, or a zero in the z-plane is replaced by its reciprocal . If a zero is to be conjugated from the upper-half to the lower-half x-plane, a cancellation operator c(t), which effects zero conjugation, should have a pole-zero pair at the conjugate location.

To explain the process of zero conjugation consider the Analytic signal given previously:

$$m(t) = 1 + a\, e^{j\Omega t} \quad , \; a > 1$$

It has x-plane zeros at:

$$x = \frac{(\pi + 2k\pi)}{\Omega} + j\frac{\ln a}{\Omega} \quad , \text{ as shown before.}$$

The cancellation operator necessary for conjugation should be of the form:

$$c(t) = \frac{1 + a\, e^{-j\Omega t}}{1 + a\, e^{j\Omega t}} \tag{2.35}$$

This has x-plane poles at:

$$x = \frac{(\pi + 2k\pi)}{\Omega} + j\frac{\ln a}{\Omega}$$

and x-plane zeros at:

$$x = \frac{(\pi + 2k\pi)}{\Omega} - j\frac{\ln a}{\Omega} \quad , \; k = o, \pm 1, \pm 2, \ldots$$

The zero-pole pattern of c(t) is shown in Figure 2.8.

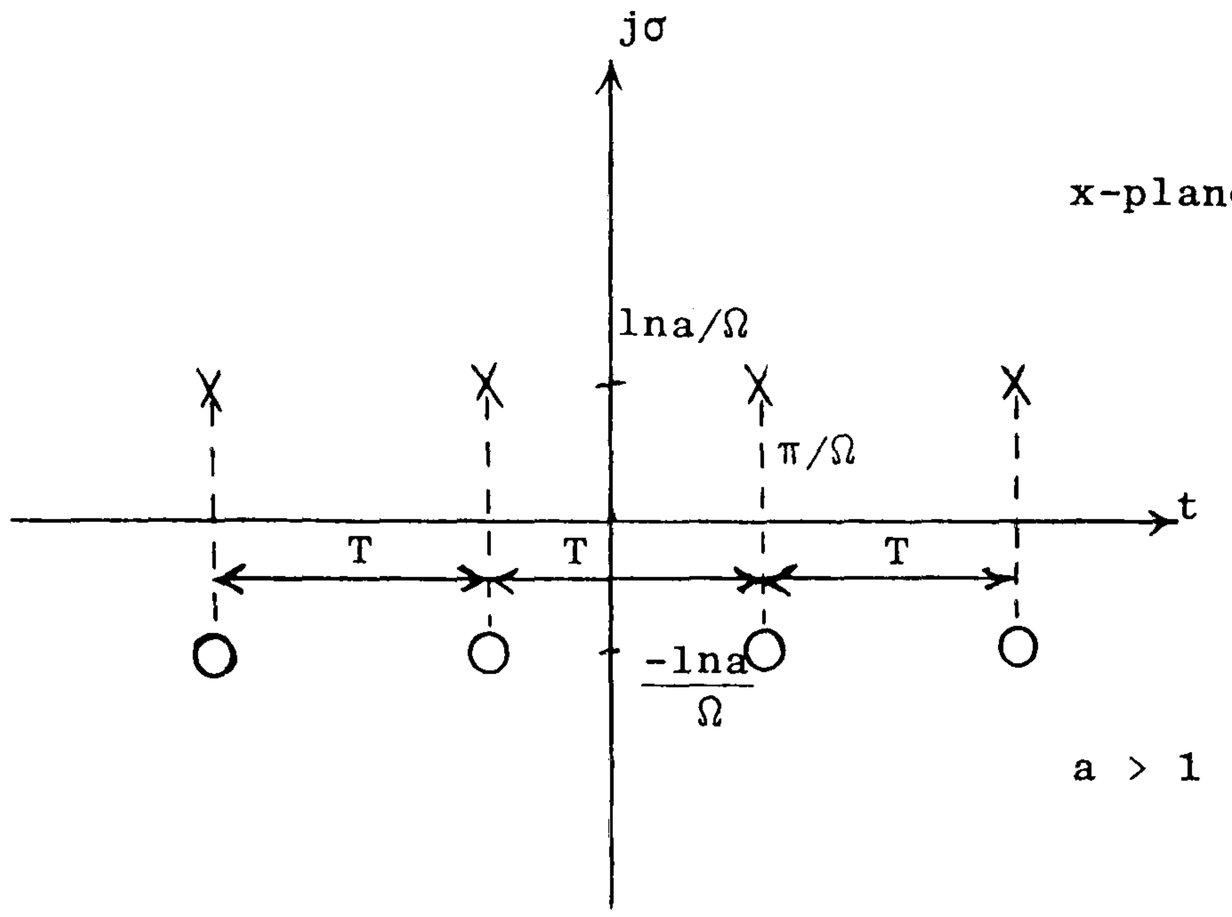

Fig. 2.8

Pole-zero pattern of c(t)

$\therefore$ m(t) c(t) = 1 + a $e^{-j\Omega t}$, which has a zero pattern as shown in Fig. 2.9

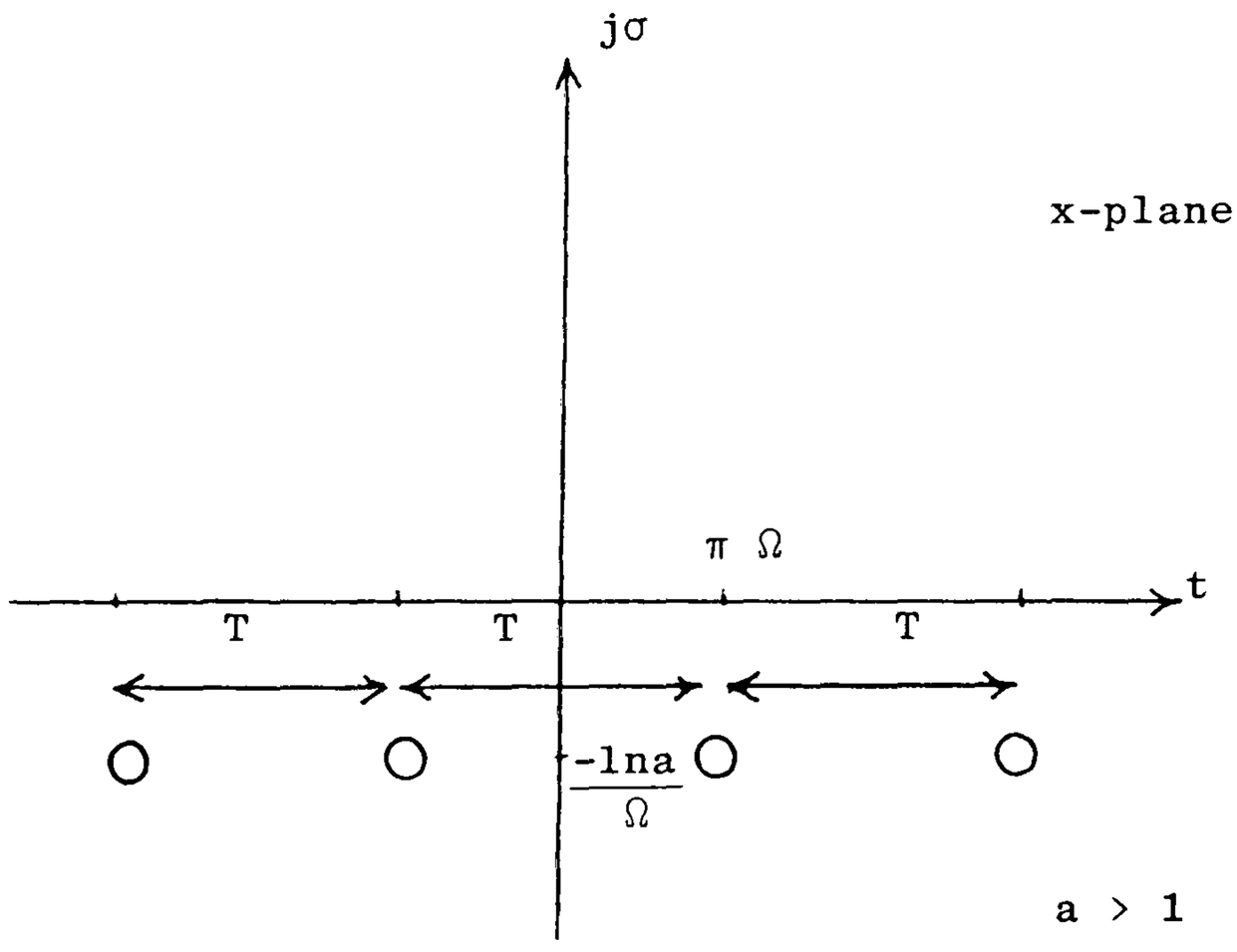

Fig. 2.9

One or more zeros can be conjugated without affecting the envelope or bandwidth of the signal, as the number of zeros per period (N) is not increased.

For a periodic signal with N zeros per period, there can be up to 2^N members, if all the zeros are complex, and of first order type (9). If all the zeros are real, there is only one member.

Example

To illustrate the idea of the common envelope set, consider the signal:

$$m(z) = 1 + az \ , \ a < 1$$

m(z) has a single zero at $z = -\frac{1}{a}$ as shown in Figure 2.10.

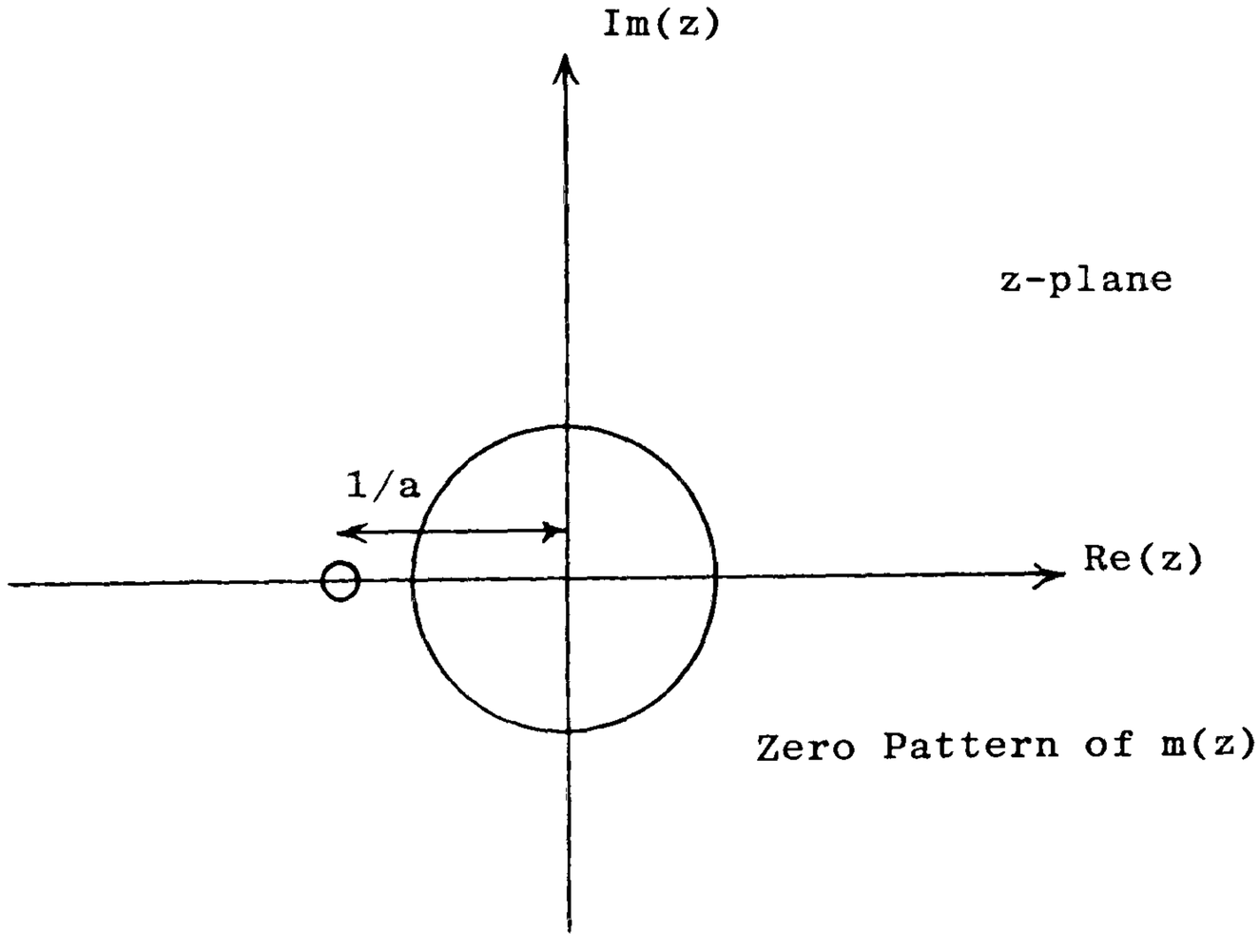

Fig. 2.10

$\therefore$ N = 1, and the number of members is $2^N = 2$.

The second member can be obtained as:

$$m^*(z) = (1 + az)^* = 1 + az^* = 1 + \frac{a}{z}$$

which has a zero at z = -a as shown in Figure 2.11.

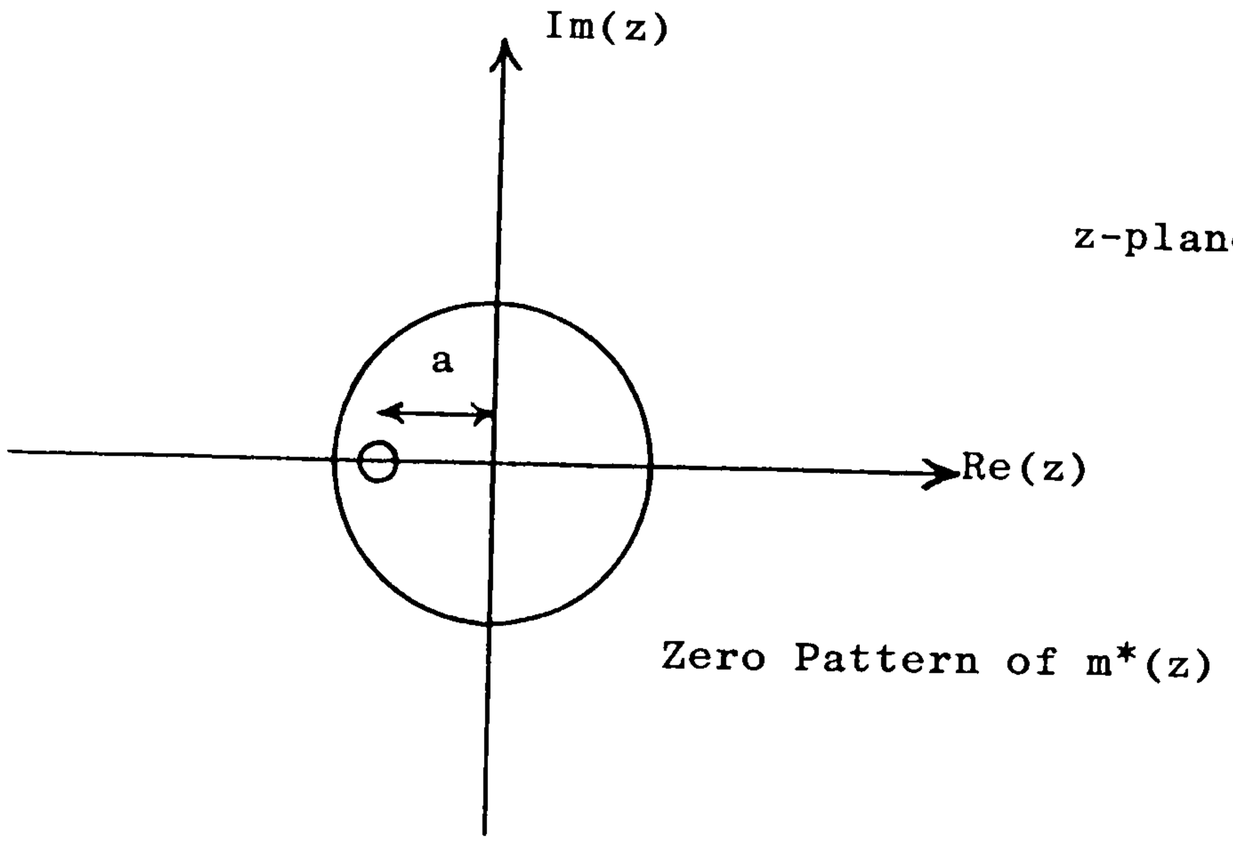

Fig. 2.11

To compare envelope and bandwidth of these two members:

$$m(t) = 1 + a\, e^{j\Omega t}$$

$$|m(t)| = \sqrt{(1 + a\cos\Omega t)^2 + (a\sin\Omega t)^2}$$

$$= \sqrt{1 + a^2 + 2a\cos\Omega t} \qquad (2.36)$$

$$\arg(m(t)) = \arctan\left(\frac{a\sin\Omega t}{1 + a\cos\Omega t}\right)$$

$$m^*(t) = 1 + a\, e^{-j\Omega t}$$

$$|m^*(t)| = \sqrt{(a + a\cos\Omega t)^2 + (-a\sin\Omega t)^2}$$

$$= \sqrt{1 + a^2 + 2a\cos\Omega t} = |m(t)| \qquad (2.37)$$

$$\arg(m^*(t)) = \arctan\left(\frac{-a\sin\Omega t}{1 + a\cos\Omega t}\right) = -\arg(m(t))$$

The above shows that $m(t)$ and $m^*(t)$ have the same envelope and bandwidth ($\frac{\Omega}{2\pi}$ Hz), but they differ in their phase functions. This is an important characteristic of the common envelope set which will be exploited and developed in the next chapter.

2.8 Zero Patterns

Algebraic and trigonometric polynomials may be represented unambiguously and uniquely by ordered sets of their zeros (plus a few parameters). The number of zeros of an algebraic polynomial is equal to the polynomial's degree. Trigonometric polynomials have an infinite number of zeros but their pattern is a periodic repetition of the finite set of zeros which occur within a period. It has been shown that the number of zeros per period is proportional to the bandwidth. The zero count of a periodic signal is the number of zeros per single period of the signal.

It was previously shown that zeros may be interpreted as informational attributes of the signal. Real zeros of a signal are overt attributes as it is easy to observe the zero crossings of the signal and hence locate its real zeros. On the other hand complex zeros of a signal are subtler attributes and they can influence the dips of the signal. For periodic signals, a factorisation of their finite Fourier series representation can give the related zero pattern.

Zero manipulation concepts (10) can be used interpretively to describe different modulation processes. It will be shown that they can also be used constructively to establish new services (13).

CHAPTER 3

ZERO SYNCHRONOUS FREQUENCY MODULATION

3.1 Introduction

This chapter is devoted to a discussion of the theoretical foundation of the proposed Zero Synchronous Frequency Modulation (ZSFM) system. A periodic signal model has been chosen to represent a general communication signal due to the simplicity of interpreting the results in both the time and frequency domains. An example of the distribution of the complex zeros of a real periodic signal is discussed. The idea of complex zero conjugation that produces the members of a "common envelope set" is considered fully in Section 3.4. A novel phase conjugating function is developed whereby the complex zero pairs can be treated individually.

The principle of ZSFM is described in Section 3.8, where a binary data signal can be superimposed on conventional DSB-AM signal without increasing bandwidth or distorting the envelope. ZSFM derives from the concept of the "common envelope set" whose members possess the same envelope and bandwidth but different phase functions. The binary data signal can be imposed by frequency modulating the carrier using a frequency modulating function related to the complex zeros of the AM signal. A prototype of a ZSFM transmitter is described in Section 3.11, and finally the possible applications of the proposed system are discussed.

3.2 Periodic Signal Model

In the previous chapter a periodic signal was written as a finite Fourier series as shown in eqn. (2.21). Factorisation of this Fourier series determines the zeros. This leads to a multiplicative signal model where zeros can be viewed as informational attributes. Choosing an elementary signal in the form:

$$m_r(t) = 1 + a_r e^{j\Omega t} \tag{3.1}$$

a general positive real, bandlimited periodic signal can be written as:

$$s(t) = \prod_{r=1}^{N} m_r(t)\, m_r^*(t)$$

$$= \prod_{r=1}^{N} (1 + a_r e^{j\Omega t})(1 + a_r^* e^{-j\Omega t}) \tag{3.2}$$

By solving for the zeros of $m_r(t)$ and $m_r^*(t)$, the above can be rewritten in the form:

$$s(t) = \prod_{r=1}^{N} (1 - e^{j\Omega(t-x_r)})(1 - e^{-j\Omega(t-x_r^*)}) \tag{3.3}$$

where $x_r = t_r + j\sigma_r$, the rth zero of $m(t)$, and $x_r^* = t_r - j\sigma_r$, the rth zero of $m_r^*(t)$, are the generally complex values of t such that $s(t) = 0$.

If the bandwidth of the elementary signal $m(t)$ is $W_r = \frac{\Omega}{2\pi} = \frac{1}{T}$ (Hz) where T is the period of $m_r(t)$, then the bandwidth of $s(t)$ is $W = \pm NW_r$ (Hz). Also the time-bandwidth product of $s(t)$ is $2NW_r\, T = 2\, N\, \frac{1}{T}\, T = 2N$, which is the zero count of $s(t)$. As $s(t)$ is a real signal by assumption, then all the zeros of $s(t)$ must be

either real or complex conjugate pairs.

It was discussed in Section 2.6 that for a zero count (2N) there can be up to 2^{2N} different members in the common envelope set. This upper bound is achieved if all the zeros are complex and of first order. For even number of zero count (2N) the exact number of members is 3^N. For example consider a real signal with two reciprocal zeros (2N = 2) in the z-plane, then there are exactly $3^{2/2} = 3$ different members whose zero configurations are shown in Figure 3.1.

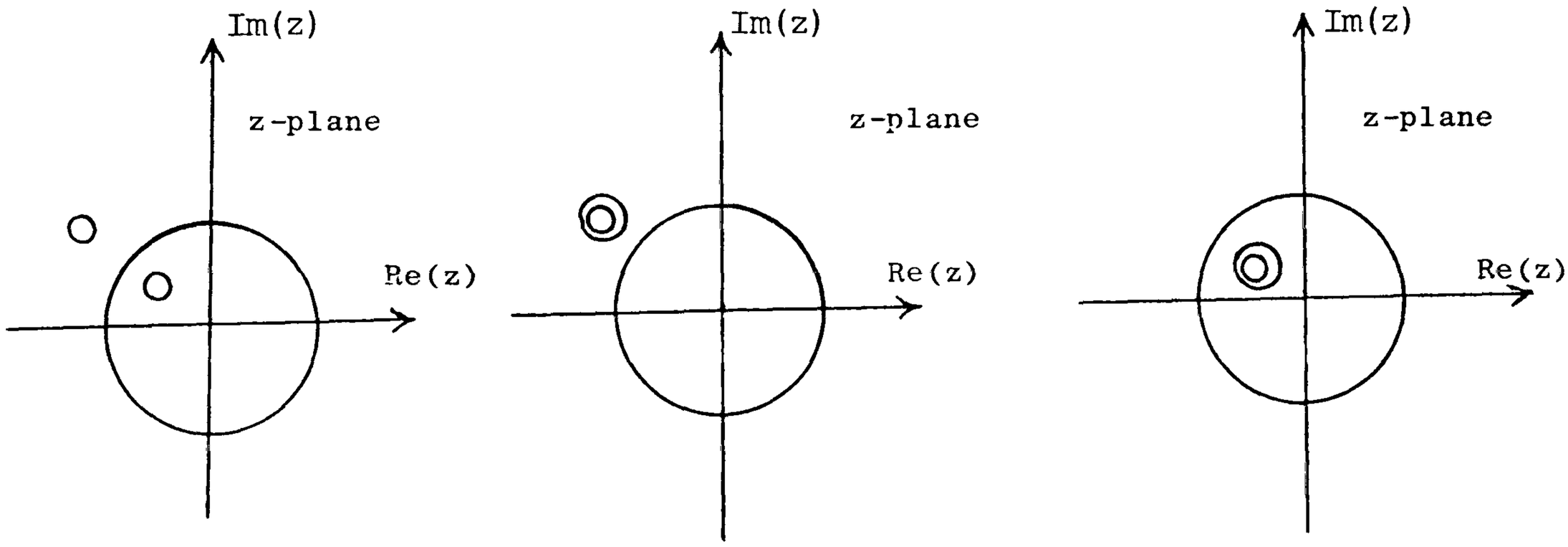

Zero patterns of three different members of a common envelope set

Fig. 3.1

Example

As an example of periodic signal zeros, consider two tones at different frequencies plus a constant. The constant is chosen so that there is no real zero crossings, i.e. all the zeros are complex.

A computer programme was written to generate this real signal and to find its zeros in both x-plane and z-plane. The total time period was taken as T = 10240 μ sec, where T = $\frac{2\pi}{\Omega}$ and the conformal transformation from the x-plane to the z-plane is via $z = e^{j\Omega x}$ as explained previously.

It was assumed that in this period (T) there are 5 cycles of f_1(i.e. $f_1 = \frac{5}{T}$) and 6 cycles of f_2(i.e. $f_2 = \frac{6}{T}$). The real signal was taken as:

$$s(t) = 4 + 2\cos(2\pi f_1 t) + 1.5\cos(2\pi f_2 t)$$

$$= 4 + 2\cos(2\pi\frac{5}{T}t) + 1.5\cos(2\pi\frac{6}{T}t)$$

$$= 4 + 2\cos(5\Omega t) + 1.5\cos(6\Omega t)$$

where $\Omega = \frac{2\pi}{T}$ (3.4)

The above signal should have a zero count of $2 \times 6 \times \frac{2\pi}{T} \times \frac{1}{2\pi} \times T = 12$ zeros per period (i.e. 12 zeros per period in the x-plane).

As the signal given in eqn. (3.4) is real and positive, all the zeros must be complex conjugate zero pairs. Expressing s(t) as a sum of exponentials:

$$s(t) = 4 + e^{j5\Omega t} + e^{-j5\Omega t} + 0.75\, e^{j6\Omega t} + 0.75\, e^{-j6\Omega t} \quad (3.5)$$

Putting $x = t + j\sigma$ and using $z = e^{j\Omega x}$ gives:

$$s(z) = 4 + z^5 + z^{-5} + 0.75\, z^6 + 0.75\, z^{-6} \quad (3.6)$$

Clearly s(z) is an algebraic polynomial in z of degree 12 and hence should have exactly 12 zeros (roots).

Eqn. (3.6) can be rearranged as follows:

$$s(z) = z^{-6}(4\ z^{6} + z^{11} + z + 0.75\ z^{12} + 0.75)$$

$$= z^{-6}\ (0.75\ z^{12} + z^{11} + 4\ z^{5} + z + 0.75) \quad (3.7)$$

To find the roots of s(z), it is required to solve for:

$$0.75\ z^{12} + z^{11} + 4\ z^{6} + z + 0.75 = 0$$

The computer programme makes use of the NAG Library subroutine CO2 AEF (14) to solve for the roots of the above polynomial, and then the corresponding x-plane zeros are computed by solving for z in $z = e^{j\Omega x}$. Figure 3.2 (a,b,c) shows the computer results where the first two show the real signal s(t) and the x-plane zeros (6 complex conjugate pairs), and it should be noted that the x-plane zeros lie at the dips (troughs) of s(t). The third figure shows the z-plane zeros which are reciprocal pairs around the unit circle. There are 12 zeros exactly as expected.

3.3 Envelope and Phase of the Elementary Signal

Consider the elementary signal as defined in eqn. (3.1):

$$m(t) = 1 + a\ e^{j\Omega t}$$

$$= |m(t)|\ e^{j\theta_m(t)}$$

where

$$|m(t)| = \sqrt{(1 + a\ \cos\Omega t)^2 + (a\ \sin\Omega t)^2}$$

$$\theta_m(t) = \arctan\left(\frac{a\ \sin\Omega t}{1 + a\ \cos\Omega t}\right) \quad (3.8)$$

Clearly both the envelope and phase of m(t) are periodic functions with period $T = \frac{2\pi}{\Omega}$. The phasor diagram of m(t) is shown in Figure 3.3.

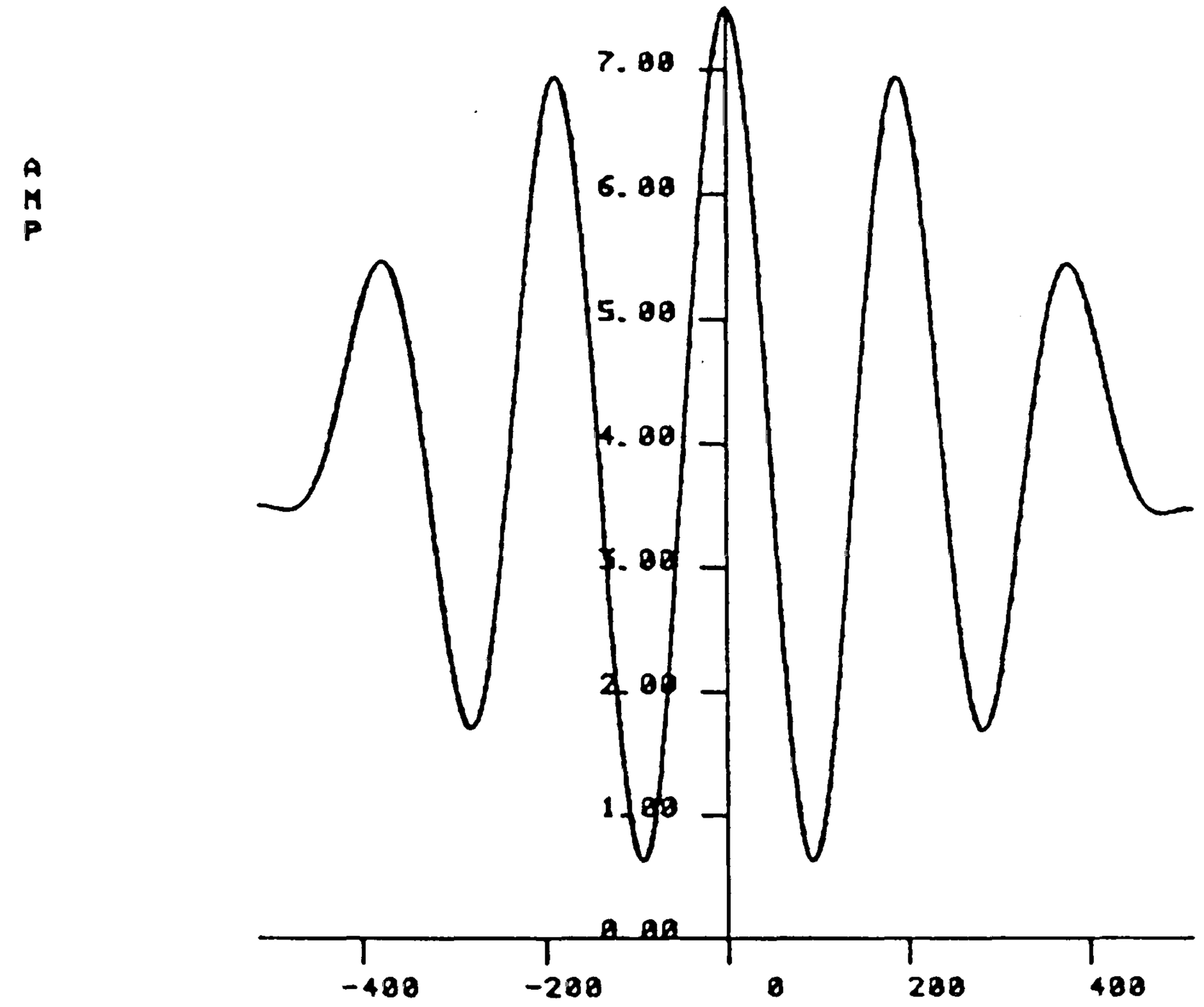

Fig. 3.2(a) The real signal s(t)

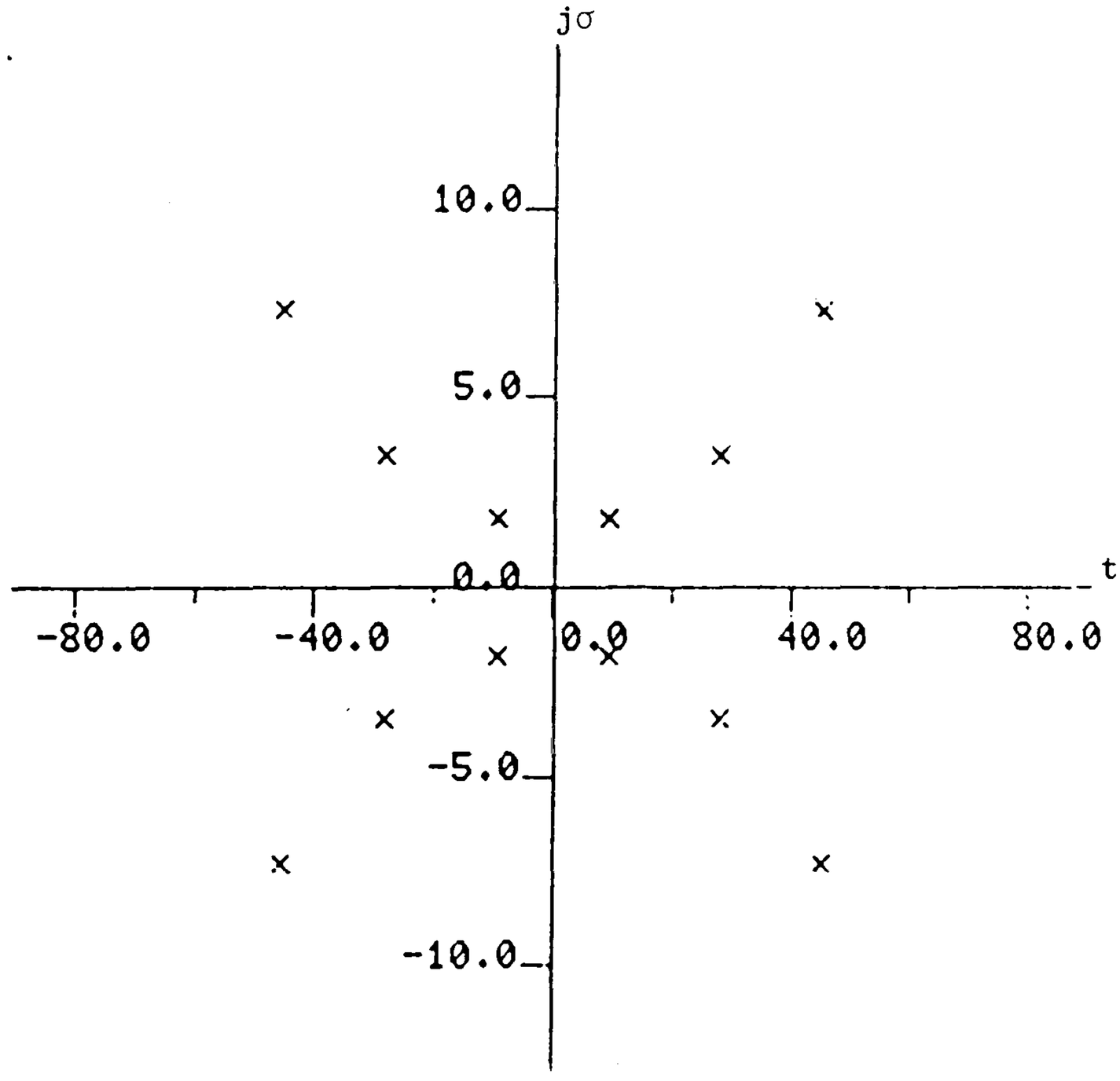

Fig. 3.2(b) x-plane zeros of s(t)

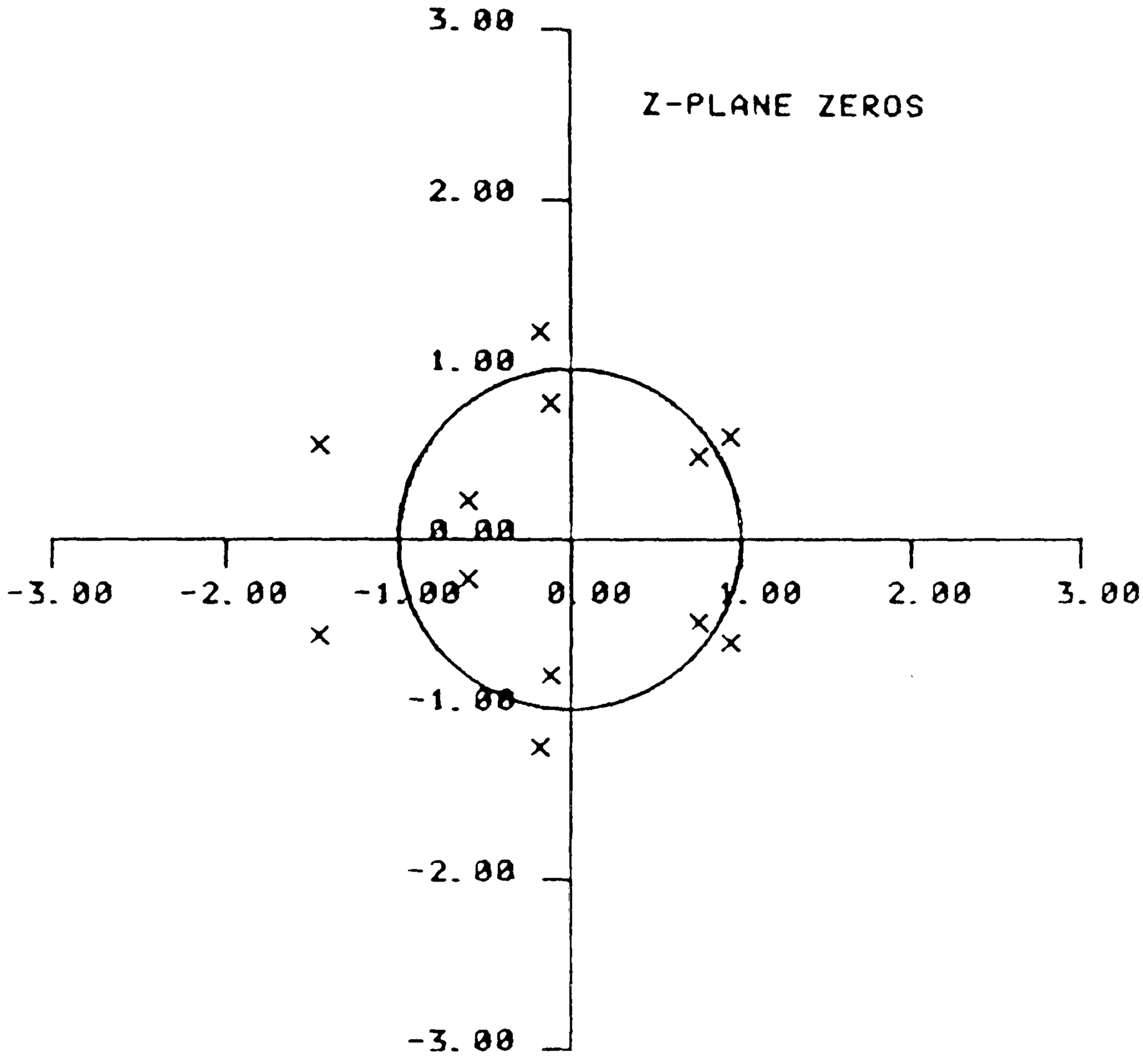

Fig. 3.2(c) z-plane zeros of s(t)

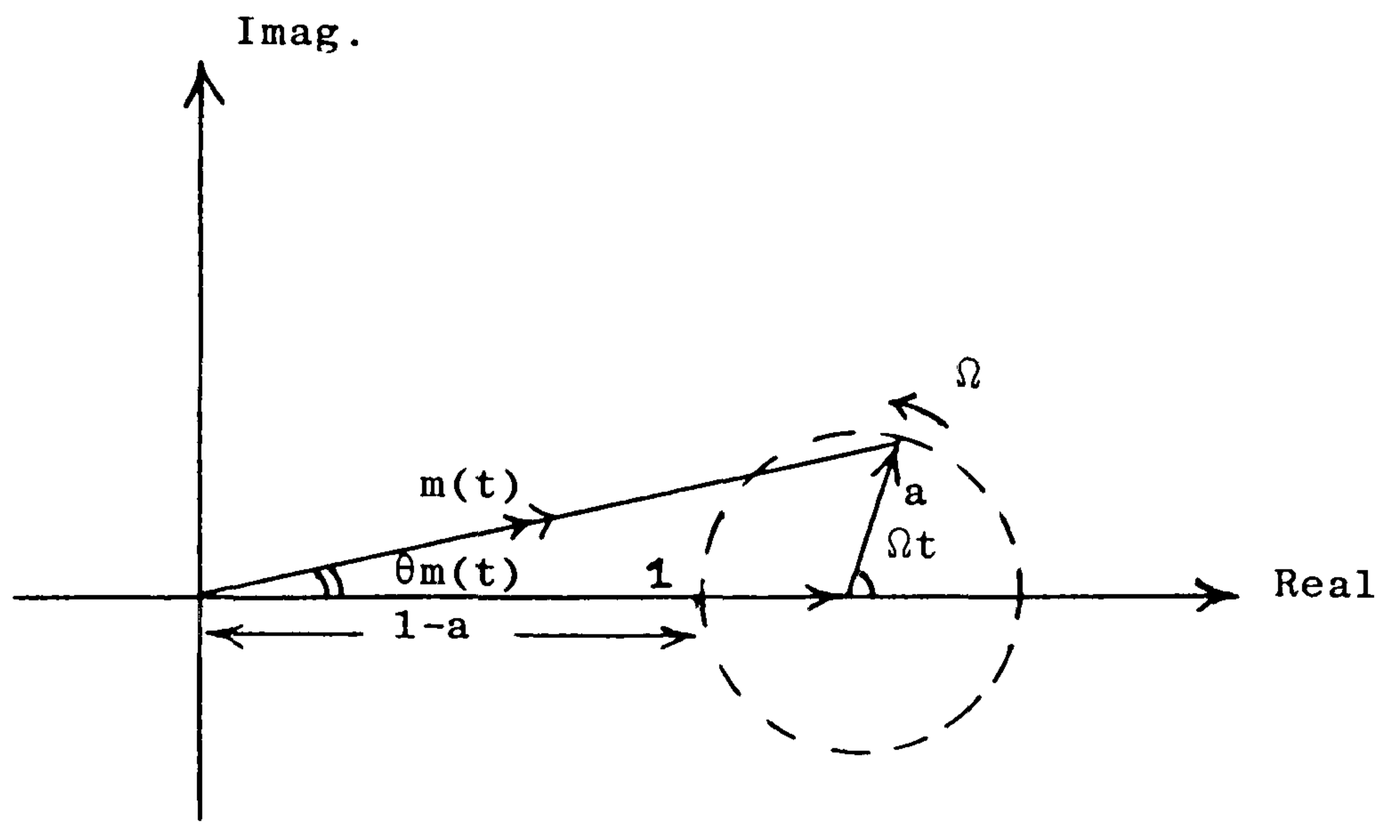

Phasor diagram of $m(t) = 1 + a\, e^{j\Omega t}$

Fig. 3.3

The following points emerge:

i) at $t = 0$

$$|m(t)| = \sqrt{1 + a^2 + 2a} = (1 + a) = \max$$

$$\theta_m(t) = 0$$

ii) at $\Omega t = \pi$ radians:

$$|m(t)| = \sqrt{1 + a^2 - 2a\cos\Omega t} = (1 - a) = \min$$

$$\theta_m(t) = 0$$

iii) It can be judged that the complex zeros of $m(t)$ occur at $\Omega t = \pi, 3\pi, 5\pi, \ldots$ i.e. at the envelope minima (dips).

iv) The instantaneous frequency $\theta_m'(t) = \frac{d}{dt}\theta_m(t)$ is maximum at the zero positions, i.e. at

$\Omega t = \pi, 3\pi, 5\pi, \ldots$

$$\theta_m'(t) = \frac{d\theta_m(t)}{dt} = \frac{1}{1 + \left(\frac{a\sin\Omega t}{1 + a\cos\Omega t}\right)^2} \times$$

$$\frac{a\Omega\cos\Omega t(1 + a\cos\Omega t) + a^2\Omega\sin^2\Omega t}{(1 + a\cos\Omega t)^2}$$

$$= \frac{1}{1 + \left(\frac{a \sin\Omega t}{1 + a \cos\Omega t}\right)^2} \quad \frac{\Omega(a^2 + a \cos\Omega t)}{(1 + a \cos\Omega t)^2}$$

$$= \frac{\Omega(a^2 + a \cos\Omega t)}{1 + a^2 + 2a \cos\Omega t} \quad \text{(rad/sec)} \tag{3.9}$$

At a = 1, the instantaneous frequency $\theta_m'(t)$ is constant and is equal to:

$$\theta_m'(t) = \frac{\Omega}{2} \quad \text{(rad/sec)}$$

v) At very small a, $\theta_m(t) \cong a \sin\Omega t$

Figure 3.4 shows five cycles of $|m(t)|$, $\theta_m(t)$, and $\theta_m'(t)$. It is apparent that the instantaneous frequency of m(t) is maximum at the positions of complex zeros of m(t).

3.4 Zero Conjugation of Periodic Signals

Consider the periodic signal model defined in eqn. (3.2). For simplicity only one pair will be considered. Let

$$s(t) = m(t) \quad m^*(t)$$

$$= (1 + a \quad ^{j\Omega t})(1 + a\, e^{-j\Omega t}),\ 0 < a < 1$$

$$= 1 + a^2 + 2a \cos\Omega t \tag{3.10}$$

Clearly the zero pattern of s(t) can be obtained by superimposing the zero patterns of m(t) and m*(t). From previous results given in section 2.6 the zero pattern of s(t) is depicted in Figure 3.5.

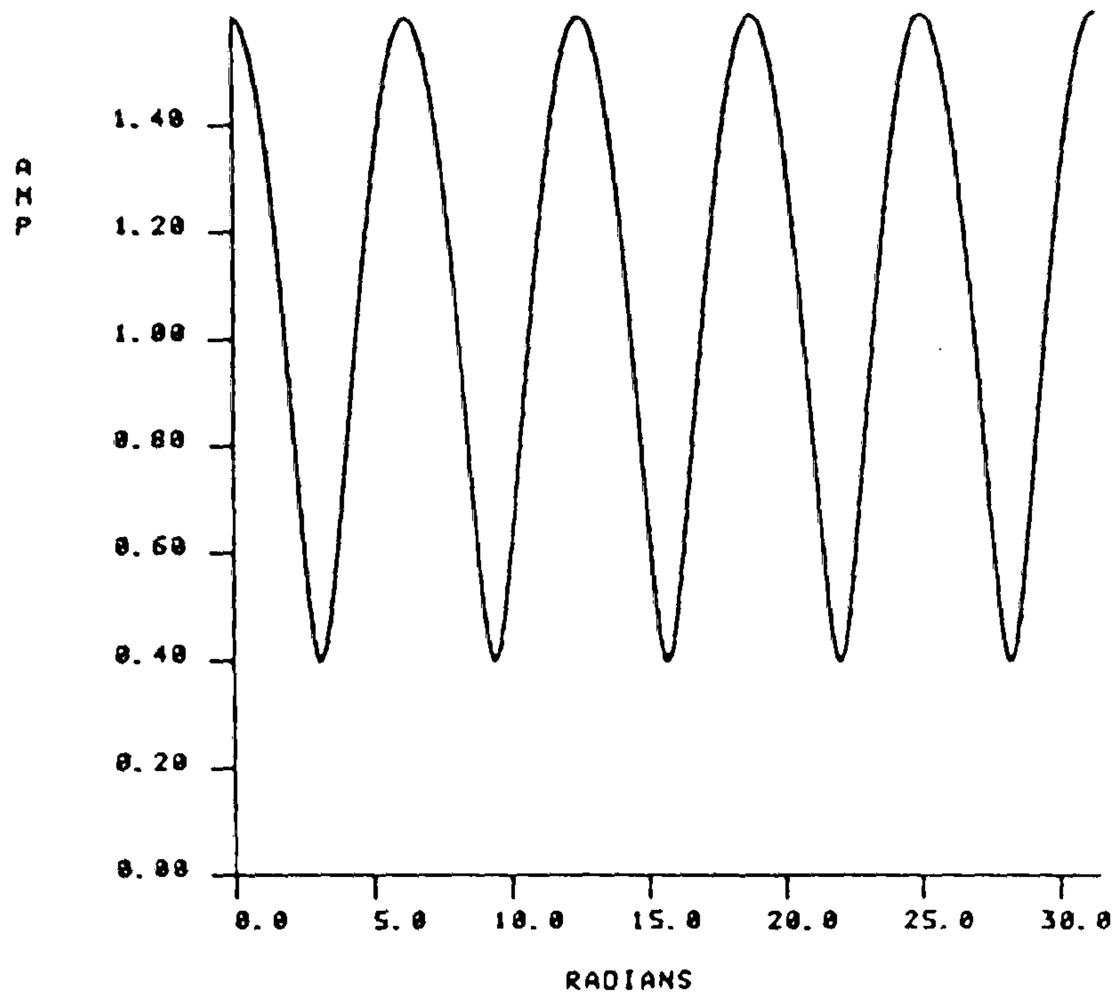

$|m(t)|$

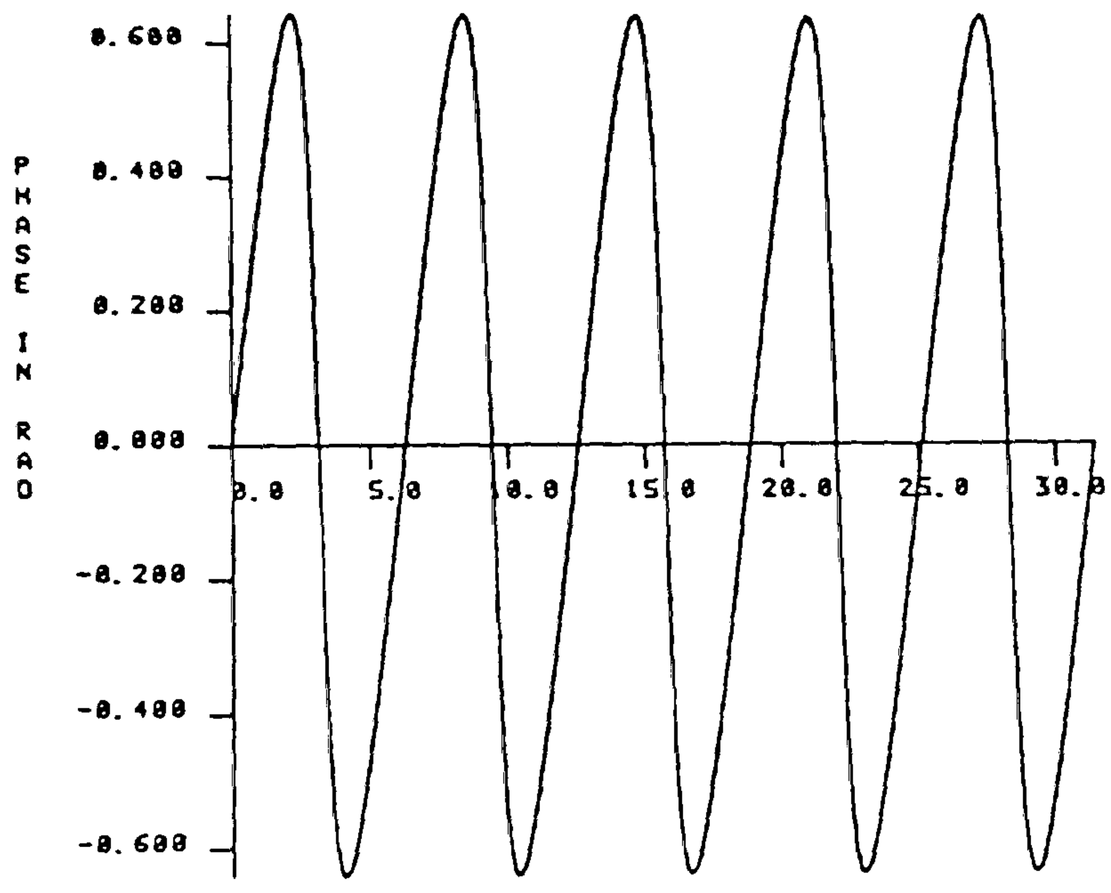

$\theta_m(t)$

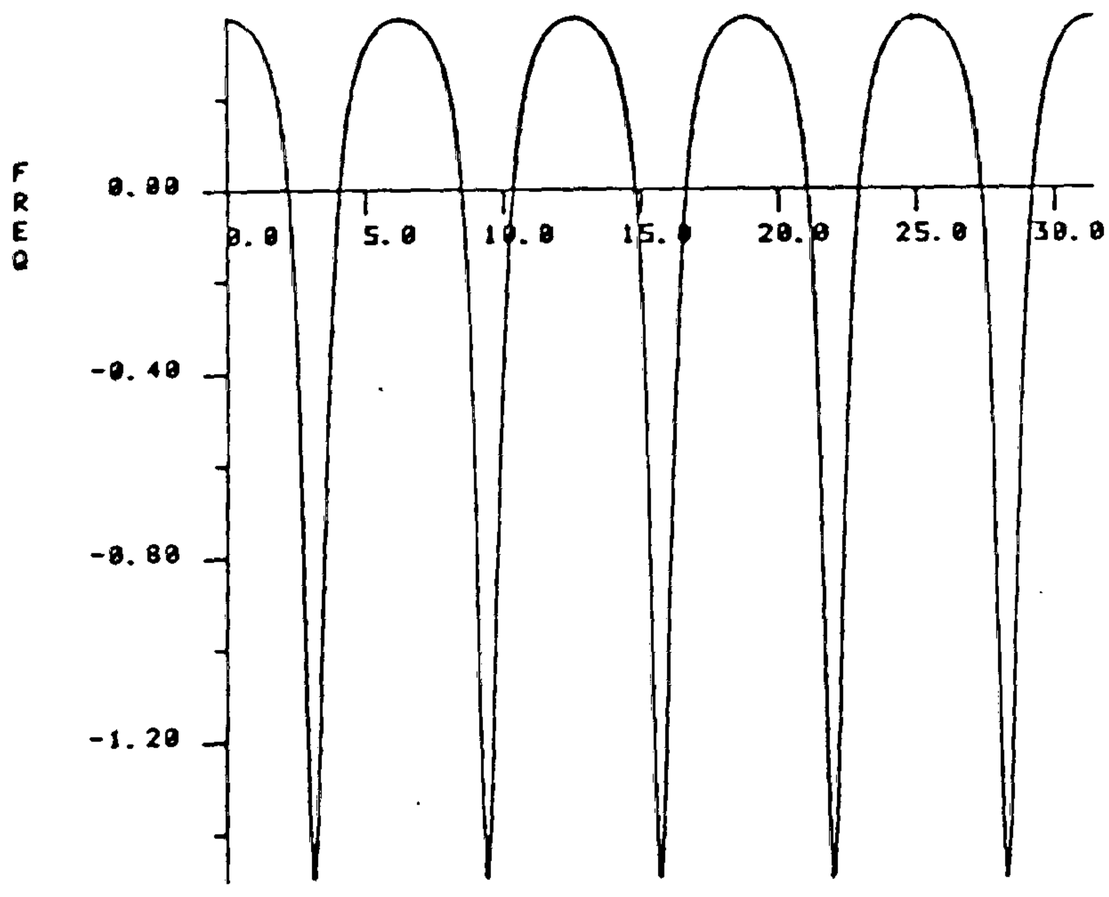

$\theta'_m(t)$

Fig. 3.4

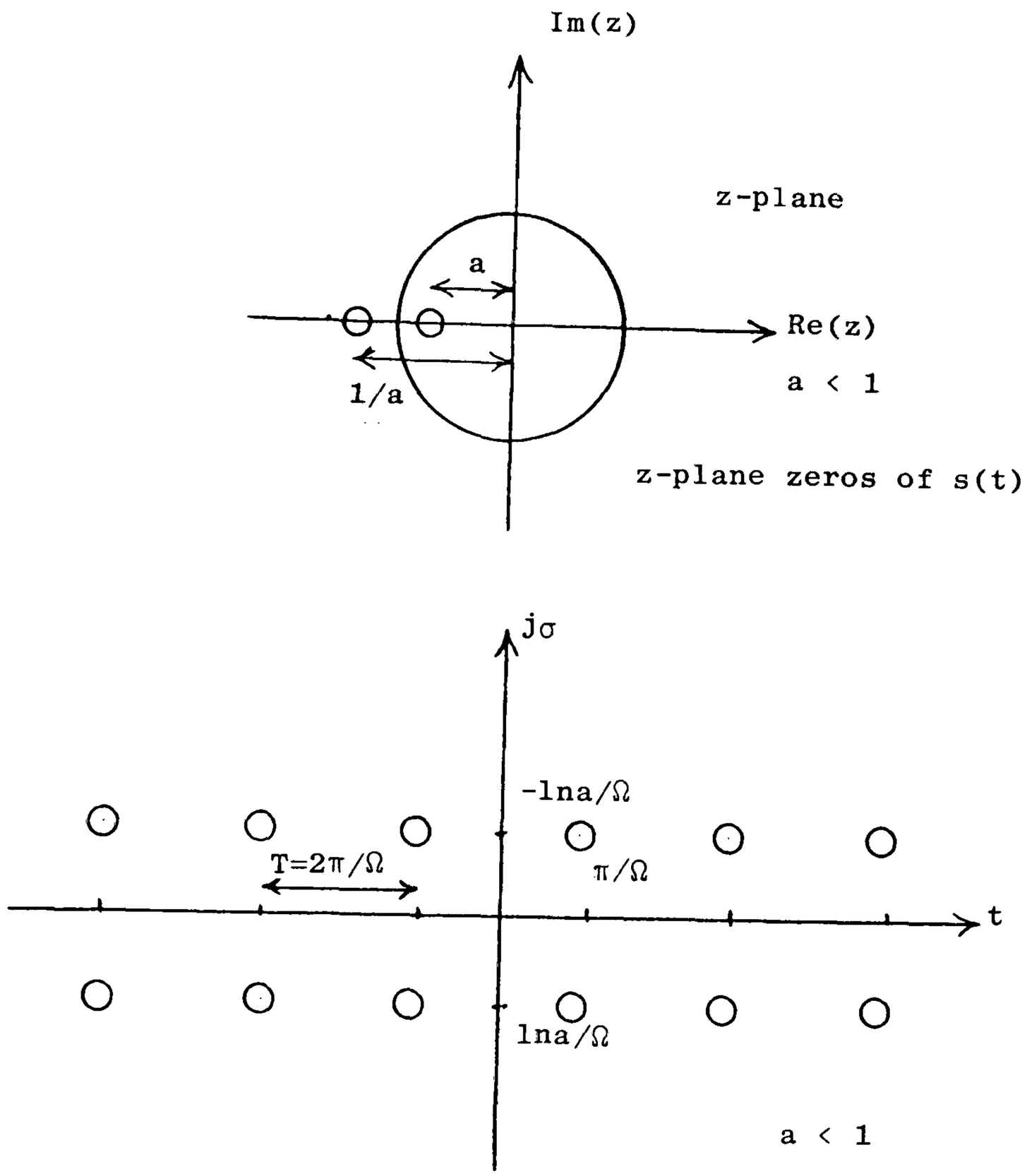

Fig. 3.5

The zero count of s(t) is 2N = 2 zeros per period and hence (see Section 3.2) there are exactly $3^{2N/2} = 3$ different members in this common envelope set. One of these members is s(t) as shown above and the two other members will be generated through a process of zero conjugation.

Let S(f) be the spectrum of s(t) then:

$$S(f) = F[1 + a^2 + 2a\cos\Omega t]$$

$$= (1 + a^2)\delta(f) + a\,\delta(f - \frac{\Omega}{2\pi}) + a\,\delta(f + \frac{\Omega}{2\pi}) \qquad (3.11)$$

where F[ ] denotes Fourier transform.

Figure 3.7(a) shows this spectrum.

To produce the second member it is necessary to conjugate all the UHP (x-plane) zeros to the LHP (x-plane) zeros of s(t).

In order to effect zero conjugation, a cancellation operator c(t), as discussed in section 2.6, must be used in the form:

$$c(t) = \frac{m(t)}{m^*(t)} = \frac{1 + a\, e^{j\Omega t}}{1 + a\, e^{-j\Omega t}}, \quad 0 < a < 1$$

$$= e^{j2\theta_m(t)} \tag{3.12}$$

where $\theta_m(t) = \arctan\left(\frac{a \sin\Omega t}{1 + a \cos\Omega t}\right)$ as given in eqn. (3.8).

Let the conjugated signal be n(t)

$$\therefore \quad n(t) = s(t)\ \ c(t) \tag{3.13}$$

$$n(t) = m(t)\ m^*(t)\ \frac{m(t)}{m^*(t)}$$

$$= m^2(t)$$

$$= (1 + a\, e^{j\Omega t})^2$$

$$= 1 + 2a\, e^{j\Omega t} + a^2\, e^{j2\Omega t} \tag{3.14}$$

and taking Fourier transform gives:

$$N(f) = \delta(f) + 2a\, \delta\left(f - \frac{\Omega}{2\pi}\right) + a^2\, \delta\left(f - \frac{2\Omega}{2\pi}\right) \tag{3.15}$$

Figure 3.7(b) shows this spectrum.

The zero pattern of n(t) is the same as that of m(t) but all the zeros are of second order type, as shown in Figure 3.6(a).

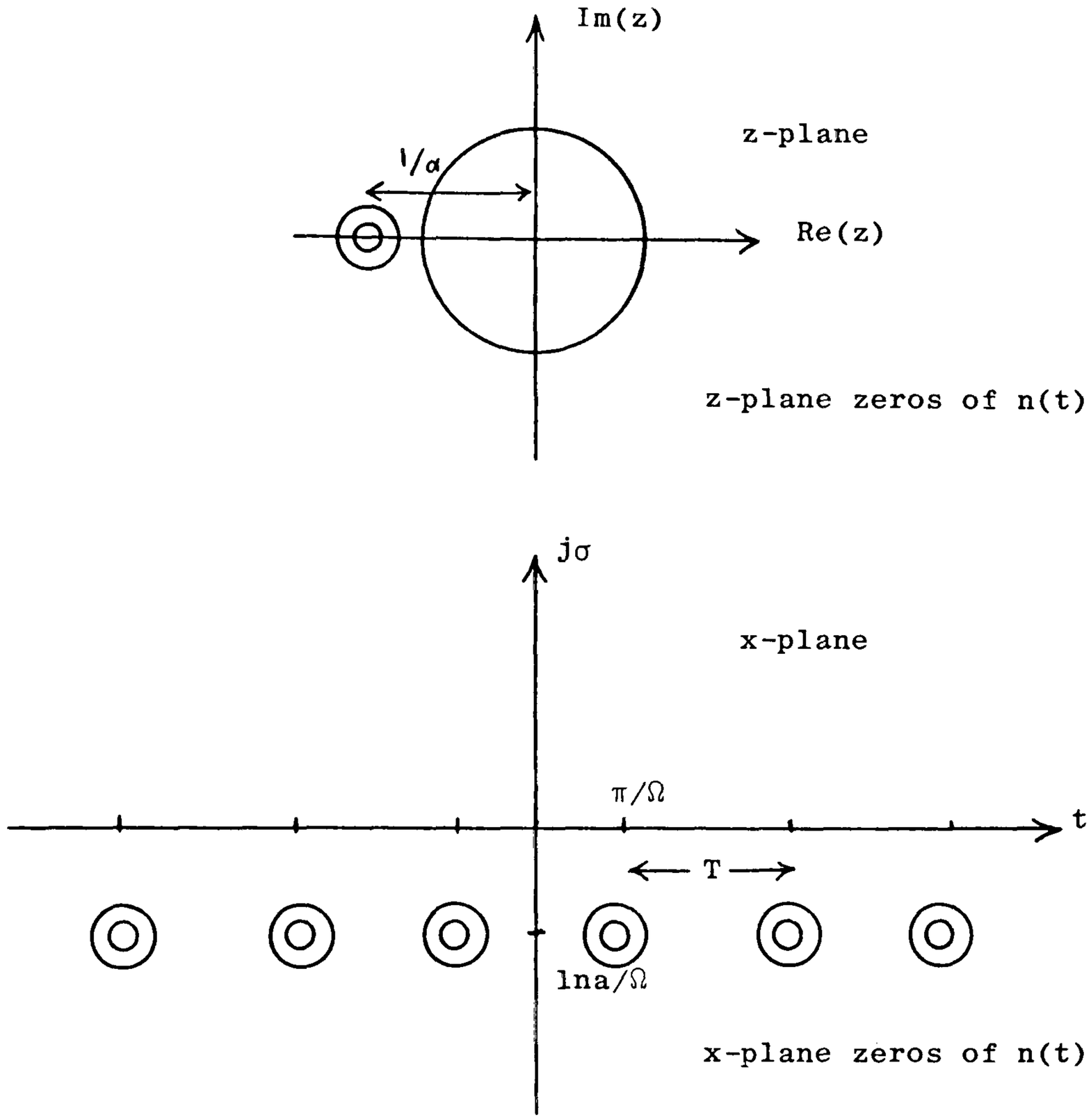

Fig. 3.6(a)

It is apparent that:

i) n(t) has the same envelope as s(t) because they are two members of a common envelope set. This can be proved by using eqn. (3.14):

$$n(t) = m(t) \quad m^*t \; \frac{m(t)}{m^*(t)}$$

$$\therefore \; |n(t)| = |m(t) \quad m^*(t)|$$

$$= |(1 + a\, e^{j\Omega t})(1 + a\, e^{-j\Omega t})|$$

$$= |1 + a^2 + 2a \cos\Omega t|$$

$$= s(t) \qquad (3.16)$$

ii) n(t) is a complex signal and is Analytic as it has no singularities in the open UHP (x-plane).

iii) As all the zeros of n(t) lie in the LHP (x-plane) then n(t) is a minimum-phase signal (Section 2.4).

iv) The zero count of n(t) is 2N = 2 which is the same as that of s(t) and hence this type of zero conjugation is bandwidth - preserving as the zero count is not changed. n(t) has the same bandwidth as that of s(t) and this is a characteristic of the common envelope set.

v) The cancellation operator c(t) which is used to effect zero conjugation conjugates all the zeros of the UHP (x-plane) from $t = -\infty$ to $t = +\infty$ and produces the zero pattern of n(t). Consequently the conjugated signal n(t) has also a periodic zero pattern.

vi) Using eqn. (3.12) and eqn. (3.13) it is evident that n(t) can be obtained by multiplying s(t) by the cancellation operator c(t) or equivalently by phase modulating s(t) with $(2\ \theta_m(t))$.

vii) The spectrum of n(t) is shifted from that of s(t) by $\frac{\Omega}{2\pi}$ Hz as shown in Figure 3.7.

To generate the third member of the common envelope set it is necessary to conjugate zeros in the reverse sense, i.e. to conjugate all the LHP (x-plane) zeros into their UHP complex conjugates. The cancellation operator required for this type of zero conjugation is:

$$c(t) = \frac{m^*(t)}{m(t)} = \frac{1 + a\, e^{-j\Omega t}}{1 + a\, e^{j\Omega t}} \quad , \; 0 < a < 1$$

$$= e^{-j2\theta_m(t)}$$

where $\theta_m(t) = \arctan\left(\frac{a \sin\Omega t}{1 + a \cos\Omega t}\right)$

The conjugated signal will be:

$$g(t) = s(t) \quad c(t)$$

$$= m(t) \quad m^*(t) \quad \frac{m^*(t)}{m(t)} = (m^*(t))^2 \qquad (3.17)$$

$$\therefore \quad g(t) = (1 + a\, e^{-j\Omega t})^2$$

$$= 1 + 2a\, e^{-j\Omega t} + a^2\, e^{-j2\Omega t} \qquad (3.18)$$

The spectrum of g(t), G(f), is given by:

$$G(f) = \delta(f) + 2a\, \delta\left(f + \frac{\Omega}{2\pi}\right) + a^2\, \delta\left(f + \frac{2\Omega}{2\pi}\right) \qquad (3.19)$$

Figure 3.7(c) shows this spectrum. The zero pattern of g(t) is the same as that of m*(t) but all the zeros are of second order type as shown in Figure 3.6 (b)

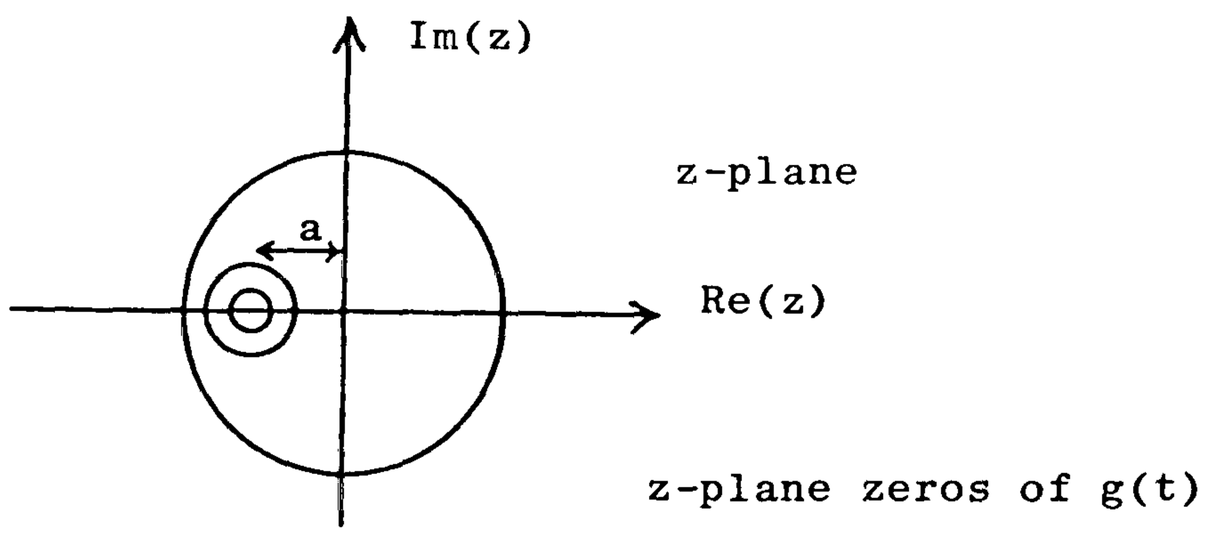

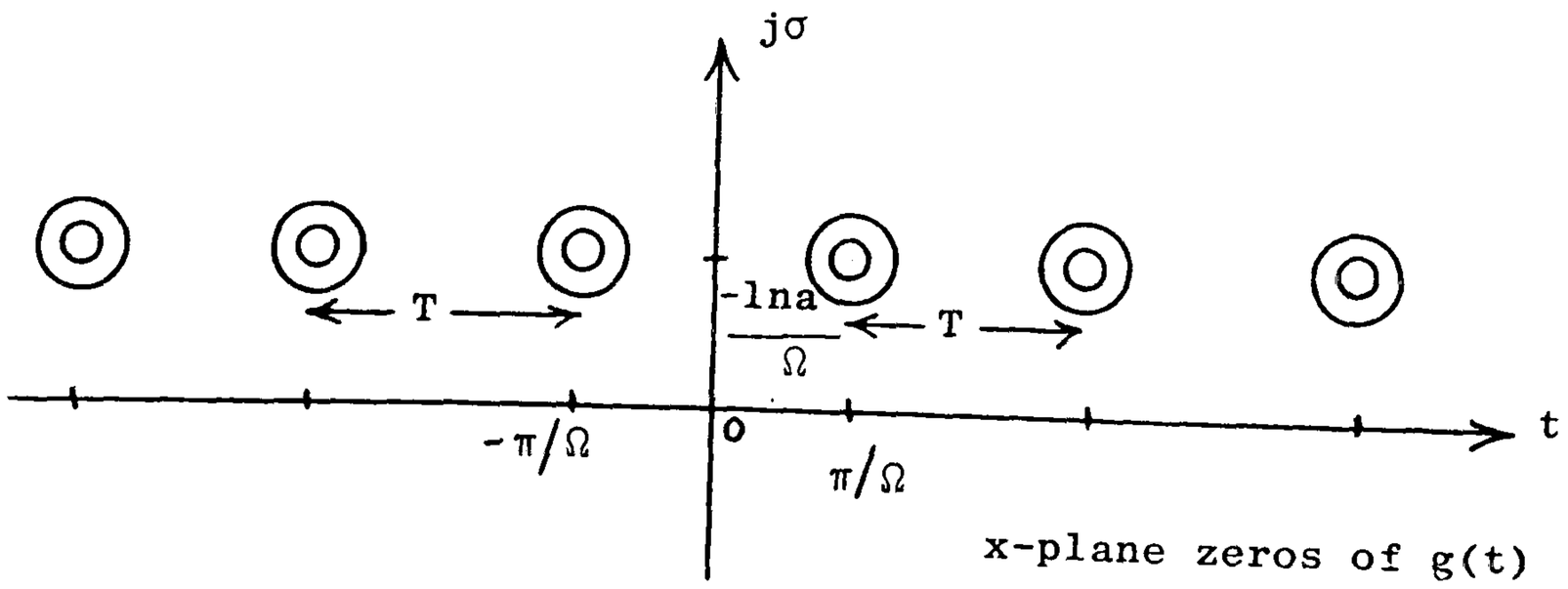

Fig. 3.6 (b)

In this case:

i) g(t) has the same envelope as s(t) and n(t) as they are members of the same common envelope set. This can be shown as follows:

$$g(t) = m(t)\ m^*(t)\ \frac{m^*(t)}{m(t)}$$

$$\therefore |g(t)| = |m(t)\ m^*(t)|$$

$$= |(1 + a\ e^{j\Omega t})(1 + a\ e^{-j\Omega t})|$$

$$= |1 + a^2 + 2\ a\ \cos\Omega t|$$

$$= s(t) = |n(t)| \qquad (3.20)$$

ii) g(t) is a complex signal and it is Image-Analytic signal as it has no singularities in the open LHP (x-plane).

iii) As all the zeros of g(t) lie in the UHP (x-plane) then g(t) is called an Image-Analytic maximum-phase signal.

iv) The zero count of g(t) is 2N = 2 which is equal to the previous two members s(t) and n(t) and consequently g(t) has the same bandwidth.

v) g(t) is a periodic signal as the cancellation operator c(t) conjugates all the zeros of the LHP (x-plane), from $t = -\infty$ to $t = +\infty$ to their conjugates.

vi) Using eqn. (3.16) and eqn. (3.17) it is possible to deduce that g(t) can be obtained by multiplying s(t) by c(t), or equivalently by phase modulating s(t) with $(-2\ \theta_m(t))$.

vii) The spectrum of g(t) is shifted from that of s(t) by $\frac{\Omega}{2\pi}$ Hz and g(t) has zero content in the positive frequencies which is a characteristic of the Image-Analytic signal. Figure 3.7(c) shows this spectrum. The results obtained in this section have theoretical interest in that they provide a satisfactory answer to the general implementation of zero conjugations and manipulations. It has been found that there is a frequency shift between the three members discussed. Provided the number of zero conjugated in one sense equals the number conjugated in the other sense, then for practical purposes the frequency range occupied by the different signals remains unchanged. The effect of unequal zero conjugation senses can be considered by generalising eqn. (3.2):

$$s(t) = (1 + a_{-N}\, e^{-jN\Omega t}) \ldots (1 + a_{-1}\, e^{-j\Omega t}) \times (1 + a_1\, e^{j\Omega t}) \ldots (1 + a_N\, e^{jN\Omega t}) \qquad (3.21)$$

By inspection the spectral limits of s(t) extend from $-N\Omega$ to $+N\Omega$ with the carrier represented by a constant at f = 0. (The double-sideband amplitude-modulated signal is just this spectrum translated by $\frac{\omega_o}{2\pi}$ Hz). Now conjugation in one sense implies replacing a factor $(1 + a_n\, e^{jn\Omega t})$ by $(1 + a_{-n}\, e^{-jn\Omega t})$ above and this changes the spectral limits to $-(N + 1)\Omega$ to $(N - 1)\Omega$. The conjugation in the other sense replaces a factor $(1 + a_{-n}\, e^{-jn\Omega t})$ by $(1 + a_n\, e^{-jn\Omega t})$ which causes a similar shift but in the positive frequency direction. In general a shift will always occur unless the number of conjugations in each sense is equal.

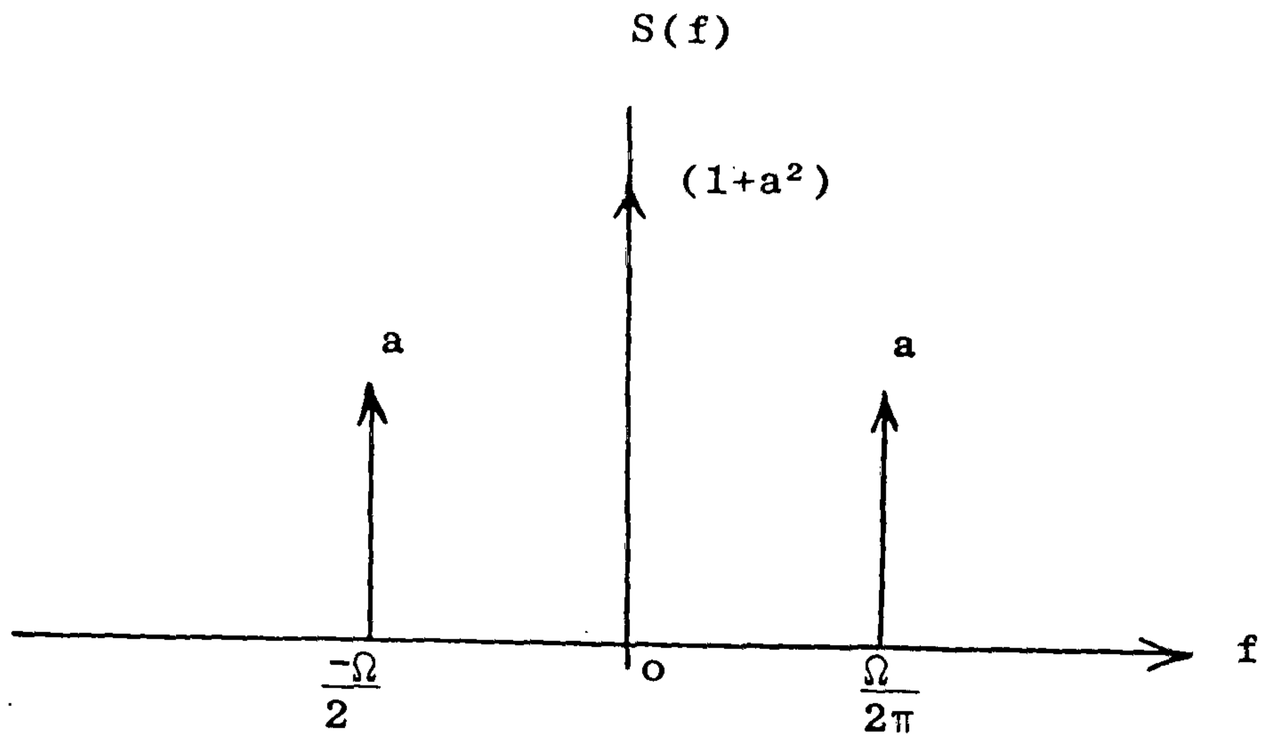

Spectrum of $s(t) = 1+a^2+2a\cos\Omega t$

(a)

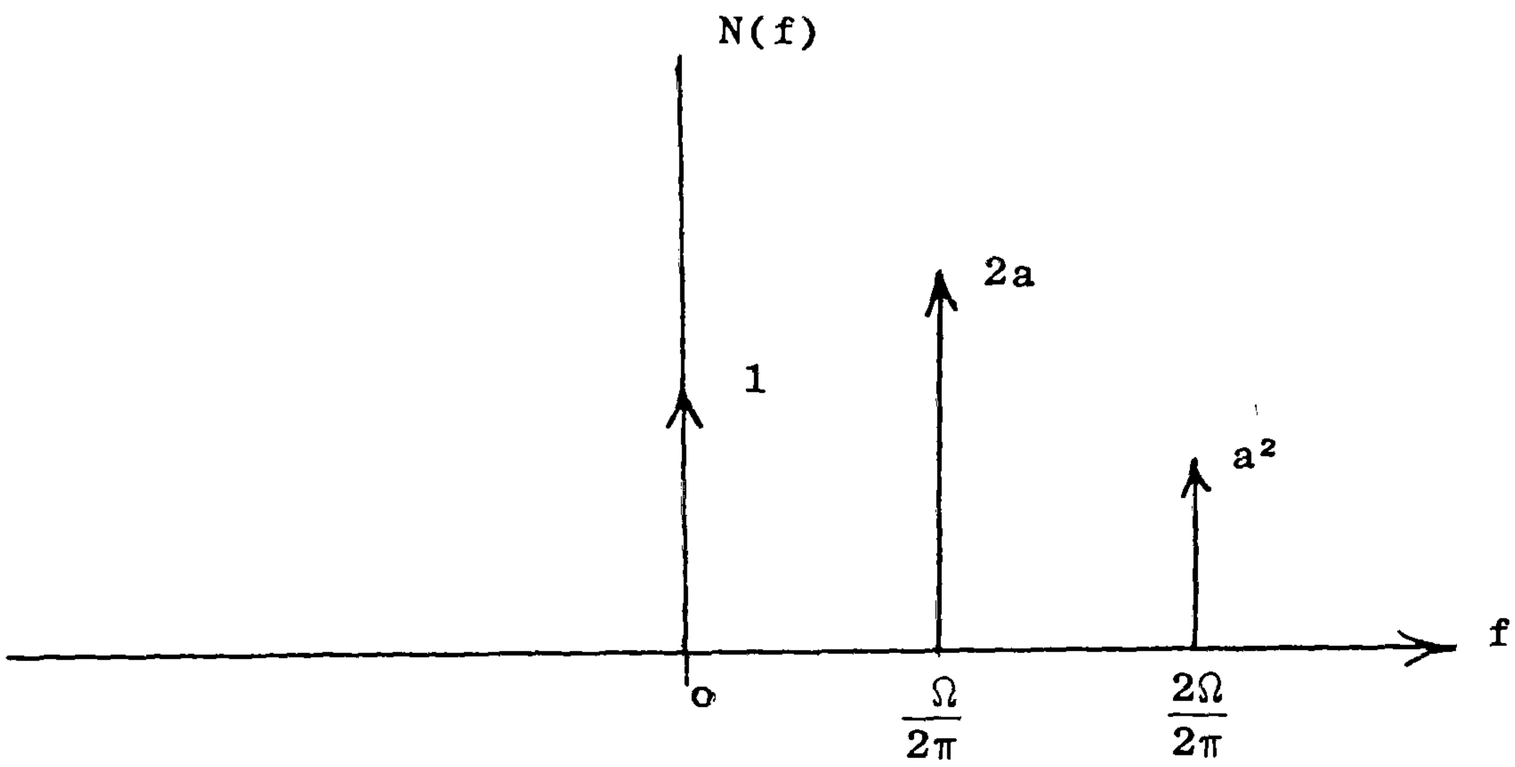

(b)

Spectrum of $n(t) = 1+2ae^{j\Omega t} + a^2e^{j2\Omega t}$

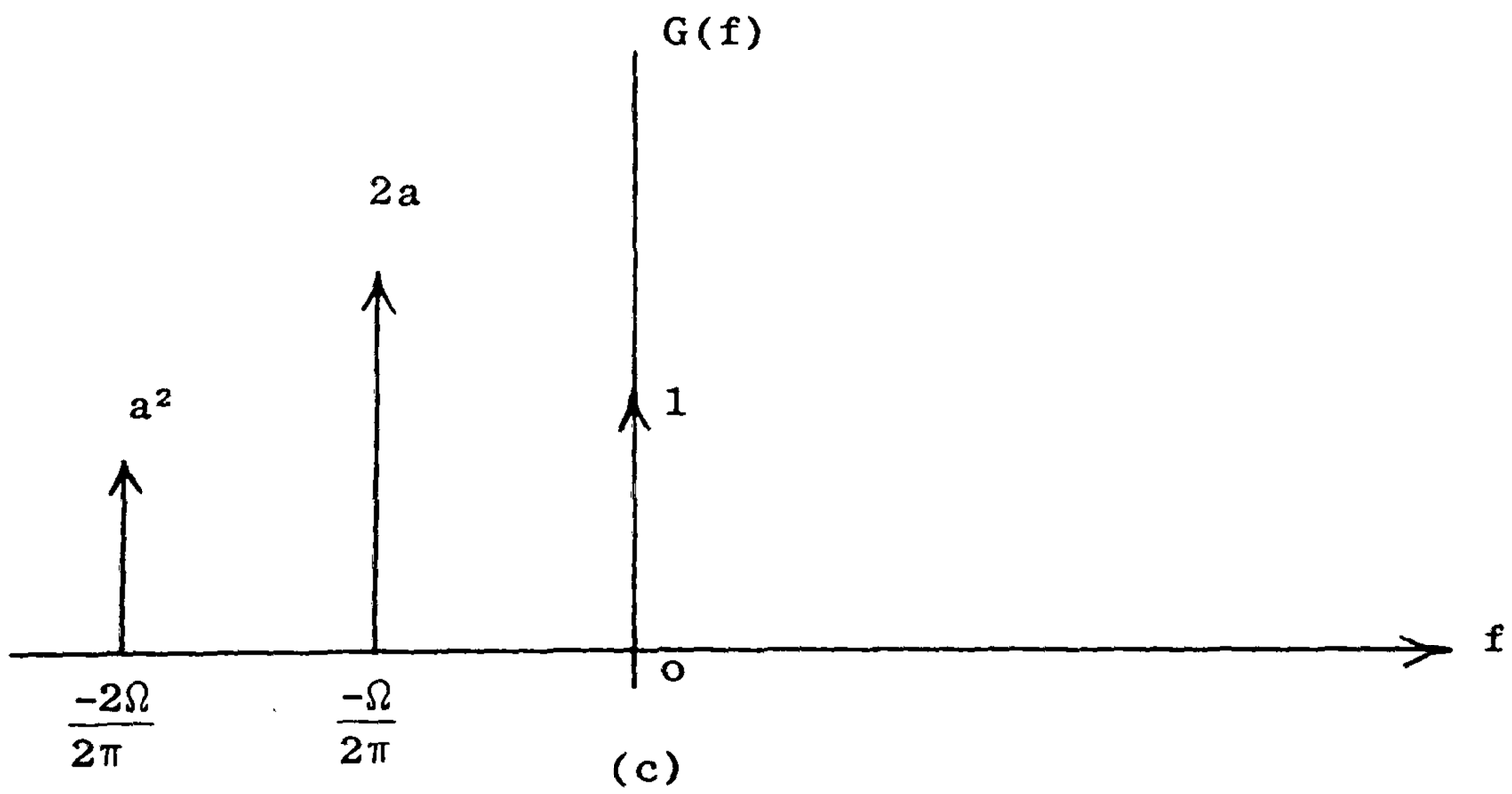

(c)

Spectrum of $g(t) = 1+2ae^{-j\Omega t} + a^2e^{-j2\Omega t}$

Fig. 3.7

3.5 Zeros in x- and z-Planes and Modelling for Aperiodic Zeros

The material discussed in this section is meant to introduce the idea of treating the zeros of a signal individually and irrespective of each other. Consider the periodic real signal s(t) defined as:

$$s(t) = m(t)\ m^*(t)$$

$$= (1 - a\ e^{j\Omega t})(1 - a\ e^{-j\Omega t}) \quad , \quad 0 < a < 1$$

$$= 1 + a^2 - 2\ a \cos\Omega t \qquad (3.22)$$

$$T = \frac{\Omega}{2\pi} = \text{period.}$$

The z-plane zeros are given by $z = a$, $z = \frac{1}{a}$ and the corresponding x-plane zeros are given by $x = \frac{2k\pi}{\Omega} \pm j\frac{\ln a}{\Omega}$

$k = 0, \pm 1, \pm 2, \ldots$ as shown in Figure 3.8.

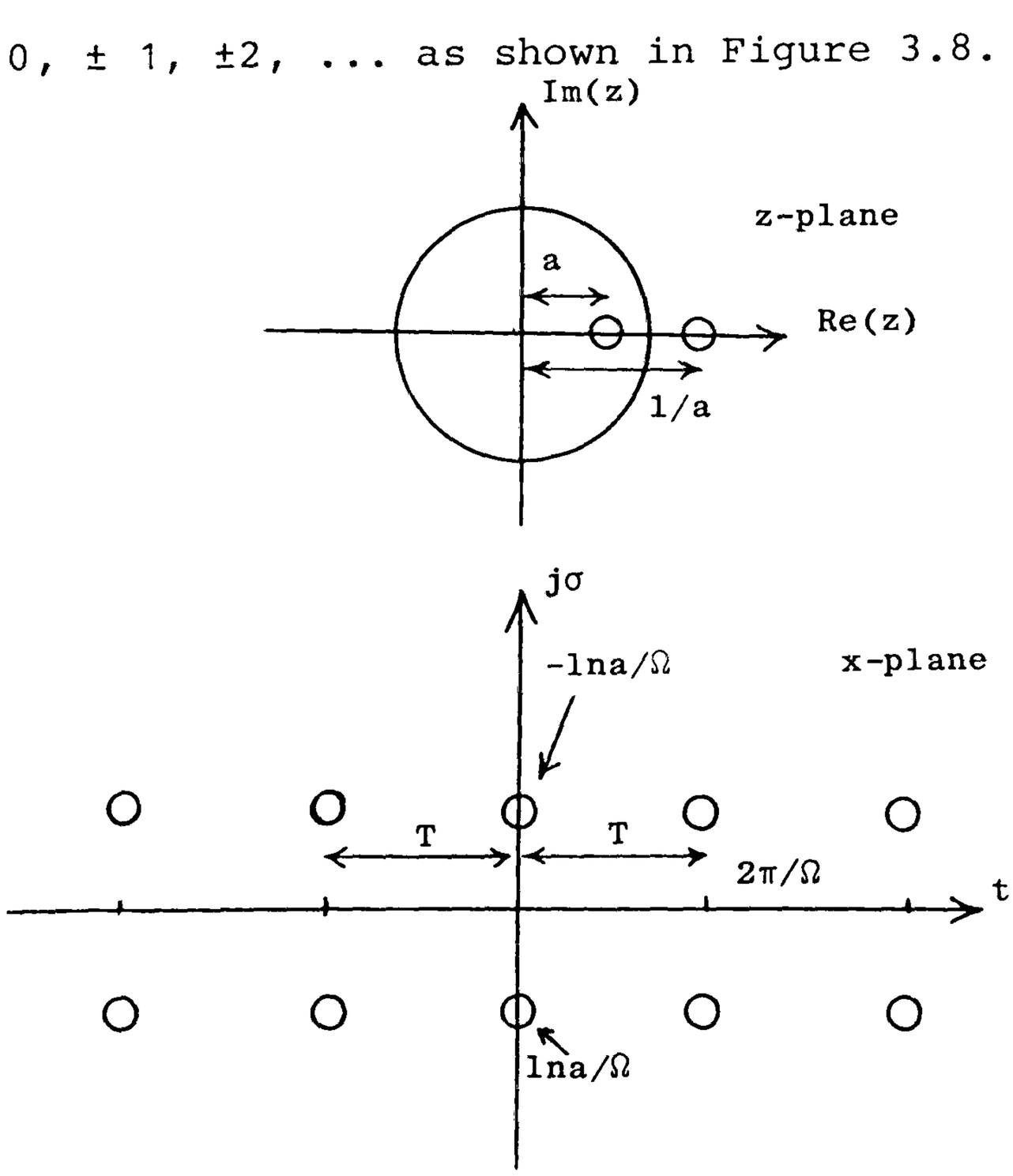

Zeros of $s(t) = 1 + a^2 - 2\ a \cos\Omega t$

Fig. 3.8

Thus the complex zeros of s(t) occur at t = kT, k = 0, ±1, ±2, ... coincided with signal dips.

For the elementary signal, m(t), the phase function $\theta_m(t)$, and the instantaneous frequency $\theta_m'(t)$ are given by:

$$\theta_m(t) = \arctan\left(\frac{-a\sin\Omega t}{1 - a\cos\Omega t}\right)$$

$$= -\arctan\left(\frac{a\sin\Omega t}{1 - a\cos\Omega t}\right)$$

$$\theta_m'(t) = \frac{a\Omega(a - \cos\Omega t)}{1 + a^2 - 2a\cos\Omega t} \qquad (3.23)$$

At the complex x-plane zeros of s(t) which occur at t = kT, k = 0, ±1, ±2 ... the phase and instantaneous frequency of m(t) have the values of:

$$\left.\begin{aligned}\theta_m(t) &= 0\\ \theta_m'(t) &= \frac{a\ \Omega}{(a - 1)}\end{aligned}\right\} \text{ at } t = kT \qquad (3.24)$$

Now consider the <u>same</u> signal m(t), as defined in eqn. (3.22), in the form:

$$m(t) = (1 - a(e^{j\frac{\Omega}{N}t})^N) \qquad (3.25)$$

The above can be interpreted as a signal having N zeros in a period NT, where $T = \frac{\Omega}{2\pi}$.

The "z" expression of eqn. (3.25) becomes:

$$m(z) = (1 - az^N) \qquad (3.26)$$

$$\text{with } z = e^{j\frac{\Omega}{N}x} = e^{-\frac{\Omega}{N}\sigma}\ e^{j\frac{\Omega}{N}t}$$

In this z-plane, we have roots given by the solution of $(1 - az^N) = 0$.

Figure 3.9 shows such a zero distribution for N = 8.

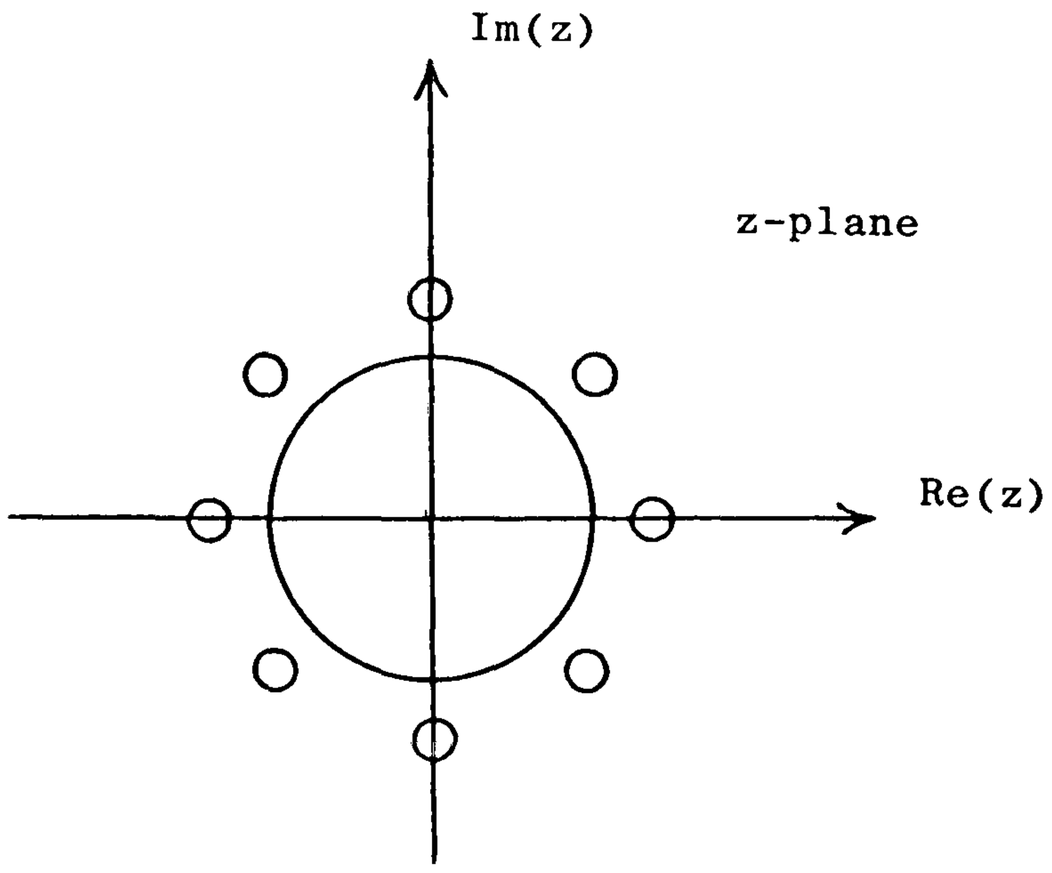

Zeros of $(1 - az^{8}) = 0$

Fig. 3.9

Looking at the zero at t = 0 we have the z-plane root given by:

$$z = (\frac{1}{a})^{1/N}$$

As time (t) progresses the other z-plane zeros will be equally spaced and all zeros have the same radius $(\frac{1}{a})^{1/N}$, i.e. dependent on N.

Let us view N periods of $(1 - a\, e^{j\Omega t})$ as a model of an infinite time signal, and we wish to examine the phase function of a single x-plane zero (say at t = 0 for convenience) for N large as shown in Figure 3.10.

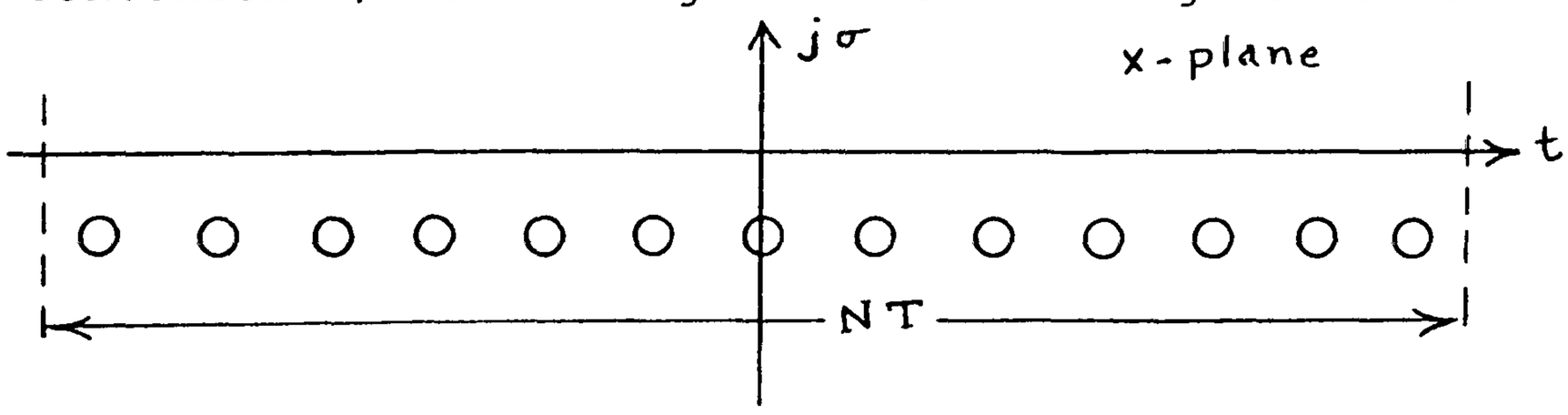

Zeros of $(1 - a\, e^{j\Omega t})$

Fig. 3.10

The z-plane factor related to the zero at t = 0 is:

$$\left[1 - \frac{z}{(\frac{1}{a})^{1/N}}\right] = (1 - a^{1/N} z), \quad z = e^{j\frac{\Omega}{N}x} \tag{3.27}$$

The phase function related to this factor is:

$$\theta_1(t) = \arg\,[1 - a^{1/N}\, e^{j\frac{\Omega}{N}t}]$$

$$= -\arctan\left[\frac{a^{1/N}\sin(\frac{\Omega}{N}t)}{1 - a^{1/N}\cos(\frac{\Omega}{N}t)}\right] \tag{3.28}$$

As N becomes larger $a^{1/N}$ tends to 1 and the phase function $\theta_1(t)$ approximates an aperiodic behaviour. Also a representation of a fixed time interval about t = 0 (say $-\frac{\tau}{2}$, $\frac{\tau}{2}$) on the circumference of the unit circle will become proportionally smaller as shown in Figure 3.11.

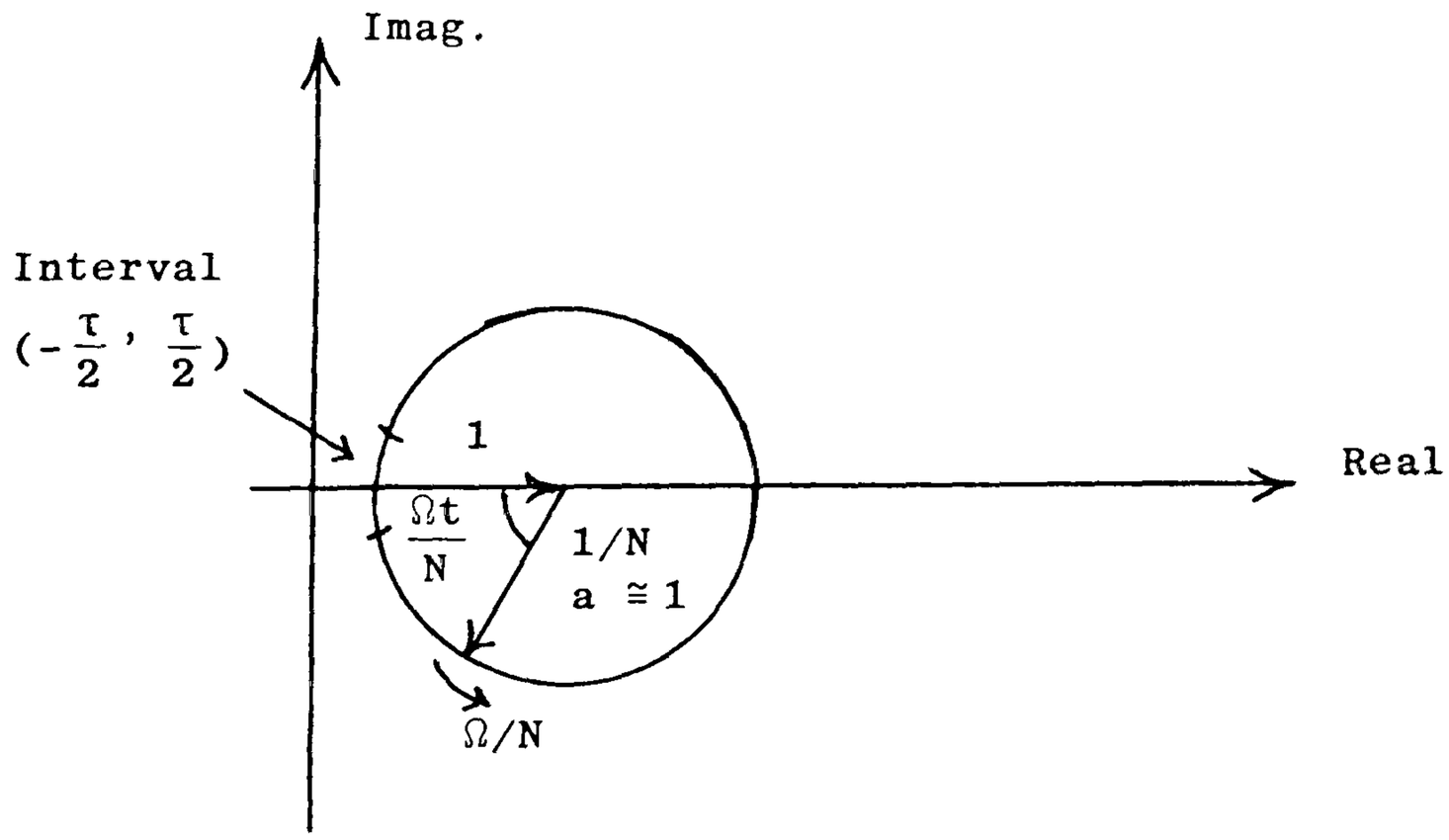

Phasor diagram of $(1 - a^{1/N}\, e^{j\frac{\Omega}{N}t})$

Fig. 3.11

The aperiodic phase function related to a single zero is considered in detail in the next section.

3.6 Single-Zero Phase Function

The phase function related to a single isolated zero is considered. This concept of treating the zeros of a signal individually is important as it permits conjugating any complex zero pair irrespective of all the other pairs. A mathematical proof follows which shows that the periodic phase function approaches the aperiodic phase when the period becomes infinitely large. Consider the periodic signal model expressed in eqn. (3.3):

$$s(t) = \prod_{r=1}^{N} (1 - e^{j\Omega(t-x_r)})\,(1 - e^{-j\Omega(t-x^*_r)})$$

$$= \prod_{r=1}^{N} f_r(t)\; f_r^*(t) \qquad (3.29)$$

where $f_r(t) = (1 - e^{j\Omega(t-x_r)})$, $f_r^*(t) = (1 - e^{-j\Omega(t-x^*_r)})$

$x_r = t_r + j\sigma_r$ = x-plane complex zero

$x^*_r = t_r - j\sigma_r$ = x-plane complex conjugate zero

* denotes complex conjugation.

In principle conjugation can be achieved by multiplying s(t) by the cancellation operator (conjugating function) c(t) as discussed in Section 3.4. Since a zero pair may be conjugated "up" or "down" the conjugating function, c(t), can be generally expressed as:

$$c(t) = \left[\frac{f_r(t)}{f_r^*(t)}\right] \pm 1 \qquad (3.30)$$

This corresponds to imposing a PM function

$\theta(t) = \arg\,[c(t)] = \pm 2 \arg\,[f_r(t)]$ on the signal s(t) as discussed previously.

These functions refer strictly to periodic conjugation; i.e. conjugation of a zero pair repeated at intervals of T seconds rather than of a single isolated zero pair. If T is made sufficiently large, then a single zero pair may be isolated for all practical purposes.

Consider the factor:

$$f_r(t) = (1 - e^{j\Omega(t-x_r)})$$

$$= 1 - \{1 + j\Omega(t-x_r) + \frac{[j\Omega(t-x_r)]^2}{2!} + \ldots\}$$

$$= - j\Omega(t-x_r) - \frac{[j\Omega(t-x_r)]^2}{2!} \quad \ldots$$

If $|\Omega(t-x_r)|$ is small then 2nd and higher order terms may be neglected and hence:

$$f_r(t) = -j\Omega(t-x_r) \tag{3.31}$$

This expression will be valid for finite values of t or x_r provided $\Omega = \frac{2\pi}{T}$ is sufficiently small. Expressing the complex zero as $x_r = t_r + j\sigma_r$ then eqn. (3.31) becomes:

$$f_r(t) = - j\Omega(t - t_r - j\sigma_r)$$

$$= - \Omega(\sigma_r + j(t - t_r)) \tag{3.32}$$

$$\therefore \theta_r(t) = \text{arc tan } (\frac{t-t_r}{\sigma_r}) \tag{3.33}$$

Then PM function is given by:

$$\theta(t) = \pm 2\ \theta_r(t) = \pm 2 \arg [f_r(t)]$$

$$= \pm 2 \text{ arc tan } (\frac{(t-t_r)}{\sigma_r}) \tag{3.34}$$

This phase function conjugates one zero pair only that occurs at $t = t_r$ and has an imaginary part of σ_r.

$\theta_r(t)$ has a zero value at the time of occurrence of the complex zero ($t = t_r$) and approaches $\pm \pi/2$ asymptotically for $\sigma_r \neq 0$.

Choosing the complex zero to lie at $t = 0$ and with an ordinate value of $\sigma_r = \frac{\ln a}{\Omega}$ then the aperiodic phase becomes:

$$\theta_r(t) = \arctan\left(\frac{\Omega t}{\ln a}\right) \tag{3.35}$$

Now consider the zero at $t = 0$ that has been shown in Section 3.5, the factor related to this zero is:

$$(1 - a^{1/N} z), \quad z = e^{j\frac{\Omega}{N}t}$$

$$\therefore \theta_1(t) = \arg\left[1 - a^{1/N} e^{j\frac{\Omega}{N}t}\right]$$

$$= -\arctan\left(\frac{a^{1/N}\sin(\frac{\Omega}{N}t)}{1 - a^{1/N}\cos(\frac{\Omega}{N}t)}\right) \tag{3.36}$$

Figure 3.12 (a,b,c) shows a phasor diagram of this factor and also the phase functions $\theta_r(t)$ and $\theta_1(t)$ as defined in eqn. (3.35) and (3.36) respectively.

As $N \to \infty$, $a^{1/N} \to 1$ and $\theta_1(t)$ changes between $\pm \frac{\pi}{2}$.

To prove mathematically that as $N \to \infty$ $\theta_1(t)$ approaches $\theta_r(t)$ as defined in eqn. (3.35), consider the sine and cosine expansions:

$$\sin x = x - \frac{x^3}{3!} + \frac{x^5}{5!} - \frac{x^7}{7!} + \ldots, \quad -\infty < x < \infty$$

$$\cos x = 1 - \frac{x^2}{2!} + \frac{x^4}{4!} - \frac{x^6}{6!} + \ldots, \quad -\infty < x < \infty$$

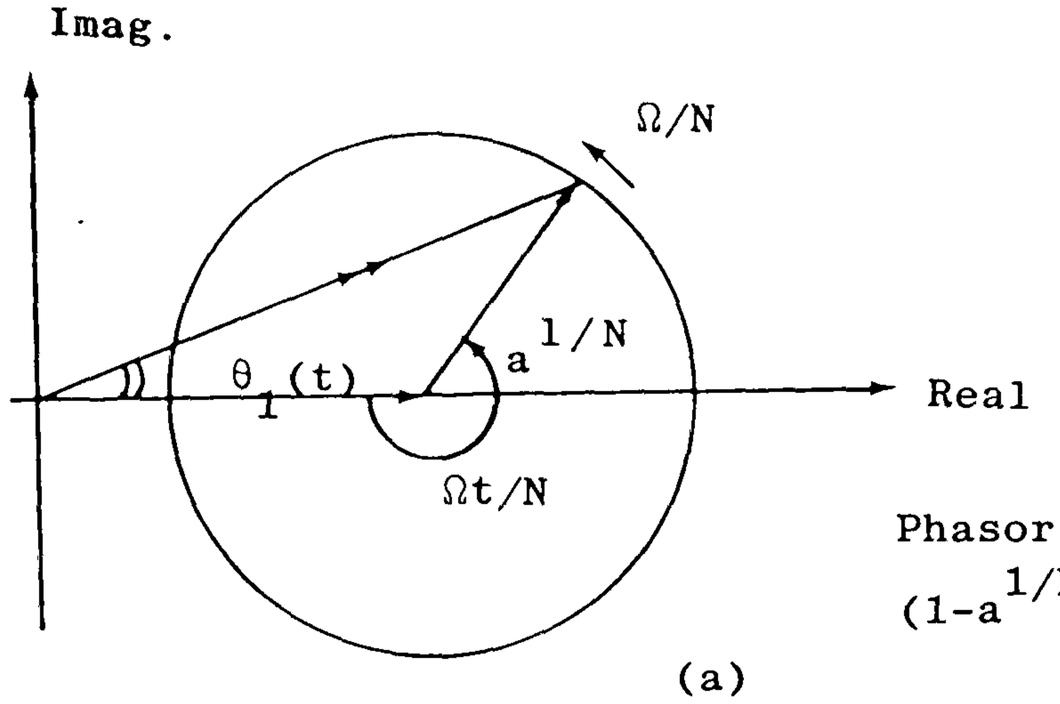

Phasor diagram of $(1-a^{1/N} e^{j\Omega t/N})$

(a)

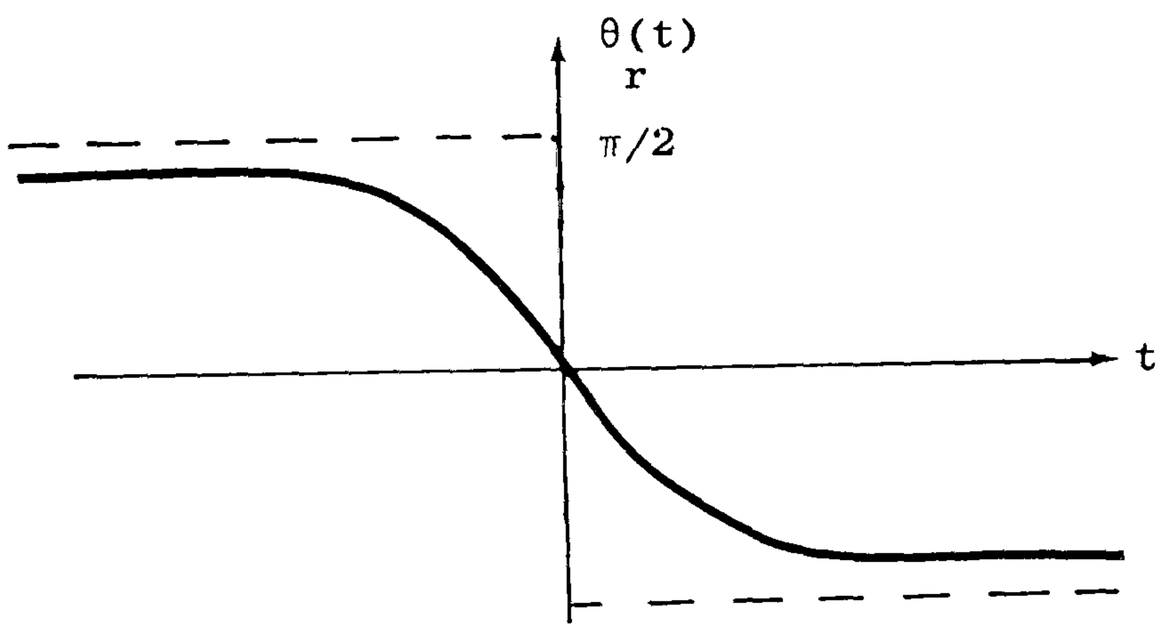

$\theta(t) = \arctan(\Omega t/\ln a)$

(b)

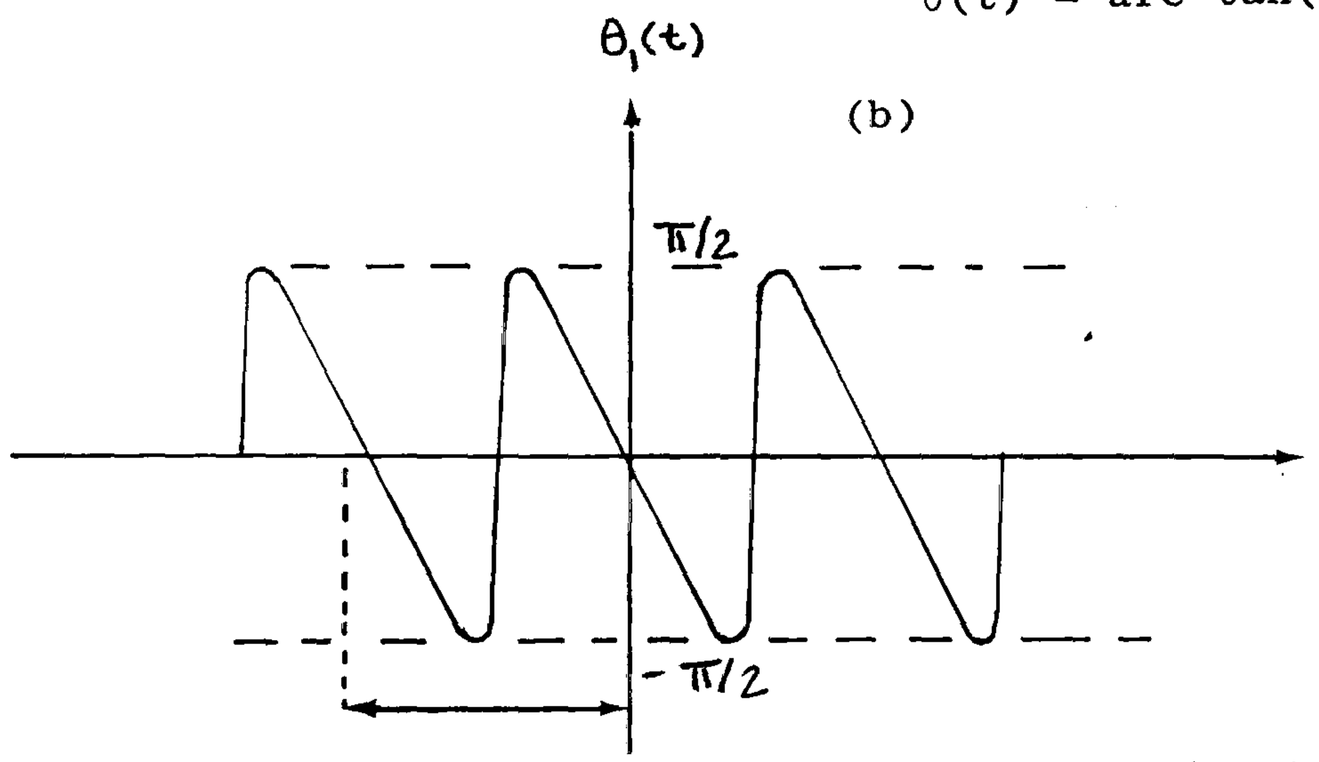

$$\theta_1(t) = -\arctan\left[\frac{a^{1/N}\sin(\frac{\Omega t}{N})}{1-a^{1/N}\cos(\frac{\Omega t}{N})}\right]$$

NT

(c)

Fig. 3.12

Using these in eqn. (3.36) gives:

$$\theta_1(t) = -\arctan\left\{\frac{a^{1/N}\left(\Omega t/N - \frac{(\Omega t/N)^3}{3!} + \frac{(\Omega t/N)^5}{5!} \ldots\right)}{1 - a^{1/N}\left(1 - \frac{(\Omega t/N)^2}{2!} + \frac{(\Omega t/N)^4}{4!} \ldots\right)}\right\} \tag{3.37}$$

$$\lim_{N\to\infty} \theta_1(t) = \lim_{N\to\infty}\left\{-\arctan\left\{\frac{a^{1/N}\left(\Omega t/N - \frac{(\Omega t/N)^3}{3!} + \frac{(\Omega t/N)^5}{5!} ..\right)}{1 - a^{1/N}\left(1 - \frac{(\Omega t/N)^2}{2!} + \frac{(\Omega t/N)^4}{4!} ..\right)}\right\}\right\}$$

To a first order approximation the above becomes:

$$\lim_{N\to\infty} \theta_1(t) = \lim_{N\to\infty}\left\{-\arctan\left\{\frac{a^{1/N}\,(\Omega t/N)}{1 - a^{1/N}}\right\}\right\} \tag{3.38}$$

Now $a^{1/N}$ can be expanded using the formula (15):

$$a^x = e^{x\ln a} = 1 + x\ln a + \frac{(x\ln a)^2}{2!} + \frac{(x\ln a)^3}{3!} + \ldots, \quad -\infty<x<\infty$$

Upon using the above expansion for $a^{1/N}$ then eqn. (3.33) becomes:

$$\lim_{N\to\infty} \theta_1(t) = \lim_{N\to\infty}\left\{-\arctan\left\{\frac{(1 + \frac{1}{N}\ln a + \frac{(\frac{1}{N}\ln a)^2}{2!} \ldots)(\Omega t/N)}{1 - (1 + \frac{1}{N}\ln a + \frac{(\frac{1}{N}\ln a)^2}{2!} \ldots)}\right\}\right\}$$

$$= -\arctan\left(\frac{\Omega t}{-\ln a}\right)$$

$$= \arctan\left(\frac{\Omega t}{\ln a}\right)$$

$$= \theta_r(t) \tag{3.39}$$

The above proof assures that the periodic phase approaches the aperiodic phase $\theta_r(t)$ when the period is large enough. In the vicinity of the complex zero both $\theta_1(t)$ and $\theta_r(t)$ are similar.

A very important point that requires emphasising at this stage is that the periodic phase function $\theta_m(t)$ conjugates all the zeros of s(t) from t = $-\infty$ to t = $+\infty$ and hence it yields also a periodic signal with periodic zero pattern as shown in Figure 3.13 (a,b). On the other hand the aperiodic phase function $\theta_r(t)$ conjugates only one zero pair when used in eqn. (3.34). Thus the conjugated signal does not have a periodic zero pattern as shown in Figure 3.13(c), and consequently the conjugated signal is no longer periodic and is not expected to have a line spectrum.

3.7 Analytical Study of the Aperiodic Conjugating Function

In the last section we discussed the aperiodic phase function that conjugates only one zero pair. This phase function is:

$$\theta_r(t) = \arctan\left(\frac{t - tr}{\sigma_r}\right)$$

For simplicity the zero can be chosen to lie at t = 0, hence:

$$\theta_r(t) = \arctan\left(\frac{t}{\sigma_r}\right) = \arg\left(1 + j\frac{t}{\sigma_r}\right)$$

Upon using the results obtained above, the conjugating function c(t) becomes:

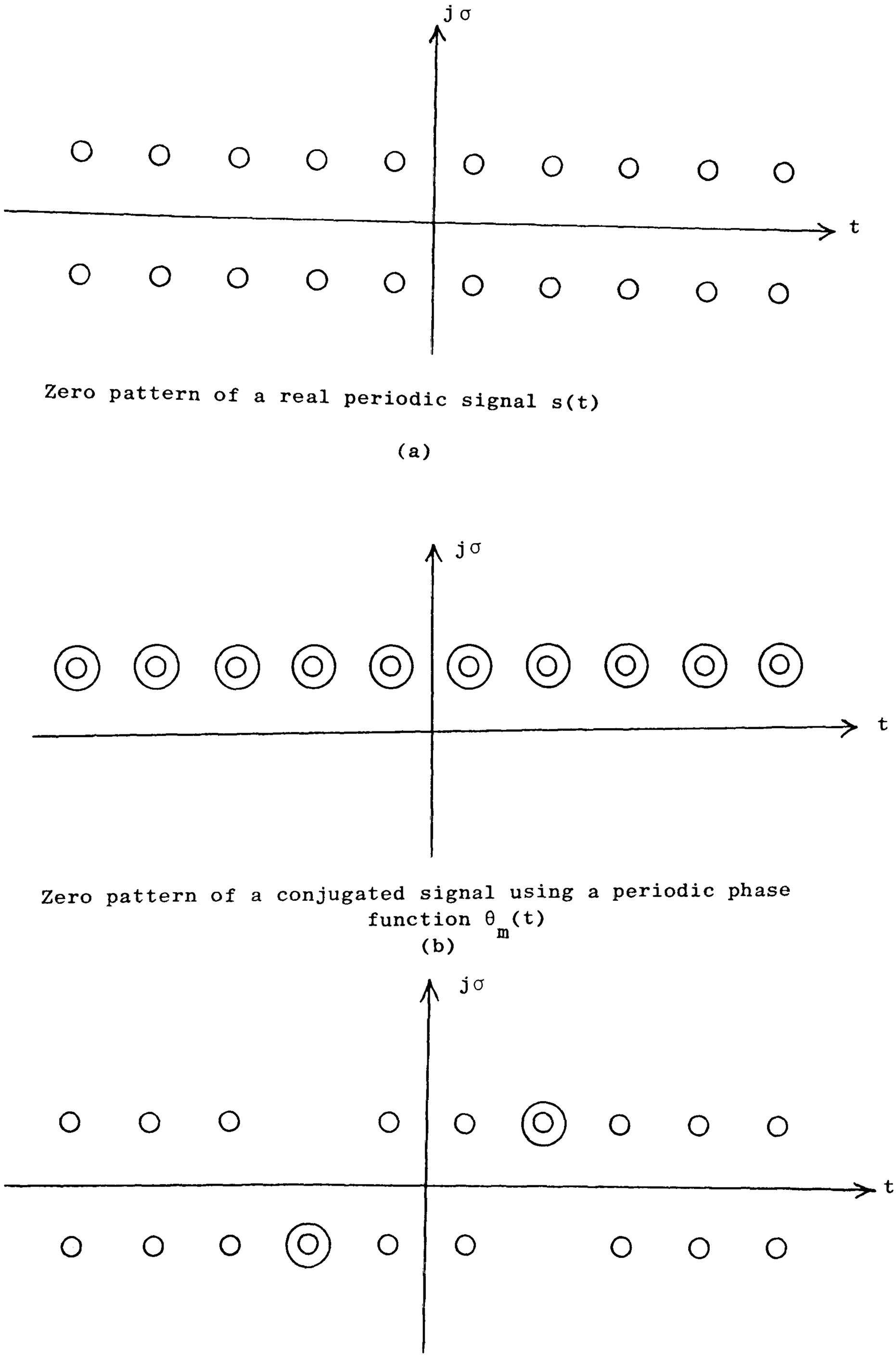

Zero pattern of a real periodic signal s(t)

(a)

Zero pattern of a conjugated signal using a periodic phase function $\theta_m(t)$

(b)

Zero pairs after conjugation using aperiodic phase function $\theta_r(t)$

(c)

Fig. 3.13

$$c(t) = e^{j2\theta_r(t)} = e^{j2\ \tan^{-1}(t/\sigma_r)}$$

$$= \frac{1 + jt/\sigma_r}{1 - jt/\sigma_r} \qquad (3.40)$$

It is worth finding the Fourier transform of c(t) since it then becomes possible to find the Fourier transform of any conjugated signal simply by convolving the Fourier transform of the real signal with C(f), the frequency spectrum of c(t).

$$\therefore C(f) = \int_{-\infty}^{\infty} c(t)\ e^{-j\omega t}\ dt$$

$$= \int_{-\infty}^{\infty} \frac{1 + jt/\sigma_r}{1 - jt/\sigma_r}\ e^{-j\omega t}\ dt$$

$$= \int_{-\infty}^{\infty} \left(\frac{1 + jt/\sigma_r}{1 - jt/\sigma_r}\right)\left(\frac{1 + jt/\sigma_r}{1 + jt/\sigma_r}\right)\ e^{-j\omega t}\ dt$$

$$= \int_{-\infty}^{\infty} \frac{(1 + jt/\sigma_r)^2}{1 + t^2/\sigma_r^2}\ e^{-j\omega t}\ dt$$

$$= \int_{-\infty}^{\infty} \left(\frac{(1 + j2t/\sigma_r - t^2/\sigma_r^2)}{1 + t^2/\sigma_r^2}\right)\ e^{-j\omega t}\ dt$$

$$= \int_{\infty}^{\infty} \left(\frac{1 - t^2/\sigma_r^2}{1 + t^2/\sigma_r^2} + j\ \frac{2t/\sigma_r^2}{1 + t^2/\sigma_r^2}\right)\ e^{-j\omega t}\ dt$$

$$C(f) = \int_{-\infty}^{\infty} \left(\frac{\sigma_r^2 - t^2}{\sigma_r^2 + t^2} + j\ \frac{2\sigma_r t}{\sigma_r^2 + t^2}\right)\ (\cos\omega t - j\sin\omega t)\,dt$$

$$= \underbrace{\int_{-\infty}^{\infty} \left[\frac{\sigma_r^2 - t^2}{\sigma_r^2 + t^2} \cos\omega t + \frac{2\sigma_r t}{\sigma_r^2 + t^2} \sin\omega t\right] dt}_{R(f)} + j \underbrace{\int_{-\infty}^{\infty} \left[\frac{2\sigma_r t}{\sigma_r^2 + t^2} \cos\omega t - \frac{\sigma_r^2 - t^2}{\sigma_r^2 + t^2} \sin\omega t\right] dt}_{X(f)}$$

Note that $X(f) = 0$ as the integrand is an odd time function, hence:

$$C(f) = \int_{-\infty}^{\infty} \left[\frac{\sigma_r^2 - t^2}{\sigma_r^2 + t^2} \cos\omega t + \frac{2\sigma_r t}{\sigma_r^2 + t^2} \sin\omega t\right] dt$$

$$= 2 \int_{0}^{\infty} \left[\frac{\sigma_r^2 - t^2}{\sigma_r^2 + t^2} \cos\omega t + \frac{2\sigma_r t}{\sigma_r^2 + t^2} \sin\omega t\right] dt$$

To integrate the above we need to use two definite integral formulae (15).

$$\int_0^{\infty} \frac{\cos mx}{x^2 + a^2} dx = \frac{\pi}{2a} e^{-ma}; \quad \int_0^{\infty} \frac{x \sin mx}{x^2 + a^2} dx = \frac{\pi}{2} e^{-ma}, \text{ m positive}$$

$$\therefore 2 \int_0^{\infty} \frac{\sigma_r^2 - t^2}{\sigma_r^2 + t^2} \cos\omega t dt = 2 \left[\sigma_r^2 \int_0^{\infty} \frac{\cos\omega t}{\sigma_r^2 + t^2} dt - \int_0^{\infty} \frac{t^2}{\sigma_r^2 + t^2} \cos\omega t \, dt\right]$$

$$= 2 \left[\sigma_r^2 \frac{\pi}{2\sigma_r} e^{-\sigma_r |\omega|} - \int_0^{\infty} \frac{t^2 + \sigma_r^2 - \sigma_r^2}{\sigma_r^2 + t^2} \cos\omega t \, dt\right]$$

$$= 2 \left[\sigma_r^2 \frac{\pi}{2\sigma_r} e^{-\sigma_r |\omega|} - \int_0^{\infty} \cos\omega t \, dt + \sigma_r^2 \int_0^{\infty} \frac{\cos\omega t}{\sigma_r^2 + t^2} dt\right]$$

$$= 2\left[\sigma_r^2 \frac{\pi}{2\sigma_r} e^{-\sigma_r|\omega|} - \int_0^\infty \cos\omega t\, dt + \sigma_r^2 \frac{\pi}{2\sigma_r} e^{-\sigma_r|\omega|}\right]$$

$$= 2\sigma_r \pi e^{-\sigma_r|\omega|} - 2\int_0^\infty \cos\omega t\, dt \qquad (3.41)$$

Now:

$$2\int_0^\infty \cos\omega t\, dt = \int_{-\infty}^\infty \cos\omega t = \frac{1}{2}\int_{-\infty}^\infty (e^{j\omega t} + e^{-j\omega t})dt$$

$$= \frac{1}{2}\left[\int_{-\infty}^\infty e^{j\omega t} dt + \int_{-\infty}^\infty e^{-j\omega t}\, dt\right]$$

$$= \frac{1}{2}\left[-\int_{\infty}^{-\infty} e^{-j\omega t}\, dt + \int_{-\infty}^\infty e^{-j\omega t}\, dt\right]$$

$$= \frac{1}{2}\left[\int_{-\infty}^\infty e^{-j\omega t}\, dt + \int_{-\infty}^\infty e^{-j\omega t}\, dt\right]$$

$$= \frac{1}{2}\left[\delta(f) + \delta(f)\right] = \delta(f)$$

where $\delta(f)$ is the delta function

$\therefore$ eqn. (3.41) becomes:

$$2\int_0^\infty \frac{\sigma_r^2 - t^2}{\sigma_r^2 + t^2} \cos\omega t\, dt = 2\sigma_r \pi e^{-\sigma_r|\omega|} - \delta(f)$$

$$2\int_0^{\infty} \frac{2\sigma_r t}{\sigma_r^{\,2}+t^2} \sin\omega t \, dt = 4\int_0^{\infty} \frac{\sigma_r t}{\sigma_r^{\,2}+t^2} \sin\omega t \, dt$$

$$= 4\ \sigma_r \frac{\pi}{2} e^{-\sigma_r|\omega|} \operatorname{sgn}(\omega)$$

where $\operatorname{sgn}(\omega) = \begin{cases} +1 & , \ \omega > 0 \\ -1 & , \ \omega < 0 \end{cases}$

$$\therefore C(f) = 2\sigma_r \pi e^{-\sigma_r|\omega|} - \delta(f) + 2\ \sigma_r \pi\ e^{-\sigma_r|\omega|} \operatorname{sgn}(\omega)$$

$$\therefore C(f) = \begin{cases} 4\sigma_r\ \pi\ e^{-\sigma_r|\omega|} - \delta(f) & , \ \omega > 0 \\ -\ \delta(f) & , \ \omega < 0 \end{cases} \qquad (3.42)$$

Therefore c(t) is Analytic as it has zero negative frequency content. For very large σ_r the exponential decay of the first term in eqn. (4.42) is fast, while for small σ_r the decay is slow. For $\sigma_r = 0$ (i.e. real zero) then the cancellation operator has a line spectrum as:

$$C(f) = -\ \delta(f)$$

For the real signal s(t) discussed in Section 3.5 the complex zeros become real (i.e. $\sigma_r = 0$) when a = 1, i.e.

$$s(t) = 2 - 2\cos\Omega t$$

$$\therefore S(f) = 2\ \delta(f) - \delta(f - \frac{\Omega}{2\pi}) - \delta(f + \frac{\Omega}{2\pi}) \qquad (3.43)$$

If the conjugated signal is n(t) then:

$$n(t) = s(t)\ c(t)$$

$$\therefore N(f) = S(f) * C(f)$$

$$= [2\ \delta(f) - \delta(f - \frac{\Omega}{2\pi}) - \delta(f + \frac{\Omega}{2\pi})] * \delta(f)$$

$$\therefore\ N(f) = 2\ \delta(f) - \delta(f - \frac{\Omega}{2\pi}) - \delta(f + \frac{\Omega}{2\pi}) \qquad (3.44)$$

The above verifies that conjugating only one zero of s(t) gives no change as all the zeros are real.

Consider the periodic cancellation operator c(t) given in eqn. (3.12):

$$c(t) = \frac{1 + a\ e^{j\Omega t}}{1 + a\ e^{-j\Omega t}}$$

The above can be written as:

$$c(t) = (1 + a\ e^{j\Omega t})(1 + a\ e^{j\Omega t})^{-1}$$

$$= (1+ae^{j\Omega t})(1-ae^{-j\Omega t}+a^2 e^{-j2\Omega t}-a^3 e^{-j3\Omega t}+a^4 e^{-j4\Omega t}\ldots)$$

$$= (1-a^2)+ae^{j\Omega t}+(a^3-a)e^{-j\Omega t}+(a^2-a^4)e^{-j2\Omega t}+(a^5-a^3)e^{-j3\Omega t}\ldots$$

This has a spectrum of:

$$C(f) = (1-a^2)\delta(f)+a\delta(f-\frac{\Omega}{2\pi})+(a^3-a)\delta(f+\frac{\Omega}{2\pi})+(a^2-a^4)\delta(f+\frac{2\Omega}{2\pi})$$

$$+(a^5-a^3)\delta(f+\frac{3\Omega}{2\pi})\ldots$$

The above shows that c(t) is non-bandlimited but has a line spectrum.

For real zero ($\sigma_r = 0$ or $a = 1$) the spectrum is band-limited as was the case for the aperiodic cancellation operator.

3.8 Superposition of Data Signals on Bandlimited Channels

The concept of the common envelope set (Section 2.7) may be exploited to study the possibility of super-imposing binary data signals on bandlimited speech channels.

Conventional double-sideband amplitude-modulation DSB-AM is widely used because of its simplicity in transmission and reception, but in a number of applications the inclusion of a data channel has become an additional requirement (5,16). This can be achieved by the use of FM for data transmission with AM in the usual way but in general, combined AM/PM will generate nonbandlimited signals for all but very slow data rates (6). It will be shown that bandlimitation may be preserved by applying FM in synchronism with the complex zeros of the amplitude-modulating signals.

This technique, named Zero Synchronous Frequency Modulation (ZSFM), requires provision for complex zero detection and combined AM/FM at the transmitter. Normal arrangements apply for envelope detection at the receiver and the additional data signal can be recovered by simple frequency modulation (e.g. phase-locked loop).

A conventional DSB-AM signal may be expressed in the general form (10):

$$x(t) = \mathrm{Re}\{s(t)\, e^{j\omega_o t}\} \tag{3.45}$$

where $s(t) > 0$ is a real modulating signal and ω_o is the carrier frequency. If $s(t)$ is periodic with period T it may be expressed as multiplicative factors representing complex conjugate zeros as given by eqn. (3.29).

$$\begin{aligned} s(t) &= \prod_{r=1}^{N} (1 - e^{j\Omega(t-x_r)})(1 - e^{-j\Omega(t-x_r^*)}) \\ &= \prod_{r=1}^{N} f_r(t)\, f_r^*(t) \end{aligned} \tag{3.46}$$

where $x_r = t_r + j\sigma_r$ and $x^*_r = t_r - j\sigma_r$ are the rth generally complex conjugate zero pair such that $s(t) = 0$.

The principle of ZSFM derives from the equality $|f_r(t)| = |f^*_r(t)|$ from which it follows that the envelope $|s(t)|$ will be unaffected if any $f_r(t)$ is replaced by its complex conjugate $f^*_r(t)$, or vice versa. Thus the envelope of the modulated signal is invariant to a process of zero conjugation in which any zero may be replaced by its complex conjugate. Since s(t) will become generally complex, arg $s(t) \neq 0$ and it is apparent that the modulated signal will be phase modulated as discussed in Section 3.4.

However, the process of zero conjugation (i.e. replacing $f_r(t)$ by $f^*_r(t)$ or vice versa) will not increase the number of multiplicative factors in eqn. (3.45) and hence the bandwidth of s(t) and hence x(t) will not be affected. However, there will be a spectral shift in the modulated signal as discussed in Section 3.4 unless the number of conjugations in each sense (i.e. "up" and "down") is equal. This condition is not difficult to meet since if s(t) models a very long signal quite long asymmetrical strings of binary data of "1" and "0" can be tolerated provided they balance in the mean.

Thus this process of complex zero conjugations preserves envelope bandwidth which is a characteristic of the "common envelope set" (13) whose members possess the same envelope and bandwidth, but different phase functions. Since a zero pair may be conjugated "up"

or "down" (resulting in a second order zero with $\sigma_r > 0$ or $\sigma_r < 0$ respectively) or left unconjugated there are 3 possibilities and therefore a total of 3^N signals exist that possess the same envelope and bandwidth as s(t) constituting a "common envelope set". It follows that by making the process of complex zero conjugation dependent on a binary data signal then the redundancy inherent in conventional DSB-AM signals can be exploited without distorting the envelope or increasing the bandwidth. It was shown in Section 3.6 that the process of conjugation can be achieved by imposing the PM function $\theta(t)$ on the modulated signal. The equivalent FM function can be obtained by differentiation.

$$\theta(t) = \pm 2 \arctan\left(\frac{t - t_r}{\sigma_r}\right)$$

$$\theta'(t) = \frac{d\theta(t)}{dt}$$

$$= \pm \frac{2\sigma_r}{\sigma_r^2 + (t - t_r)^2} \qquad (3.47)$$

Imposition of either PM or FM function will be sufficient to conjugate a single zero pair without affecting bandwidth or envelope. $\theta'(t)$ is symmetrical about $t = t_r$ and falls asymptotically to zero with t^2. Thus in practice $\theta'(t)$ may be truncated within a finite time interval of P seconds centred on t_r with an approximation error which can be reduced by increasing P. The effect of truncating $\theta'(t)$ is discussed in Section 5.10.

Since the above analysis can be applied to any zero pairs represented in eqn. (4.46), conjugation of any combination of zeros can be achieved by forming the product of s(t) and the related conjugating functions or, equivalently, superimposing the associated PM or FM functions on the carrier. Thus in general for FM:

$$\theta'(t) = \sum_r \frac{2\, b_r \sigma_r}{\sigma_r^2 + (t - t_r)^2} \qquad (3.48)$$

where $b_r = \pm 1$ denotes the binary data signal (1 or 0) required for transmission.

Figures 3.14(a) and 3.24(b) shows a series of zero pairs before and after conjugation for data transmission (binary code 101100), while Figure 3.14(c) shows FM function as given by eqn. (3.48) denoting the 6-bit data signal 101100.

The combined AM/FM signal carrying both channels can be obtained by frequency modulating the carrier with the FM function $\theta'(t)$ and also amplitude modulating the carrier with the amplitude modulating signal s(t) in the conventional way. Using eqn. (3.45) this can be written as:

$$x(t) = \mathrm{Re}\{s(t)\, e^{j\theta(t)}\, e^{j\omega_o t}\}$$

$$= s(t) \cos [\omega_o t + \theta(t)] \qquad (3.49)$$

where the FM function $\theta'(t)$ relates to the complex zeros of s(t) and must be applied in synchronism with the time of occurrence of the complex zeros of s(t) as explained before.

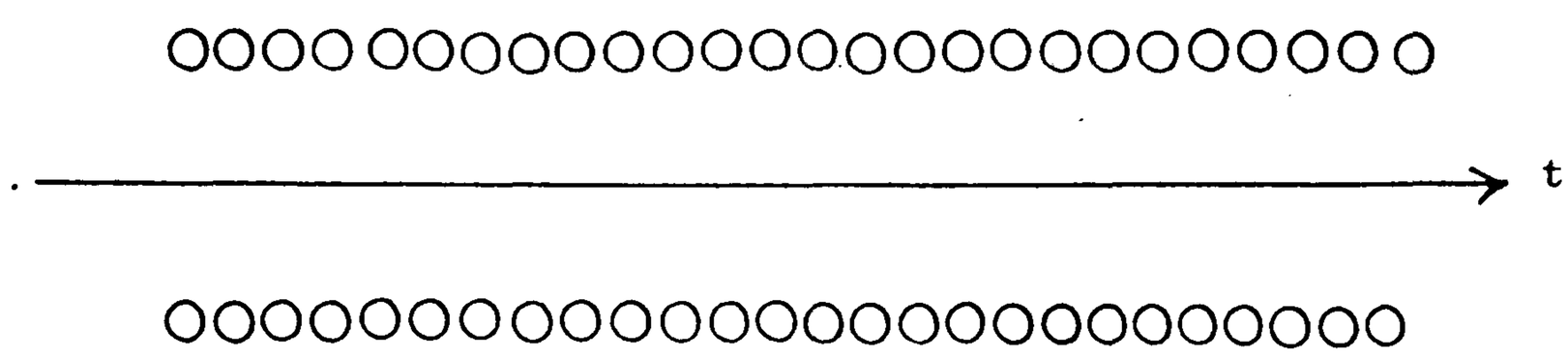

Complex zeros before conjugation

(a)

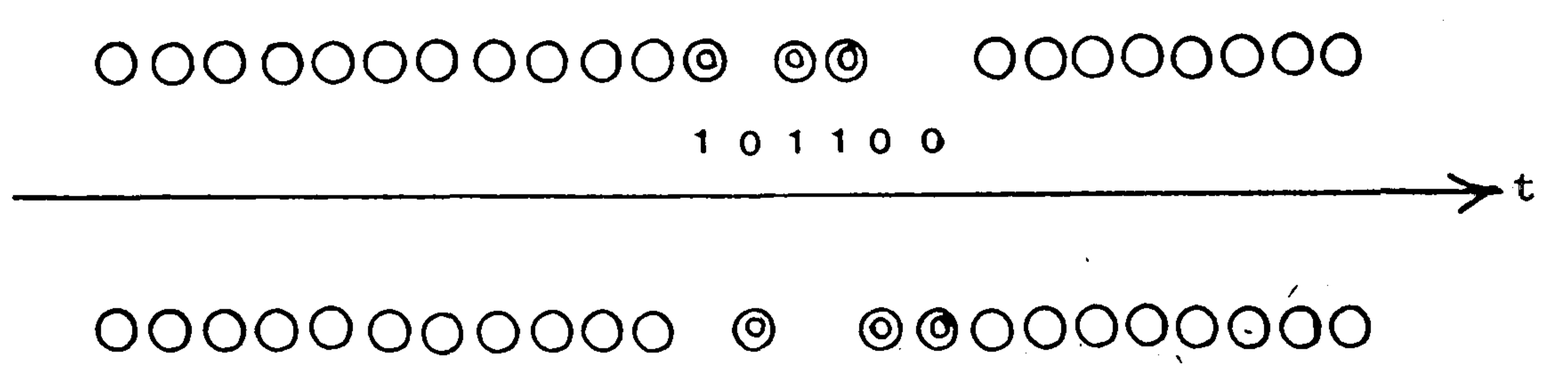

(b)

Complex zeros after conjugation

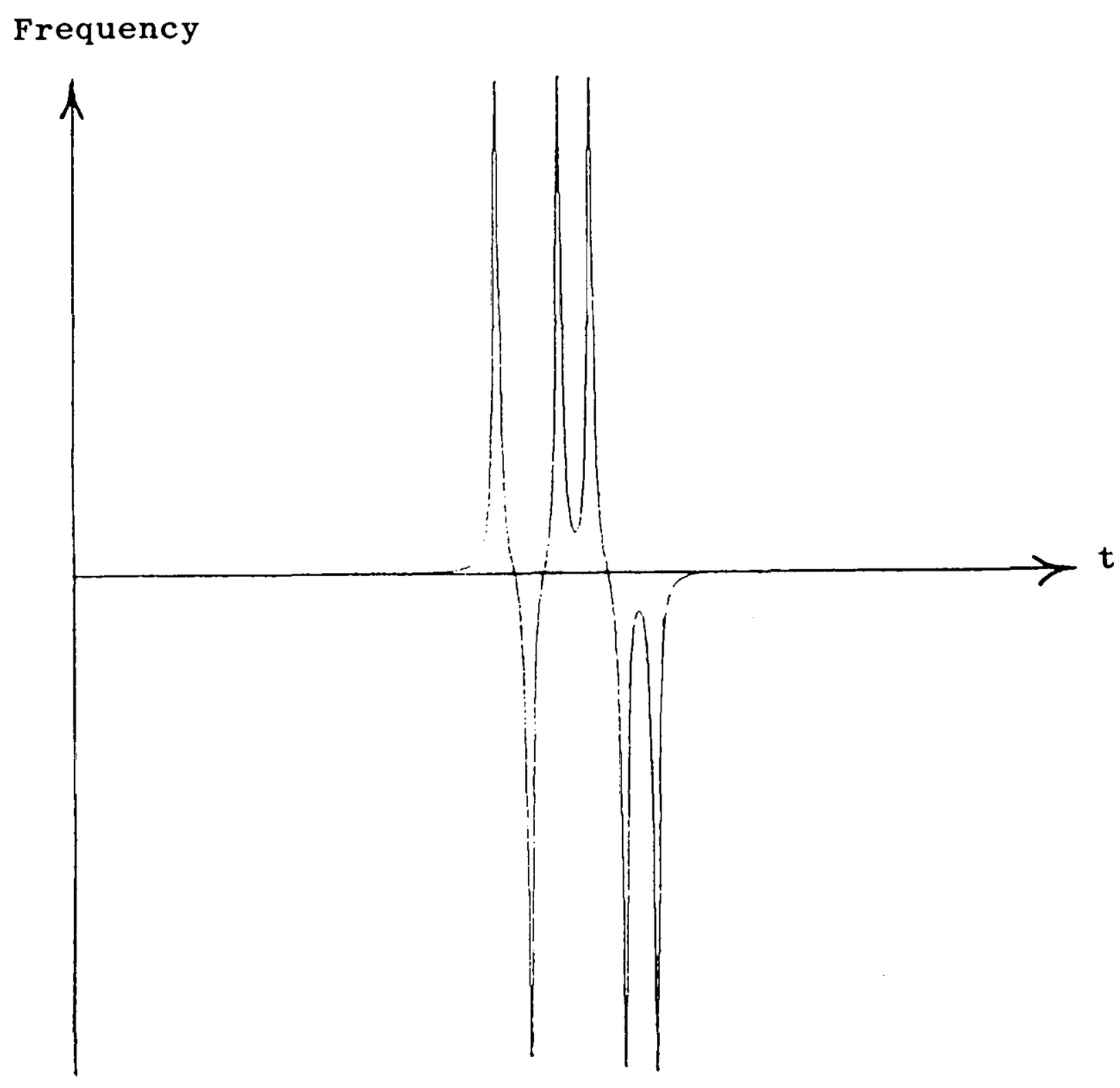

(c)
FM function

Fig. 3.14

Theoretically ZSFM permits data transmission to be superimposed on conventional DSB-AM signals without increasing bandwidth or distorting the envelope. Thus x(t) has the same bandwidth as s(t) and can be generated by imposing either the PM or the FM function on the carrier. For example, the function $\theta'(t)$ might be applied to a voltage-controlled oscillator (VCO) which will produce $\cos[\omega_o t + \theta(t)]$.

3.9 Data Rates of ZSFM

The maximum data rate for ZSFM depends on the average rate of occurrence of complex zeros of the positive amplitude modulating signal s(t). For N complex zero pairs during a period T, the data rate will be:

$$R = \frac{N}{T} \text{ bits/sec} \qquad (3.50)$$

The above assumes that all the complex zeros may be associated with a data bit, i.e. all the complex zeros are detected and suitable for conjugation. Using eqns. (3.45) and (3.46), the bandwidth of s(t) and hence of x(t) is:

$$W = \frac{2N\Omega}{2\pi} = \frac{2N}{T} \text{ Hz}$$

The data rate is therefore (17):

$$R = \frac{W}{2} \text{ bits/sec} \qquad (3.51)$$

Thus in principle data rate up to 5 kbits/sec may be transmitted over a 10 kHz broadcast channel, but in practice not all the available complex zeros are usable

for conjugation. For very small σ_r the envelope modulation depth approaches 100% in which case frequency detection of the transmitted data signal during the envelope trough will be unreliable due to low signal-to-noise ratios. For very large σ_r eqn. (3.48) shows that the frequency deviation ($\frac{2}{\sigma_r}$ rad/sec) becomes insufficient for detection at the receiver. Nevertheless it is known (18) that the majority of the complex zeros of bandlimited signals are distributed in the vicinity of the real axis and hence it is expected that most of the complex zeros are amenable to conjugation. If a fraction v of the available complex zero pairs are detectable and suitable for conjugation, then only vN complex zero pairs may be conjugated causing the data rate to become:

$$R = v \frac{W}{2} \text{ bits/sec} , \quad v < 1 \qquad (3.52)$$

It was discussed in Section 3.4 that unless the number of conjugations in each sense (i.e. "up" and "down") is equal, there will be a spectral shift in the conjugated signal. This condition is not difficult to meet since if s(t) models a very long signal then asymmetrical strings of 1's and 0's can be tolerated provided they balance in the mean. In practice, however, s(t) is effectively limited to a "time window", but if necessary a redundant complementary bit may be sent after each information bit , thus ensuring equal numbers of 1's and 0's.

This results in a reduction in the data rate by one half. If 50% of the available complex zero pairs is used only then the data rate becomes:

$$R = 0.5\ \frac{10}{2} = 2.5 \text{ bits/sec}$$

In the last section it was shown that the complex zero pair can be either conjugated "up" or "down" or left unconjugated giving 3 possibilities and therefore for N complex zero pairs during a period T the date rate is:

$$R = \frac{1}{T} \log_2 3^N = \frac{N}{T} \log_2 3 \text{ bits/sec}$$

Quoting the result of eqn. (3.51) the above becomes:

$$R = \frac{W}{2} \log_2 3 \tag{3.53}$$

The above gives a data rate of 7.93 kbits/sec over a 10 kHz broadcast channel, but this requires complex zero detection at the receiver which would significantly complicate the circuitry and increase costs.

3.10 Zero Detection

This section introduces the complex filter that detects complex zeros of a signal very briefly, whereas the next chapter is devoted mainly to complex zero detection. Complex zero detection is necessary for the conjugation process, and consequently for data transmission in ZSFM.

Real zeros of a signal are simple to detect, but complex zeros, in general, do not have an obvious

physical interpretation. It will be shown in Chapter 4 that if the signal $s(t + j\sigma_r)$ can be formed, then all the complex zeros of $s(t)$ with imaginary part σ_r will transform into easily detected real zeros. If the Fourier transform of $s(t)$ is $S(f)$ then the Fourier transform of $s(t + j\sigma_r)$ is:

$$F[s(t + j\sigma_r)] = e^{-2\pi f\sigma_r} S(f) \quad \text{(time translation theorem)}$$
$$= e^{-\omega\sigma_r} S(f) \qquad (3.54)$$

Thus $s(t + j\sigma_r)$ is obtained by passing $s(t)$ through a filter with frequency response:

$$H(\omega) = e^{-\omega\sigma_r} \qquad (3.55)$$

This filter is complex for $\sigma_r \neq 0$ and has a complex impulse response, but in practice such a filter may be approximated in a number of ways (19). For example, this filter may be realised by two tapped delay lines having weights representing real and imaginary parts respectively of the sampled impulse response, the weights being obtained from the inverse Fourier transform of the filter frequency response which is equivalent to the sampled impulse response. Each delay line is connected to a respective summing circuit and a logic circuit indicates when both summing circuits have zero weighted sums, indicating a complex zero. Since the filter detects complex zeros of $s(t)$ with imaginary part σ_r, a bank of such filters must be used for different σ_r values if complex zeros within a range of σ_r values are to be detected.

3.11 A ZSFM System

A possible implementation for a ZSFM transmitter is now described with reference to Figure 3.15. The amplitude modulating signal is applied to the bank of complex filters so that the complex zero pairs are transformed into real zeros that can be detected by real zero detectors. This signal may, for example, be an audio signal (speech, music) but it must contain a d.c. component of sufficient value to prevent zero crossings occurring. The filters are described in more detail later in Chapter 4. Each filter output is connected to a real zero detector which envelope detects the filter output and signifies by means of an internal comparator when the envelope passes through a real zero, thus indicating the presence of a complex zero in the corresponding signal output. The logic circuit coupled to the real zero detectors provides a first output indicating that a complex zero pair has been detected, and a second output giving the imaginary part of the complex zero (σ_r). These two outputs are passed to the conjugation function generator. After a complex zero pair has been detected at $t = t_r$, a conjugation according to the data signal is achieved by imposing the FM function given by eqn. (3.48) on the carrier. This function is generated by the conjugation function generator which outputs the correct positive or negative function according to the binary data signal. This function generator provides an output voltage each time

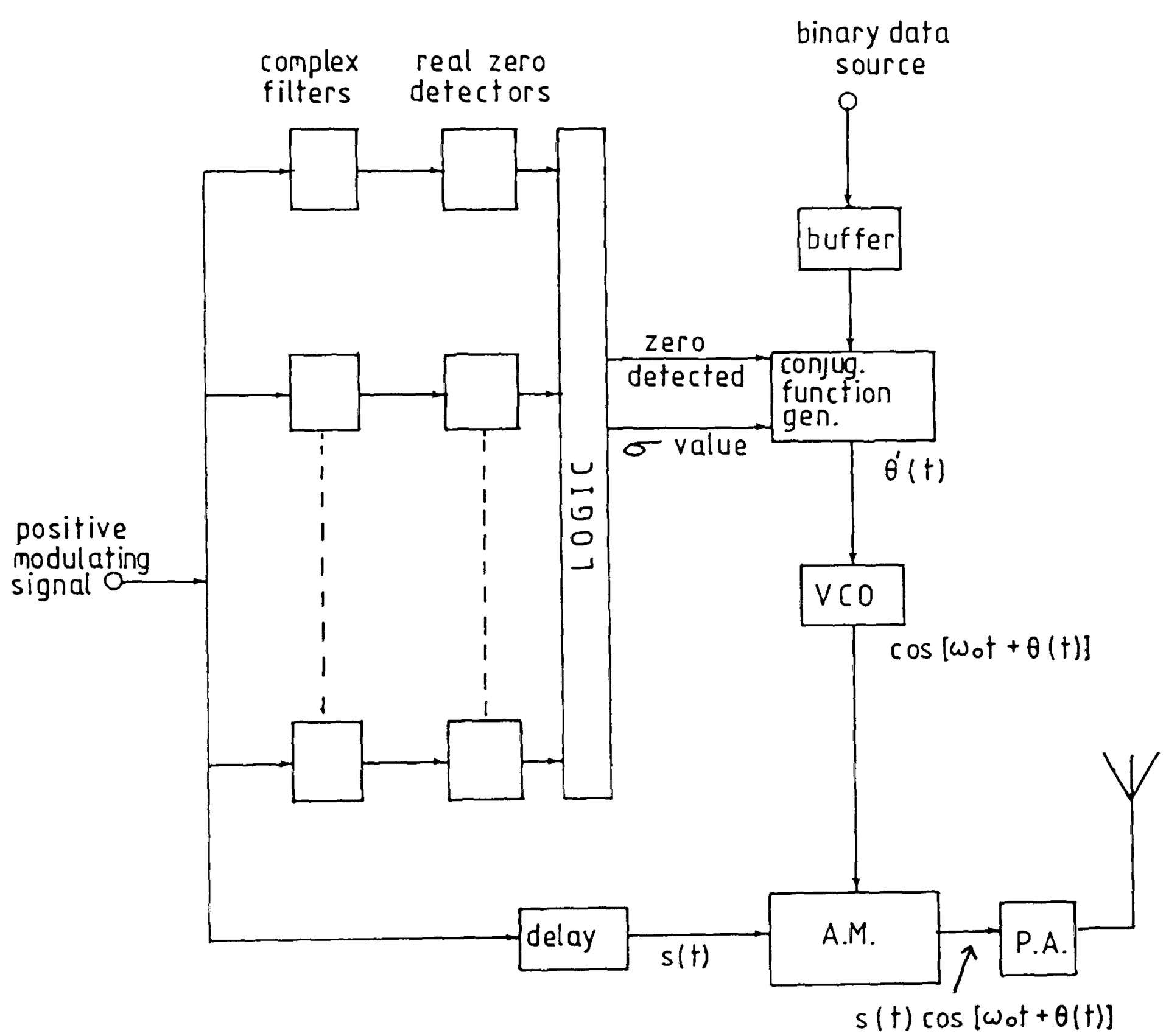

A ZSFM Transmitter

Fig. 3.15

a zero is detected. The conjugation function generator may comprise a number of shift registers, one for each imaginary part of the zero (σ_r) detected by the bank of complex filters. Each shift register has taps weighted according to samples of the function $\frac{2\sigma_r}{\sigma_r^2 + (t - t_r)^2}$ evaluated in the region $t = t_r$; that is each weight corresponds to a value of $\frac{2\sigma_r}{\sigma_r^2 + (t - t_r)^2}$ for the value of σ_r for that shift register and for values of t in the region $t = t_r$. On detection of complex zero, a binary bit is applied to the appropriate shift register which is clocked in accordance with increments of t, and a sampled version of the required function is generated by a summing circuit connected to the tap outputs. A low-pass filter is preferably used to smooth the summed outputs.

The conjugation function generator may also be based on digital techniques, for example, samples of the required function may be stored in read-only memory and addressed by values of σ_r and t. It is then required to use digital-to-analogue converter at the output of the generator.

In order to take account of the binary data signal the function generator may include a circuit which inverts the signal from the low-pass smoothing filter if, for example, the binary value is zero.

In practice the FM function is truncated within a duration of P second as was discussed in Section 3.8,

and the effect of this truncation on the bandwidth of the modulated signal will be studied in Chapter 5.

If a constant data source is used then an expanding/contracting buffer must be employed since the FM must be imposed synchronously with zeros which, in general, will not occur regularly in time.

The voltage function from the conjugation function generator is passed to frequency modulate the voltage controlled oscillator which provides the carrier signal. This carrier signal is then amplitude modulated by the input signal s(t) and thus producing the combined AM/FM signal given by eqn. (3.49).

Since the FM function is impressed only within an interval $(t_r \pm \frac{P}{2})$ seconds, the amplitude modulating signal must be delayed by $\frac{P}{2}$ seconds before amplitude modulation takes place. The delay must also incorporate the time required to detect zeros due to the delay introduced by a physically-realisable filter bank.

The output of the amplitude modulator is passed to a transmitter for transmission according to known techniques.

From the preceding information it is clear that the ZSFM technique requires no modification at the transmitter other than provision for carrier frequency modulation as well as complex zero detection by bank of filters.

At the receiver, envelope detection is carried out in the usual way to recover the amplitude modulating signal. The data signal can be recovered by hard limiting the received signal followed by frequency demodulation using a phase-locked loop to detect positive or negative frequency deviations from the carrier.

It should be noted that zero detection at the receiver is not required since demodulation of a binary data signal can be performed without the need to locate the time positions of zeros.

Figure 3.16 shows a possible ZSFM receiver.

3.12 Applications of ZSFM

The additional data capacity made available by ZSFM technique can be utilised in many different ways. Applications include the provision of advisory services (for example, monitoring weather conditions and motoring information), signalling for regular time checks to reset a free-running quartz clock in the receiver and thus providing a highly accurate but low cost clock. Station identification with particular relevance to medium wave broadcasting is also feasible.

The additional data signal may also provide control and display functions at the receiver (5,16). The control functions include a network identification code where a programme search in automatic tuning becomes possible, and also programme type code (e.g. news, music) can be used. The display functions can include a

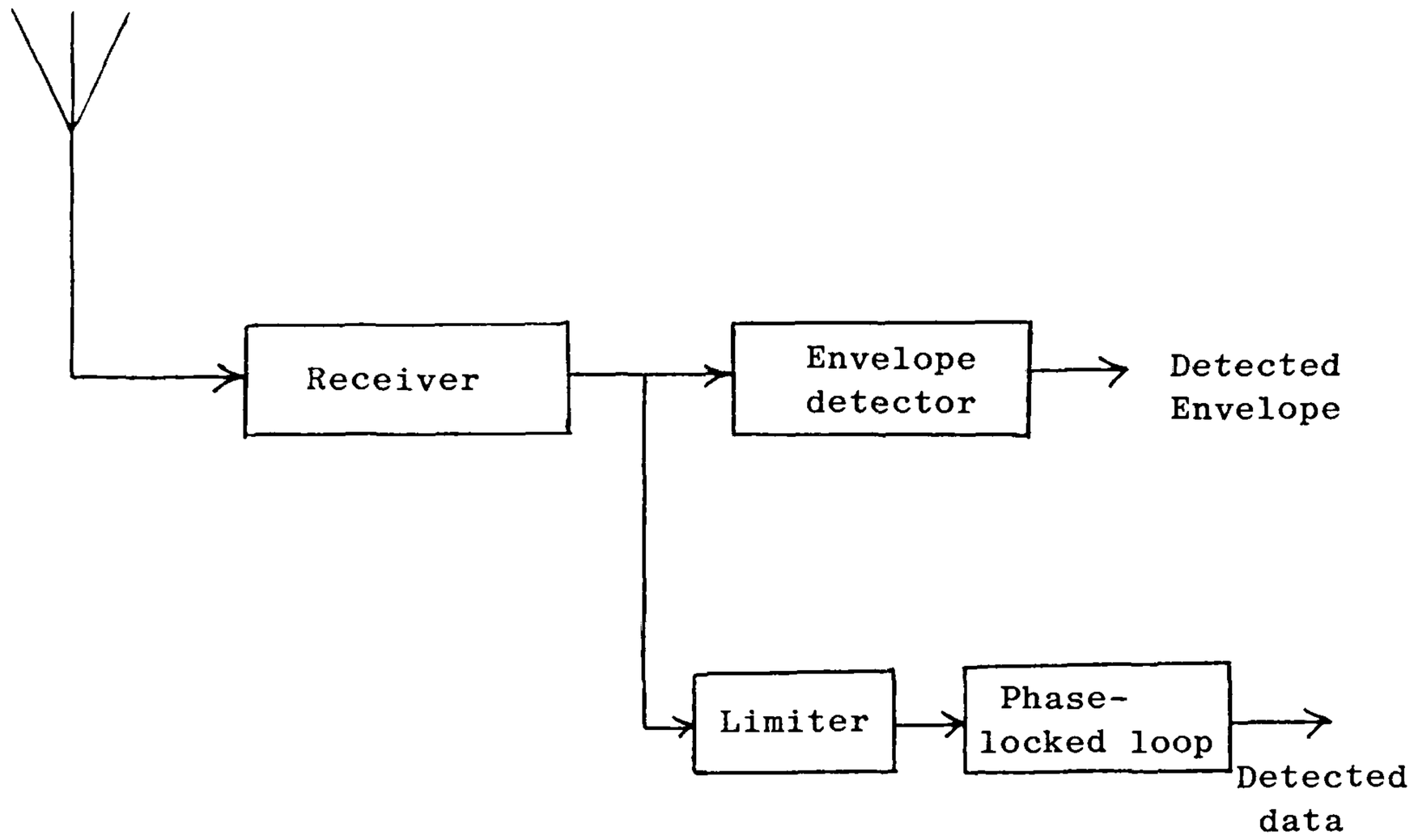

Fig. 3.16 ZSFM receiver

display of network name (e.g. BBC LON for BBC Radio London), and also a display of the programme type such as news or music.

The importance of adding the additional data signal to the broadcast radio signals at m.f. and v.h.f. was considered by the BBC (4). However, according to their technique, at m.f. the data rate is limited to 30 bits/sec, while at v.h.f. the data signal can be added to the multiplex signal by modulating a subcarrier (located at the gaps in the spectrum of the conventional stereo multiplex signal) by the data signal. This BBC suggested system for v.h.f. has a data rate of 1187.5 bits/sec, while the ZSFM provides, in principle, a maximum data of 5 kbits/sec for medium wave broadcast.

It should be noted that the additional data signals are imperceptible to listeners with existing receivers and they cause no impairment to the main programme reception on existing receivers. However, suitably equipped future receivers will be able to detect and use the data signals in the aforementioned ways.

3.13 Final Remarks

It has been shown that in principle, ZSFM will permit the transmission of data signals at high rates to be superimposed on conventional DSB-AM signal without introducing envelope distortion or increasing the bandwidth. The different possible applications of ZSFM

have been discussed where the facilities it would offer for automatic tuning and the different control functions would be significant steps forward in making the best use of the available broadcast channels.

In practice the effects of cross-talk between AM and FM channels due to propagation and IF filtering at the receiver may affect the ZSFM technique. This will be studied fully in Chapter 5 where a computer simulation is developed. The FM function imposed on the carrier will be truncated within a finite time window in a practical transmitter. This situation will be viewed and investigated in Chapter 5.

CHAPTER 4

ZERO DETECTION AND COMPLEX FILTERING

4.1 Introduction

In the last chapter, zero conjugation of a real signal was discussed, but in order to implement zero conjugation the complex zeros must be detected first. This chapter introduces the fundamental idea of complex filtering where the complex zeros of a real signal are transformed into easily detected real zeros. The impulse response of the complex filter is discussed together with possible realisations of a complex filter.

In principle, inspection of a signal's waveform sometimes can provide information on the location of its complex zeros, but yet the quantitative method for finding complex zeros involves the numerical factorisation of a trigonometric polynomial.

The means of zero detection may include a bank of complex filters having characteristics related to respective imaginary values of complex zeros and respective envelope detectors coupled to the filters for generating an output when a real zero occurs. Alternatively, the zero detection may be realised using digital signal processing techniques. It is shown that the complex filter can be envisaged as a series of differentiators which can be implemented using non-recursive digital filters.

4.2 Envelope Minima

It was shown in Section 3.2 that typically a com-

plex zero pair produces a dip in the envelope of the real signal s(t) at the corresponding instant of time. Also Section 3.3 described how the complex zeros of the complex elementary signal m(t) lie at the dips of the envelope m(t). A direct approach to locating the time of occurrence of the zeros is to find derivatives of the envelope. If the first derivative of the envelope is zero at a specific point then that point might be a minimum, a maximum, or an inflection point. However, the sign of the second derivative tells whether the envelope is concave upward (i.e. a minimum point) or concave downwards (i.e. a maximum point). If the second derivative is positive at that point at which the first derivative is zero then that point represents a minimum value. On the other hand negative second derivative means a maximum point. Figure 4.1 shows graphically the signal s(t) with its first and second derivatives where point B represents a minimum, point C an inflection point, and point D a maximum point.

The signal s(t) is said to have a local or relative minimum at point $t = t_1$ if $s(t_1) < s(t_1+h)$ for all positive and negative values of h sufficiently near zero (20). Local minimum is used to distinguish such a point from an absolute minimum which would happen at $t = t_1$ if $s(t_1) < s(t)$ for all t as shown in Figure 4.2.

However, the detection of complex zeros by observing the envelope minima is misleading due to the possibility of having more than one complex zero pair corresponding to the same envelope trough.

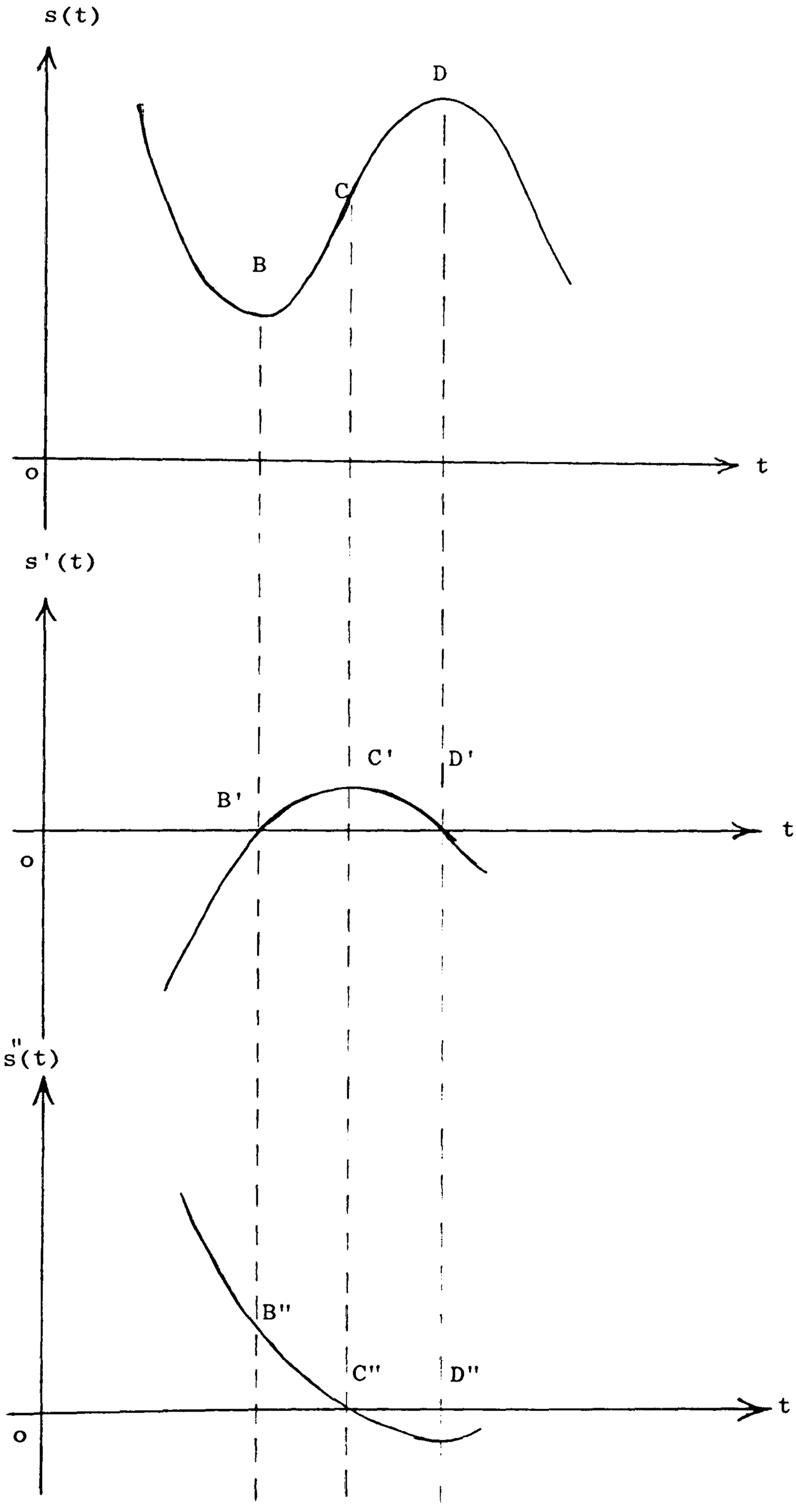

Fig. 4.1

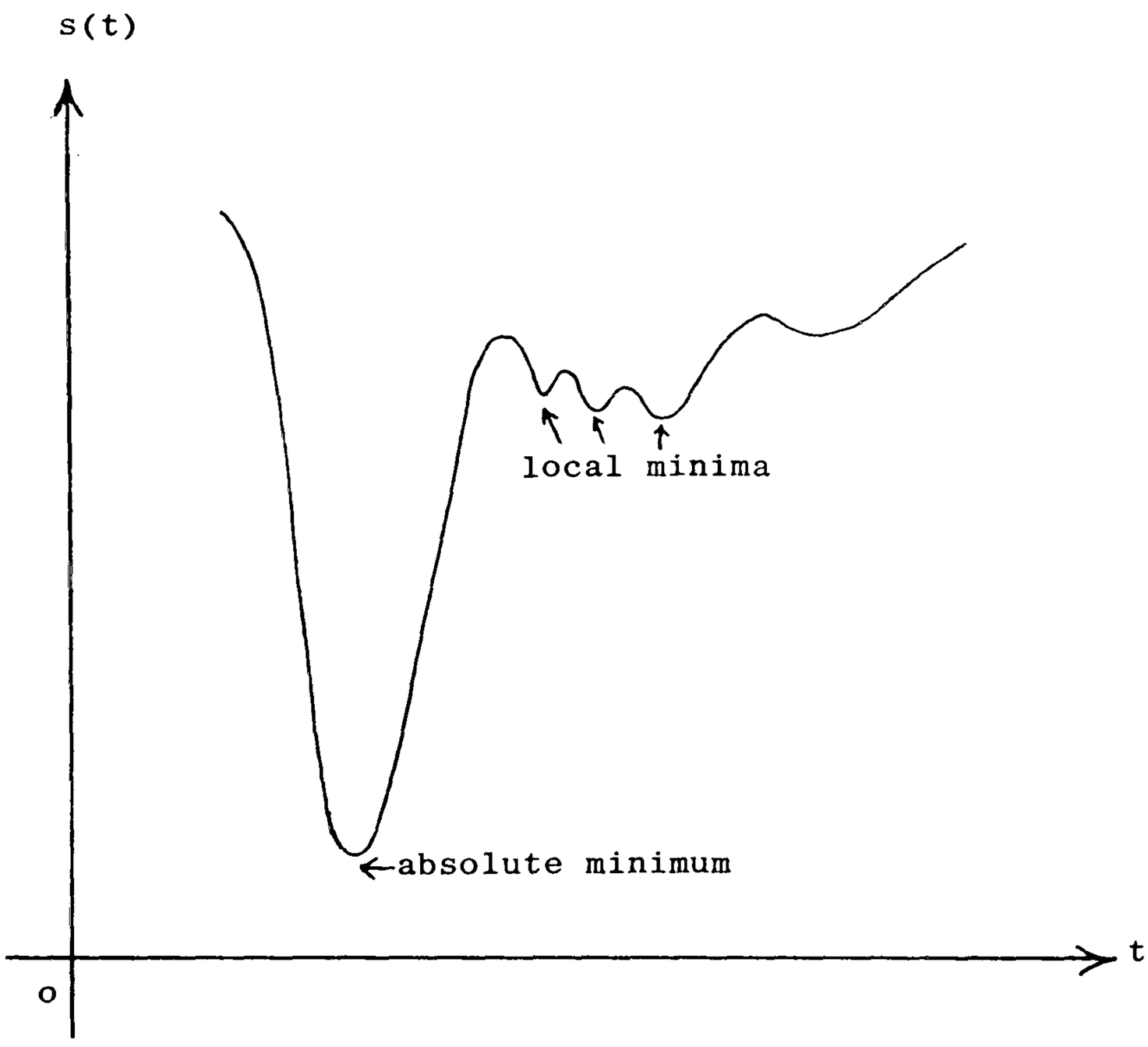

Fig. 4.2

Example:

Let us consider the positive real signal s(t) of the form:

$$s(t) = (1 - a\, e^{j\Omega t})(1 - a\, e^{-j\Omega t})(1 - b\, e^{j\Omega t})(1 - b\, e^{-j\Omega t})$$

$$0 < a < 1\ ,\ 0 < b < 1\ ,\ b < a \qquad (4.1)$$

The z-plane zeros of s(t) are given by the zeros of the factors as:

$(1 - a\, e^{j\Omega t})$ has a zero at $z = \frac{1}{a}$

$(1 - a\, e^{-j\Omega t})$ has a zero at $z = a$

} reciprocal zero-pair

$(1 - b\, e^{j\Omega t})$ has a zero at $z = \frac{1}{b}$

$(1 - b\, e^{-j\Omega t})$ has a zero at $z = b$

} reciprocal zero-pair

Figure 4.3 shows the z-plane zeros and the corresponding x-plane zeros of s(t) as given by eqn. (4.1).

The signal s(t) can be rewritten in the form:

$$s(t) = (1 + a^2 - 2\, a \cos\Omega t)\ (1 + b^2 - 2\, b \cos\Omega t) \qquad (4.2)$$

Figure 4.4 shows 5 cycles of s(t) as given above and it is apparent by comparison with Figure 4.3 that at every envelope dip there are two complex zero pairs. It is also evident that the added zero pair has the effect of sharpening the maximum edge of s(t), and in the limit when the number of complex zero pairs per period of s(t) is unbounded then the maximum edge of s(t) becomes a cusp point and s(t) a non-bandlimited periodic signal. The envelope minima technique is therefore not an efficient way of determining the complex zeros.

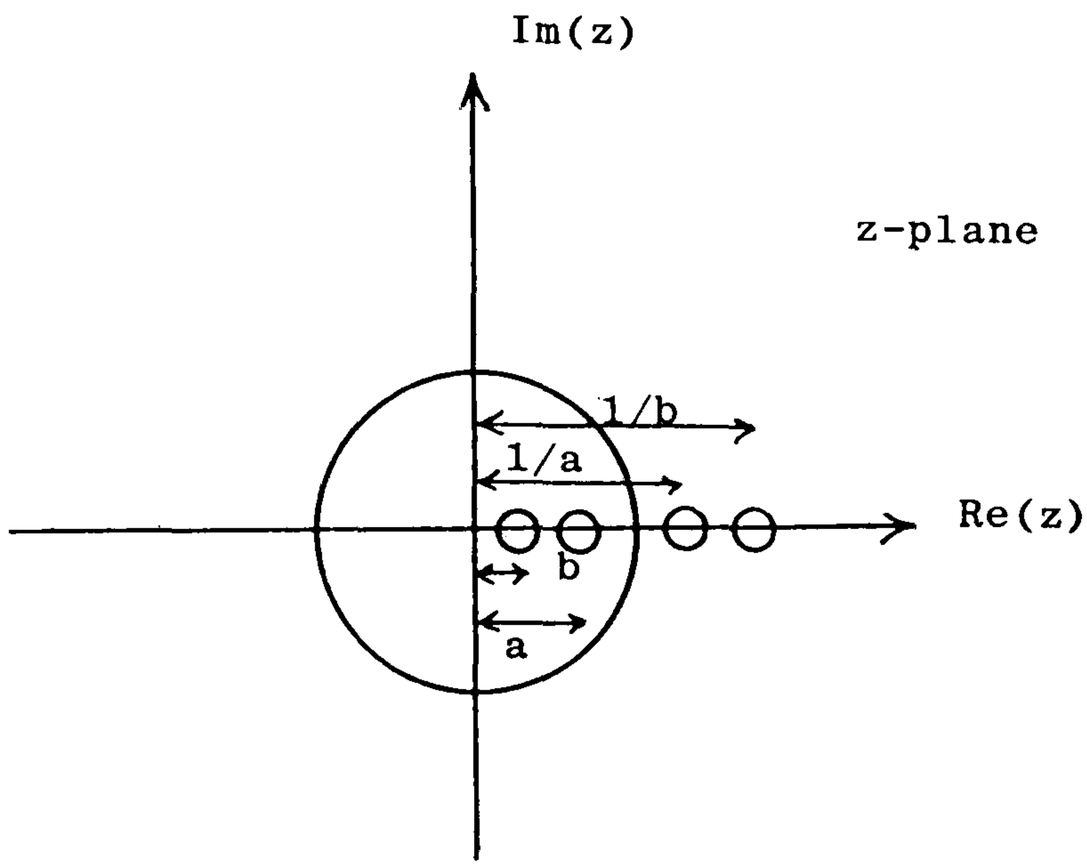

z-plane zeros of s(t)

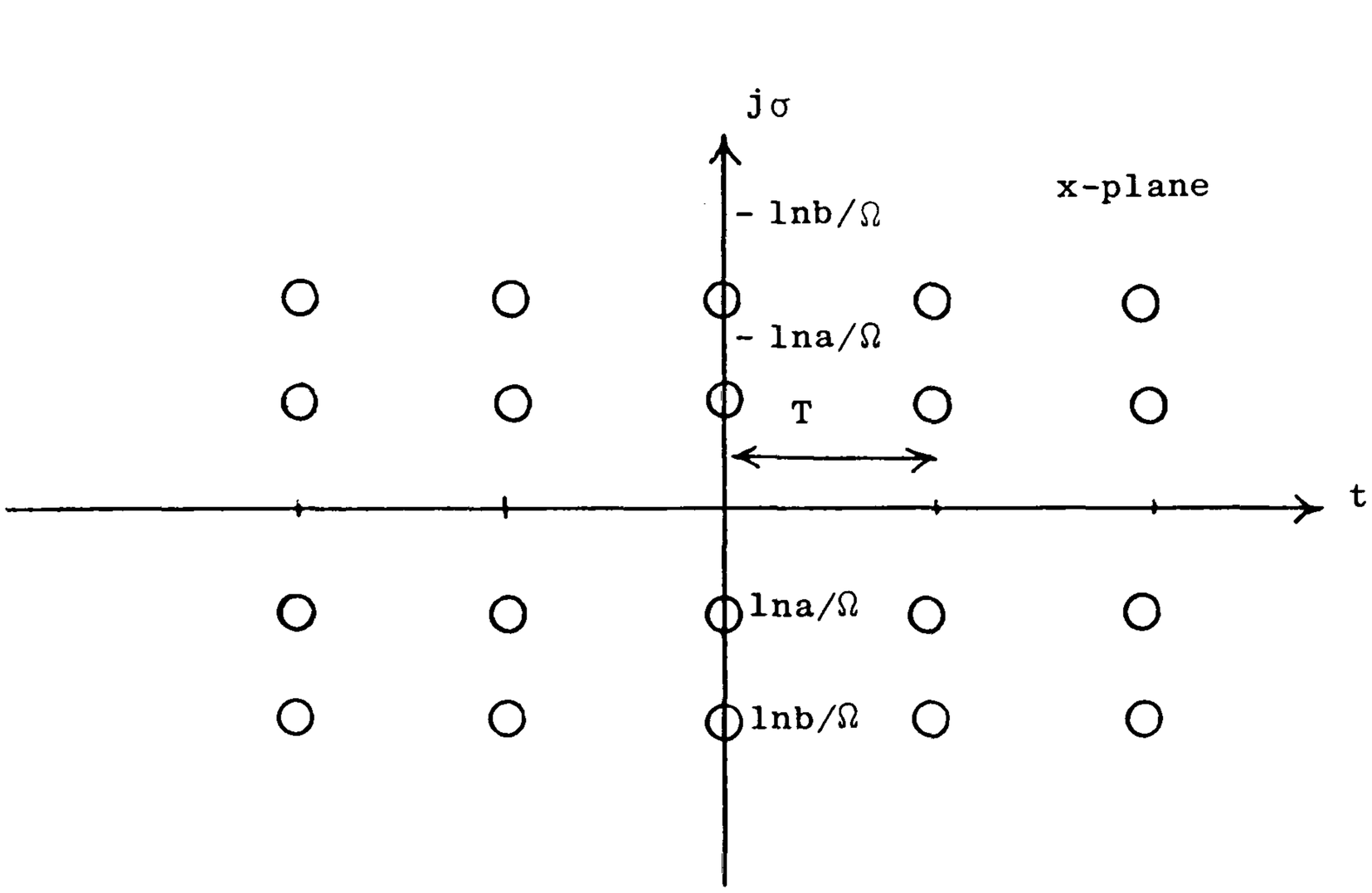

x-plane zeros of s(t)

Fig. 4.3

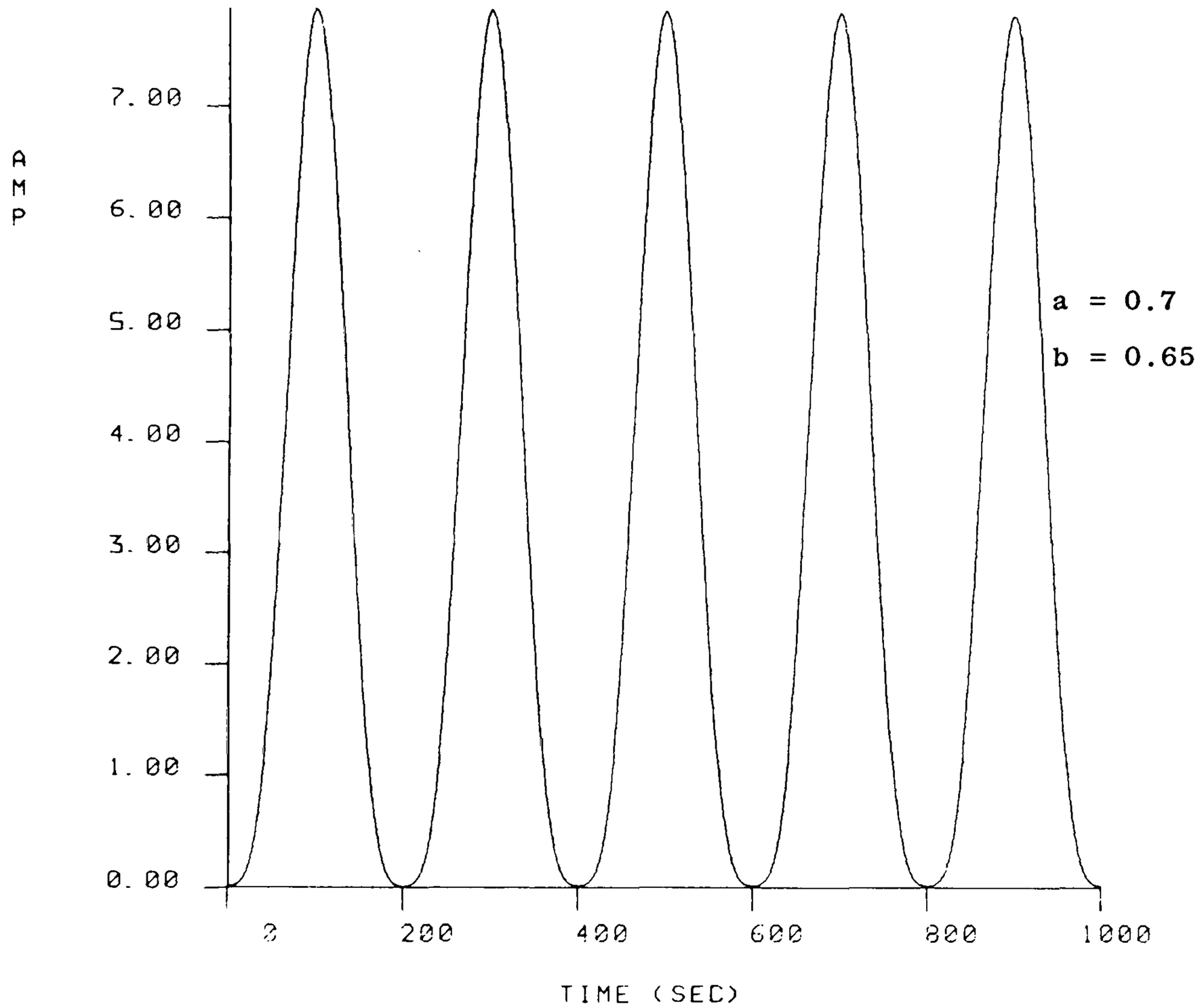

Fig. 4.4 Five cycles of s(t)

Now let us consider another situation in which one of the zero pairs of s(t) given by eqn. (4.1) has shifted slightly and changed its position. This results in considering s(t) as follows:

$$s(t) = (1-a\ e^{jd}e^{j\Omega t})(1-a\ e^{-jd}e^{-j\Omega t})(1-b\ e^{j\Omega t})(1-b\ e^{-j\Omega t}) \quad (4.3)$$

$$0 < a < 1\ ,\ 0 < b < 1\ ,\ b < a$$

where d is a real constant and represents the shift in radians.

$(1 - a\ e^{jd}e^{j\Omega t})$ has a zero at $z = \frac{1}{a}e^{-jd}$

$(1 - a\ e^{-jd}e^{-j\Omega t})$ has a zero at $z = a\,e^{-jd}$

} reciprocal zero-pair

Figure 4.5 shows the z-plane zeros of s(t) and also the x-plane zeros (found by substituting $z = e^{j\Omega x}$ and solving for x as mentioned before) of the signal s(t). The signal s(t) as given by eqn. (4.3) can be written in the following way:

$$s(t) = [1 + a^2 - 2\ a\ \cos(\Omega t + d)][1 + b^2 - 2\ b\ \cos\Omega t] \quad (4.4)$$

The effect of the shifted zero pair, through d radians, is another possible noticeable dip in the envelope of s(t).

Figure 4.6 shows 5 cycles of s(t) as given in eqn. (4.4) and for d = 0.9 radians and it can be seen that the extra dip caused by the shifted zero pair is not very noticeable.

Figure 4.7 shows 5 cycles of s(t) and for d = 1.4 radians, and it is apparent that the shifted zero pair has produced a noticeable extra dip in s(t).

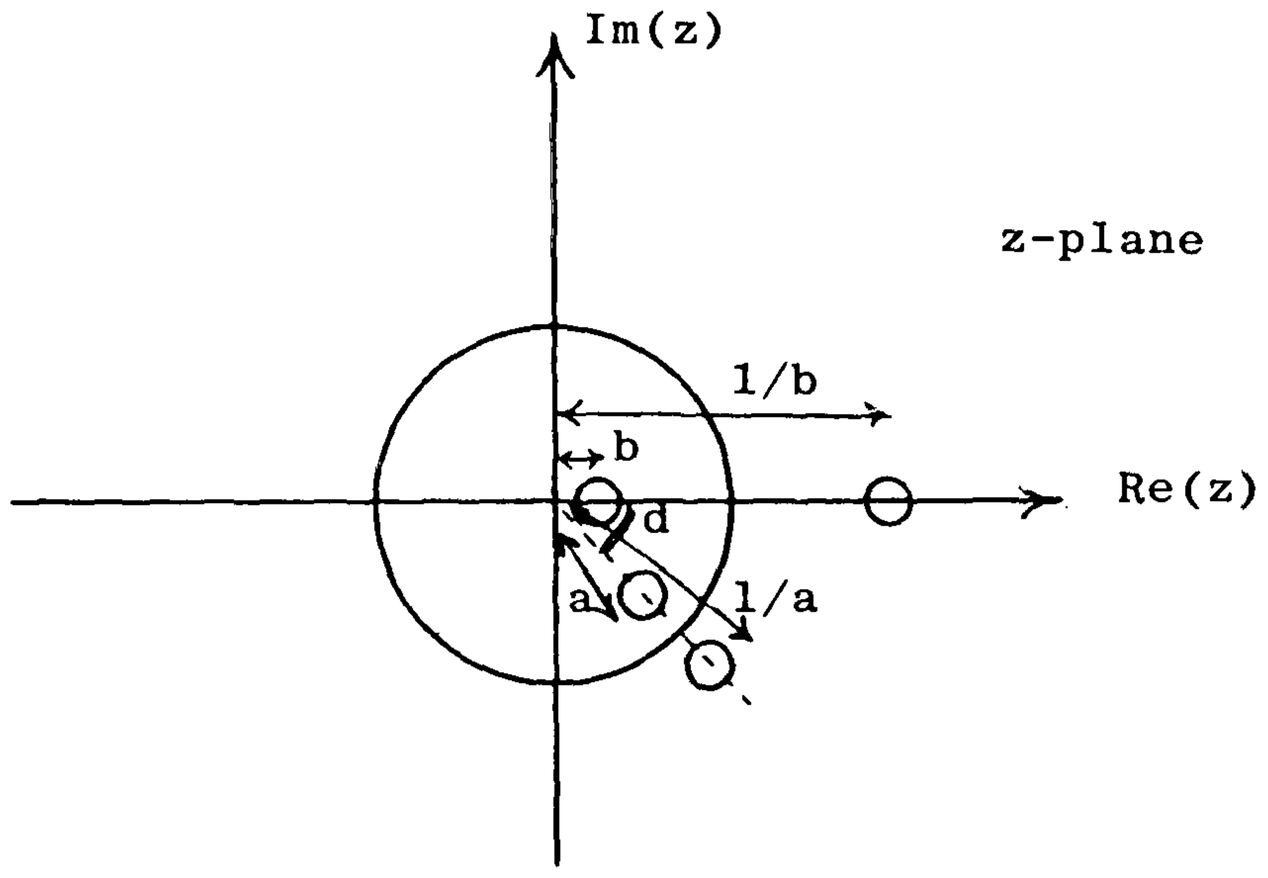

z-plane zeros of s(t)

x-plane zeros of s(t)

Fig. 4.5

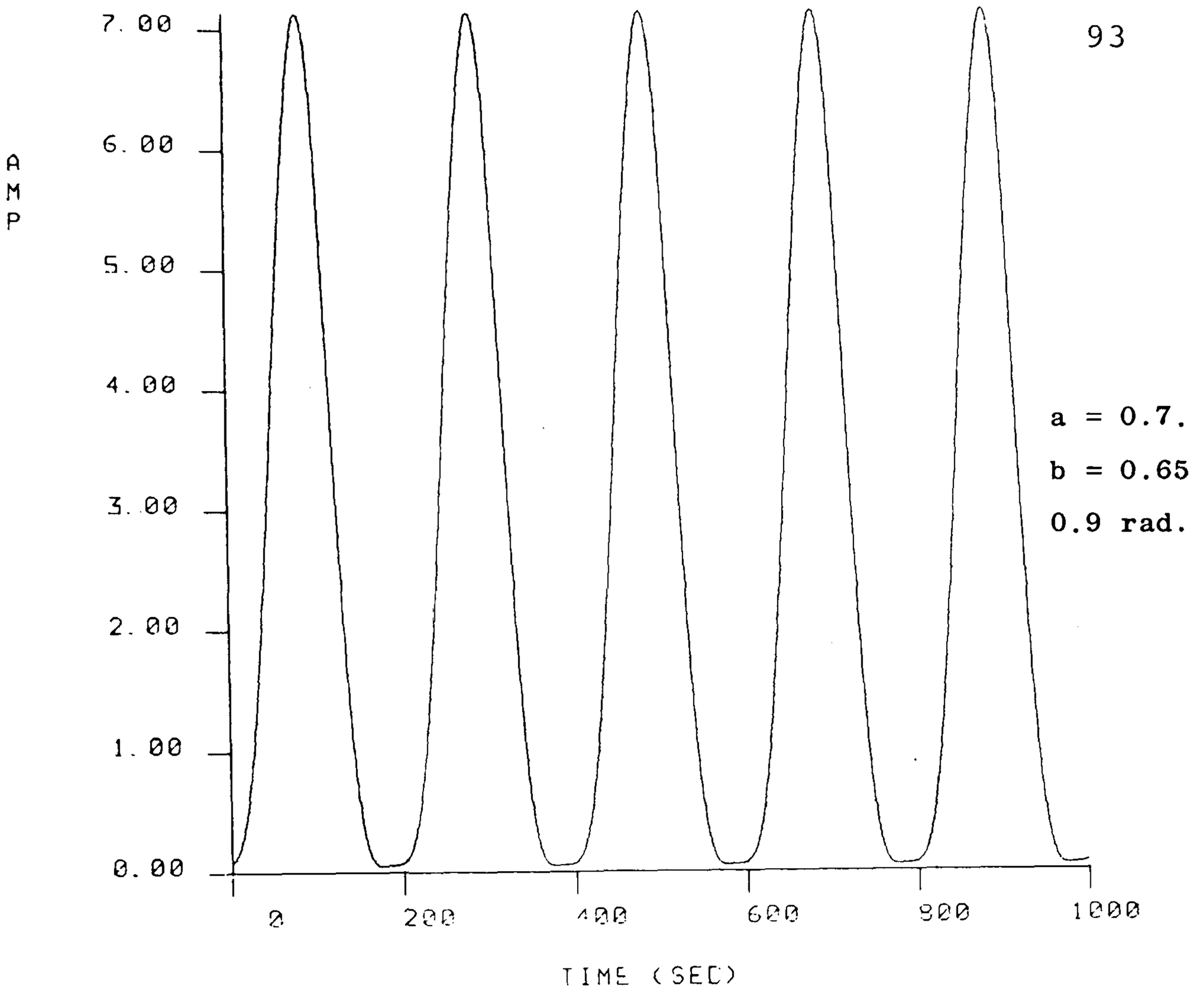

Fig. 4.6 s(t) for d = 0.9 rad.

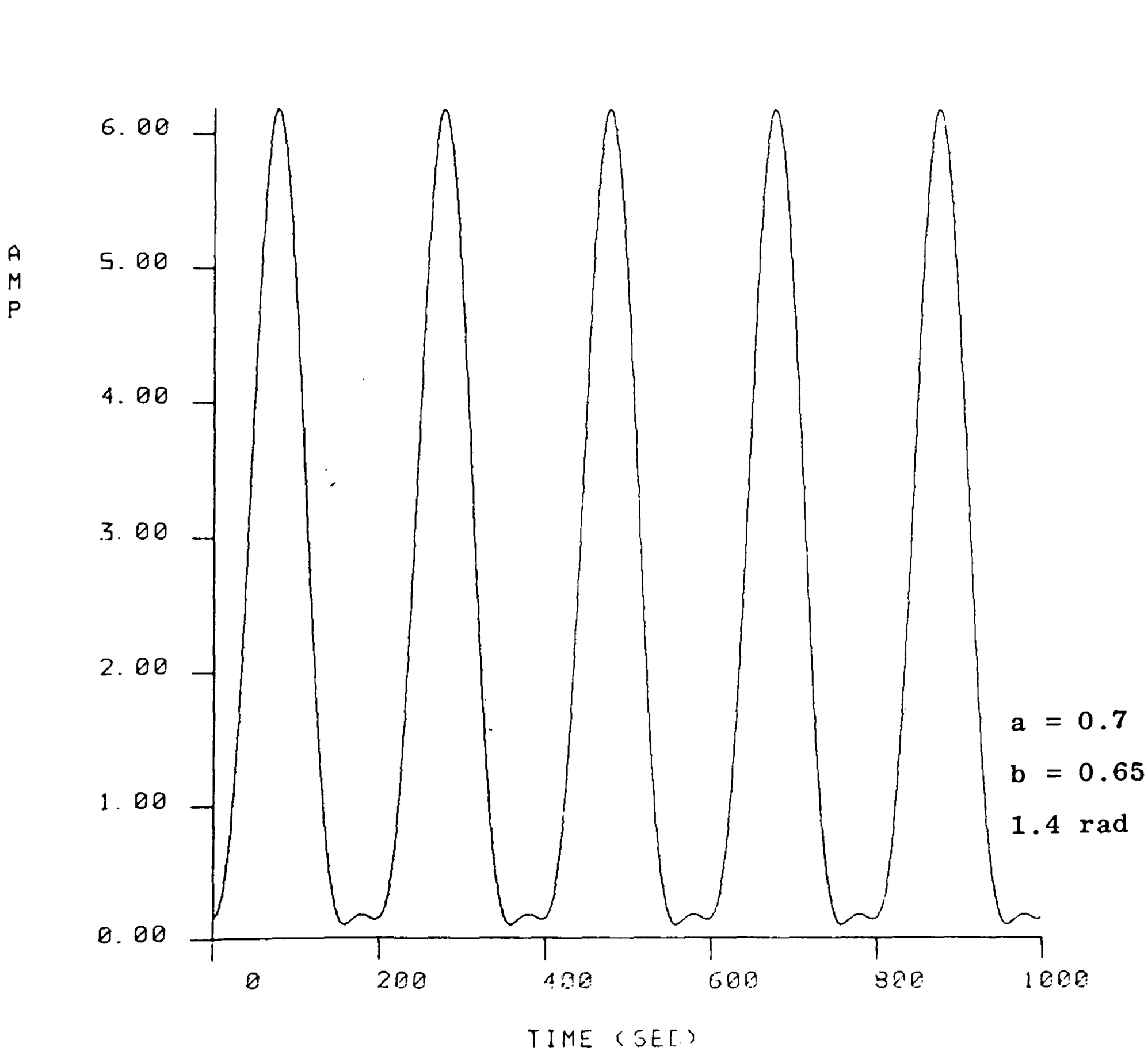

Fig. 4.7 s(t) for d = 1.4 rad.

Now it is possible to generalise the idea that to every dip of a positive real signal there must correspond at least one pair of complex zeros. However, when any two zero pairs get closer and occur nearby each other in real time, then the two envelope dips corresponding to each pair get less pronounced until they become a single dip when the two zero pairs coincide (i.e. occur at the same instant of time).

As a final comment it is apparent that detecting the envelope minima does not determine the complex zeros. In order to conjugate zero pairs, it is essential to determine both the time of occurrence of the zero pair (t_r) and the imaginary part of the complex zero (σ_r) as discussed in Chapter 3. Hence another approach for detecting the complex zeros should be utilised.

4.3 Complex Filters

This section describes how a complex filter transforms the complex zeros of a real signal into easily detected real zeros. Complex filters are derived with their transfer functions, while the possible realisations of complex filters are discussed in Section 4.5.

Given a real signal with complex conjugate zeros, the relation of the zeros of s(t) with those of $s(t - j\,\sigma_r)$ is considerd where σ_r is a real constant. Let the Fourier transforms of s(t) and $s(t - j\,\sigma_r)$ be S(f) and L(f) respectively, then by using the time-

translation property of the Fourier transform (21) it is possible to write:

$$L(f) = F[s(t - j\,\sigma_r)] = S(f)\; e^{-j2\pi f(j\,\sigma_r)}$$

$$= S(f)\; e^{2\pi f\sigma_r}$$

$$= S(f)\; H_{\sigma_r}(f) \qquad (4.5)$$

where $H_{\sigma_r}(f)$ represents a transfer function of a filter which is complex due to its asymmetrical frequency response. The impulse response of this filter is complex and can be implemented in a number of ways as will be discussed. Figure 4.8 shows frequency responses of the complex filter for positive and negative values of σ_r. Thus $s(t - j\,\sigma_r)$ can be obtained by passing $s(t)$ through a complex filter with transfer function $H_{\sigma_r}(f)$ as shown by eqn. (4.5). If σ_r is chosen to be equal to the ordinate value of the complex zero of $s(t)$, then $s(t - j\,\sigma_r)$ has a real zero at the same real time position as the following example shows.

<u>Example:</u> Consider the real signal $s(t)$:

$$s(t) = (1 - a\,e^{-j0.1}e^{j\Omega t})(1 - a\,e^{j0.1}e^{-j\Omega t}),\quad a < 1$$

$(1 - a\,e^{-j0.1}e^{j\Omega t})$ has a z-plane zero at $z = \frac{1}{a}e^{j0.1}$

$(1 - a\,e^{j0.1}e^{-j\Omega t})$ has a z-plane zero at $z = ae^{j0.1}$

} reciprocal zero-pair

$(1 - a\,e^{-0.1}e^{j\Omega t})$ has x-plane zero at $x = \frac{0.1 + 2m\pi}{\Omega} - j\frac{\ln a}{\Omega}$

$(1 - a\,e^{j0.1}e^{-j\Omega t})$ has x-plane zero at $x = \frac{0.1 + 2m\pi}{\Omega} + j\frac{\ln a}{\Omega}$

} $m = 0, \pm 1, \pm 2,$

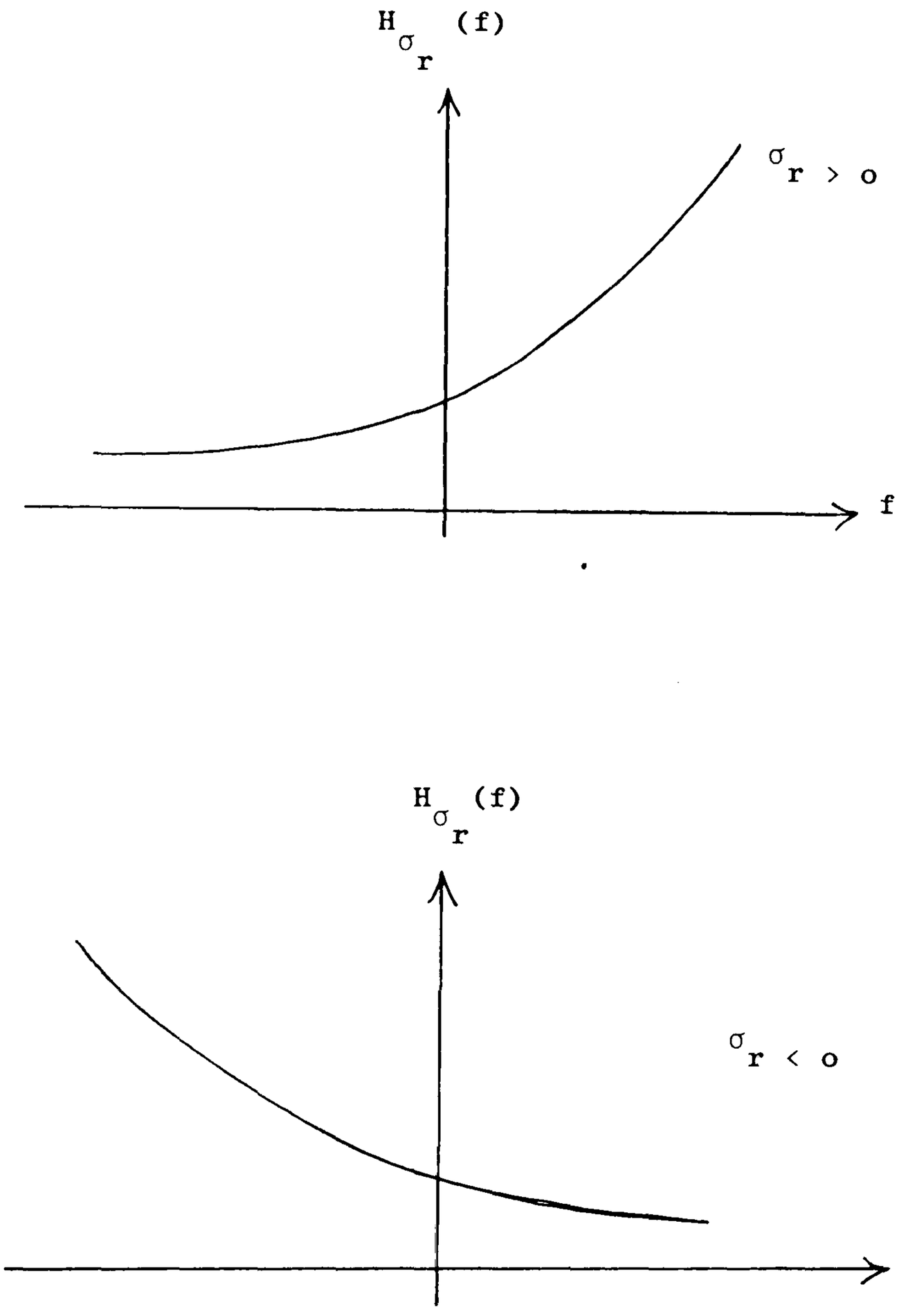

Frequency response of the complex filter

Fig. 4.8

Figure 4.9 shows both the z- and x-plane zeros of s(t). Now let σ_r be equal to the imaginary part of the zero of s(t), then $s(t - j\sigma_r)$ becomes:

$$s(t - j\sigma_r) = (1 - a\, e^{-j0.1} e^{j\Omega(t-j\sigma_r)})(1 - a\, e^{j0.1} e^{j\Omega(t-j\sigma_r)})$$

On substituting $\sigma_r = -\frac{\ln a}{\Omega}$:

$$s(t-j\sigma_r) = (1 - a\, e^{-j0.1} e^{-\ln a} e^{j\Omega t})(1 - a\, e^{j0.1} e^{\ln a} e^{-j\Omega t})$$

$$= (1 - a\tfrac{1}{a} e^{-j0.1} e^{j\Omega t})(1 - a.a\, e^{j0.1} e^{-j\Omega t})$$

$$= (1 - e^{-j0.1} e^{j\Omega t})(1 - a^2 e^{j0.1} e^{-j\Omega t}) \qquad (4.6)$$

$(1 - e^{-j0.1} e^{j\Omega t})$ has a z-plane zero at $z = e^{j0.1}$

$(1 - a^2\, e^{j0.1} e^{-j\Omega t})$ has a z-plane zero at $z = a^2 e^{j0.1}$

Note that the z-plane zeros of $s(t - j\sigma_r)$ are not reciprocals as those of s(t).

$(1 - e^{-j0.1} e^{j\Omega t})$ has x-plane at $x = \frac{0.1 + 2m\pi}{\Omega}$

$(1 - a^2\, e^{j0.1} e^{-j\Omega t})$ has x-plane zero at $x = \frac{0.1+2m}{\Omega} - j2\frac{\ln a}{\Omega}$ $\Big\}$ m=0, ±1, ±2,..

The x-plane zeros are not complex conjugates as those of s(t). Figure 4.10 shows both the z- and x-plane zeros of $s(t - j\sigma_r)$.

The following points emerge:

i) $s(t - j\sigma_r)$ is a complex signal as its complex zeros do not occur in conjugate pairs as shown above. This is because of the effect of the complex filter $H_{\sigma_r}(f)$ which converts the real signal s(t) into the complex signal $s(t - j\sigma_r)$.

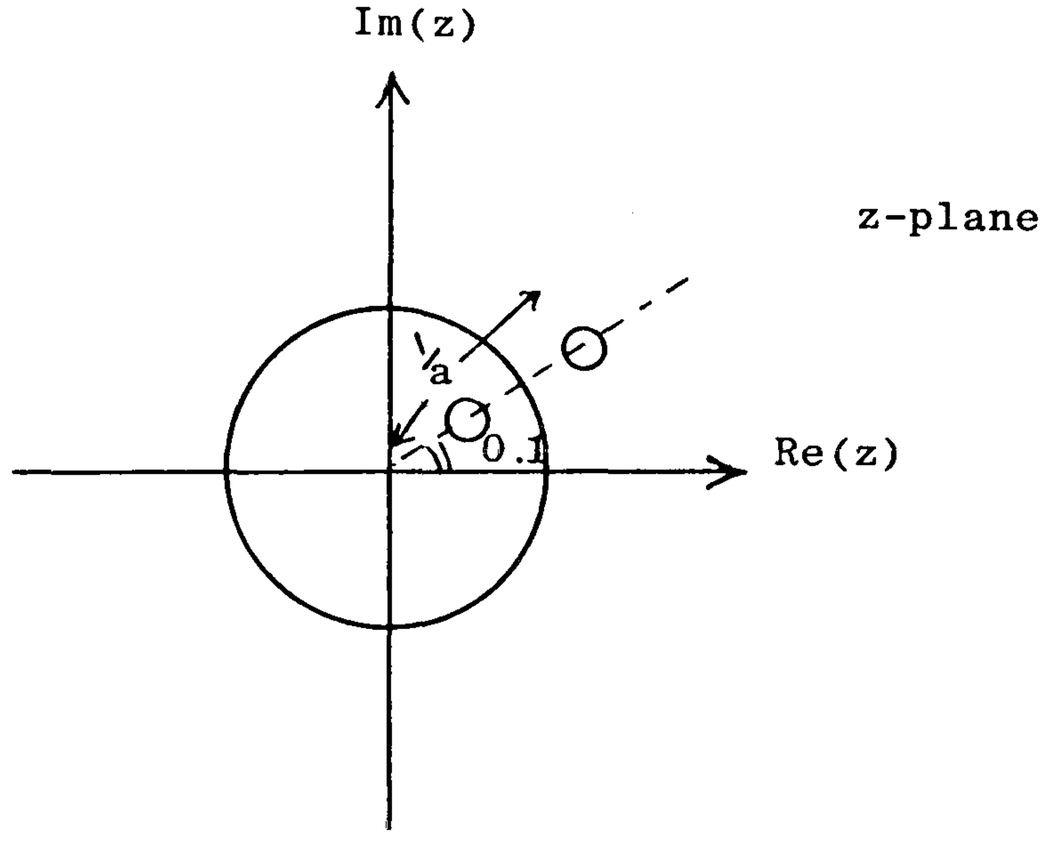

z-plane zeros of s(t)

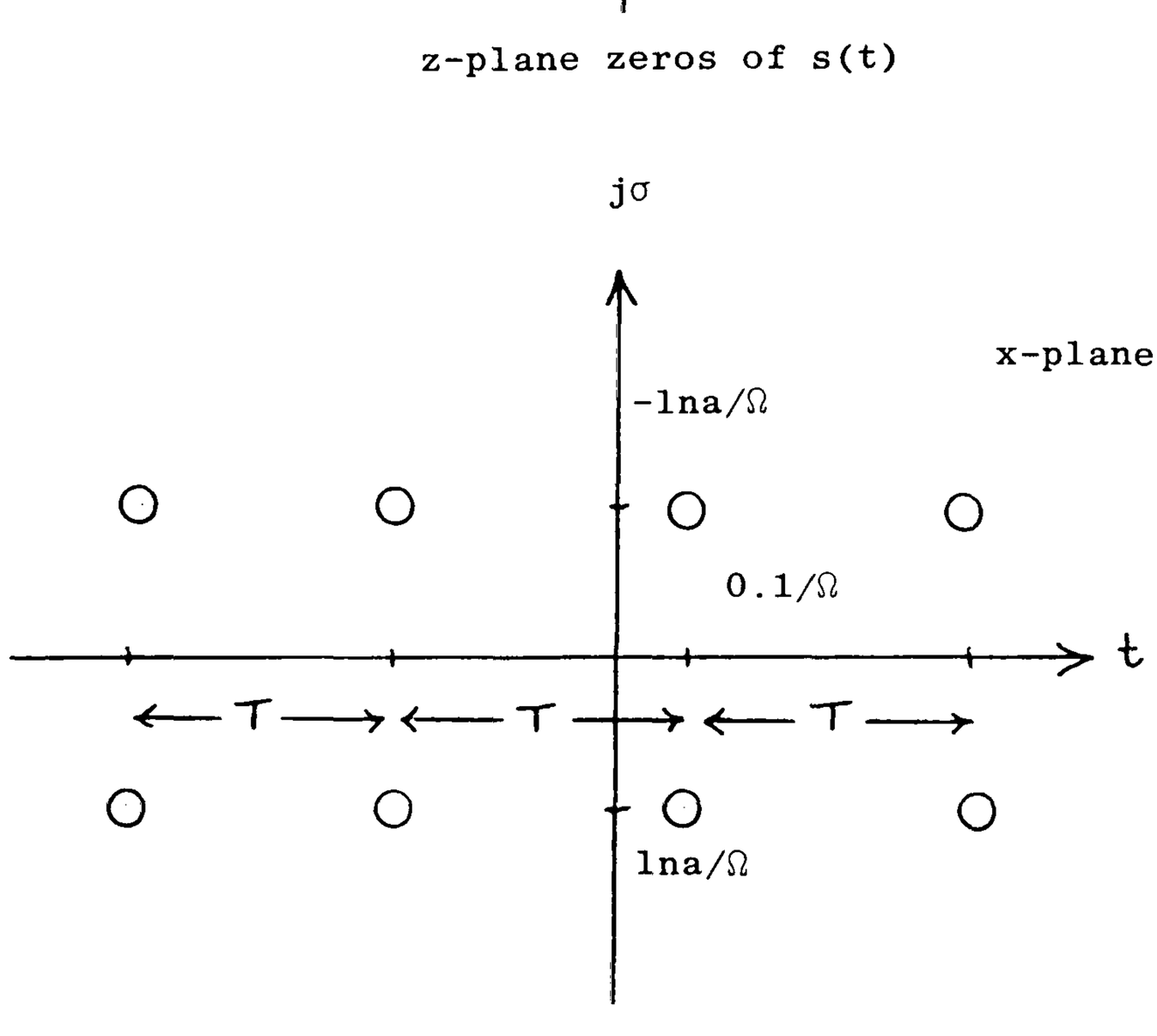

x-plane zeros of s(t)

Fig. 4.9

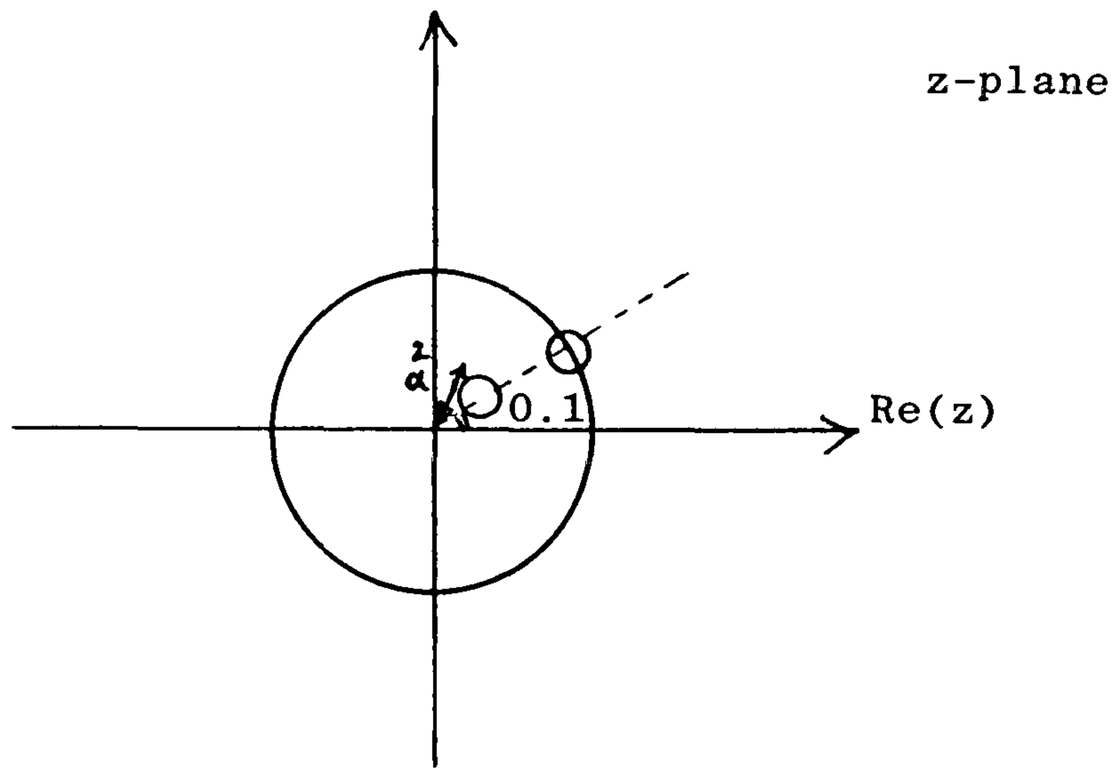

z-plane zeros of $s(t-j\sigma_r)$

x-plane zeros of $s(t-j\sigma_r)$

Fig. 4.10

ii) It is clear that one of the complex zeros of s(t) has changed into a real zero at the same real time position after being passed through the complex filter. However, the vertical separation between the zeros of $s(t - j\sigma_r)$ is still $2\frac{\ln a}{\Omega}$.

iii) It is therefore possible for a complex filter $H_{\sigma_r}(f)$ to convert one of the complex zeros at $x = t_r \pm j\sigma_r$ into a real zero at $x = t_r$. In other words a complex zero pair of ordinate value $\pm \sigma_r$ can be detected whenever the envelope of $s(t - j\sigma_r)$ has a real zero.

iv) In practice we need a bank of such complex filters, each designed to detect a zero with different σ_r value or range of σ_r, so that different complex zeros can be detected. At the output of each complex filter there is a real zero detector which envelope detects the output of the complex filter as was described in Section 3.11. To understand how the real zeros of the envelope of $s(t - j\sigma_r)$ correspond to the complex zeros of s(t) consider the signal:

$$s(t) = 1 + a^2 - 2a\cos\Omega t$$

The x-plane zeros of s(t) above are given by:

$$x = \frac{2m\pi}{\Omega} \pm j\frac{\ln a}{\Omega}, \quad m = 0, \pm 1, \pm 2, \ldots$$

as found in Section 3.5

The complex filtered signal is:

$$s(t - j\sigma_r) = 1 + a^2 - 2\,a\,\cos\Omega(t - j\sigma_r)$$

$$= 1 + a^2 - 2a[\cos\Omega t \cos j\Omega\sigma_r + \sin\Omega t \sin j\Omega\sigma_r]$$

Using the relations cosjy = coshy, sinjy = j sinhy the above can be written as:

$$s(t - j\sigma_r) = 1 + a^2 - 2a[\cos\Omega t \cosh\Omega\sigma_r + j \sin\Omega t \sinh\Omega\sigma_r] \quad (4.7)$$

Now taking the modulus of $s(t - j\sigma_r)$ gives:

$$|s(t-j\sigma_r)| = \sqrt{(1+a^2-2a\cos\Omega t \cosh\Omega\sigma_r)^2 + (2a\sin\Omega t \sinh\Omega\sigma_r)^2} \quad (4.8)$$

The above is never negative.

If $\sigma_r = \frac{\ln a}{\Omega}$, then $\cosh\Omega\sigma_r = \cosh(\ln a) = \frac{e^{\ln a} + e^{-\ln a}}{2} = \frac{1+a^2}{2a}$

and also if $t = \frac{2m\pi}{\Omega}$, $m = 0, \pm 1, \pm 2, \ldots$ then $\sin\Omega t = 0$

and the modulus becomes:

$$|s(t - j\sigma_r)| = \sqrt{(1 + a^2 - 2a\,\frac{1+a^2}{2a})^2} = 0$$

which is a real zero corresponding to the complex zero of s(t). For $\sigma_r \neq \frac{\ln a}{\Omega}$ the envelope is always non-zero and therefore there are no extra real zeros of $|s(t - j\sigma_r)|$ that do not correspond to complex zeros of s(t). A plot of $|s(t - j\sigma_r)|$ is shown in Section 5.9.

v) Most of the zeros of bandlimited signals are close to the real axis ([18]), and hence zeros with very high σ_r values can be neglected, restricting the required number of complex filters. An important point which will be considered is the increment between successive values of σ_r in the bank of filters.

4.4 Impulse Response

The impulse response of the complex filter discussed in the last section will be derived, and a a practical bandlimited version of the complex filter described. Given the transfer function of the complex filter $H_{\sigma_r}(f)$, the impulse response can be found by taking the inverse Fourier transform of $H_{\sigma_r}(f)$. From eqn. (4.5):

$$H_{\sigma_r}(f) = e^{2\pi f\sigma_r}$$

$$\therefore h_{\sigma_r}(t) = \int_{-\infty}^{\infty} H_{\sigma_r} e^{j2\pi ft}\, df$$

$$= \int_{-\infty} e^{2\pi f\sigma_r} e^{j2\pi ft}\, df$$

$$= \int_{-\infty}^{\infty} e^{j2\pi f(t-j\sigma_r)}\, df \qquad (4.9)$$

Using the relation that a delta-function and 1 are a Fourier transform pair, then eqn. (4.9) above becomes:

$$\therefore h_{\sigma_r}(t) = \delta(t - j\sigma_r) \qquad (4.10)$$

However, the effective complex filter transfer function is bandlimited within a finite frequency range (say $\pm f_c$ Hz), then the bandlimited version of the complex filter has a transfer function as

$$H_c(f) = e^{2\pi f\sigma_r}\ \mathrm{rect}\left(\frac{f}{2f_c}\right) \qquad (4.11)$$

where $\text{rect}\left(\frac{f}{2f_c}\right) = \begin{cases} 1, & |f/2f_c| \leq \frac{1}{2} \\ 0, & \text{otherwise} \end{cases}$

Figure 4.11 shows the transfer function of the bandlimited version of the complex filter, where f_c gives the cut-off frequency of the filter. In practice, if the filter is designed to detect complex zeros of speech signals then f_c may be chosen as 5 kHz. The impulse response of the bandlimited version of the filter can be obtained by taking the inverse Fourier transform of $H_c(f)$ as given by eqn. (4.11), i.e.

$$h_c(t) = \int_{-\infty}^{\infty} H_c(f)\, e^{j\omega t}\, df$$

$$= \int_{-f_c}^{f_c} H_c(f)\, e^{j2\pi ft}\, df$$

$$= \int_{-f_c}^{f_c} e^{2\pi f\sigma_r}\, e^{j2\pi ft}\, df$$

$$= \int_{-f_c}^{f_c} e^{j2\pi f(t-j\sigma_r)}\, df$$

$$H_c(f) = e^{2\pi f\sigma_r}\ \mathrm{rect}(f/2f_c)$$

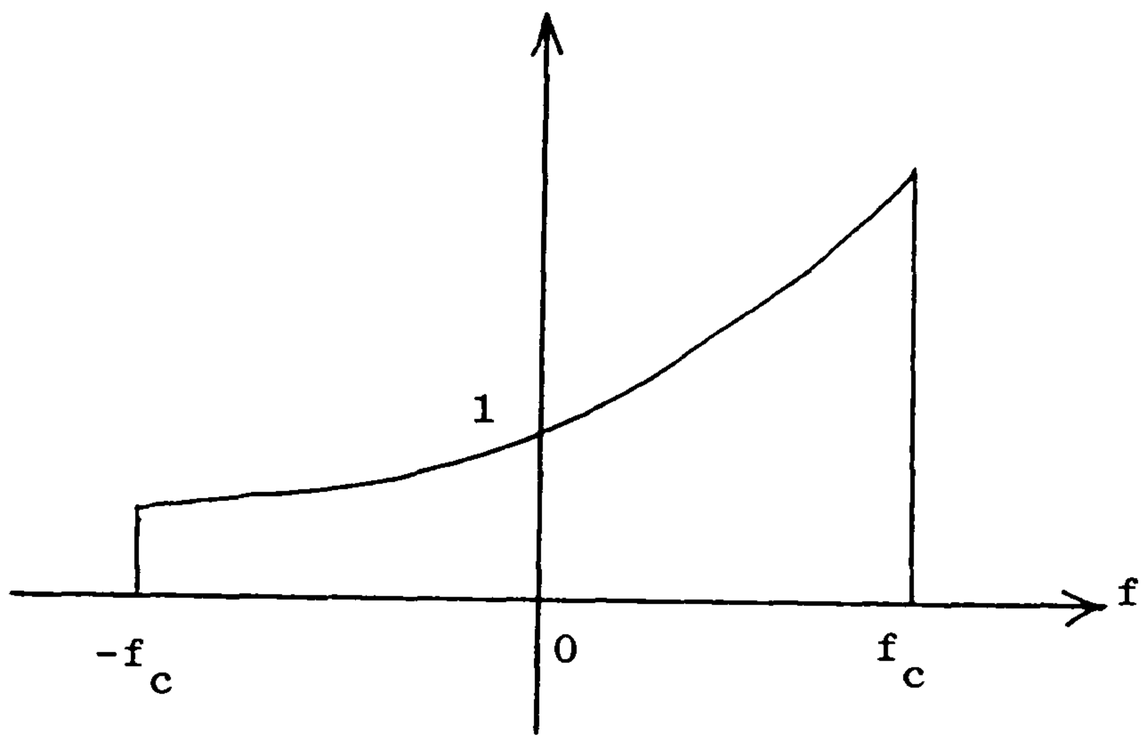

Fig. 4.11

Bandlimited version of the complex filter.

$$= \left[\frac{e^{j2\pi f(t-j\sigma_r)}}{j2\pi(t-j\sigma_r)} \right]_{-f_c}^{f_c}$$

$$= \frac{e^{j2\pi f_c(t-j\sigma_r)} - e^{-j2\pi f_c(t-j\sigma_r)}}{j2\pi(t-j\sigma_r)}$$

$$= \frac{\sin[2\pi f_c(t-j\sigma_r)]}{\pi(t-j\sigma_r)} = \frac{\sin[\omega_c(t-j\sigma_r)]}{\pi(t-j\sigma_r)}$$

$$= \frac{\sin\omega_c t \cos j\omega_c\sigma_r - \cos\omega_c t \sin j\omega_c\sigma_r}{\pi(t-j\sigma_r)} \qquad (4.12)$$

$$h_c(t) = \frac{\cosh\omega_c\sigma_r \sin\omega_c t - j \sinh\omega_c\sigma_r \cos\omega_c t}{\pi(t-j\sigma_r)} \qquad (4.13)$$

$$h_c(t) = \frac{[\cosh\omega_c\sigma_r \sin\omega_c t - j \sinh\omega_c\sigma_r \cos\omega_c t][t + j\sigma_r]}{\pi(t^2 + \sigma_r^2)}$$

If $h_c(t) = r(t) + j\, q(t)$, where $r(t)$ and $q(t)$ are real functions of time, then:

$$\left.\begin{aligned} r(t) &= \frac{t \sin\omega_c t \cosh\omega_c\sigma_r + \sigma_r \sinh\omega_c\sigma_r \cos\omega_c t}{\pi(t^2 + \sigma_r^2)} \\ q(t) &= \frac{\sigma_r \sin\omega_c t \cosh\omega_c\sigma_r - t \sinh\omega_c\sigma_r \cos\omega_c t}{\pi(t^2 + \sigma_r^2)} \end{aligned}\right\} \qquad (4.14)$$

It should be noted that $r(t)$ is an even function of time as $r(t) = r(-t)$, and $q(t)$ is odd as $q(t) = -q(-t)$. It will be shown that the real and imaginary parts of the impulse response have amplitude and frequency variations and the envelope diminishes with $|t|$.

Let $A = \cosh\omega_c\sigma_r$, $B = \sigma_r \sinh\omega_c\sigma_r$ then $r(t)$ can be written as follows:

$$r(t) = \frac{A\ t\ \sin\omega_c t + B\ \cos\omega_c t}{\pi(t^2 + \sigma_r^2)}$$

$$r(t) = \frac{\sqrt{(At)^2 + B^2}}{\pi(t^2 + \sigma_r^2)} \left[\frac{At}{\sqrt{(At)^2 + B^2}} \sin\omega_c t + \frac{B}{\sqrt{(At)^2 + B^2}} \cos\omega_c t \right]$$

$$= \frac{\sqrt{(At)^2 + B^2}}{\pi(t^2 + \sigma_r^2)} [\sin\phi(t)\sin\omega_c t + \cos\phi(t)\cos\omega_c t]$$

$$= \frac{\sqrt{(At)^2 + B^2}}{\pi(t^2 + \sigma_r^2)} \cos[\omega_c t - \phi(t)] \qquad (4.15)$$

where $\phi(t) = \arctan\left(\frac{At}{B}\right)$

Thus r(t) has amplitude variations as well as frequency variation, imposed by $\phi(t)$, but the frequency variation is nearly negligible because $\phi(t)$ changes very slowly compared to $(\omega_c t)$. Also, r(t) diminishes with time. Similarly, q(t) can be analysed by letting $C = \sigma_r \cosh\omega_c\sigma_r$, $D = \sinh\omega_c\sigma_r$ in eqn. (4.14).

$$q(t) = \frac{C\ \sin\omega_c t - D\ t\ \cos\omega_c t}{\pi(t^2 + \sigma_r^2)}$$

$$= \frac{\sqrt{C^2 + (Dt)^2}}{\pi(t^2 + \sigma_r^2)} \left[\frac{C}{\sqrt{C^2 + (Dt)^2}} \sin\omega_c t - \frac{Dt}{\sqrt{C^2 + (Dt)^2}} \cos\omega_c t \right]$$

$$= \frac{\sqrt{C^2 + Dt)^2}}{\pi(t^2 + \sigma_r^2)} [\cos\phi(t)\ \sin\omega_c t - \sin\phi(t)\ \cos\omega_c t]$$

$$= \frac{\sqrt{C^2 + (Dt)^2}}{\pi(t^2 + \sigma_r^2)} \sin[\omega_c t - \phi(t)] \qquad (4.16)$$

where $\phi(t) = \arctan\left(\frac{Dt}{C}\right)$

Therefore q(t) can be viewed as having envelope variation and frequency variation imposed by $\phi(t)$. The envelope diminishes as $|t|$ increases, and approaches zero in the limit when $|t| \to \infty$. A similar expression can be derived for the magnitude of the impulse response (i.e. $|h_c(t)|$).

Using equ.(4.13) we have:

$$\therefore \quad |h_c(t)| = \frac{\sqrt{\cosh^2 \omega_c \sigma_r \sin^2 \omega_c t + \sinh^2 \omega_c \sigma_r \cos^2 \omega_c t}}{\pi \sqrt{t^2 + \sigma_r^2}}$$

$$= \frac{\sqrt{(1 + \sinh^2 \omega_c \sigma_r) \sin^2 \omega_c t + \sinh^2 \omega_c \sigma_r \cos^2 \omega_c t}}{\pi \sqrt{t^2 + \sigma_r^2}}$$

$$= \frac{1}{\pi \sqrt{t^2 + \sigma_r^2}} \sqrt{\sin^2 \omega_c t + \sinh^2 \omega_c \sigma_r}$$

$$= \frac{\sinh \omega_c \sigma_r}{\pi \sqrt{t^2 + \sigma_r^2}} \sqrt{1 + \frac{\sin^2 \omega_c t}{\sinh^2 \omega_c \sigma_r}} \qquad (4.17)$$

For f_c = 5 kHz, σ_r = 100 μsec, $\sinh^2 \omega_c \sigma_r$ = 133.37, hence:

$$|h_c(t)| = \frac{3.68}{\sqrt{t^2 + 10^{-8}}} \sqrt{1 + \frac{\sin^2 \omega_c t}{133.37}}$$

The dependence of $|h_c(t)|$ on $\sin^2 \omega_c t$ is negligible for the values given above as the factor $\sqrt{1 + \frac{\sin^2 \omega_c t}{133.37}}$ varies between $1 \to 1.0037$ as $\sin^2 \omega_c t$ varies between $0 \to 1$. Hence for f_c = 5 kHz and $\sigma_r \geq$ 100 μsec the effect of the term $\sin^2 \omega_c t$ can be neglected and $|h_c(t)|$ approximated as:

$$|h_c(t)| \cong \frac{\sinh\omega_c\sigma_r}{\pi\sqrt{t^2 + \sigma_r^2}} \qquad (4.18)$$

Figures 4.12, 4.13 and 4.14 show the real part, the imaginary part, and the magnitude of the impulse response respectively for f_c = 5kHz and σ_r = 100 μseconds and it is clear that they all diminish with time.

4.5 Realisation of the Complex Filter

Some of the possible realisations of the complex filter, discussed in the last two sections, will be described in more detail.

a) Delay line approximation

The tapped delay line is one of the simplest ways of implementing the practical bandlimited version of the complex filter.

Although the impulse response of the complex filter is complex, having real and imaginary parts, each filter can be realised by two tapped delay lines having weights representing real and imaginary parts of the impulse response of the filter. The weights are obtained from the inverse Fourier transform of the filter transfer function which is equivalent to the impulse response. Each delay line is connected to a respective summer and a comparator can be used to indicate when both summers have zero sums implying a complex zero. Implementation

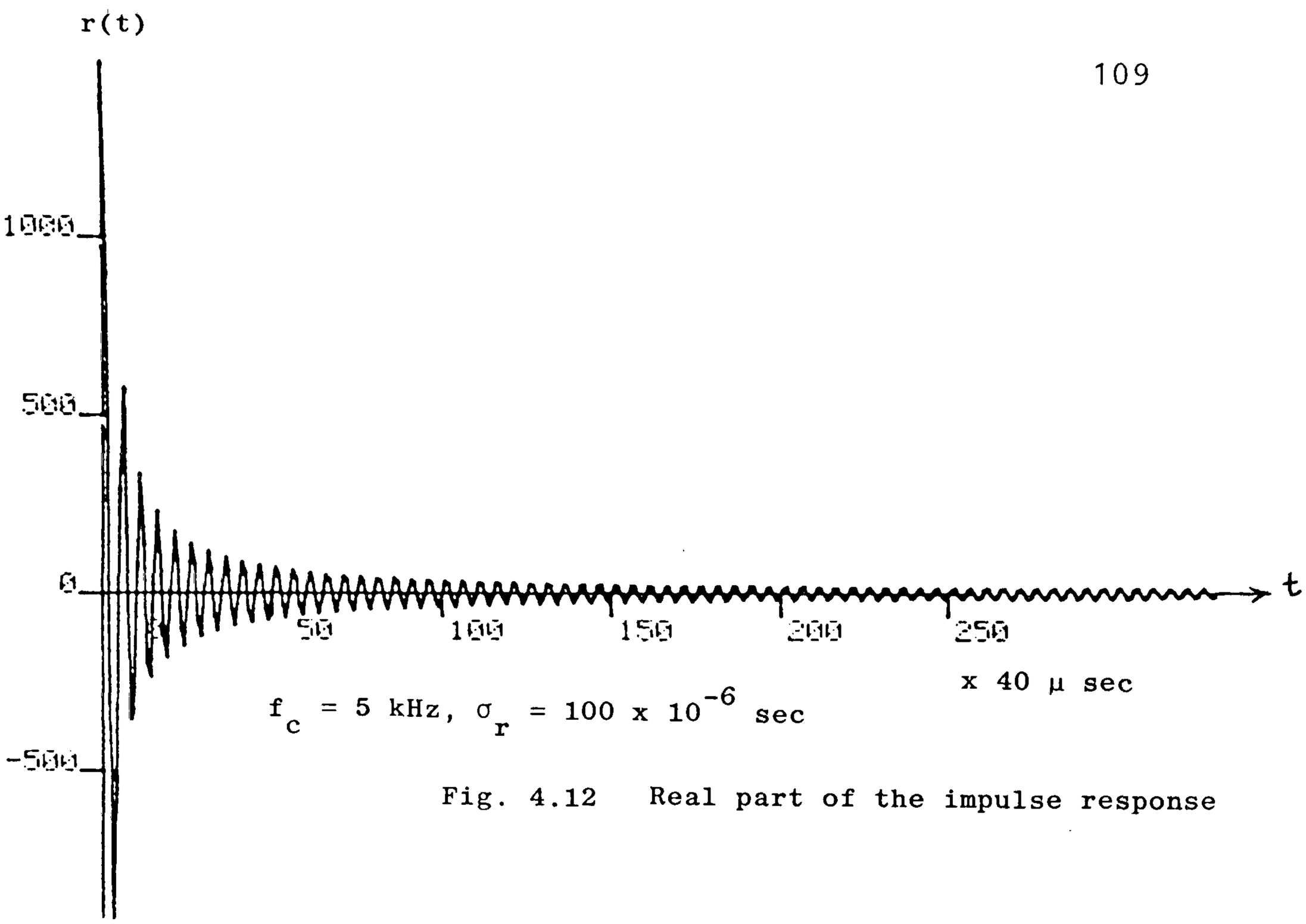

f_c = 5 kHz, σ_r = 100 x 10^{-6} sec

Fig. 4.12 Real part of the impulse response

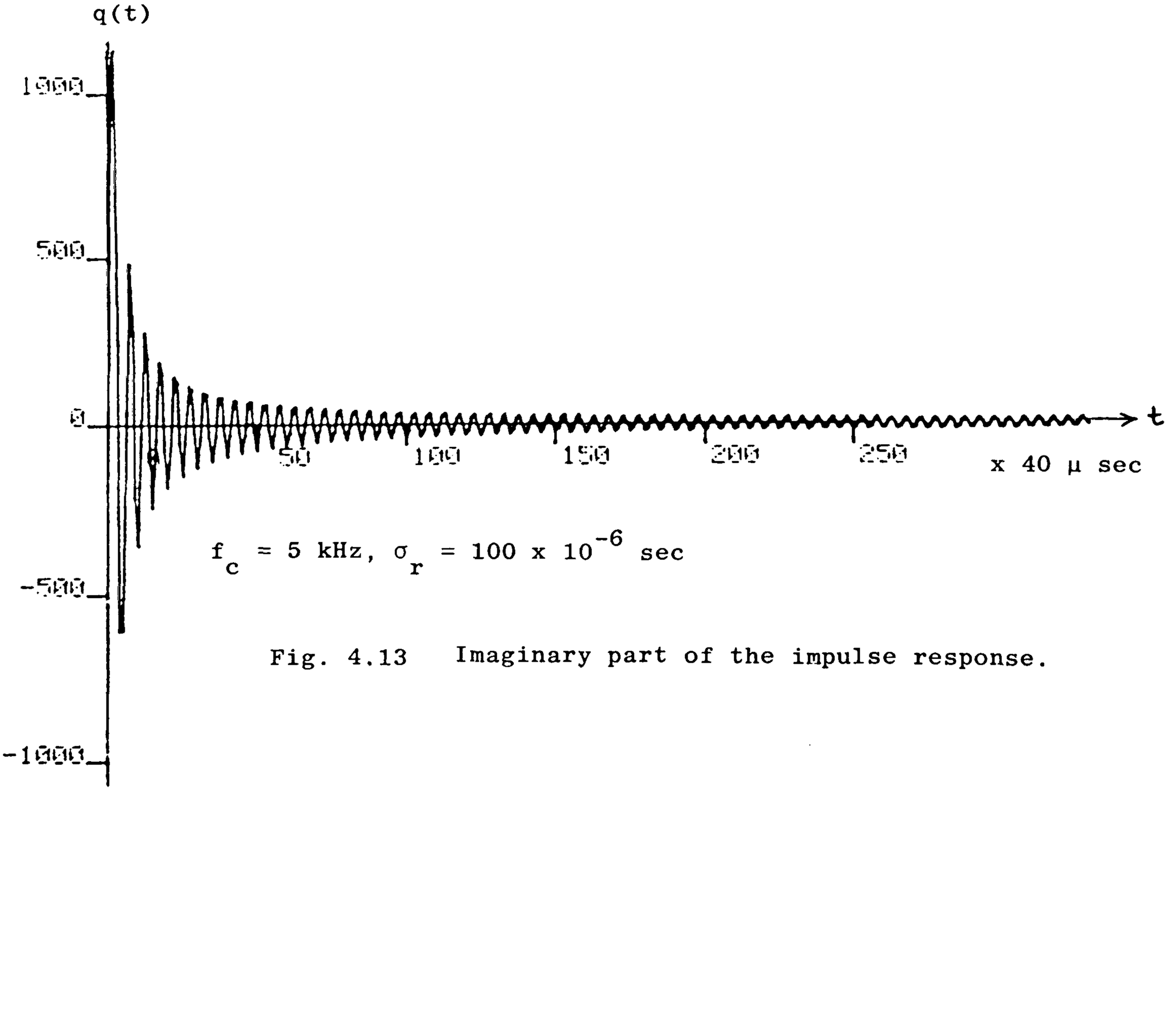

f_c = 5 kHz, σ_r = 100 x 10^{-6} sec

Fig. 4.13 Imaginary part of the impulse response.

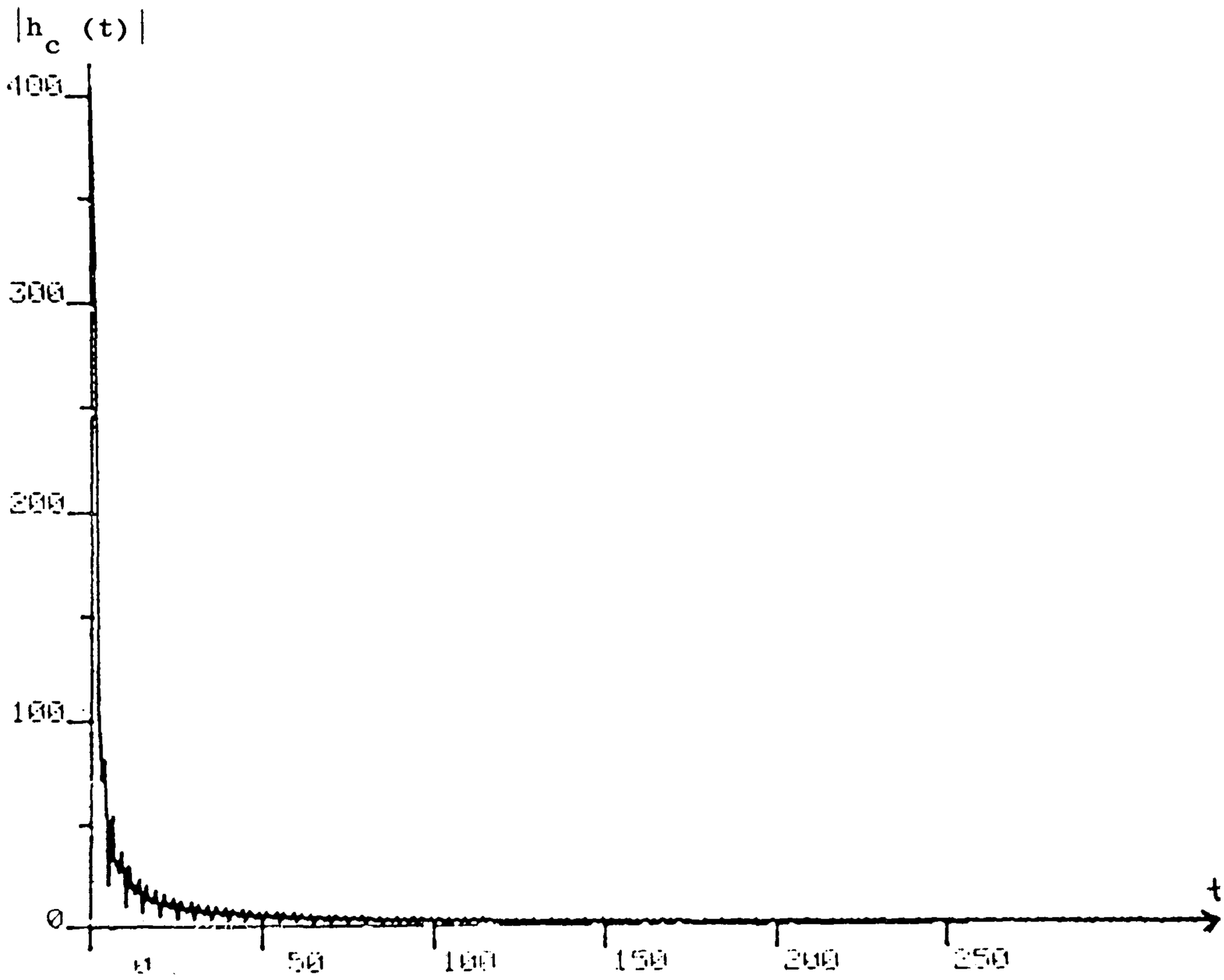

f_c = 5 kHz, σ_r = 100 x 10^{-6} sec

Magnitude of the impulse response

Fig. 4.14

using the well-known analogue transversal filter is the simplest approach for detection of complex zeros. The transversal filter is a linear network since it utilises delay, multiplication by a constant and summation (22). A digital transversal filter can be similarly implemented provided that the input signal is passed through an analogue-to-digital converter. In this case the weights represent the sampled impulse response, and a logic circuit can be used to indicate when both summers have zero output implying a complex zero.

It is also possible to use one tapped-delay line with half the weights representing the real part of the impulse response and the remainder representing the imaginary part.

If s(t) is a real input signal, and h(t) is the complex impulse response of the filter then the output complex signal $s(t - j\sigma_r)$ is:

$$s(t - j\sigma_r) = s(t) * h_c(t) \qquad (4.19)$$

where * means convolution.

$$\therefore s(t - j\sigma_r) = s(t) * [r(t) + j\, q(t)]$$

where $h_c(t)$ is expressed as a sum of real and imaginary parts

$$\therefore s(t - j\sigma_r) = s(t) * r(t) + j\, s(t) * q(t) \qquad (4.20)$$

Using eqn. (4.21), the envelope of $s(t - j\sigma_r)$ is:

$$|s(t - j\sigma_r)| = |s(t) * r(t) + j\, s(t) * q(t)|$$

$$= \sqrt{[s(t) * r(t)]^2 + [s(t) * q(t)]^2} \qquad (4.21)$$

Thus it is apparent that the envelope is zero only when both [s(t) * r(t)] and [s)t) * q(t)] are zero. Figure 4.15 shows a possible delay line implementation of the complex filter where the upper weighting resistors represent the real part of the impulse response while the lower weights represent the imaginary part. At the outputs of the upper and lower summing circuits we have [s(t) * r(t)] and [s(t) * q(t)] respectively. Two squaring circuits are then used to give $[s(t) * r(t)]^2$ and $[s(t) * q(t)]^2$ At the summer to the right-most, a logic circuit can be used to indicate when the sum is zero.

For a delay line with 32 taps it can be assumed that 16 correspond to positive time samples of r(t) and q(t), while the other 16 correspond to negative time samples of r(t) and q(t). Assuming the delay between any two successive taps is 32 μseconds, then the delay between the centre and the end taps is 16 x 32 = 512 μseconds. The expressions for the amplitude variations of r(t) and q(t) are given by eqns. (4.15)and (4.16) respectively. The following results, assuming f_c = 5 kHz and σ_r = 100 μseconds, may be obtained:

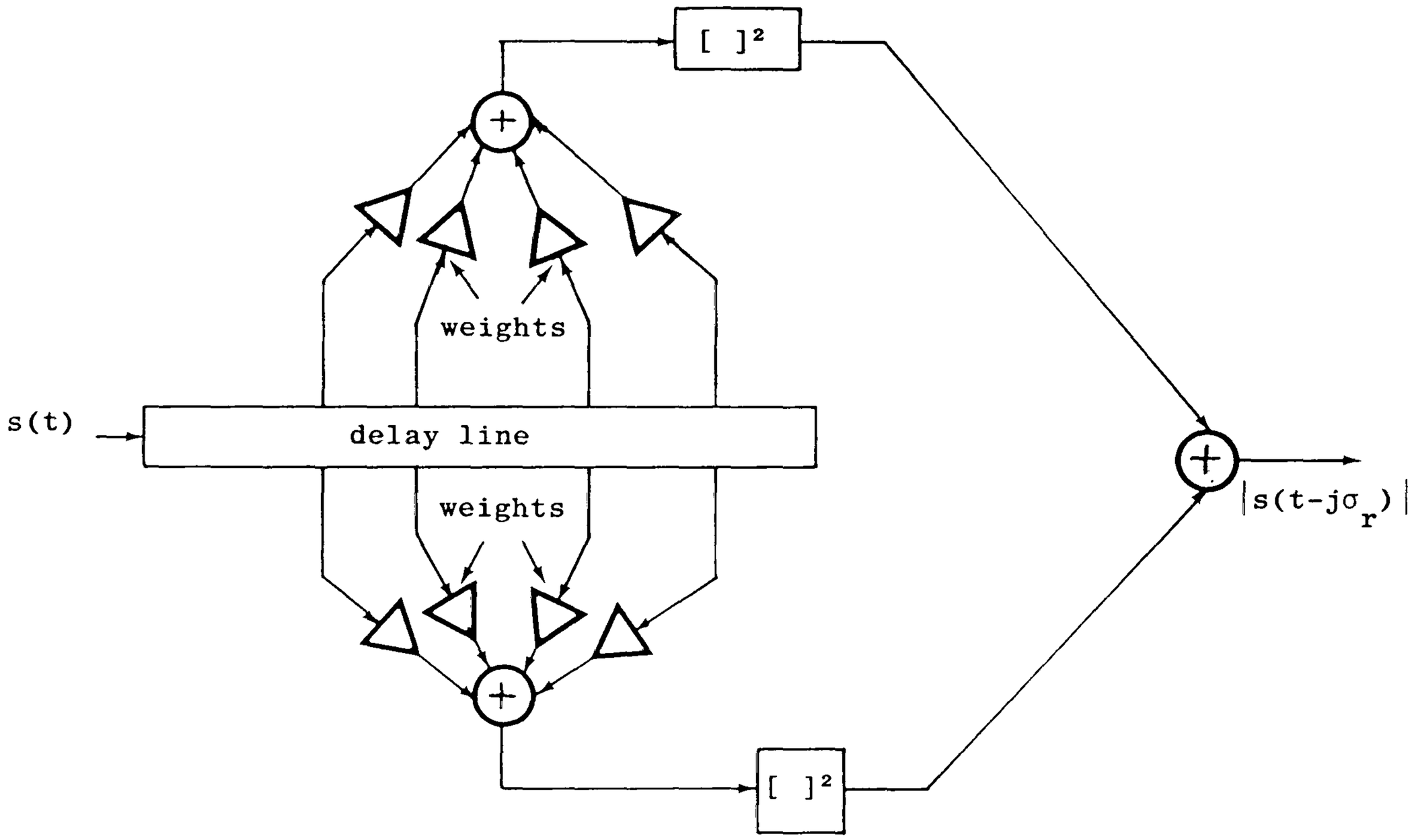

Fig. 4.15 Delay line implementation of the complex filter

t	$\frac{\sqrt{(At)^2 + B^2}}{\pi(t^2 + \sigma_r^2)}$	$\frac{\sqrt{C^2 + (Dt)^2}}{\pi(t^2 + \sigma_r^2)}$
0	36760.654	36898.482
512×10^{-6}	7072.119	7047.640

The ratio between the end to the centre taps is about 0.19 which might be a tolerable approximation to the decaying nature of the impulse response discussed in Section 4.4. If the number of taps is doubled then the ratio will roughly be halved to 0.1.

b) Cascaded differentiators

An alternative realisation of the complex filter can be derived from eqn. (4.5):

$$L(f) = S(f)\, e^{2\pi f\sigma_r}$$

where $S(f)$ is the Fourier transform of the real signal $s(t)$ input at the filter, $e^{2\pi f\sigma_r}$ is the transfer function of the filter, and $L(f)$ is the Fourier transform of the output complex signal $s(t - j\sigma_r)$ as mentioned previously. The exponential transfer function can be expressed as an expansion:

$$L(f) = S(f)\, e^{2\pi f\sigma_r}$$

$$= S(f)\ \left[1 + (2\pi f\sigma_r) + \frac{(2\pi f\sigma_r)^2}{2!} + \frac{(2\pi f\sigma_r)^3}{3!} + \ldots\right] \qquad (4.22)$$

$$= S(f)\ \left[1 + (j2\pi f)(-j\sigma_r) + (j2\pi f)^2\frac{(-j\sigma_r)^2}{2!} + (j2\pi f)^3\ \frac{(-j\sigma_r)^3}{3!} + \ldots\right] \qquad (4.23)$$

Taking inverse Fourier transform of eqn. (4.23) and using the property $\frac{d^n s(t)}{dt^n} \leftrightarrow (j2\pi f)^n S(f)$ gives:

$$s(t-j\sigma_r) = s(t) + (-j\sigma_r)\frac{ds(t)}{dt} + \frac{(-j\sigma_r)^2}{2!}\frac{d^2s(t)}{dt^2} + \frac{(-j\sigma_r)^3}{3!}\frac{d^3s(t)}{dt^3} + \ldots \quad (4.24)$$

Therefore the complex filter can be realised by cascaded differentiators, weighting resistors, and a summer. Figure 4.16 shows such an implementation of the complex filter. It is also possible to truncate this complex filter by decreasing the number of differentiators as the multiplying weights become negligible with increasing order ($\sigma_r/5, \sigma_r/6, \ldots$) of differentiation as is apparent from Figure 4.16.

It is also possible to derive eqn. (4.24) directly through the use of Taylor's series of complex variable (11) as shown:

$$f(z) = f(a) + (z-a)f'(a) + (z-a)^2\frac{f''(a)}{2!} + \ldots + (z-a)^n\frac{f^{(n)}(a)}{n!}$$

Applying this to the complex signal $s(t - j\sigma_r)$ and substituting $z = t - j\sigma_r$, it is then possible to obtain:

$$s(t-j\sigma_r) = s(t) + (-j\sigma_r)\, s'(t) + (-j\sigma_r)^2\frac{s''(t)}{2!} + \ldots$$

which is the same as eqn. (4.25).

Similar to the delay-line realisation, the envelope of the output signal $s(t - j\sigma_r)$ is the important thing whose real zeros correspond to complex zeros of s(t).

Example:

As an example on the cascaded differentiators implementation of the complex filter let us consider the real signal given as:

$$s(t) = 1 + a^2t^2 \qquad (4.25)$$

The zeros of the above polynomial representing a real signal are complex conjugate zeros given by: $x = \pm j\frac{1}{a}$; i.e. the two complex zeros have ordinate part of $\pm \sigma_r = \pm\frac{1}{a}$. As s(t) is a polynomial of degree two, then only two differentiators are required.

The filtered signal is:

$$\begin{aligned} s(t-j\sigma_r) = 1 + a^2(t-j\sigma_r)^2 &= 1 + a^2(t-j\frac{1}{a})^2 \\ &= 1 + a^2(t^2-j\frac{2t}{a} - \frac{1}{a^2}) \\ &= a^2t^2 - j2at \end{aligned} \qquad (4.26)$$

$s(t-j\sigma_r)$ has two x-plane zeros, one real zero at x =0, and one complex zero at $x = j\frac{2}{a}$.

Figure 4.17 shows the complex filter for s(t) realised as two cascaded differentiators. To prove that the envelope of $s(t-j\sigma_r)$ does not have extra real zeros that do not correspond to complex zeros of s(t) let us assume in eqn. (4.26) that $\sigma_r \neq \frac{1}{a}$ then we have:

$$\begin{aligned} s(t-j\sigma_r) &= 1 + a^2(t-j\sigma_r)^2 \\ &= 1 + a^2(t^2-j2\sigma_r t - \sigma_r^2) \\ &= 1 + a^2t^2 - a^2\sigma_r^2 - j2a^2\sigma_r t \end{aligned} \qquad (4.28)$$

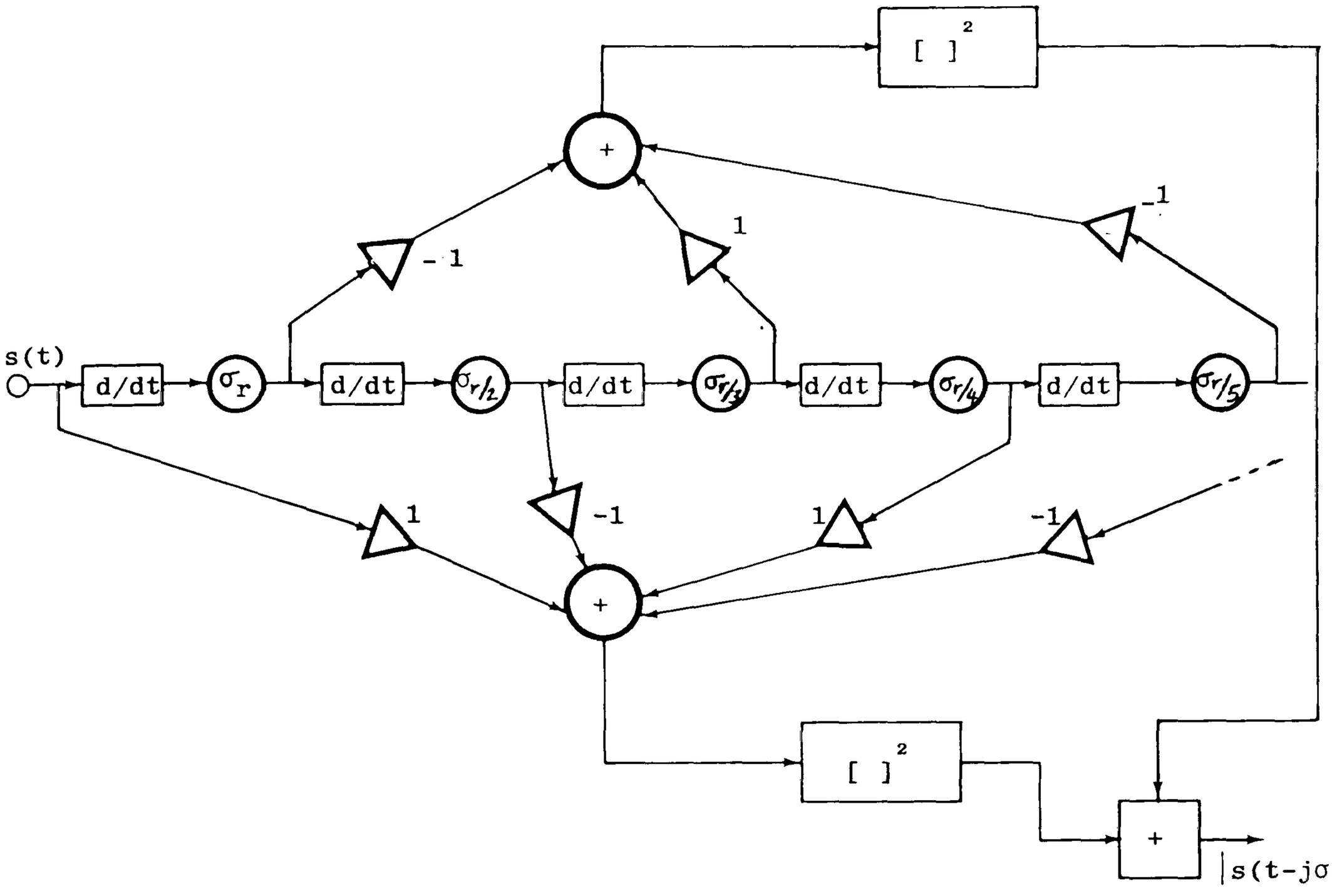

Fig. 4.16 Complex filter implemented as cascaded differentiators

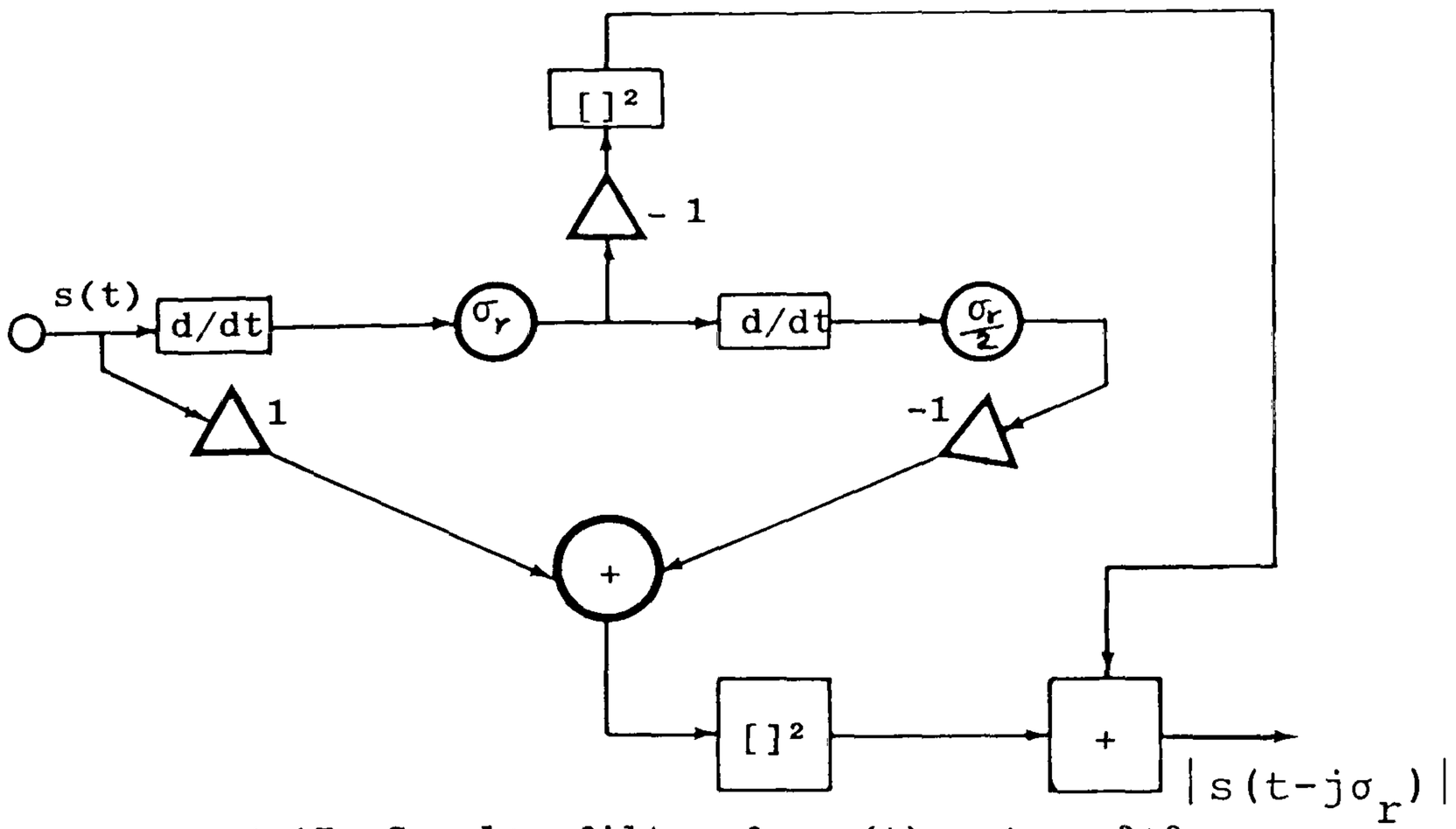

Fig. 4.17 Complex filter for $s(t) = 1 + a^2t^2$

The envelope of $s(t-j\sigma_r)$ is given by:

$$|s(t-j\sigma_r)| = \sqrt{(1 + a^2t^2 - a^2\sigma_r{}^2)^2 + 4\ a^4\sigma_r{}^2t^2} \quad (4.28)$$

The above is always positive unless $\sigma_r = \frac{1}{a}$ in which case it becomes:

$$|s(t-j\sigma_r)| = \sqrt{(1 + a^2t^2 - a^2\frac{1}{a^2})^2 + 4\ a^4\frac{1}{a^2}t^2}$$

$$= \sqrt{a^4t^4 + 4\ a^2t^2}$$

which becomes zero at t = 0 where the complex zeros of s(t) occur, thus indicating a zero detection.

In practice a differentiator can be implemented digitally by a non-recursive filter (23) with a finite impulse response. This guarantees stability as all non-recursive filters have no feedback and hence are stable (24).

Figure 4.18 shows a non-recursive digital filter with one delay element and a summer, x_n representing the samples at the input and y_n representing the output samples. This first order non-recursive filter represents a crude differentiator as its output samples are proportional to the rate of change of the input samples. The relation between the output sequence and the input sequence of the filter can be written in the from:

$$y_n = x_n - x_{n-1} \quad (4.29)$$

The above has a z-transform as:

$$Y(z) = X(z) - X(z)\ z^{-1} \quad (4.30)$$

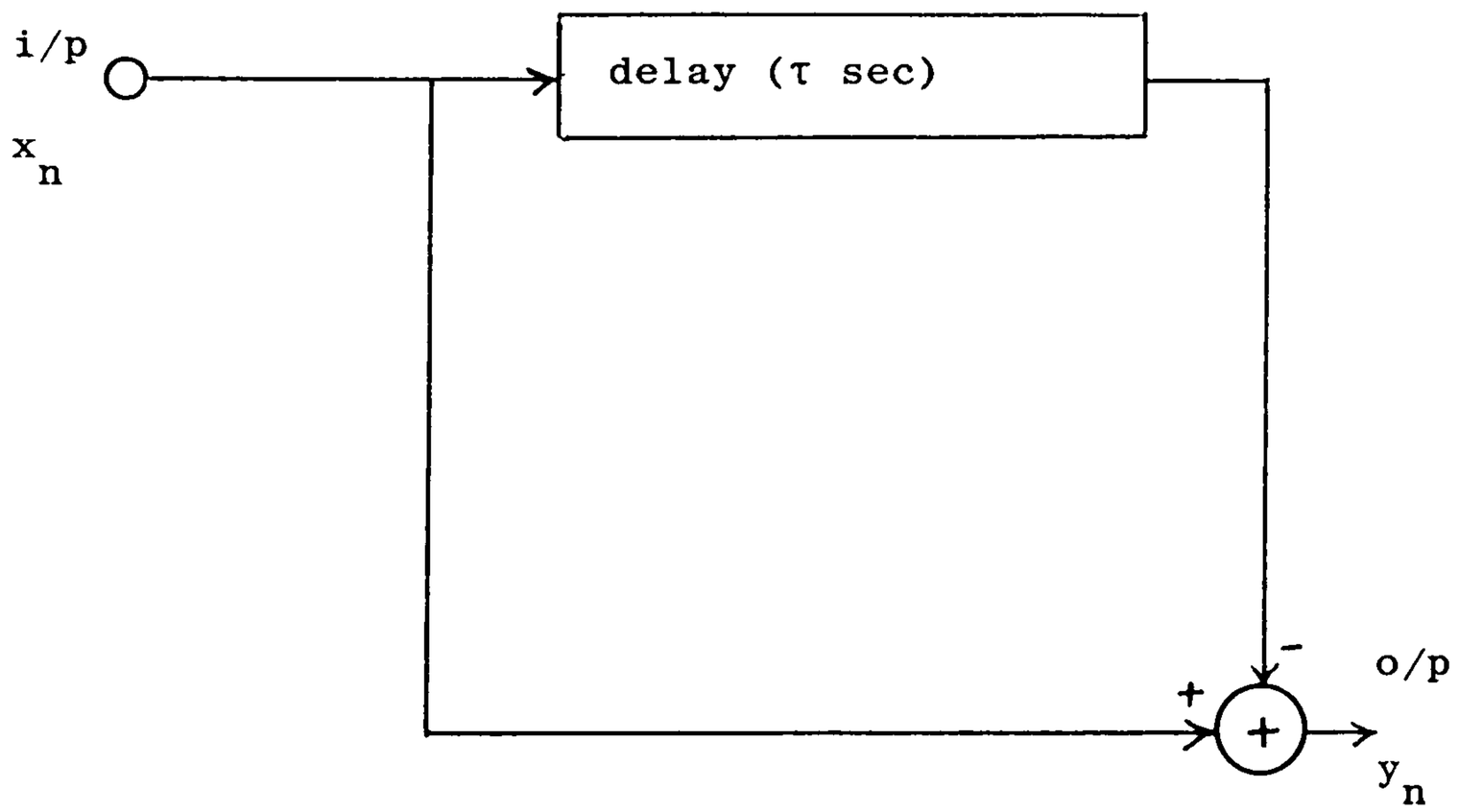

First order Non-Recursive Filter

Fig. 4.18

where $z^{-1} = e^{-j\omega\tau}$, τ is the sampling period.

If H(z) is the transfer function of the digital filter then:

$$H(z) = \frac{Y(z)}{X(z)} = (1 - z^{-1})$$

The frequency response of the above can be obtained by substituting $z^{-1} = e^{-j\omega\tau}$,

$$H(e^{j\omega\tau}) = (1 - e^{-j\omega\tau})$$

$$\therefore |H(e^{j\omega\tau})| = |(1 - e^{-j\omega\tau})|$$

$$= \sqrt{2(1 - \cos\omega\tau)}$$

$$\therefore \arg(H(e^{j\omega\tau}) = \text{arc tan } (\frac{\sin\omega\tau}{1 - \cos\omega\tau}) \qquad (4.31)$$

A computer implementation of this differentiator will be described in Chapter 5.

Figure 4.19 shows the magnitude and phase frequency responses of the digital filter given by eqn. (4.31) where the periodic nature of the response is clear. An ideal differentiator has a transfer function of the form:

$$H(\omega) = j\omega$$

$$\therefore |H(\omega)| = \omega$$

$$\therefore \arg[H(\omega)] = \frac{\pi}{2} \text{ radians} \qquad (4.32)$$

A comparison between eqns. (4.31) and (4.32) reveals that at very low frequencies the non-recursive digital filter gives a good approximation to the ideal differentiator. Smaller τ gives better approximation. However, there are more sophisticated ways of realising a better differentiator.

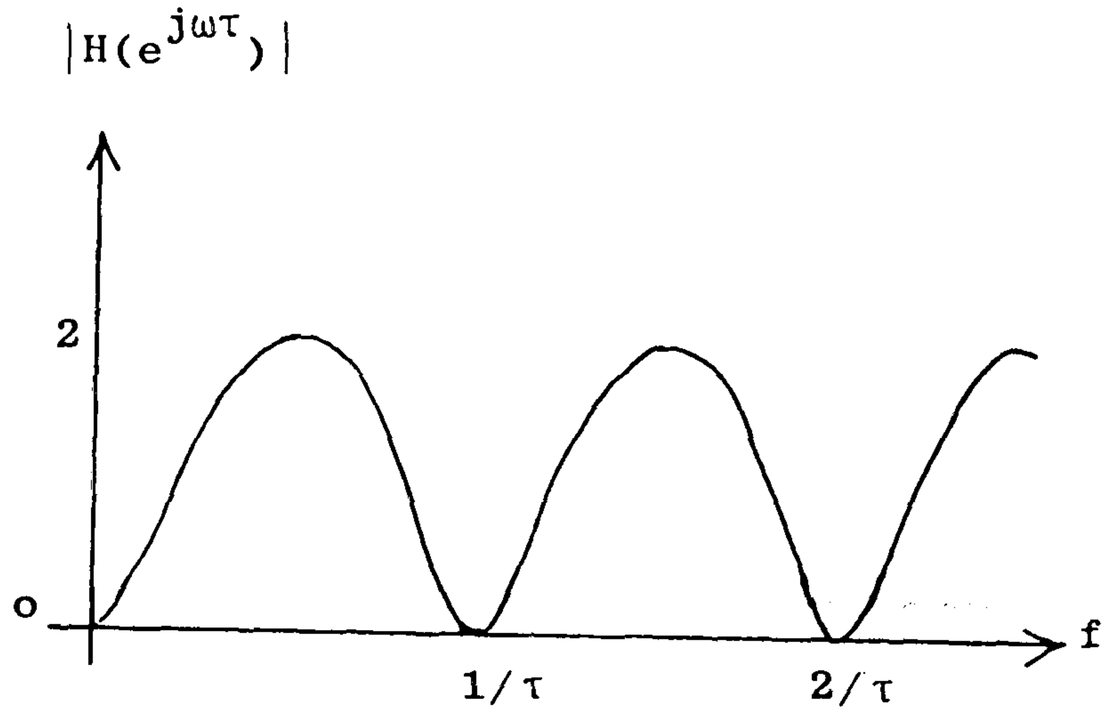

Magnitude and Phase Frequency Responses of a Digital Differentiator

Fig. 4.19

c) Computer Implementation

An alternative means of realising the complex filter is through the use of a computer for real-time signal processing. In this case the input signal is sampled and quantised and passed to the computer. This quantised input signal is then processed in blocks by the fast Fourier transform routine giving the frequency domain samples of the signal. The resulting Fourier coefficients are digitally weighted by the respective filter frequency reponses (that is by values of $e^{2\pi f\sigma r}$) such that this product corresponds to the complex filtered frequency samples. An inverse Fourier transform will generate the time samples of the filtered signal as previously discussed in Section 4.3. A complex zero is detected if the computer indicates that the real and the imaginary parts of the sample (i.e. its envelope) are simultaneously zero.

Although a specific embodiment of the complex filter has been described it is worthwhile to emphasise that the aforementioned examples of realisation are not exhaustive and there may be many other ways of implementing complex filtering in practice.

4.6 Final Remarks

The theoretical foundation of complex filtering has been developed and also a practical realisation of the new technique has been described in three different

ways. The squaring circuits used in Section 4.5 can be replaced by full-wave rectifiers that give modulus of the signals. The new complex filtering technique confirms that although complex zeros of real signals do not generally have an obvious physical interpretation, it is still possible to detect complex zeros contrary to what was thought (25).

As discussed before a bank of complex filters having different σ_r values is required in order to detect different complex zeros. It will be shown that values of σ_r corresponding to potential complex zeros have to be selected in specifying the filter bank, and only "medium" values of σ_r are considered of practical use. Due to filter imperfections, each filter in the bank must correspond to a small range of σ_r values. If these ranges cover all the σ_r values of interest, only a few filters are required. This will be considered in Chapter 6.

CHAPTER 5

SIMULATION OF ZERO SYNCHRONOUS FREQUENCY MODULATION SYSTEM

5.1 Introduction

The performance of the Zero Synchronous Frequency Modulation (ZSFM), introduced in Chapter 3, is investigated in this chapter by means of digital computer simulation with the objective of evaluating the performance under different conditions. Bandlimitation of the modulated signal is considered first using the periodic and aperiodic phase functions for zero conjugation. An ideal channel and a receiver are simulated with envelope and frequency demodulation.

The first source of degradation to be considered is that of additive Gaussian noise which is present in any communication channel. Signal-to-noise ratios (SNR) of the detected envelope are measured.

The effect of the nonlinear IF filtering characteristic at the receiver is also considered. This gives rise to AM/PM conversion effect causing cross-talk problems between the data channel and the main envelope modulation. A practical IF transformer is simulated with its specified magnitude and phase responses so that the cross-talk effect on the detected envelope due to phase non-linearity can be investigated. A condition of mistune is also considered with its degrading effects. The signal-to-distortion ratios of the detected envelope signal are measured showing

the significance of the distortion introduced due to non-linearities.

Multipath fading is also considered with its implications for reception of both envelope and data signals.

Two implementations of the complex filters are presented in this chapter; as cascaded differentiators and as blocks of FFT in the frequency domain.

The effect of truncating the FM function generator which has been discussed in Section 3.11, is investigated in order to evaluate its effect on system performance.

All simulation is performed at baseband for simplicity of computation. Finally, a simple circuit is used as a frequency demodulator utilising phase-locked loop to detect the data signal.

5.2 Bandlimitation Test

In this section computer simulation of a ZSFM signal is considered including the bandwidth of the signal whose complex zeros have been conjugated according to the binary data signal as explained in Section 3.8. The test signal used is a single-tone deterministic signal of known bandwidth. This has the advantage that the time positions of the signal complex zeros can be predetermined analytically before conjugation. The test signal considered is:

$$s(t) = (1 - ae^{j\Omega t})(1 - ae^{-j\Omega t}) \quad , \; 0 < a < 1$$

$$= 1 + a^2 - 2\,a\cos\Omega t \qquad (5.1)$$

where s(t) has a bandwidth of $W = \pm \frac{\Omega}{2\pi}$ Hz and its zeros are given by:

$$x = \frac{2k\pi}{\Omega} \pm j \frac{\ln a}{\Omega} \quad , \; k = 0, \pm 1, \pm 2, \ldots$$

as shown in Section 3.5.

For $0 < a < 1$ the signal s(t) is always positive and all the zeros are complex conjugate pairs. The signal s(t) given in eqn. (5.1) can be written in the form:

$$\begin{aligned} s(t) &= 1 + a^2 - 2a \cos\Omega t \\ &= (1 + a^2)\left(1 - \frac{2a}{1 + a^2} \cos\Omega t\right) \\ &= (1 + a^2)(1 - m \cos\Omega t) \end{aligned} \qquad (5.2)$$

where $m = \frac{2a}{1 + a^2}$ is the modulation depth of s(t), and s(t) can represent a DSB-AM signal with the d.c. term $(1 + a^2)$ corresponding to the carrier component and the two tones at $\pm \frac{\Omega}{2\pi}$ Hz corresponding to upper and lower sidebands of the DSB-AM signal.

The signal s(t) is represented on the computer by 1024 time samples over which a block of 64 cycles of s(t) is generated within a time duration of 10240 μ seconds. The bandwidth of this specific test signal is therefore given by:

$$W = \pm \frac{\Omega}{2\pi} = \pm \frac{1}{2\pi} \; \frac{64}{10240 \times 10^{-6}} = \pm 6.25 \text{ kHz}$$

The number of the complex zero pairs is N = 64 and the 64 cycles of s(t) can be viewed as a model of a long time signal.

Figure 5.1 shows the 64 cycles of s(t) for 60% modulation depth (m = 0.6). The frequency spectrum of s(t) can be calculated by the Fast-Fourier Transform (FFT) subroutine and this is illustrated in Figure 5.2.

In order to simulate the conjugated signal on the computer it is necessary to generate the phase function $\theta(t)$ and then to form the product:

$$c(t) = s(t)\ e^{j\theta(t)} \tag{5.3}$$

where c(t) is the conjugated signal and $\theta(t)$ is the PM function. For the periodic case $\theta(t)$ is given by eqn. (3.28):

$$\theta(t) = \pm 2 \text{ arc tan } \left\{ \frac{a^{1/N} \sin(\frac{\Omega}{N}t)}{1 - a^{1/N} \cos(\frac{\Omega}{N}t)} \right\} \tag{5.4}$$

while for the aperiodic phase conjugating function related to a single zero pair it is given by eqn. (3.34):

$$\theta(t) = \pm 2 \text{ arc tan } (\frac{t - t_r}{\sigma_r}) \tag{5.5}$$

as discussed in Section 3.6.

After the conjugated signal c(t) is formed, then the frequency spectrum can be found by the FFT subroutine.

Consider first the conjugated signal spectrum with the periodic phase conjugating function as given by eqn. (5.4), and N = 64 for the signal s(t). Six zero pairs of s(t) at the middle are chosen for conjugation. These are the 27th, 29th, 31st, 33rd, 35th and 37th pairs respectively. The conjugation depends on the binary data code, and if the code used is 101010 the number of con-

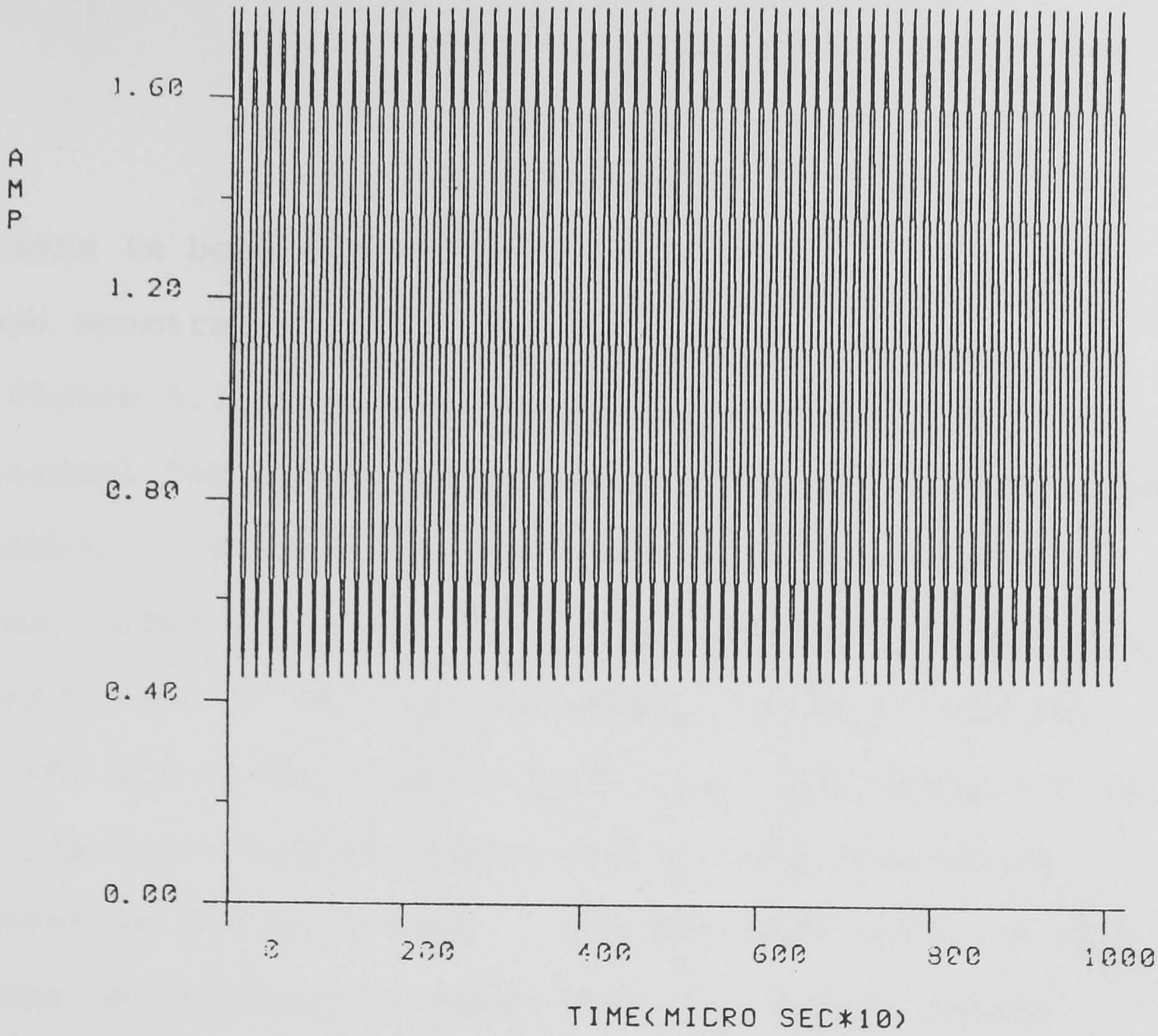

Fig. 5.1 Real signal s(t)

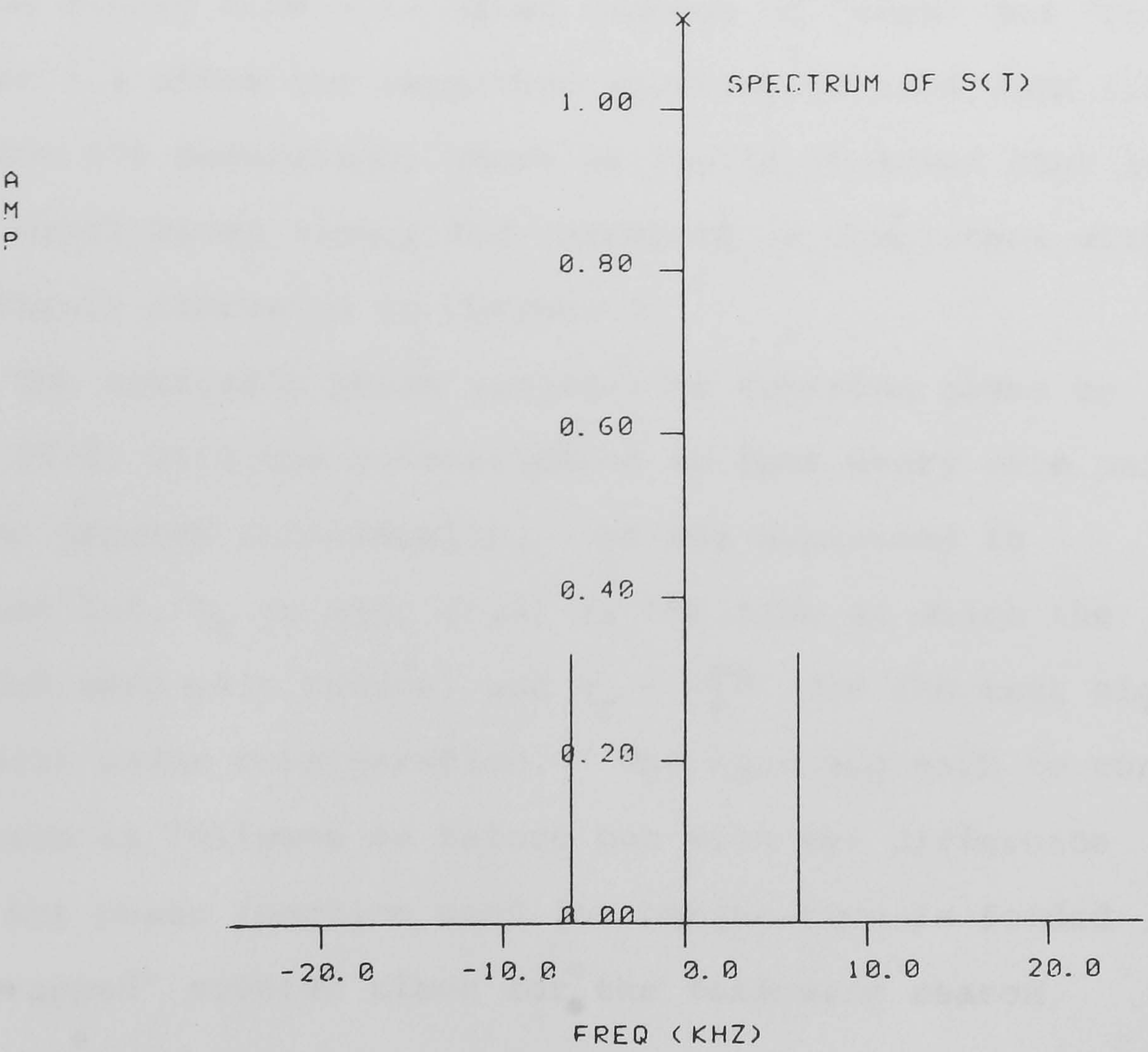

Fig. 5.2 Spectrum of s(t)

jugations in both directions is equal ensuring that the average spectral shift of the carrier is zero.

Figure 5.3 shows the magnitude spectrum of the ZSFM signal for 60% modulation and it can be observed that the signal is bandlimited to $\pm \frac{\Omega}{2\pi} = \pm 6.25$ kHz. The spectral components that lie between the tone components correspond to the superimposed binary signal (101010), while the out-of-band components, that fall about 115 dB below the tone components, are due to numerical noise generated in the programme. The spectral shift is also zero due to conjugating equal numbers in both senses. Next, all the zero pairs (64) of s(t) are conjugated using the periodic phase conjugating function and a random binary code with equal numbers of "ones" and "zeros". Figure 5.4 shows the magnitude spectrum of this ZSFM signal for 60% modulation, where it can be observed that it is a bandlimited signal and therefore is consistent with the theory discussed in Chapter 3.

The aperiodic phase conjugating function given by eqn. (5.5) will now be considered so that every zero pair can be treated individually. As was explained in Section 3.6, t_r in eqn. (5.5) is the time at which the related zero pair occurs, and $\sigma_r = \frac{\ln a}{\Omega}$ for the test signal s(t) under consideration. The same approach to conjugation is followed as before but with the difference that the phase function used for conjugation is folded or "wrapped" several times for the following reason.

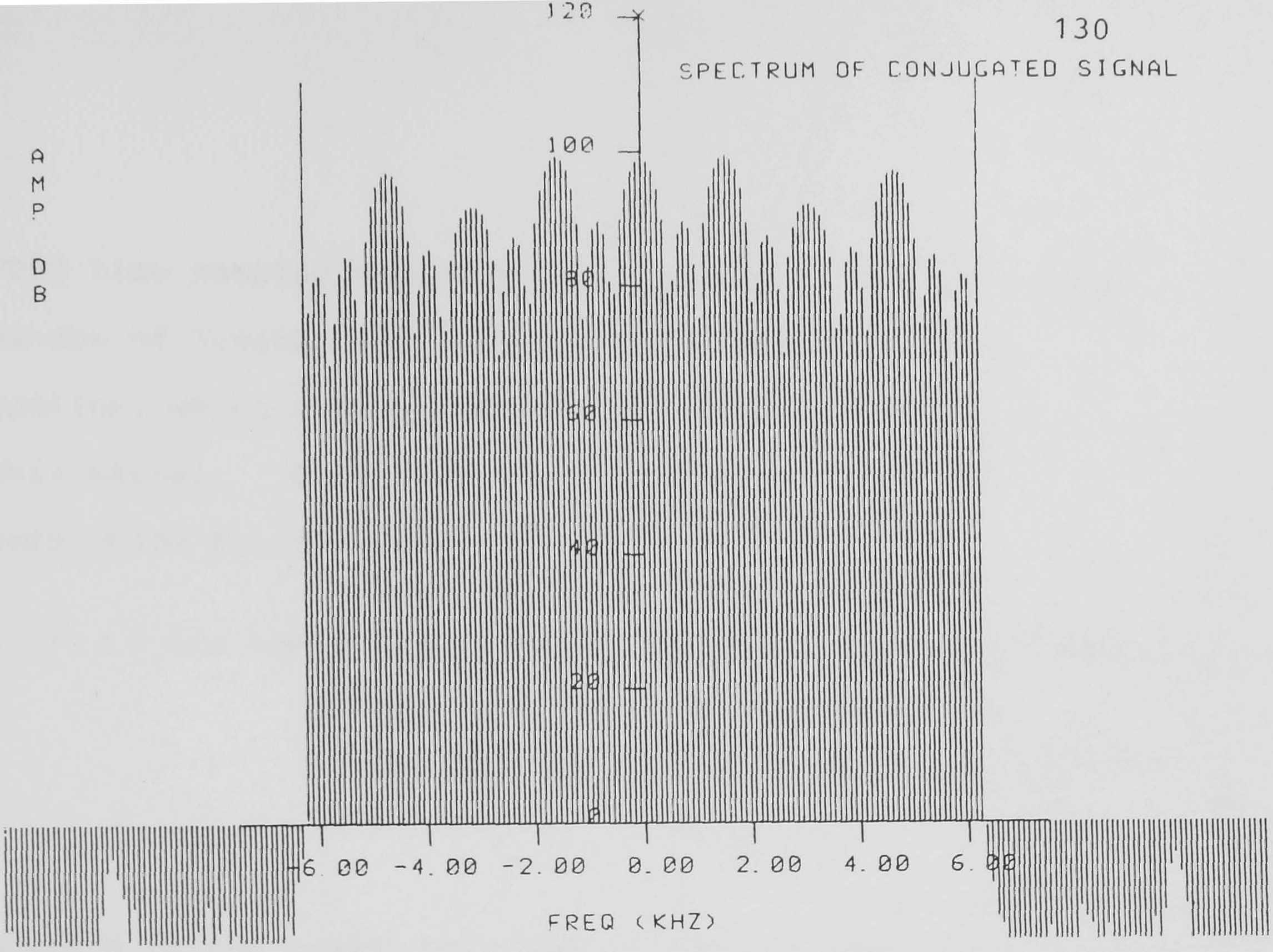

Fig. 5.3 Spectrum of the ZSFM signal,
6 zero pairs conjugated.

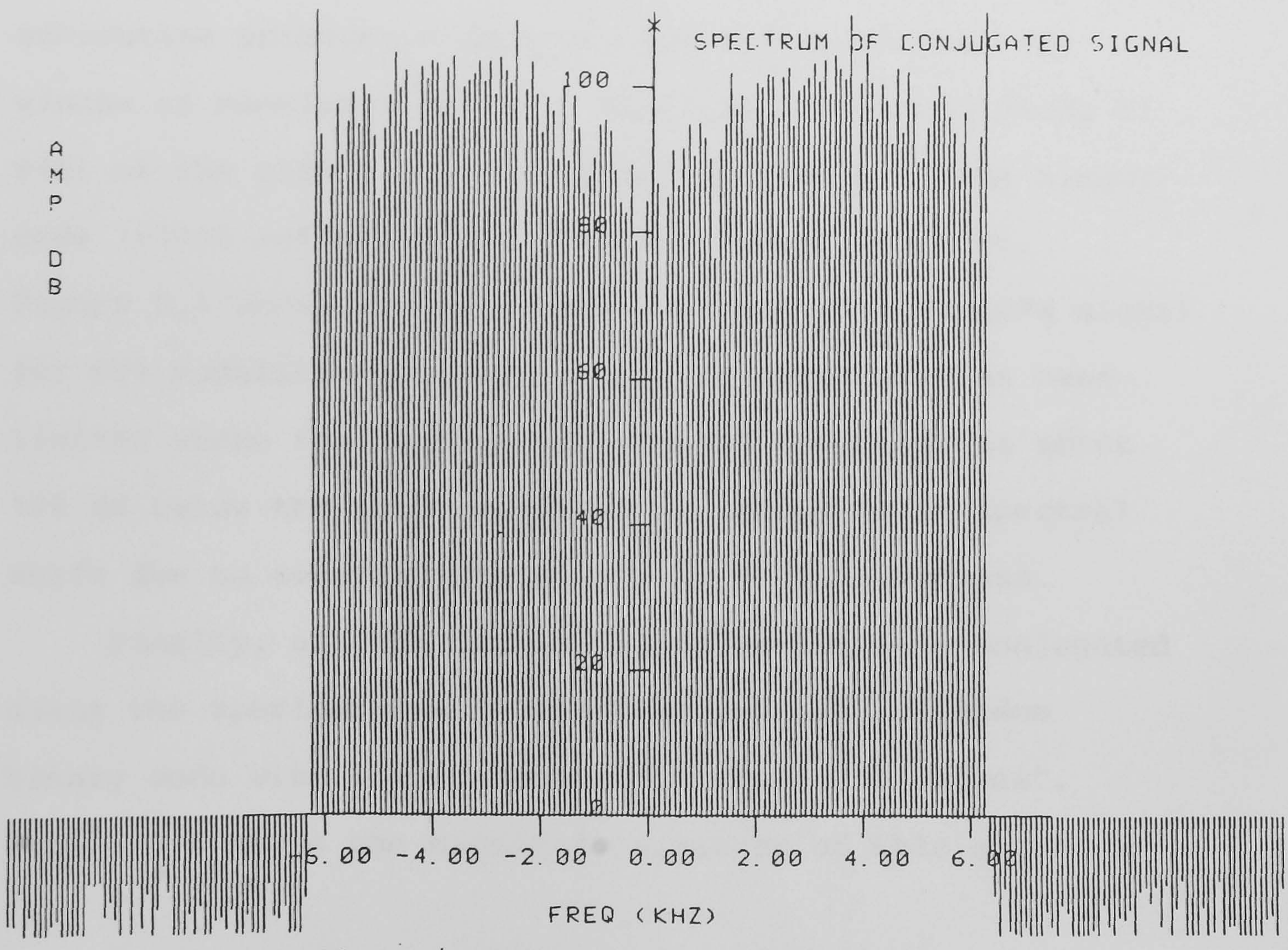

Fig. 5.4 Spectrum of the ZSFM signal,
all zero pairs conjugated.

1024 time samples representing the signal s(t) in a time window of length 10240 μ sec are fed to the FFT subroutine, which then produces a periodic repetition of this signal. Considering the zero pair at $t_r = 0$, then phase folding can be achieved as:

$$\theta(t) = \pm 2 \text{ arc } \tan\left(\frac{t}{\sigma_r}\right) \pm 2 \text{ arc } \tan\left(\frac{t-10240}{\sigma_r}\right) \pm 2 \text{ arc } \tan\left(\frac{t+10240}{\sigma_r}\right) \pm \ldots$$

$$\pm 2 \text{ arc } \tan\left(\frac{t-nx10240}{\sigma_r}\right) \pm 2 \text{ arc } \tan\left(\frac{t+nx10240}{\sigma_r}\right) \qquad (5.6)$$

where n is the number of times the phase function is folded. This folding is used for all the conjugated zero pairs and n is chosen as 4. The essence of folding the phase function is to take into consideration the fact that the FFT subroutine produces a periodic repetition of the time window as mentioned above. Similarly, six zero pairs of s(t) at the middle are conjugated according to the binary code 101010 and using the aperiodic phase function. Figure 5.5 shows the magnitude spectrum of this ZSFM signal for 60% modulation and the signal is considered as band-limited where the highest out-of-band component is about 100 dB below the tone components. There is no spectral shift due to conjugating equally in both directions.

Finally, all the 64 zero pairs of s(t) are conjugated using the aperiodic phase function and also a random binary code with equal numbers of "ones" and "zeros". Figure 5.6 shows the magnitude spectrum of this signal

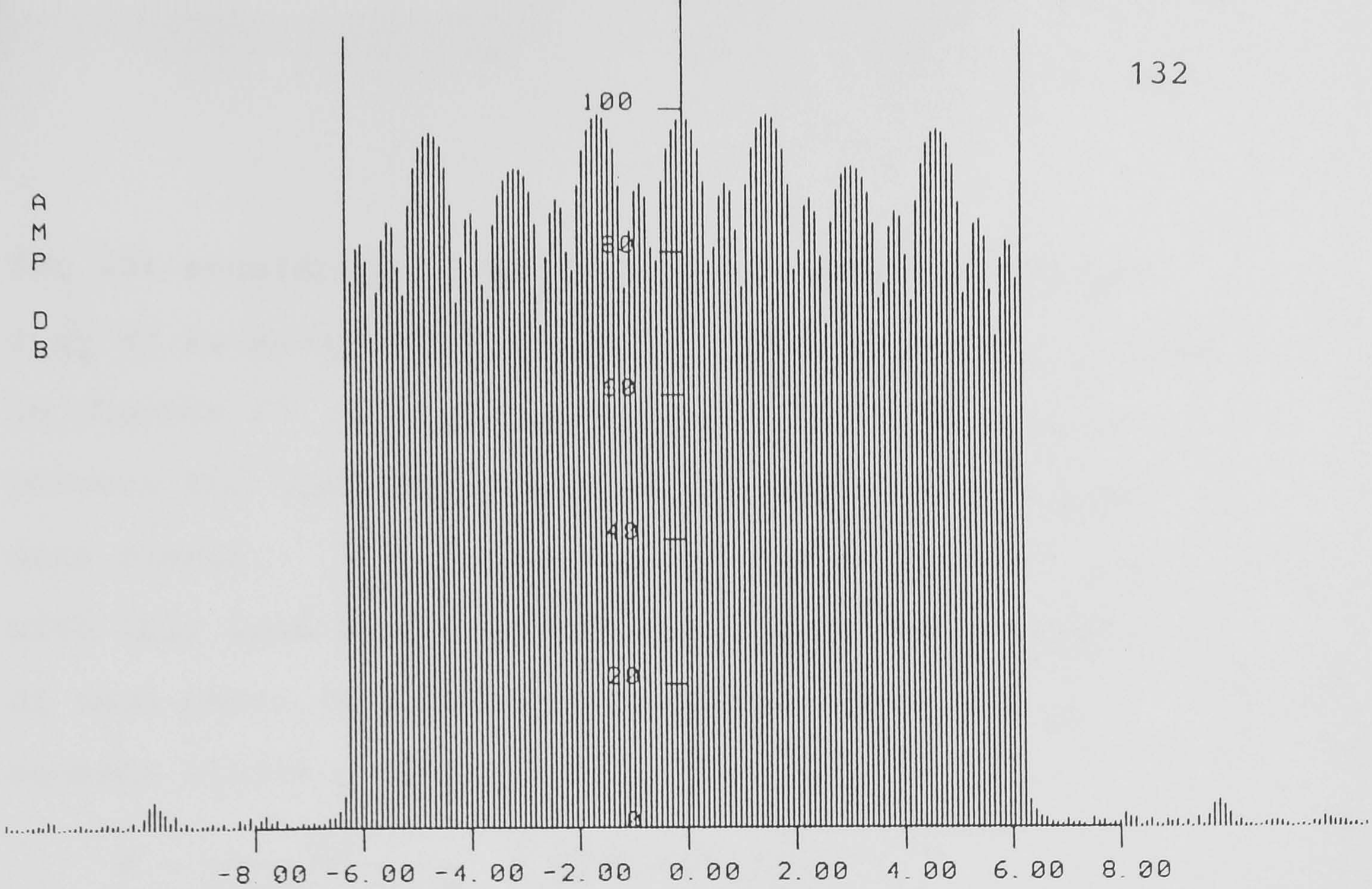

Fig. 5.5 Spectrum of the ZSFM signal,
6 zero pairs conjugated.

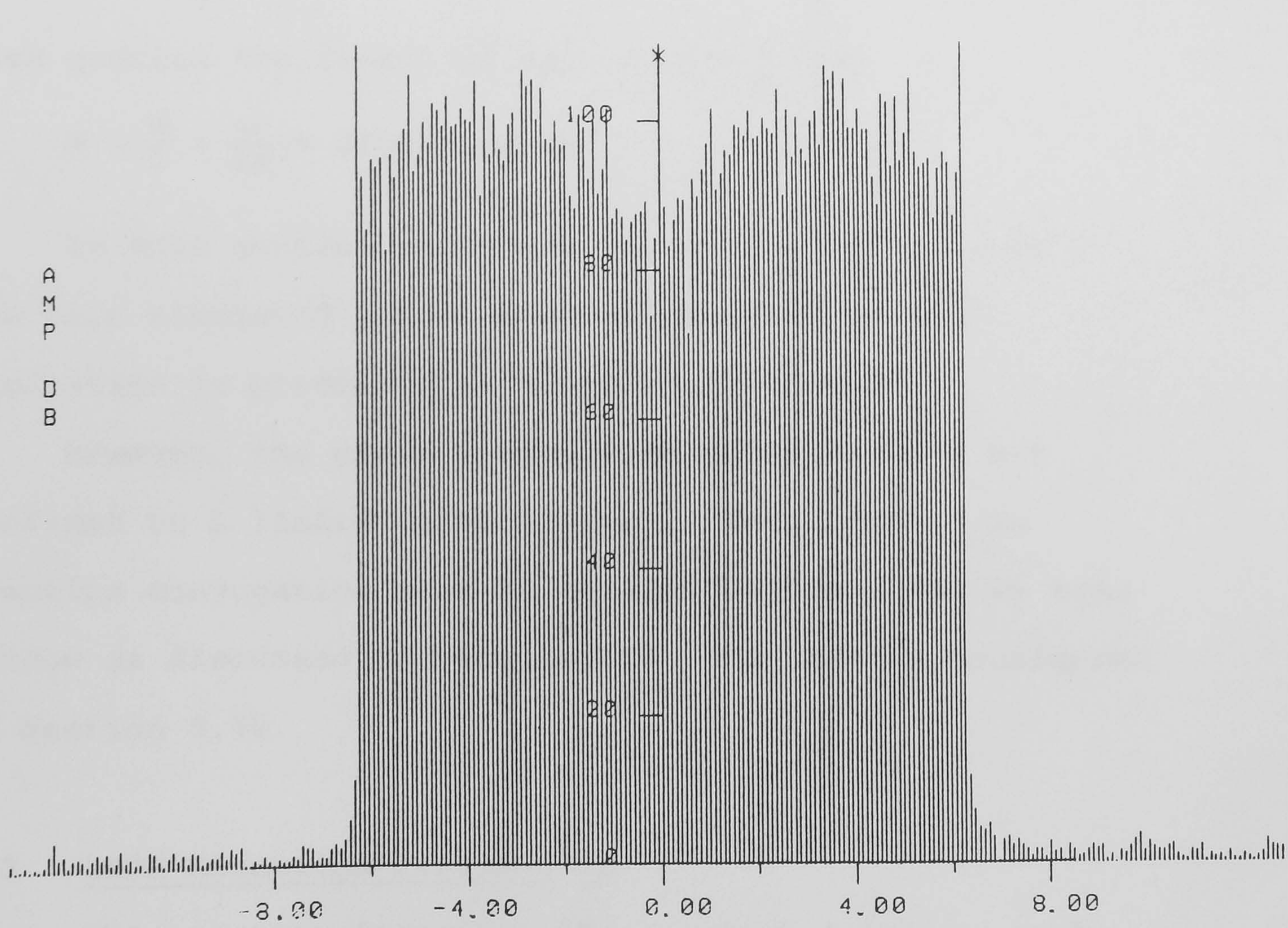

Fig. 5.6 Spectrum of the ZSFM signal,
all zero pairs conjugated.

for 60% modulation. Bandlimitation is preserved to $\pm \frac{\Omega}{2\pi}$ Hz in consistence with the theory of ZSFM explained in Chapter 3. The spectral components contained in between the tone components correspond to the binary data signal. The maximum data rate that can be used with this test signal is the ratio between the number of zero pairs (64) and the length of the signal in seconds (10240 μ sec) i.e.

$$R = \frac{64}{10240 \times 10^{-6}} = 6250 \text{ bits/sec}$$

Considering the double-sided bandwidth of the signal s(t) as W then:

$$W = \pm \frac{2\Omega}{2\pi} \text{ Hz}$$

then quoting the result of eqn. (3.51) gives:

$$R = \frac{W}{2} = \frac{\Omega}{2\pi} = 6250 \text{ bits/sec}$$

In this section, only the ideal ZSFM signal itself has been simulated and it has been shown that band-limitation is preserved as expected in theory.

However, the phase conjugating functions are not confined to a limited time window in this test. In practice conjugation must be applied within a finite time window as discussed in Section 3.8, and this is considered in Section 5.10.

5.3 ZSFM Reception Performance

This section describes the approach taken in implementing the simulated receiver. Simulation of an ideal

channel with constant frequency response is performed. Also white Gaussian noise is added with specified carrier-to-noise ratio (CNR) in order to investigate the performance of ZSFM under such conditions. A fading channel is considered in Section 5.8.

The detected envelope and phase (data) signals can be simulated by the following approach. If c(t) is the ZSFM signal then it can be expressed as shown in eqn. (5.3):

$$c(t) = s(t)\ e^{j\theta(t)} = \text{ZSFM signal.}$$

where s(t) is a real envelope signal and $\theta(t)$ is the phase conjugating function which is also real. In all the tests to be described, $\theta(t)$ is used as defined in eqn. (5.5) in which case any complex zero pair is conjugated individually irrespective of all the other zero pairs.

If C(f) is the Fourier transform of the ZSFM signal, c(t), then C(f) must be bandlimited and must have the same bandwidth as s(t) as was shown in Section 5.2. The samples obtained at the output of the FFT subroutine represent the frequency components of C(f). Both s(t) and c(t) are bandlimited to $\pm \frac{\Omega}{2\pi}$Hz as they are members of the same common envelope set. Nevertheless, c(t) will not be bandlimited if the phase function used for conjugation utilises a different σ_r value from that of the complex zero.

If $c_{BL}(t)$ is the bandlimited ($\pm \frac{\Omega}{2\pi}$Hz) version of c(t), that has some out-of-band components, then $c_{BL}(t)$ can be expressed as:

$$c_{BL}(t) = F^{-1}\{C(f)\ H_R(f)\} \tag{5.7}$$

where F^{-1} means inverse Fourier transform and $H_R(f)$ is the receiver I.F. filter which is assumed to have a constant magnitude over the band of interest and a single-sided bandwidth of $\frac{\Omega}{2\pi}$ Hz with linear phase characteristics. The FFT subroutine can be used in the reverse direction to produce time samples of $c_{BL}(t)$. Thus the magnitude $|c_{BL}(t)|$ gives the detected envelope signal, while the binary data signal can be obtained by taking the imaginary part of the logarithm of $c_{BL}(t)$ and then differentiating with respect to time, i.e.

$$\ln [c_{BL}(t)] = \ln|c_{BL}(t)| + j \arg[c_{BL}(t)]$$

$$\therefore \text{Im}\ [\ln\{c_{BL}(t)] = \arg\ [c_{BL}(t)]$$

$$\therefore \frac{d}{dt}\ \text{Im}[\ln\{c_{BL}(t)\}] \text{ gives the binary data signal.}$$

A forward-difference formula is used to estimate the numerical differentiation in the simulation. Figure 5.7 shows the detected evelope of the ZSFM signal whose spectrum is shown in Fig. 5.5 and for 60% modulation also. The IF filter used is of constant magnitude response and linear phase, and has a bandwidth of $\pm \frac{\Omega}{2\pi} = \pm$ 6.25 kHz. A comparison between Figures 5.7 and 5.1 reveals that the detected envelope of this ZSFM signal is only a replica of the original modulation signal s(t). Figure 5.8 shows the detected binary data signal 101010, where the positive frequency deviation from the carrier (zero here) represents the binary "1" and the negative frequency

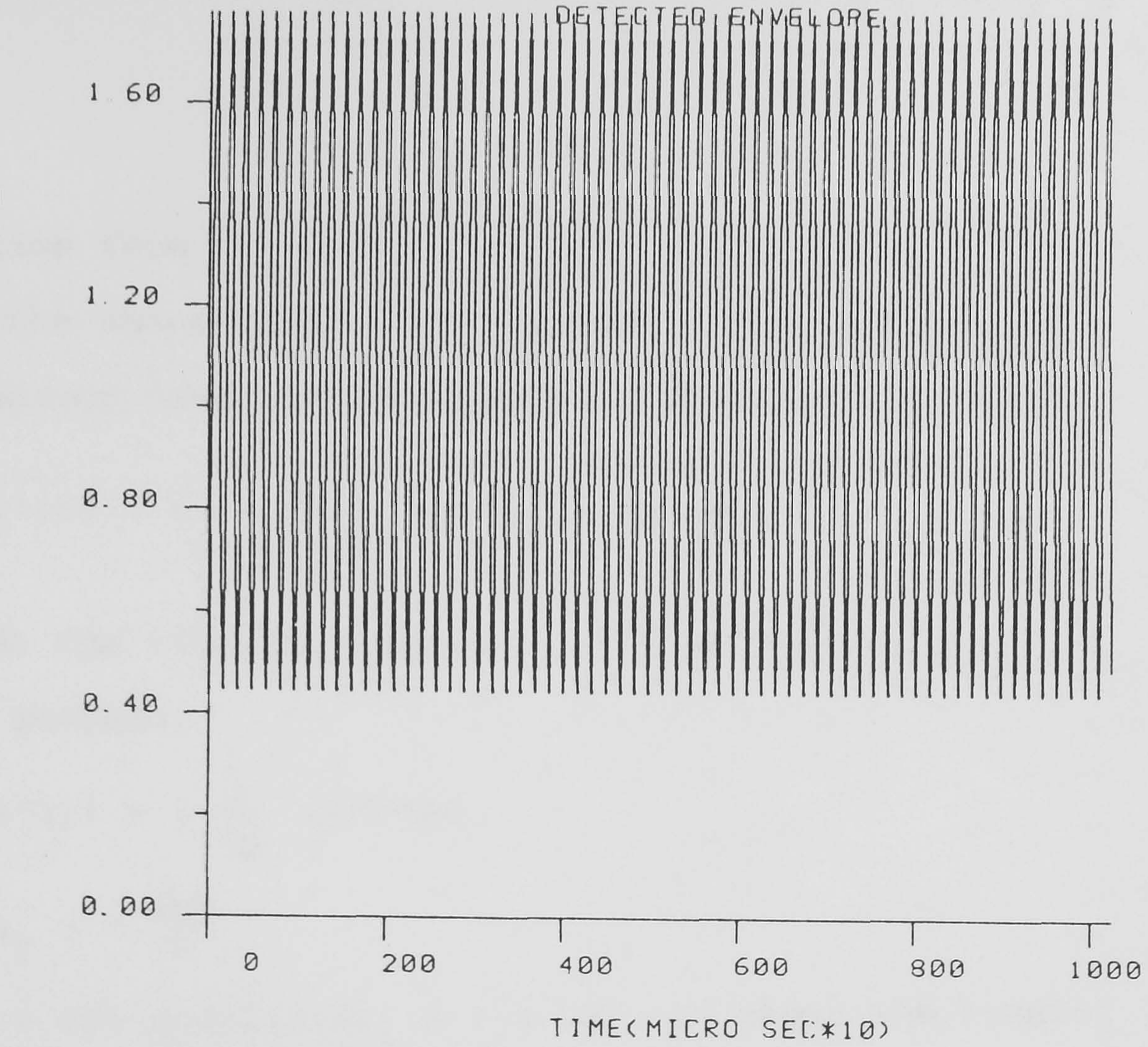

Fig. 5.7 Detected envelope of the ZSFM signal.

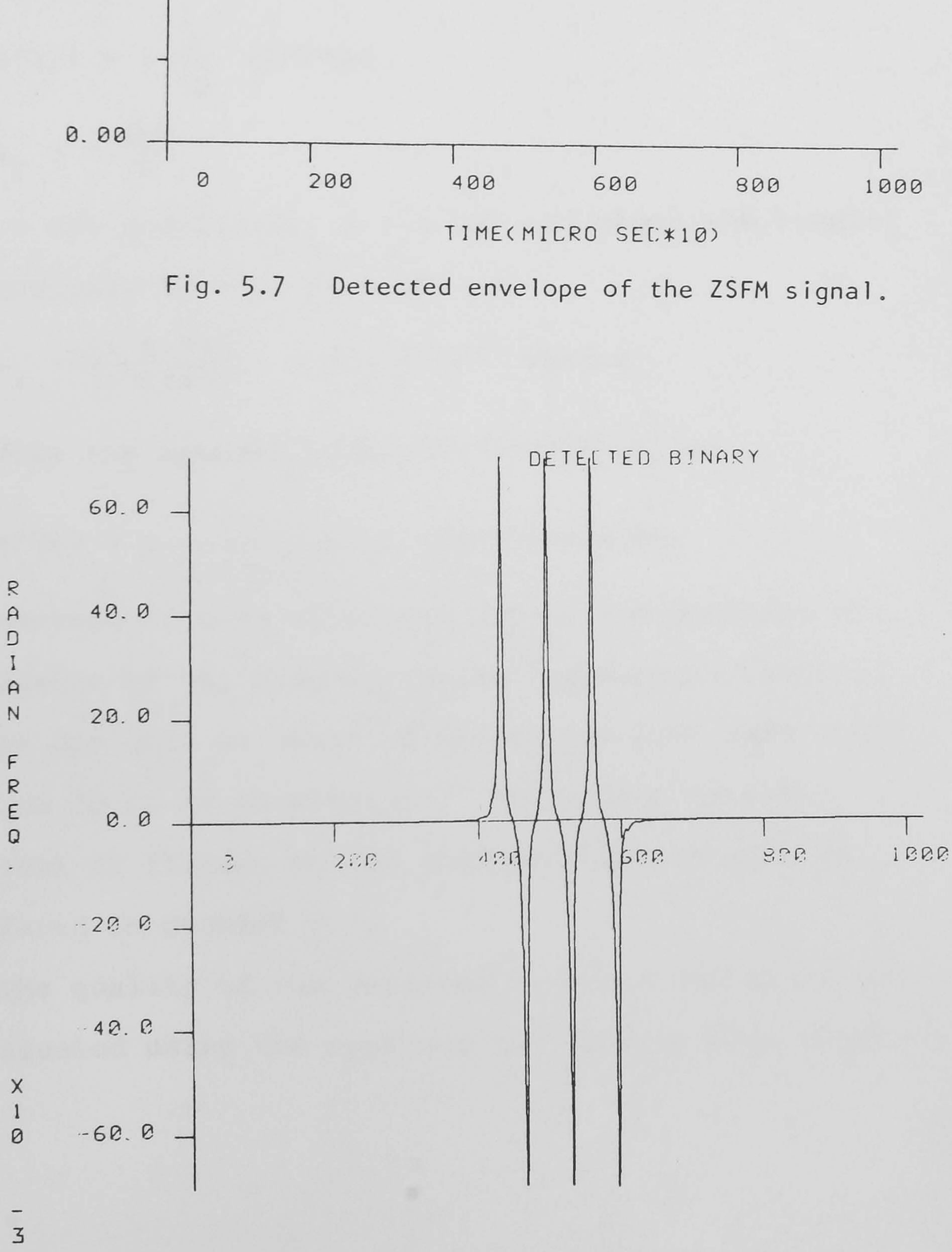

Fig. 5.8 Detected data signal of ZSFM.

deviation from the carrier represents the binary "0". Using the theoretical result given by eqn. (3.47), the FM function used for zero conjugation is in the form:

$$\theta'(t) = \pm \frac{2\sigma_r}{\sigma_r^2 + (t - t_r)^2} \quad \text{rad/sec}$$

Thus at the time of occurrence of a zero pair, $t = t_r$, $\theta'(t)$ becomes:

$$\theta'(t) = \pm \frac{2}{\sigma_r} \quad \text{rad/sec}$$

$$\sigma_r = \pm \frac{\ln a}{\Omega}$$

For m = 60% modulation, a = 0.333 and hence the complex zero ordinate of s(t) is given by:

$$\sigma_r = \pm \frac{\ln 0.333}{2\pi \times 6250} = \pm 2.8 \times 10^{-5} \text{ second}$$

Therefore the maximum frequency deviation is:

$$\theta'(t) = \pm \frac{2}{2.8 \times 10^{-5}} = \pm 71428.6 \text{ rad/sec}$$

A comparison of this value and Figure 5.8 confirms the resemblance of the simulation and theoretical results.

So far only an ideal IF filter has been used which gives no PM to AM conversion. The effect of using practical IF filters on the ZSFM performance will be considered in Section 5.5.

The quality of the detected envelope and phase will be evaluated using the approach outlined in this section.

5.4 SNR Calculation and Quality of Detected Data

In this simulation, Gaussian noise samples are added in the channel before reception permitting evaluation of ZSFM performance under noisy conditions. The NAG Library subroutine GØ5DDF (14) is used to generate noise samples having a Gaussian distribution. For a random variable x, the statistical average or mean value ($\bar{x}$) is the numerical average of the value of x weighted by their probabilities (26), i.e.

$$\bar{x} = \lim_{n\to\infty} \Sigma_m \, x_m \frac{n_m}{n} = \Sigma_m \, x_m \, P(x_m) \qquad (5.8)$$

where $P(x_m)$ is the probability.

In order to add noise to the channel, it is necessary to specify the standard deviation of the noise. This can be determined from a specified carrier-to-noise ratio (CNR).

If B_N = noise bandwidth

= receiver IF filter bandwidth (single-sided)

and $\frac{\eta}{2}$ = noise spectral density (watt/Hz)

then the noise power is:

$$N = \eta \, B_N \qquad (5.9)$$

For a random variable x, the variance is given by

$$\text{variance} = \overline{[(x - \bar{x})^2]}$$

$$= \overline{x^2} - \bar{x}^2 \qquad (5.10)$$

The standard deviation is the square root of the variance, i.e.

$$\text{standard deviation} = \sqrt{\overline{x^2} - \bar{x}^2} \qquad (5.11)$$

For processes with zero mean value ($\bar{x} = 0$) the standard deviation becomes:

$$\text{standard deviation} = \sqrt{\overline{x^2}}$$

$$= \sqrt{\text{mean power (N)}}$$

$$= \sqrt{\eta\ B_N}$$

If C is the carrier power then:

$$\text{CNR} = 10 \log \left(\frac{C}{N}\right) \quad \text{(dB)}$$

$$\therefore N = \frac{C}{10^{0.1\ \text{CNR}}} \tag{5.12}$$

Using eqns. (5.9) and (5.12) we can express the spectral density as:

$$\eta = \frac{N}{B_N} = \frac{C}{B_N \times 10^{0.1\ \text{CNR}}} \tag{5.13}$$

The above shows how the standard deviation is calculated from a given CNR. In the SNR tests, zero mean Gaussian samples are assumed throughout the experiments.

The signal-to-noise ratio at the output of the envelope detector is defined as:

$$\left(\frac{S}{N}\right)_D \equiv \frac{\text{full load signal power}}{\text{noise power available in the absence of modulation}}$$

The full load signal power (i.e. without any noise added) can be calculated, then from the given CNR Gaussian noise is added to the carrier only with zero modulation and the noise power at the output of the detector can thus be calculated. For the test signal

$$s(t) = 1 + a^2 - 2\ a \cos\Omega t$$

the d.c. term corresponding to the carrier in the absence of modulation (a = 0) is 1. Regarding the quality of the detected binary data the error rate is more useful than the measured SNR value. There is the possibility of the detected noise clicks being interpreted as a transmitted "one" or "zero" and hence giving an error. In a noisy channel the noise clicks will always be present at the output of the frequency detector due to the fact that noise is added to the envelope and phase of a ZSFM signal.

Criterion for evaluating quality of detected data

The frequency deviation from the carrier is given by the FM conjugating function $\theta'(t)$ defined as:

$$\theta'(t) = \pm \frac{2\ \sigma_r}{\sigma_r^2 + (t - t_r)^2}$$

as explained previously. At the time of occurrence of a conjugated zero pair, $t = t_r$, the deviation is maximum and equal to $\pm\ 2/\sigma_r$. It will be shown in Section 6.6 that complex zeros with σ_r values larger than 200 μsec can be neglected and this gives a lower bound of $\theta'(t)$ equal to:

$$\theta'(t) = \frac{2}{200 \times 10^{-6}} = 10000 \text{ rad/sec}$$

The above figures can be taken as a threshold value and therefore if the noise clicks at the output of the frequency detector are below 10000 rad/sec then the quality of the detected binary is regarded as "good".

This is because of the fact that when all the noise clicks are below 10000 rad/sec, then there is no error, i.e. a noise click being interpreted as binary "1" or "0". If some of the noise clicks are approximately equal to the threshold value of 10000 rad/sec, the quality is considered as "fair" and the detected data might have some error. Finally, if the noise clicks are considerably greater than 10000 rad/sec then the quality is regarded as "bad" and the above-threshold noise clicks give erroneous detection.

The next three experiments show the simulation results of the measured SNR and also the quality of the detected data for different carrier-to-noise (CNR), while the modulation depth is varied in each experiment. The ZSFM signal used is the same as expressed in Section 5.2, i.e.

$$c(t) = s(t)\ e^{j\theta t}$$

where $$s(t) = 1 + a^2 - 2a\cos\Omega t$$

$$\theta(t) = \pm 2 \arctan\left(\frac{t - t_r}{\sigma_r}\right)$$

A cluster of six zero pairs at the centre are conjugated according to the binary code 101010, while the signal s(t) generated has 64 zero pairs. Throughout the three experiments the measured SNR and quality of detected data are observed repeatedly but with the first and sixth zero pairs conjugated using different σ_r values from the actual value required for conjugation. The objective is to

EXPERIMENT 1

CNR = 30 db

Modulation depth	% $\frac{\Delta\sigma_r}{\sigma_r}$	SNR of detected envelope dB	Quality of detected binary	Highest noise click rad/sec
10%	0	6.973	good	2320
20%	0	13.076	good	2700
30%	0	16.741	good	3340
40%	0	19.451	good	4300
50%	0	21.690	good	5766
60%	0	23.659	good	8220
70%	0	25.535	fair*	12890
80%	0	27.457	bad*	23710
90%	0	29.688	bad*	88670
30%	5	16.701	good	3350
30%	10	16.663	good	3360
40%	5	19.423	good	4300
40%	10	19.395	good	4310
50%	5	21.661	good	5770
50%	10	21.642	good	5780
60%	5	23.646	good	8230
60%	10	23.632	good	8240
70%	5	25.527	fair*	12900
70%	10	25.519	fair*	12910
80%	5	27.453	bad*	23730
80%	10	27.448	bad*	23750

* The detected binary data are still recognizable and not lost in the noise clicks, i.e. binary "1" is not interpreted as binary "0" or vice versa.

EXPERIMENT 2

CNR = 40 dB

Modulation depth	% $\frac{\Delta\sigma_r}{\sigma_r}$	SNR of detected envelope dB	Quality of detected binary	Highest noise click rad/sec
10%	0	16.976	good	680
20%	0	23.080	good	780
30%	0	26.744	good	940
40%	0	29.454	good	1190
50%	0	31.684	good	1570
60%	0	33.662	good	2176
70%	0	35.538	good	3250
80%	0	37.460	good	5560
90%	0	39.691	bad*	18070
30%	5	26.704	good	950
30%	10	26.66	good	950
40%	5	29.426	good	1200
40%	10	29.398	good	1200
50%	5	31.664	good	1570
50%	10	31.645	good	1570
60%	5	33.649	good	2170
60%	10	33.636	good	2170
70%	5	35.530	good	3250
70%	10	35.522	good	3250
80%	5	37.456	good	5560
80%	10	37.452	good	5560

* The data code 101010 is not lost in the noise clicks.

EXPERIMENT 3

CNR = 50 dB

Modulation depth	% $\frac{\Delta\sigma_r}{\sigma_r}$	SNR of detected envelope dB	Quality of detected binary	Highest noise click rad/sec
10%	0	27.977	good	200
20%	0	33.081	good	230
30%	0	36.746	good	280
40%	0	39.455	good	350
50%	0	41.685	good	460
60%	0	43.663	good	630
70%	0	45.539	good	940
80%	0	47.461	good	1590
90%	0	49.692	good	4540
30%	5	36.705	good	280
30%	10	36.667	good	280
40%	5	39.427	good	350
40%	10	39.400	good	350
50%	5	41.665	good	460
50%	10	41.646	good	460
60%	5	43.650	good	630
60%	10	43.637	good	630
70%	5	45.531	good	940
70%	10	45.522	good	940
80%	5	47.457	good	1590
80%	10	47.453	good	1600

notice the effect of using slightly different σ_r for conjugation on the quality of detected signal. The receiver filter simulated is of constant magnitude over the passband and has a linear-phase response. The receiver IF filter has a bandwidth of $\pm \frac{\Omega}{2\pi} = \pm 6.25$ kHz, i.e. equal to the ZSFM signal bandwidth.

The last three experiments showed that the degradation in the SNR of the detected envelope due to using incorrect σ_r values for conjugation is tolerable. The degradation is less than 0.1 dB for an error up to 10%.

In Experiment 1 the detected binary has an error for modulation depth $\geq$ 70%, while in Experiment 2 the detected binary is error-free up to 90% modulation depth. It was noticed that the noise clicks in the detected binary increase as the modulation depth increases for any given CNR. For low modulation depth the envelope trough is far from zero and the corresponding complex zero has a high σ_r value. Hence the binary data, imposed through the frequency function $\theta'(t)$, are not highly affected by noise as mentioned in Section 3.9. While for high modulation depth the envelope trough is close to zero and the corresponding zero has a low σ_r value. Therefore the binary data are highly affected by noise and the noise clicks are higher and can be misleading,

i.e. noise clicks can be interpreted as "1" or "0" at the receiver. Figure 5.9 shows the detected envelope for 60% modulation and 40 dB CNR, and Figure 5.10 shows the detected binary code (101010) for the same condition.

A test was carried out to measure the highest noise clicks available in the detected binary data for different modulation depths. The same signal is used as that of the last experiments and $\Delta\sigma_r$ is kept equal to zero throughout, i.e. a correct value of σ_r is used. Figure 5.11 shows the noise click variation against the modulation depth for 40 dB CNR. The noise clicks are unharmful and do not exceed 10000 rad/sec up to 87% modulation depth. Figure 5.12 shows the noise clicks for 45 dB CNR and it is noticeable that noise clicks are less than 10000 rad/sec for modulation depths $\leq$ 90%. Thus the hazard of noise clicks being interpreted as a conjugated zero pair is tolerable for modulation depths less than 90%, and consequently zero conjugation and data transmission can be performed safely for signal modulation depth up to 85% - 90%. In practice the modulation depth rarely exceeds 80% in radio broadcast transmission.

The error performance of ZSFM can be studied by observing the detected data of a prototype real ZSFM system. Three types of errors are expected in the detected system of ZSFM; the first type is a noise click being interpreted as binary "1" or "0" when it exceeds the threshold value of ± 10000 rad/sec. The second type occurs when binary "1" is being interpreted as binary "0" and vice versa, and the third type of error occurs when binary "1" or "0" is so badly corrupted by noise that it gives, on detection, a deviation less than 10000 rad/sec in magnitude. Probability of error can then be found for different CNR values by counting the errors that occur in the time of record.

The second and third types of errors were not detected in the last three experiments of this section, even under the worst considered noise condition of 30 dB CNR. However, the first type of error was detected and it can significantly affect performance at high modulation depths and high noise level. For higher CNR values the detected binary was error-free for modulation depths up to 90%.

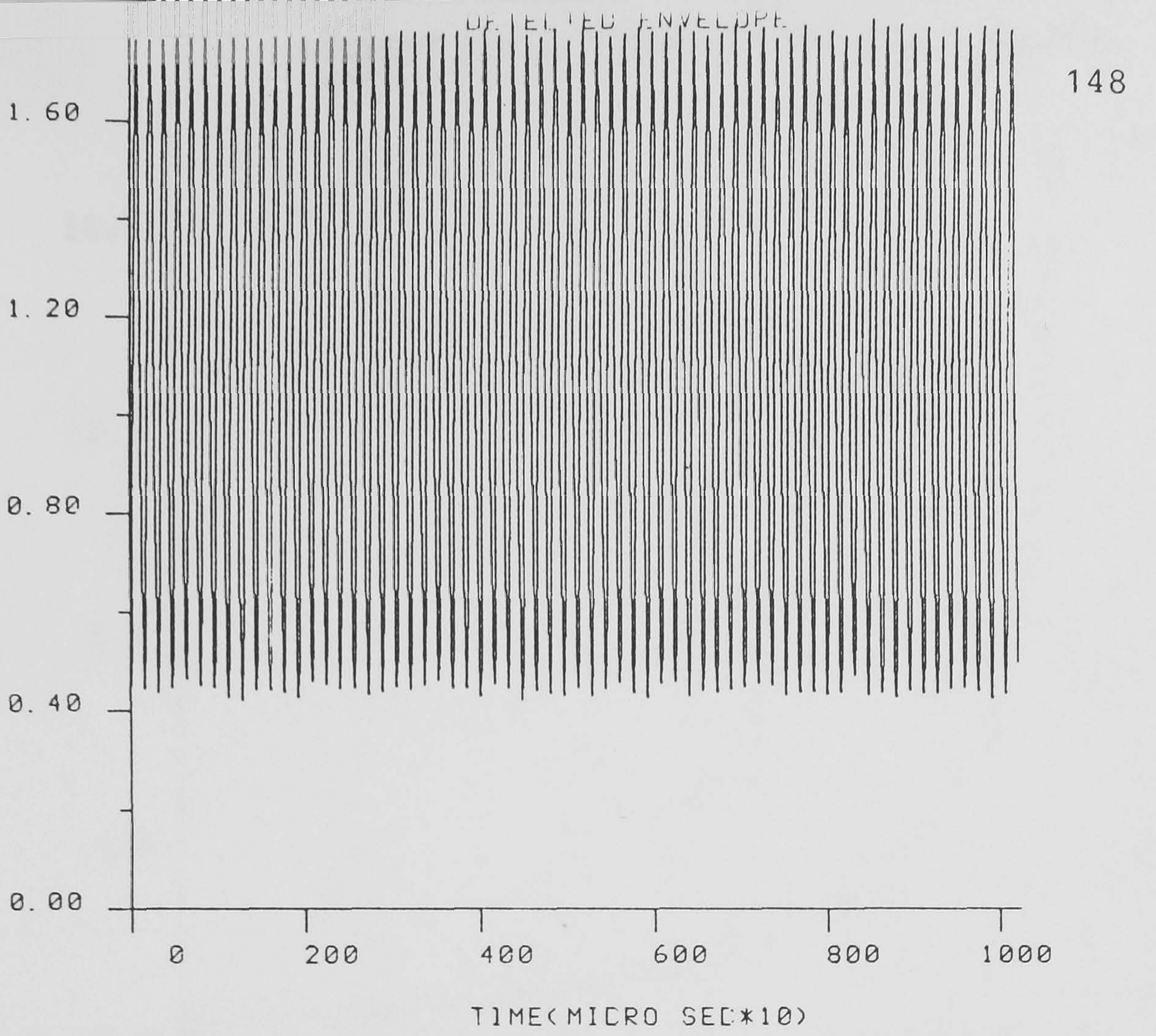

Fig. 5.9 Detected envelope signal for 60% modulation and 40 dB CNR.

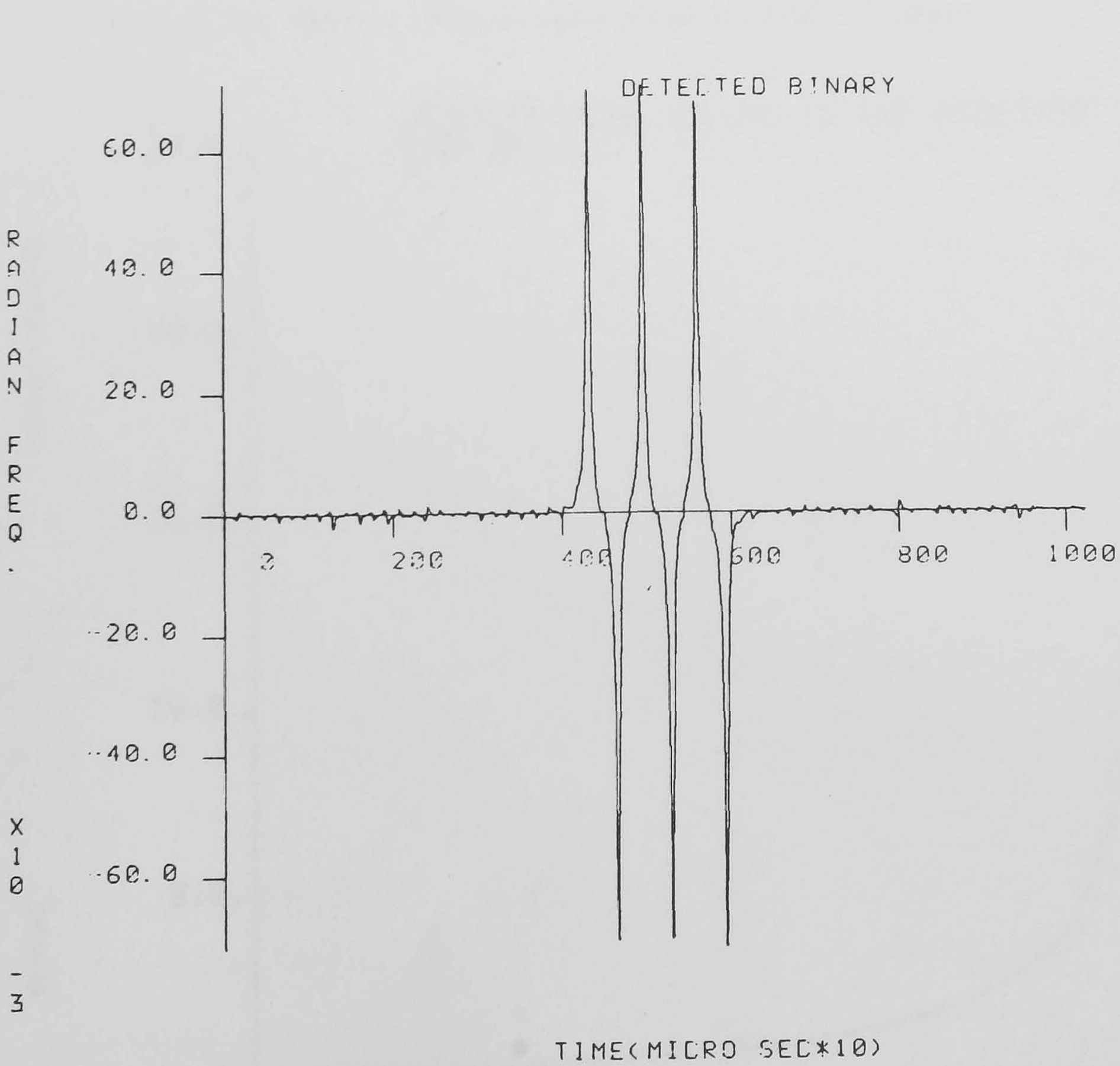

Fig. 5.10 Detected data for 60% modulation and 40 dB CNR.

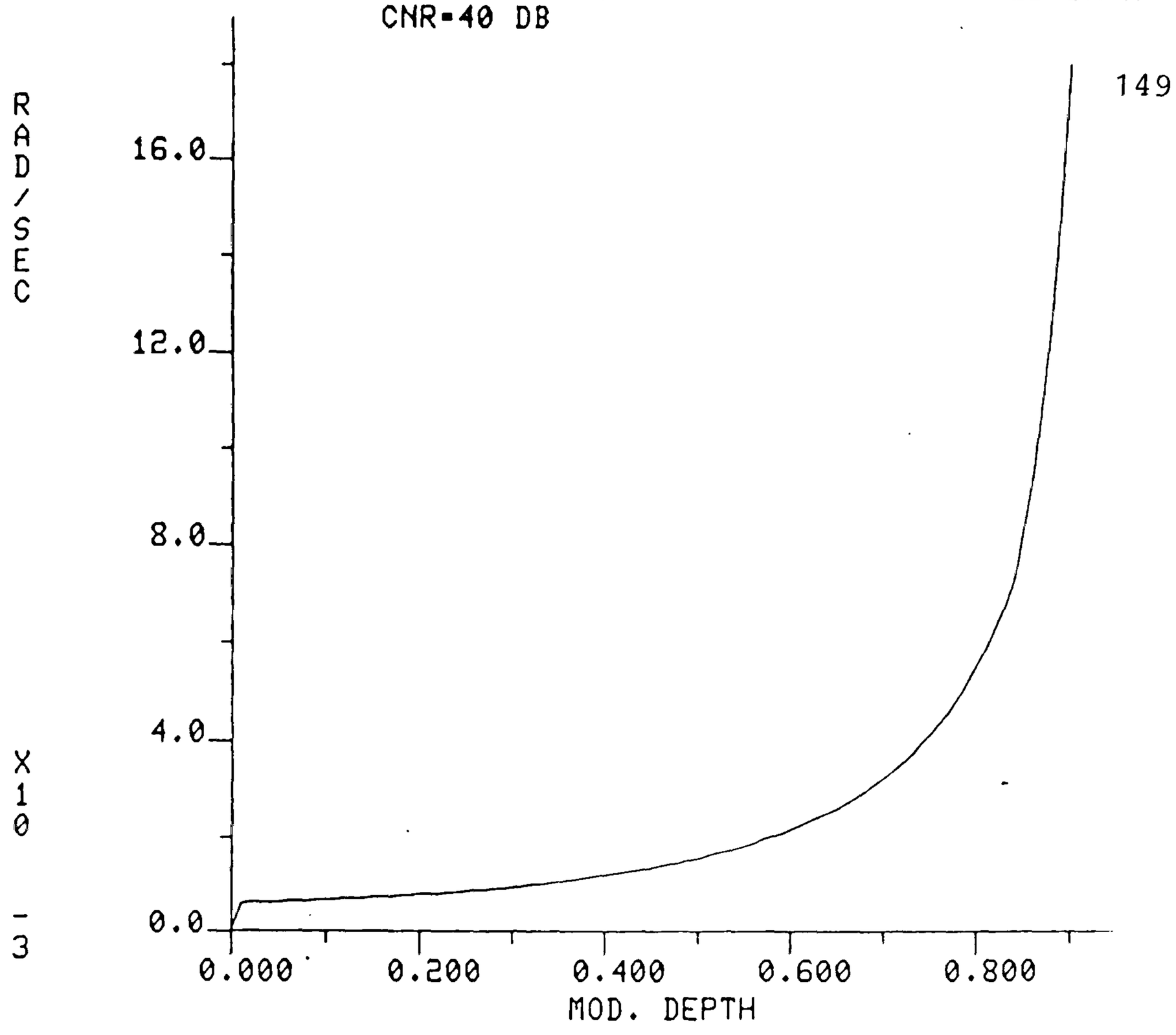

Fig. 5.11 Noise clicks variation for 40 dB CNR

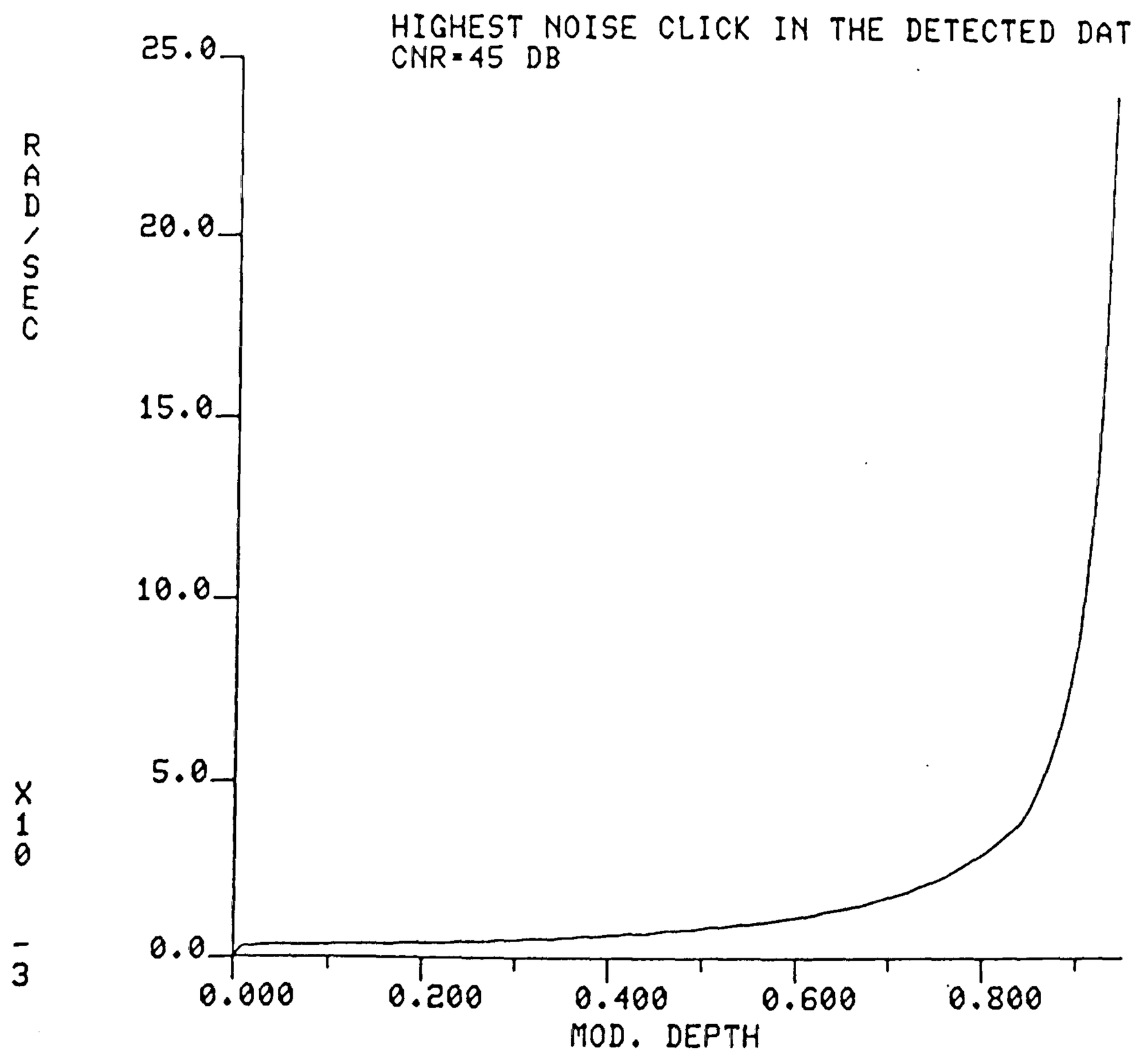

Fig. 5.12 Noise clicks variation for 45 dB CNR.

5.5 Simulation of IF Cross-Talk

In the previous section an ideal IF filter was used, having a constant magnitude over the passband and linear-phase response. This ideal IF filter gives no p.m. to a.m. conversion and hence it is important to investigate the effect of using practical IF filter on the detection performance of ZSFM. For every linear-phase filter the group delay (also called envelope delay) is constant, and it describes a constant delay of a packet of frequencies which is highly desirable in FM systems. For such a linear-phase response the group delay is constant for all components of the FM signal, and there is no distortion introduced (27).

In the domestic AM receiver the IF amplifier comprises coupled tuned circuits operating at a fixed frequency (28,29,30). High selectivity (narrow bandwidth) needs high Q values for the coil. Single-tuned circuits are not normally used in IF amplifier as they give a narrow selectivity and poor attenuation in the stopband. Coupled circuits give more satisfactory curve and usually they have identical L, C, and R values.

We will consider the IF tuned transformer with mutual inductance coupling, and study its magnitude and phase frequency responses. The equivalent circuit diagram (30) for the double-tuned transformer with mutual inductance coupling and a derivation of the magnitude and phase responses are given in Appendix (3). Quoting the results of Appendix (3), the magnitude and phase responses of a practical IF transformer can be expressed in the form:

$$|H_{IF}(F)| = \frac{2\,Qk}{\sqrt{[1 + Q^2(k^2 - F^2)]^2 + 4\,Q^2F^2}} \qquad (5.14)$$

$$\phi_{IF}(F) = \arg H_{IF}(F) = \arctan \frac{1 + Q^2(k^2 - F^2)}{2\,QF}$$

where Q is the Q-factor of the coil, k is the coupling coefficient ($k << 1$), $F = \frac{2\Delta f}{f_o}$, f_o = central frequency (mid-band frequency) and Δf is the off-tune frequency from f_o.

The assumptions made in order to obtain the above expressions lead only to small errors with normal couplings at an IF of f_o = 465 kHz or over and off-tune (Δf) frequencies up to ± 50 kHz.

The phase response $\phi_{IF}(F)$ has little significance in AM reception, but it is of considerable importance in FM reception because the non-linear characteristic over the passband range can cause distortion of the modulation content of the signal.

The simulation of this IF stage in the computer is performed by generating the corresponding magnitude and phase responses, $|H_{IF}(F)|$ and $\phi_{IF}(F)$ given by eqn. (5.14), and multiplying this response with the spectrum of the received ZSFM signal before detection takes place. This allows the effect of phase non-linearities on the detected signal to be estimated, and the problem of cross-talk (due to the data signal in ZSFM) can be evaluated. A value of Qk = 1 is used as it is the common figure for commercial IF transformers in domestic receivers (31). For critically-coupled double-tuned circuits the bandpass

double-sided bandwidth is given by:

$$B = \frac{\sqrt{2}\ f_o}{Q} \tag{5.15}$$

A value of Q is chosen such that the 3-dB bandwidth of the IF transformer is 5 kHz (i.e. Δf = 5 kHz and B = 10 kHz). This can be calculated from eqn. (5.15) where the IF mid-band frequency is f_o = 470 kHz.

$$B = 2\Delta f = 10 \text{ kHz} = \frac{\sqrt{2}\ f_o}{Q}$$

$$10 \text{ kHz} = \frac{\sqrt{2} \times 470 \text{ kHz}}{Q}$$

$$\therefore Q = 66.468$$

But Qk = 1

$$\therefore k = 0.015045$$

Now these values for Q and k, when used in the magnitude and phase characteristics of the IF stage, give the required IF response with 5 kHz 3-dB bandwidth.

Figure 5.13 shows the magnitude response of the IF transformer and it can be noticed that at 5 kHz the magnitude is 0.707 (3 dB point).

Figure 5.14 shows the phase response. Now the problem of cross-talk can be investigated by observing the detected envelope and data signals of ZSFM using this practical IF filter. The ZSFM signal considered is:

$$c(t) = s(t)\ e^{j\theta(t)}$$

where a block of 64 cycles of $s(t) = 1 + a^2 - 2a\cos\Omega t$ is generated in a time duration of 40960 μ second which gives a modulating frequency of $\frac{\Omega}{2\pi}$ = 1.5625 kHz, i.e. it lies in the IF passband range.

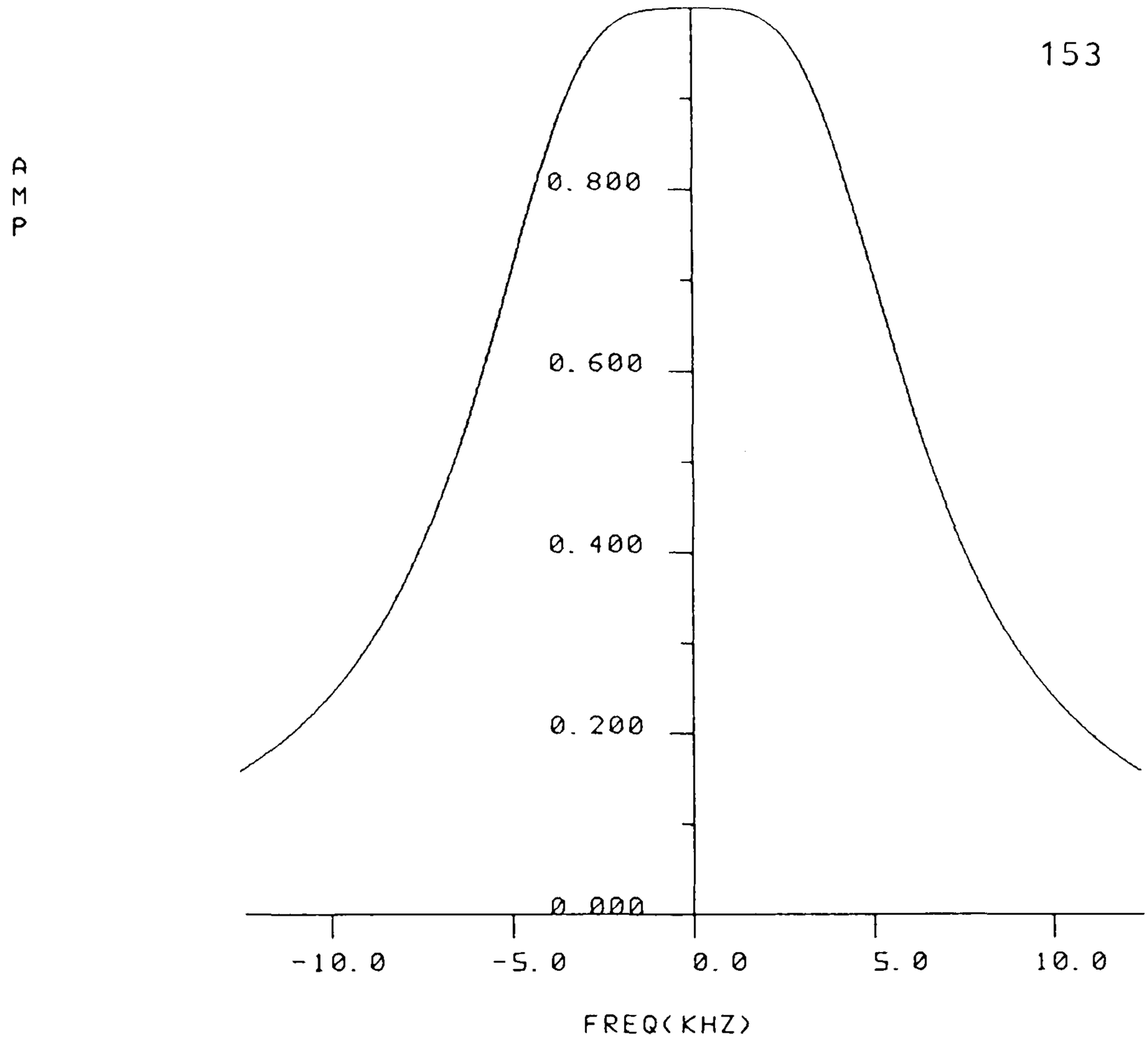

Fig. 5.13 Magnitude response of the IF transformer.

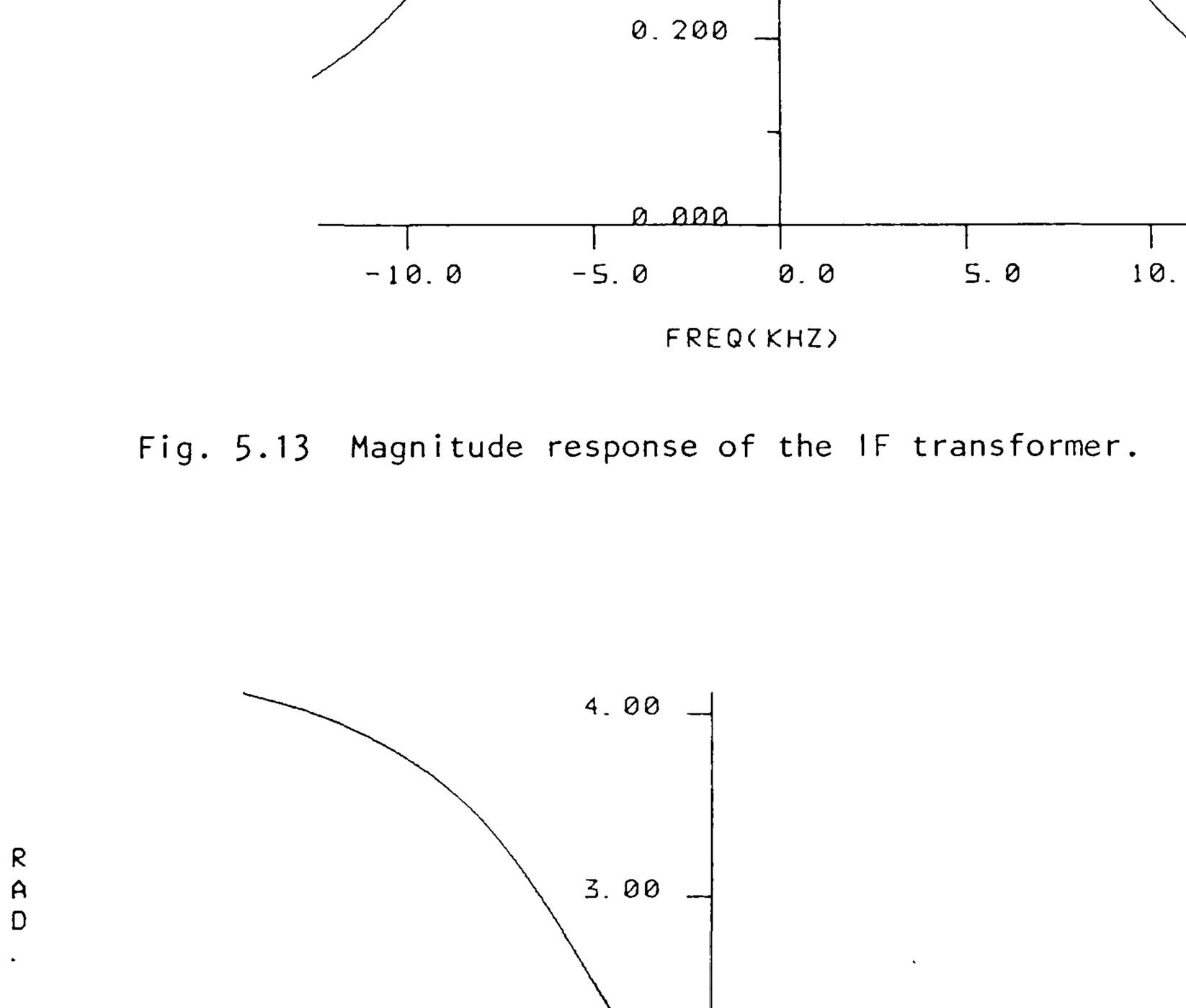

Fig. 5.14 Phase response of the IF transformer.

The PM function is as usual given by:

$$\theta(t) = \pm 2 \arctan\left(\frac{t - t_r}{\sigma_r}\right)$$

A cluster of six zero pairs at the middle of s(t) are conjugated according to the binary code (101010).

Figure 5.15 shows the detected envelope for 60% modulation depth. It is apparent that the detected envelope signal is almost free of distortion and hence the IF transformer does not appear to significantly degrade p.m. to a.m. conversion.

Figure 5.16 shows the spectrum of the detected envelope signal from which the distortion components can be seen to fall about 60 dB below the envelope tone. A quantitative study of the degradation of the detected envelope due to the distortion introduced by the IF transformer is discussed in Section 5.7.

Figure 5.17 shows the detected binary signal (101010). From the theoretical result given by eqn. (3.47), the FM function used for zero conjugation is:

$$\theta'(t) = \pm \frac{2\sigma_r}{\sigma_r^2 + (t - t_r)^2} \quad \text{rad/sec}$$

At the time of occurrence of a zero pair $t = t_r$ the FM function becomes:

$$\theta'(t) = \pm \frac{2}{\sigma_r}$$

For 60% modulation $\sigma_r = \pm 1.12 \times 10^{-4}$ second

$$\therefore \quad \theta'(t) = \pm 17856.3 \text{ rad/sec}$$

This value is confirmed in Figure 5.17.

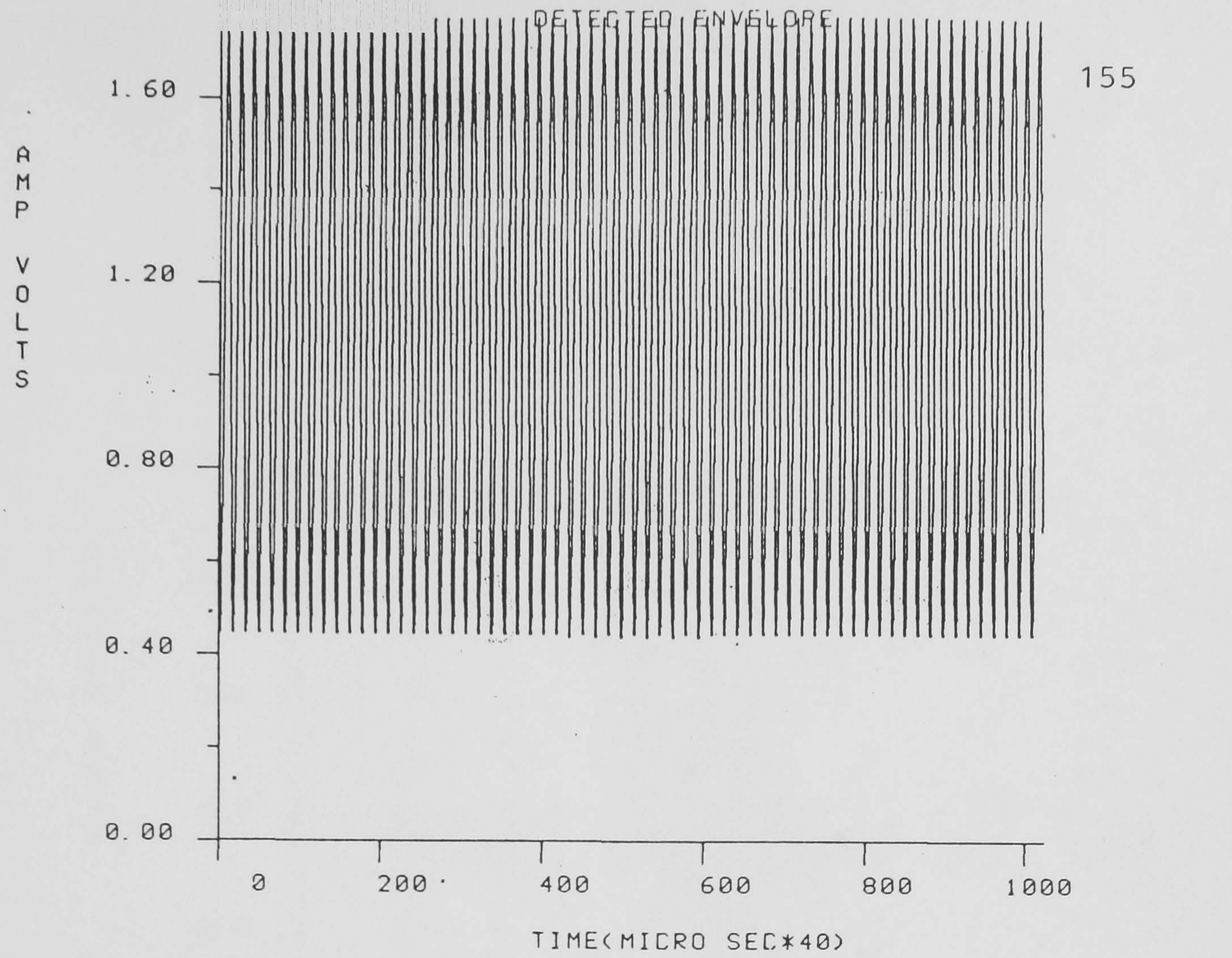

Fig. 5.15 Detected envelope signal for 60% modulation.

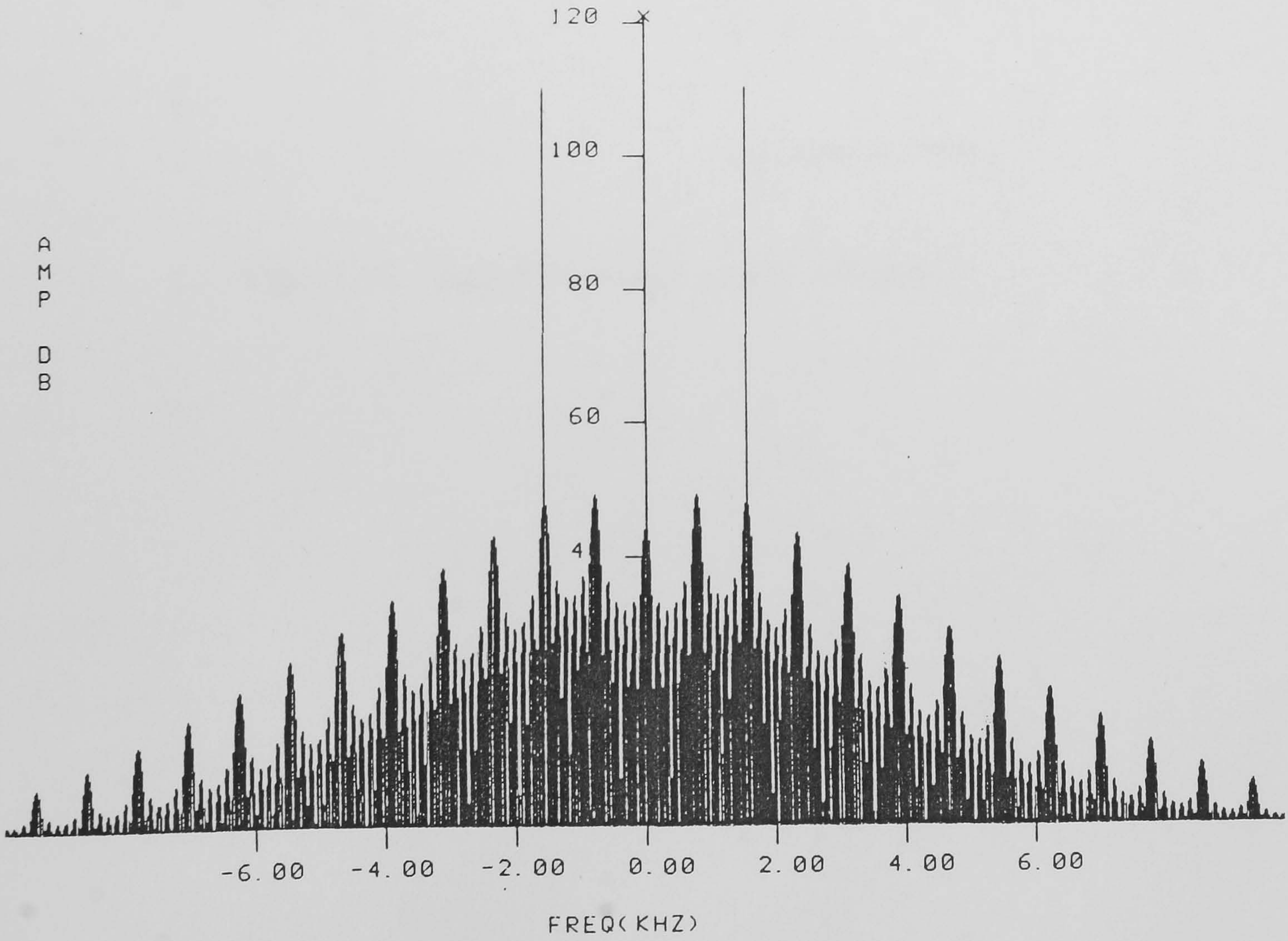

Fig. 5.16 Spectrum of the detected envelope.

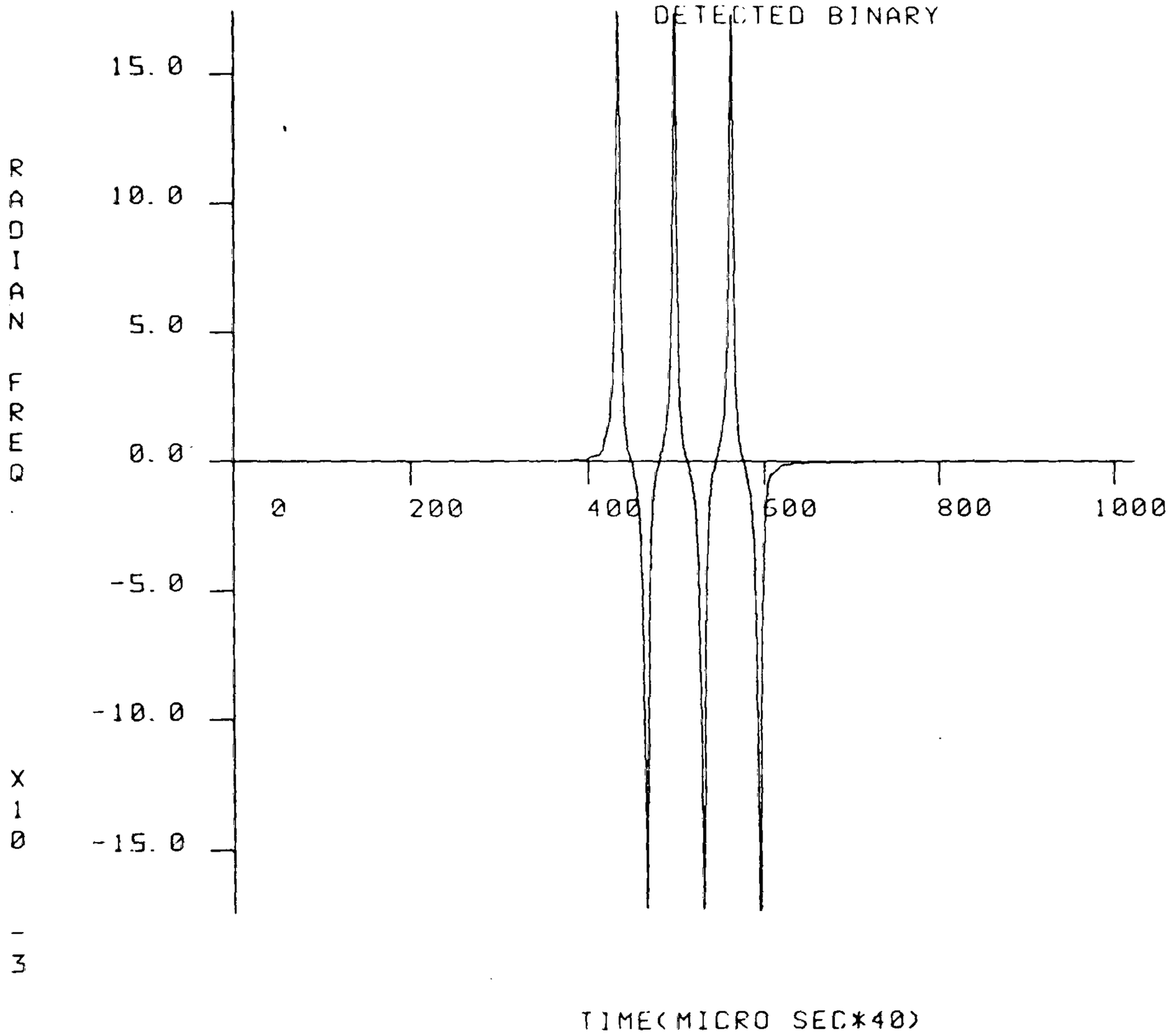

Fig. 5.17 Detected binary signal (101010).

Another ZSFM signal was simulated in which all the 64 complex zero pairs are conjugated according to a random binary code that has equal numbers of "ones" and "zeros". Figure 5.18 shows the detected envelope signal for 60% modulation depth. Figure 5.19 shows the spectrum of the detected envelope signal, and it is apparent that the distortion components are about 70 dB below the envelope tone. The envelope harmonics that are more than 50 dB below the fundamental are filtered out easily by the low pass filter after envelope detection.

Figure 5.20 shows the detected binary code that has equal numbers of randomly varying "ones" and "zeros".

The last three experiments discussed in Section 5.4 for calculating the SNR of the detected envelope and observing the quality of the detected binary data in presence of noise, can be repeated using the practical IF transformer. In calculating the SNR, the receiver IF filter bandwidth (B_N) used to obtain the noise spectral density is made equal to the 3-dB bandwidth of the IF filter, i.e. 5 kHz. The same criterion for the quality of the detected data signal is used. The ZSFM signal considered in the next three experiments has six zero pairs at the centre conjugated according to the binary code (101010). Different carrier-to-noise ratio (CNR) are considered.

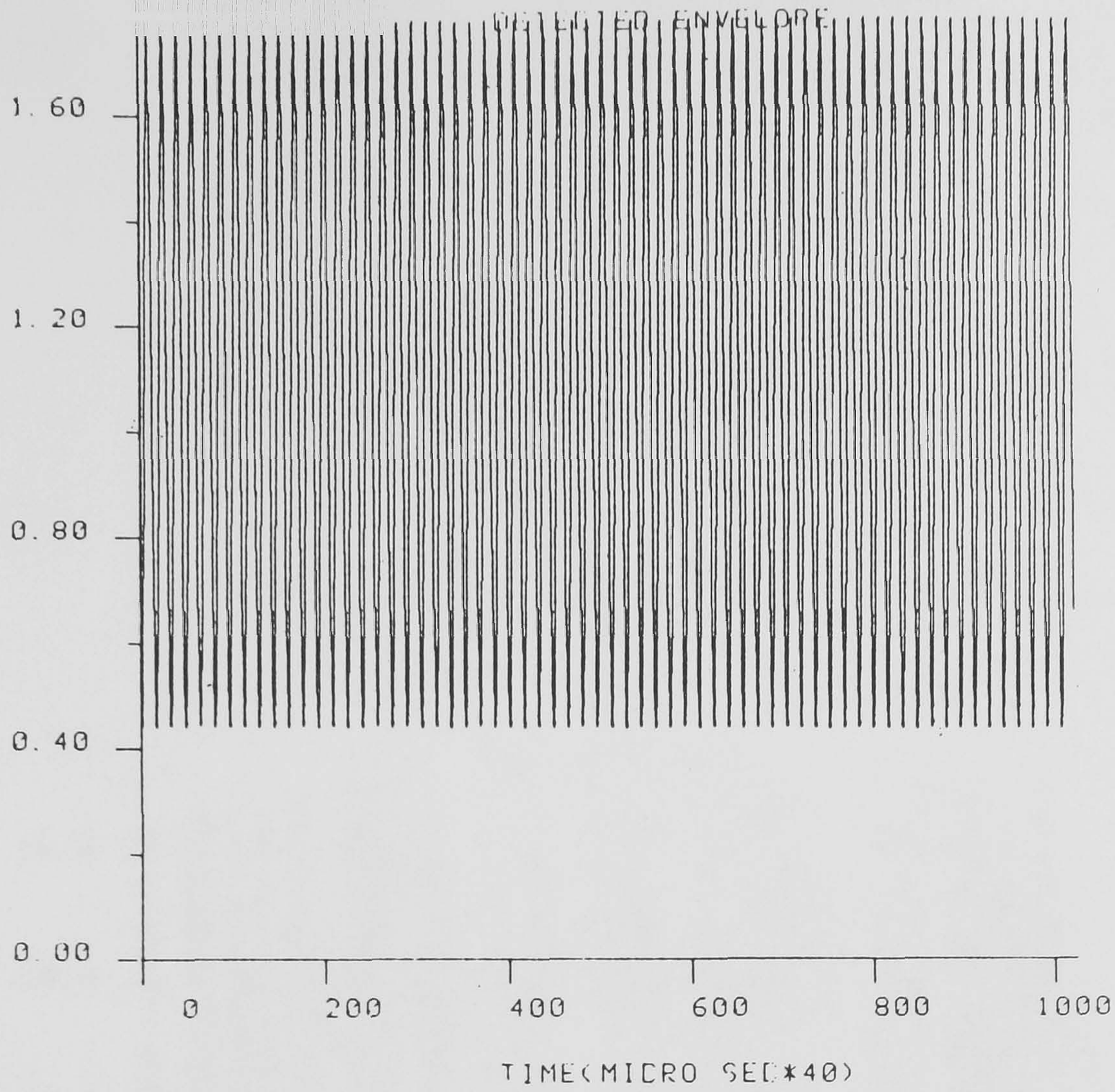

Fig. 5.18 Detected envelope for 60% modulation, and all zero pairs conjugated.

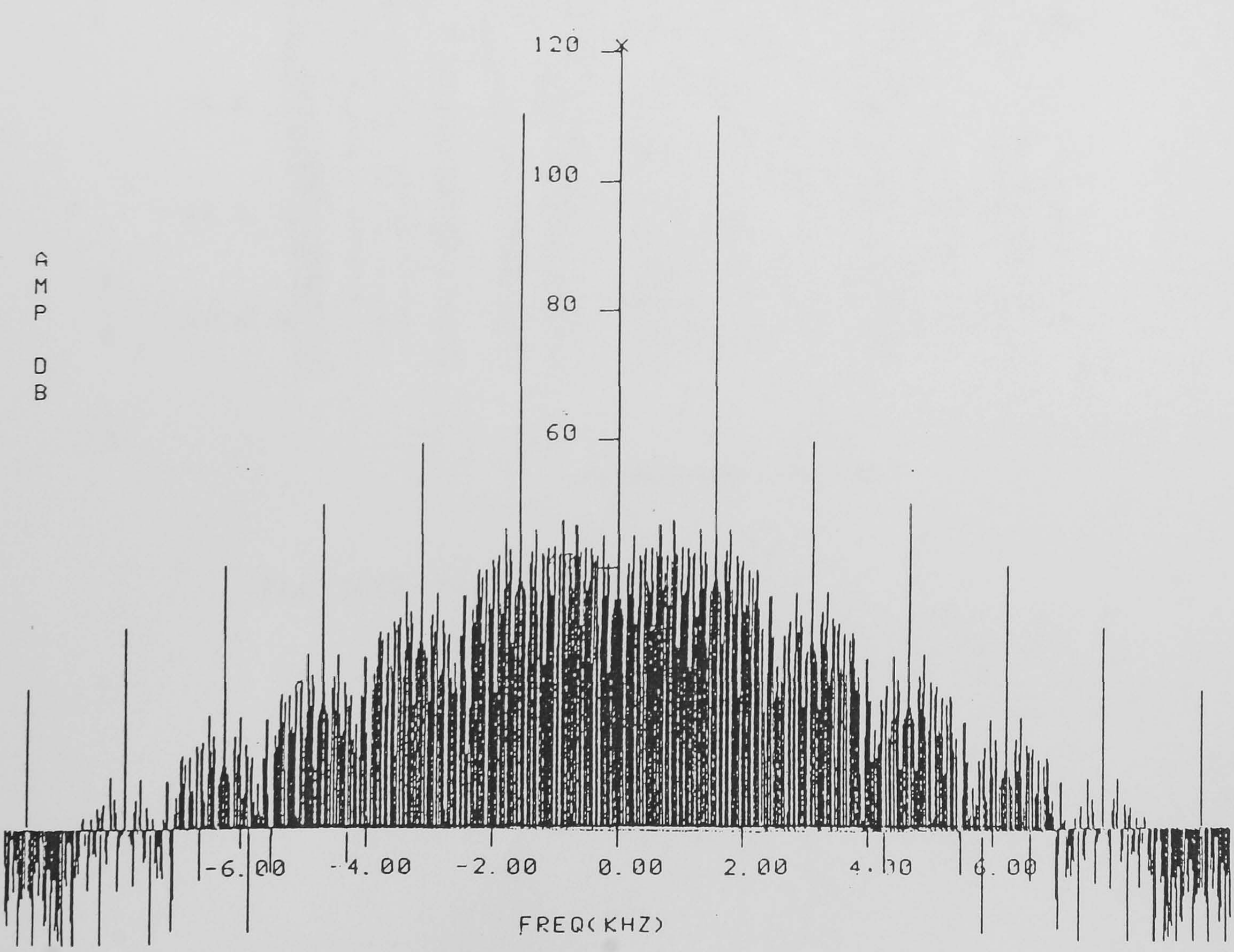

Fig. 5.19 Spectrum of the detected envelope.

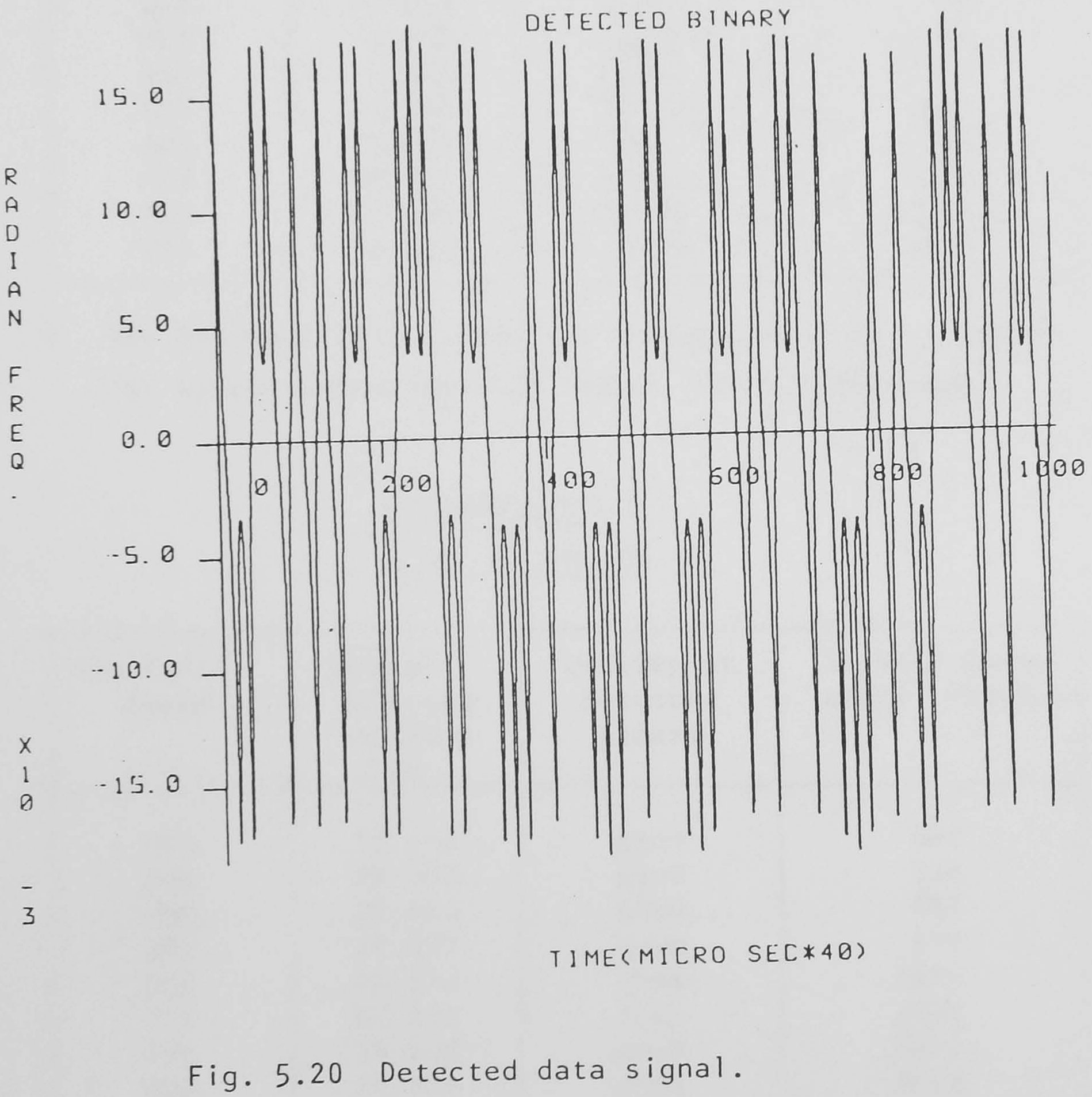

Fig. 5.20 Detected data signal.

EXPERIMENT 4

CNR = 30 dB

Modulation depth	SNR of detected envelope dB	Quality of detected binary	Highest noise click rad/sec
10%	6.851	good	2113
20%	12.954	good	2228
30%	16.618	good	2518
40%	19.328	good	2956
50%	21.557	good	3561
60%	23.536	good	4459
70%	25.413	good	5927
80%	27.336	good	8725
90%	29.568	bad*	15675

* The detected binary data are recognisable, i.e. binary "1" is not interpreted as binary "0" or vice versa.

EXPERIMENT 5

CNR = 40 dB

Modulation depth	SNR of detected envelope dB	Quality of detected binary	Highest noise click rad/sec
10%	16.846	good	654
20%	22.949	good	714
30%	26.614	good	827
40%	29.323	good	977
50%	31.553	good	1187
60%	33.531	good	1502
70%	35.408	good	2030
80%	37.331	good	3079
90%	39.563	good	5935

EXPERIMENT 6

CNR = 50 dB

Modulation depth	SNR of detected envelope dB	Quality of detected binary	Highest noise click rad/sec
10%	26.840	good	204
20%	32.943	good	225
30%	36.607	good	262
40%	39.317	good	310
50%	41.546	good	378
60%	43.525	good	480
70%	45.402	good	652
80%	47.325	good	994
90%	49.557	good	1937
95%	51.042	good	3320

The last three experiments show that the detection performance of ZSFM using an IF stage with non-linear characteristics appears satisfactory.

A comparison of these experiments with those in Section 5.4 shows that the SNR of the detected signal is not degraded by more than 0.1 dB when using the practical IF filter. The detected data have proved very satisfactory and there was only noise click exceeding 10000 rad/sec at 90% modulation and for 30 dB CNR.

After simulating a practical IF transformer it can be concluded that the problem of IF cross-talk is almost negligible, as the detected envelope and data signals do not appear to have been affected significantly due to non-linearities of the IF tuned circuit.

5.6 Condition of Mistune

In practice it cannot be assumed that a perfect tune to a specific station is obtained as this varies from person to person. In such a case where a receiver is slightly mistuned to a station, more distortion can be expected in the detected envelope signal and some of the data signals may possibly become perceptible. Therefore an investigation of the detection performance of ZSFM becomes necessary under such conditions.

In order to simulate such a mistune condition on the computer, it is only required to shift the transfer function of the IF transformer $H_{IF}(f)$ from the centre frequency f_o. In the present computer simulation this corresponds to shifting $H_{IF}(f)$ from the zero frequency as the simulation is performed at baseband as illustrated by Figure 5.21. This can be achieved by multiplying the impulse response of the IF transformer, $h_{IF}(t)$, in the time domain by $e^{j2\pi f_{mis} t}$ where f_{mis} is the mistune frequency. Taking the discrete Fourier transform using the FFT subroutine then gives the required shifted IF transformer characteristics, i.e.

$$F[h_{IF}(t)] = H_{IF}(f)$$

$$F[h_{IF}(t)\ e^{j2\pi f_{mis} t}] = H_{IF}(f - f_{mis}) \qquad (5.16)$$

where F [ ] denotes Fourier transform.

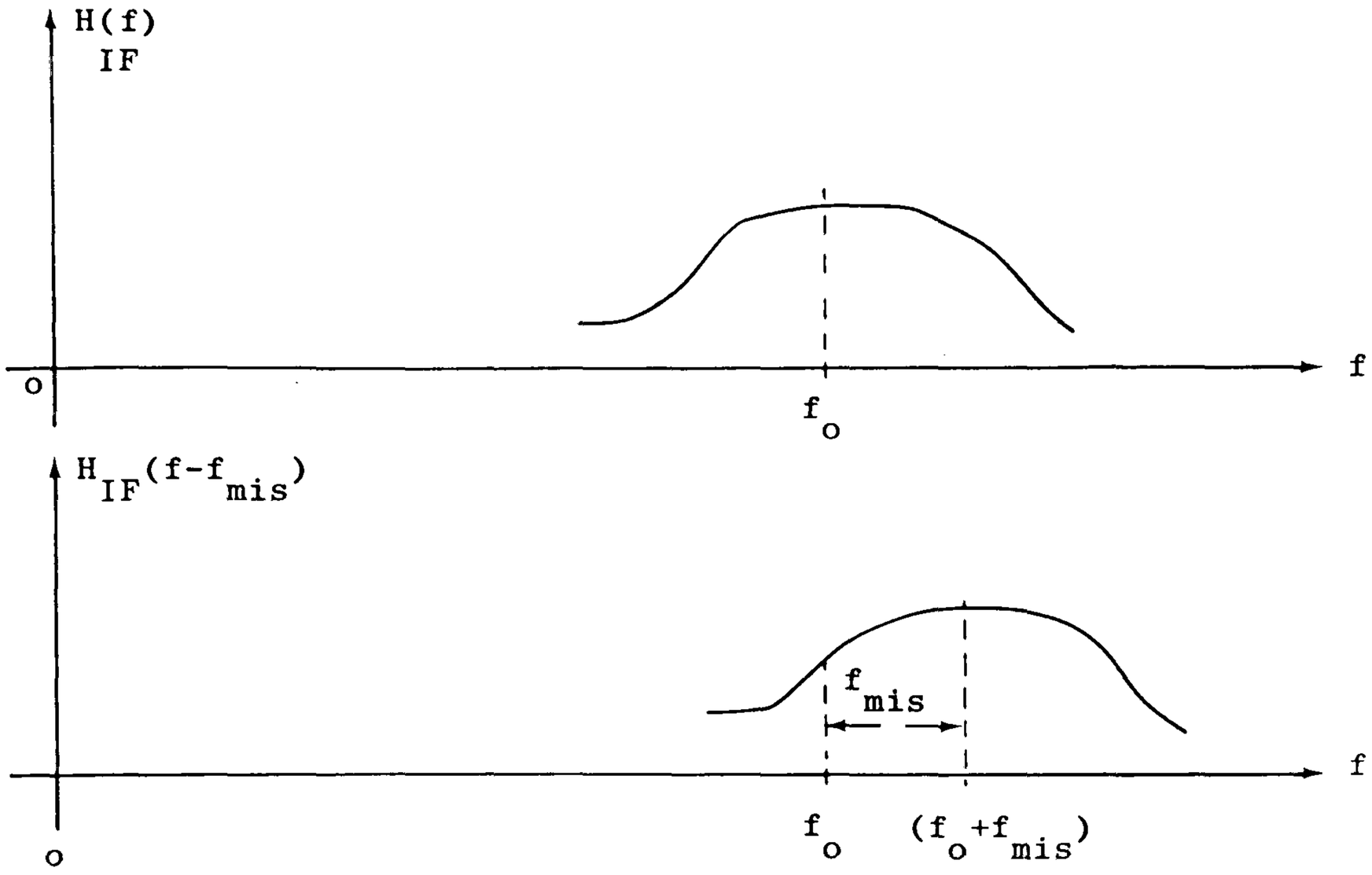

Mistune at f_o

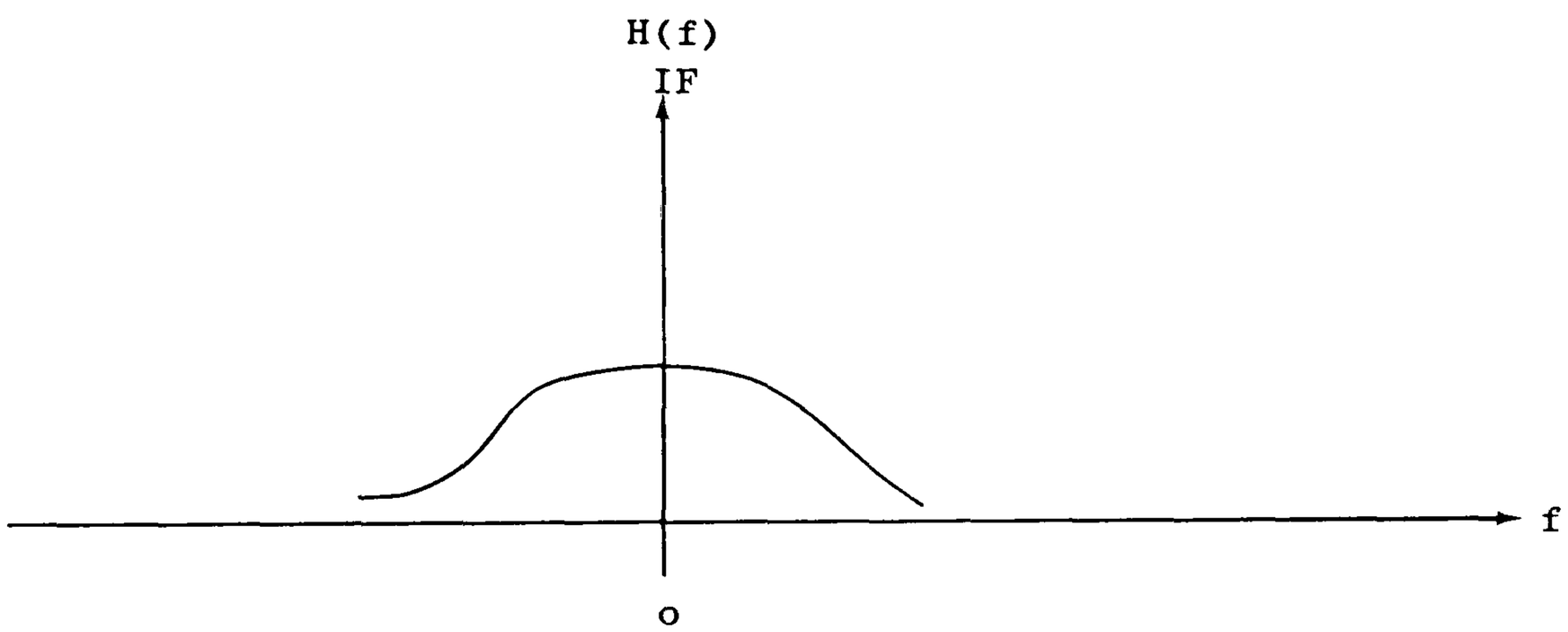

Mistune at baseband

Fig. 5.21

The same ZSFM signal, described in the previous section with six zero pairs at the centre conjugated according to the code (101010), is used to investigate the effect of a mistune condition. A mistune of 1 kHz ($\frac{1\ kHz}{10\ kHz}$ x 100% = 10% mistune) is considered. Figure 5.22 shows the detected envelope for 60% modulation depth. Figure 5.23 shows the spectrum of the detected envelope signal from which the distortion components can be seen to fall about 55 dB below the envelope tone components. A quantitative study of the degradation of the detected envelope signal due to mistune will be made in the next section. Figure 5.24 shows that the detected binary signal (101010) is clearly recognisable. It is apparent that a.m./p.m. conversion occurs in this case of receiver mistune as the upper and lower sidebands of the DSB-AM signal are unequal.

The performance of ZSFM is apparently satisfactory even in the condition of 10% mistune.

The next three experiments show the ZSFM detection performance in noisy conditions and also in a 10% mistune condition. The same procedures in calculating the SNR and observing the quality of detected binary apply as before. Different carrier-to-noise ratios (CNR) are considered.

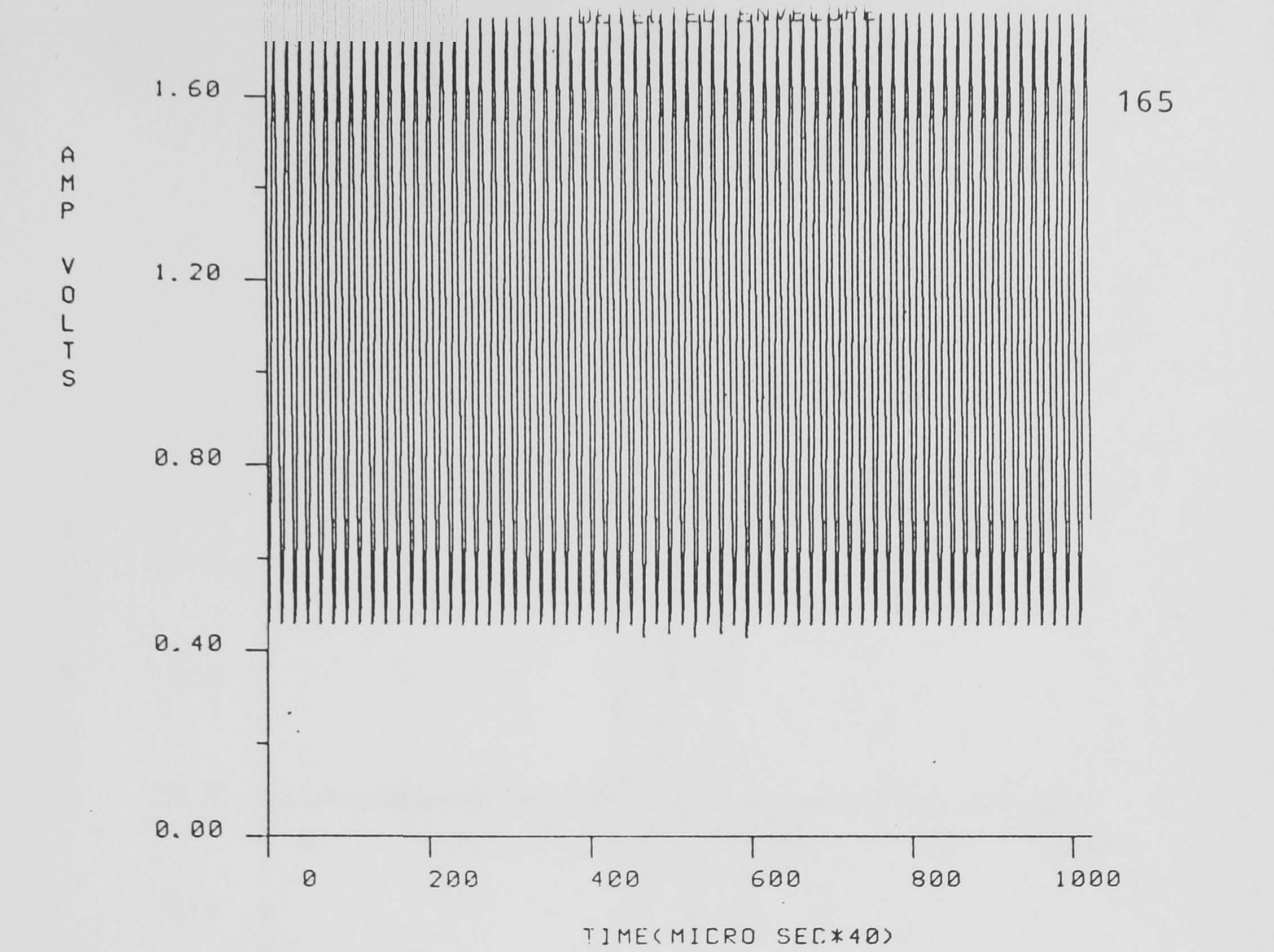

Fig. 5.22 Detected envelope for 60% modulation, and 10% mistune.

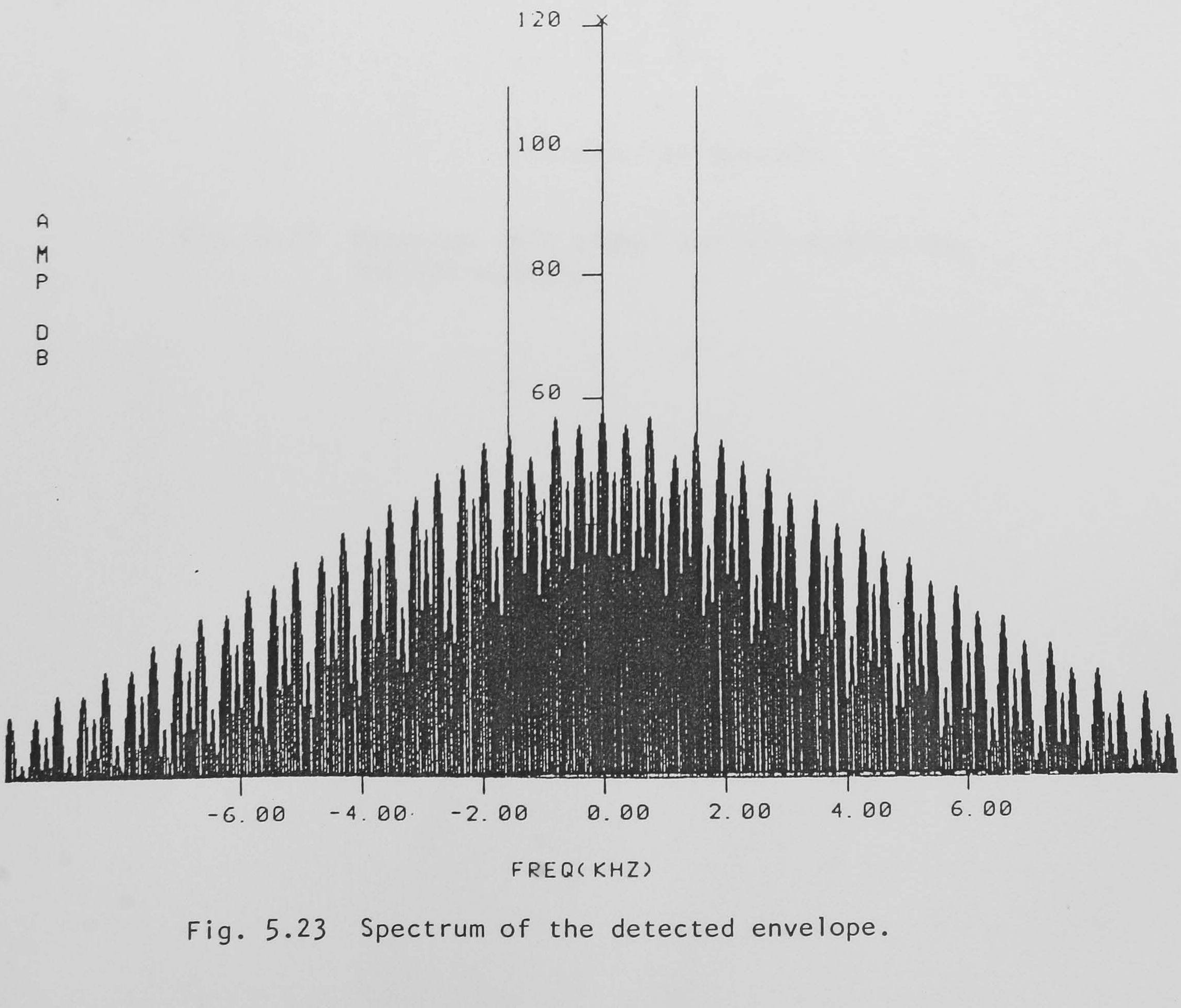

Fig. 5.23 Spectrum of the detected envelope.

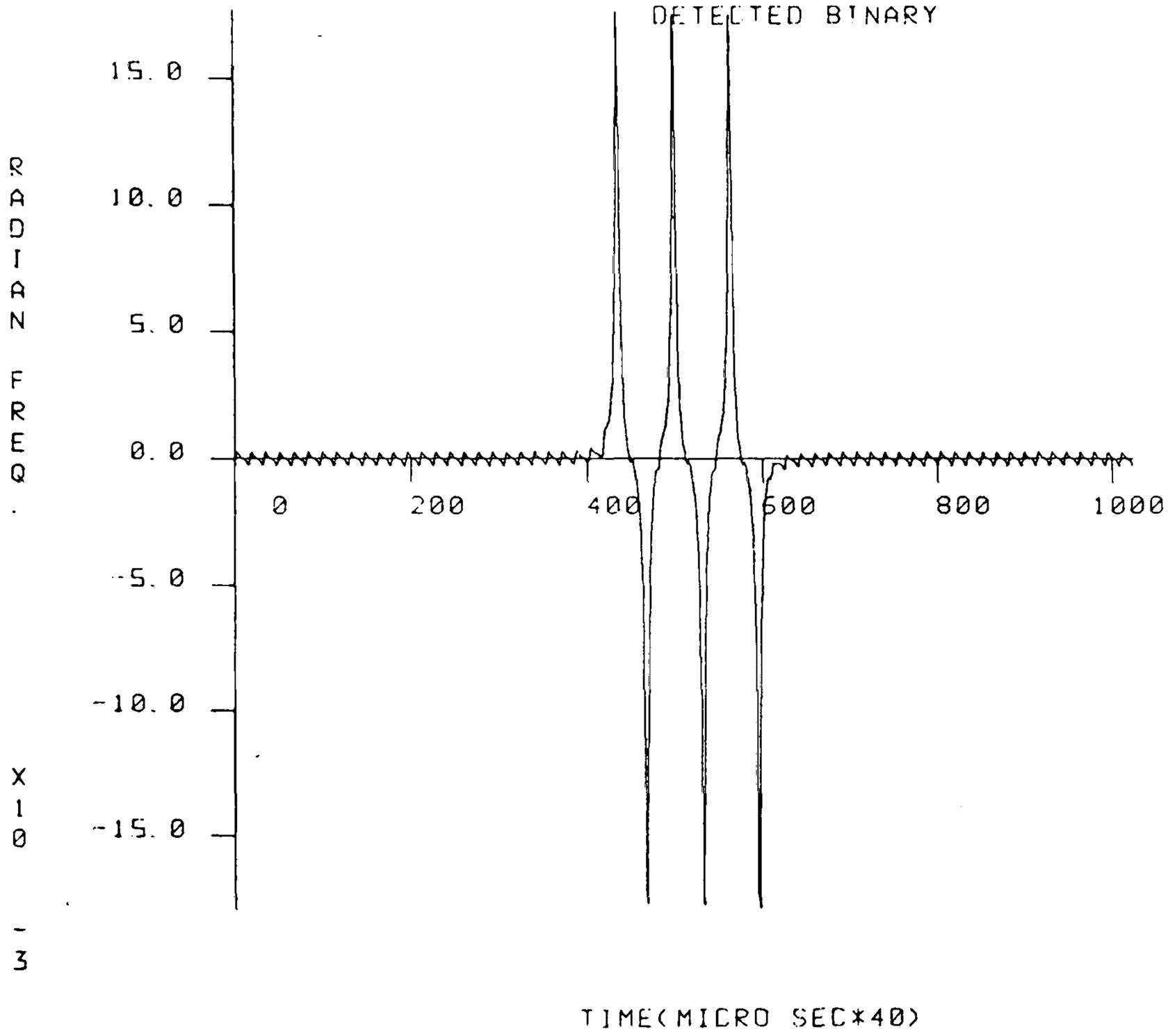

Fig. 5.24 Detected data signal for 60% modulation, and 10% mistune.

EXPERIMENT 7

CNR = 30 dB, f_{mis} = 1 kHz (10% mistune)

Modulation depth	SNR of detected envelope dB	Quality of detected binary	Highest noise click rad/sec
10%	6.722	good	2310
20%	12.822	good	2239
30%	16.486	good	2254
40%	19.195	good	2628
50%	21.426	good	3129
60%	23.405	good*	3862
70%	25.283	good*	4955
80%	27.208	good*	7008
90%	29.443	bad*	17344

* Positive and negative frequency excursions are unequal in magnitude.

EXPERIMENT 8

CNR = 40 dB, f_{mis} = 1 kHz (10% mistune)

Modulation depth	SNR of detected envelope dB	Quality of detected binary	Highest noise click rad/sec
10%	16.564	good	722
20%	22.663	good	749
30%	26.327	good	769
40%	29.037	good	873
50%	31.267	good	1052
60%	33.246	good	1356
70%	35.125	good	1811
80%	37.050	good	2768
90%	39.285	good	7198

EXPERIMENT 9

CNR = 50 dB, f_{mis} = 1 kHz (10% mistune)

Modulation depth	SNR of detected envelope dB	Quality of detected binary	Highest noise click rad/sec
10%	25.264	good	236
20%	31.364	good	264
30%	35.028	good	288
40%	37.737	good	332
50%	39.968	good	448
60%	41.947	good	626
70%	43.825	good	908
80%	45.750	good	1601
90%	47.985	good	4622

These experiments reveal that the quality of the detected envelope and data signals of ZSFM in a Gaussian noise condition appears acceptable even with 10% mistune of the IF transformer. It is possible to notice by comparing these experiments with those of Section 5.5 that the degradation in the SNR of detected envelope is not more that 1 dB for 10% mistune. The detected binary data signal is also acceptable and it should be noted that the positive and negative frequency deviations from the carrier are not always equal in magnitude. This effect occurs because of the asymmetry of the IF stage characteristics in a mistune condition. It is more likely to happen with small CNR values and high modulation depth in which case the detection of the data signal becomes unreliable due to low CNR as discussed in Section 3.9.

It can therefore be concluded that the problem of IF cross-talk due to a practical IF transformer does not

appear to significantly affect performance, even in the condition of mistune. The distortion introduced to the detected envelope signal is negligible and should be imperceptible. There will be some distortion introduced to the detected data signal due to the a.m./p.m. conversion in the case of mistune.

5.7 Envelope Distortion Measurement

This section discusses a quantitative approach to determine the distortion in the detected envelope signal of ZSFM due to a non-ideal IF stage which may produce some perceptible cross-talk. The signal-to-distortion (S/D) ratio can be calculated from the spectrum of the detected envelope signal which will contain the envelope components and distortion components. When calculating the signal-to-distortion ratio, no noise is added to the signal in the channel as the aim is to evaluate the deterioration of the envelope due to the IF stage.

The signal power (S) and the distortion power (D) can be calculated from the spectral components of the detected envelope signal, with some modifications to account for d.c. de-coupling and low-pass filtering as shown below. Consider the spectrum of the detected envelope signal (single-tone) shown in Figure 5.25

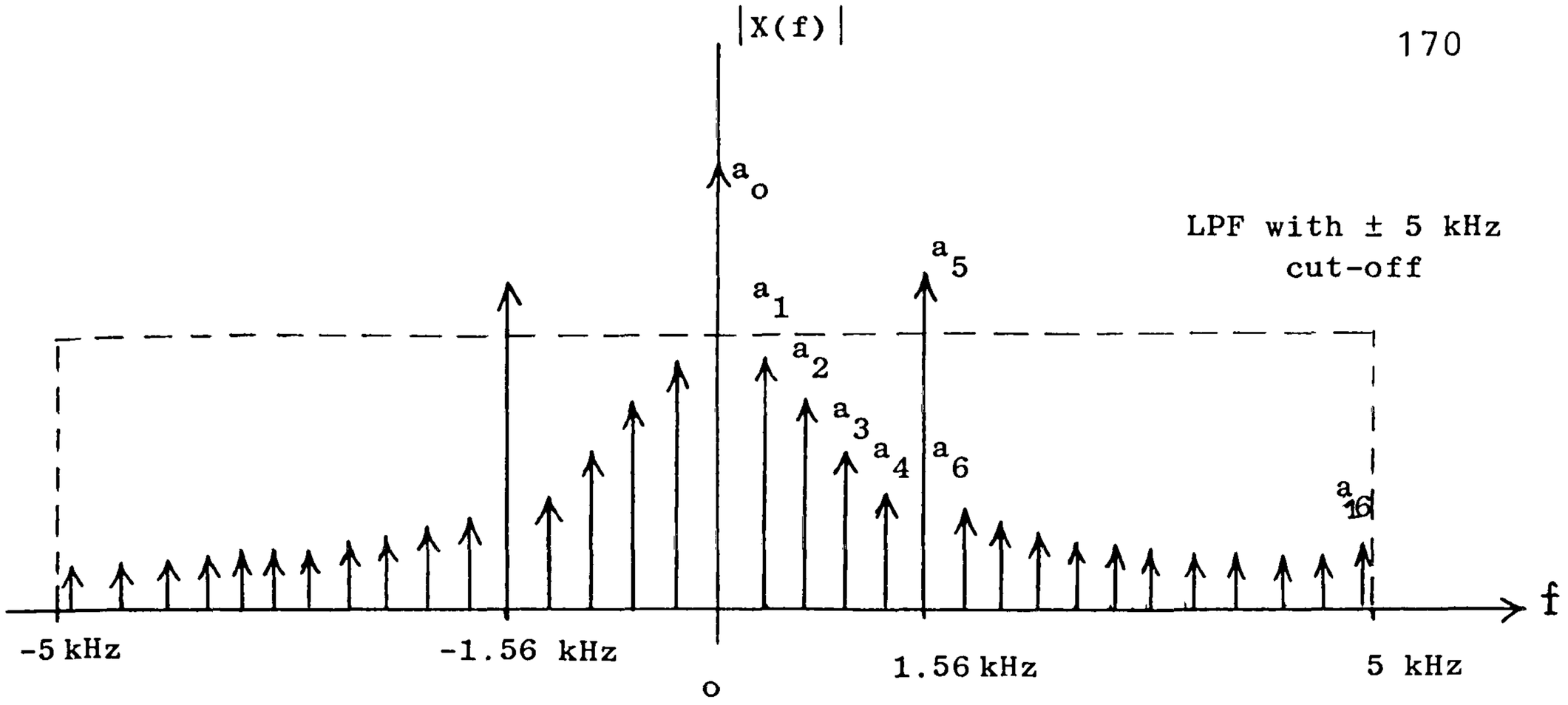

Fig. 5.25

Only positive frequency components will be considered because of spectral symmetry. Assuming that the spectral component a_{16} lies just below 5 kHz, then the components a_{17}, a_{18}, ... are neglected since these will not normally be perceptible due to low-pass filtering effect at the receiver. The d.c. spectral component a_o is not considered in the calculation as the carrier term is removed after detection. If x(t) is the detected envelope and a_1, a_2, ... a_{16} are in volts, then the related power $\overline{x^2(t)}$ is:

$$\overline{x^2(t)} = \left[\frac{|a_1|^2}{2} + \frac{|a_2|^2}{2} + \ldots + \frac{|a_{16}|^2}{2}\right]$$

= (signal + distortion) power

= S + D (5.17)

Assuming that a_5 represents the signal tone then the signal power is given by:

$$S = \frac{|a_5|^2}{2}$$

Therefore the distortion power is given by:

$$D = \overline{x^2(t)} - S = \overline{x^2(t)} - \frac{|a_5|^2}{2}$$

$$\therefore S/D = \frac{|a_5|^2/2}{\overline{x^2(t)} - |a_5|^2/2} \qquad (5.18)$$

Experiment 10

This experiment measures the S/D ratio of the detected envelope signal of ZSFM for different modulation depths. The ZSFM signal used is the same as in Section 5.6, with a cluster of six zero pairs at the centre conjugated according to the code (101100). The same IF stage is used with 5 kHz 3-db bandwidth. Figure 5.26 shows the calculated S/D ratio where the envelope signal is low-pass filtered to 5 kHz. It is apparent that the S/D ratio is more than 40 dB even for a very small modulation depth (10%). This implies that the distortion is unlikely to be perceptible in the envelope signal.

Experiment 11

Experiment 10 was repeated but with a 1 kHz mistune (i.e. 10% mistune). Figure 5.26 shows the S/D ratio which has fallen by almost 10 dB below the S/D ratio without mistune.

Experiment 12

In this experiment the modulation depth is kept constant at 50%, while the mistune frequency of the IF

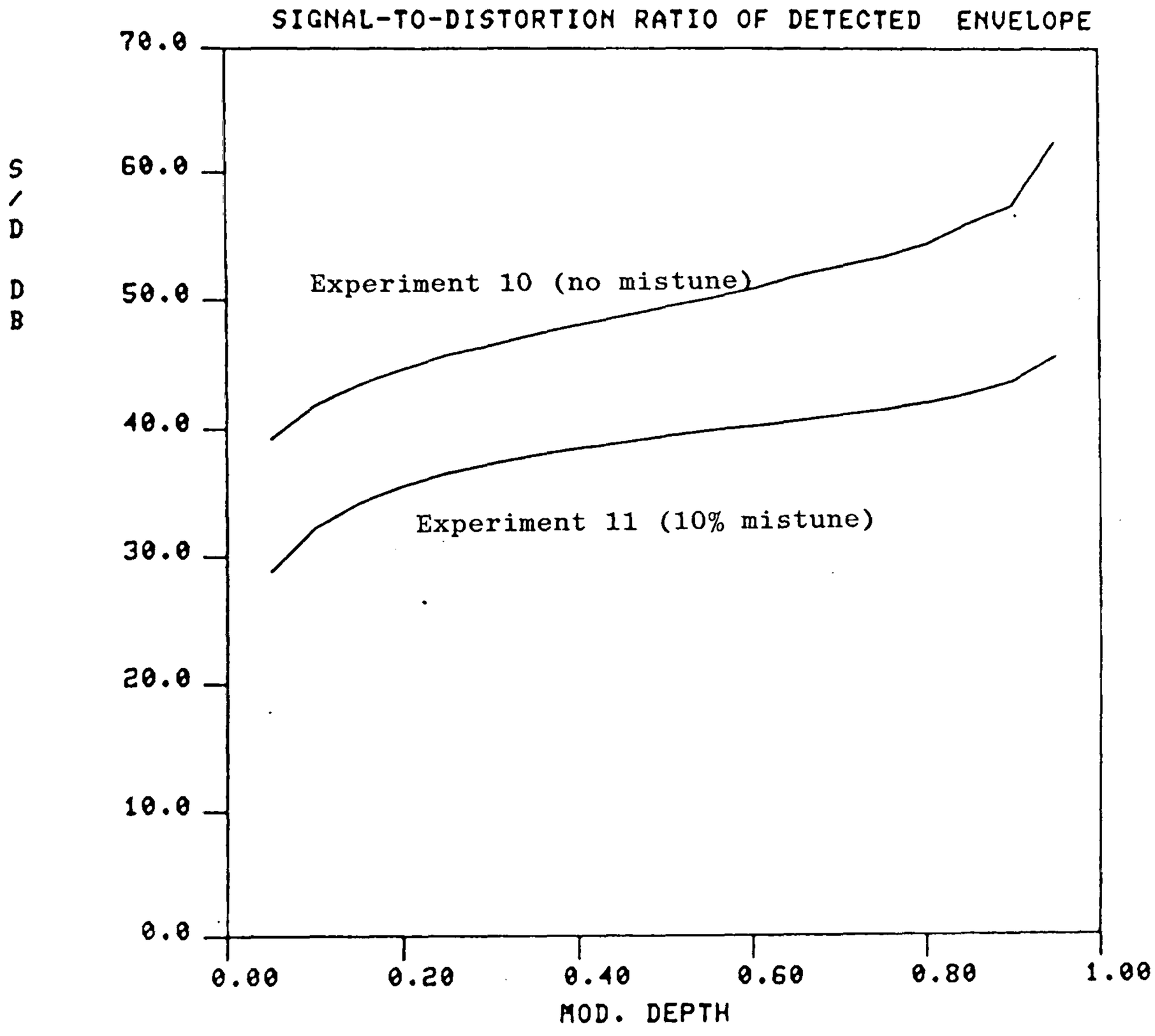

Fig. 5.26 Signal/distortion power ratio.

stage is varied from 0 to 2 kHz. The same ZSFM signal and IF stage are used as in the last two experiments. The degradation of the S/D ratio of the detected envelope signal is calculated against different mistune frequencies. Figure 5.27 shows the result, and the degradation is apparently worst (20 dB) for 2 kHz mistune (20% mistune). The envelope signal deteriorates significantly for mistune frequencies larger than 1 kHz. It can therefore be inferred that the distortion introduced due to the IF non-linearities does not degrade ZSFM performance significantly. The problem of cross-talk being perceptible in the main programme has been found to be negligible. However, if crystal filters with linear-phase can be used in the IF stage then this will even improve the performance of ZSFM. Crystal filters will complicate receiver circuitry and increase costs.

5.8 Multipath Fading

For the l.f. transmission the propagation mechanism is surface-wave giving stable transmission for distances up to 1500 km. For the medium wave (m.f.) band the propagation mechanism is surface-wave for short distances and sky-wave over longer distances which is subject to fading (32). The surface-wave is the direct wave produced by energy propagating close to the ground and guided by it to follow the same curvature as the earth. The sky-wave is the indirect signal produced by waves

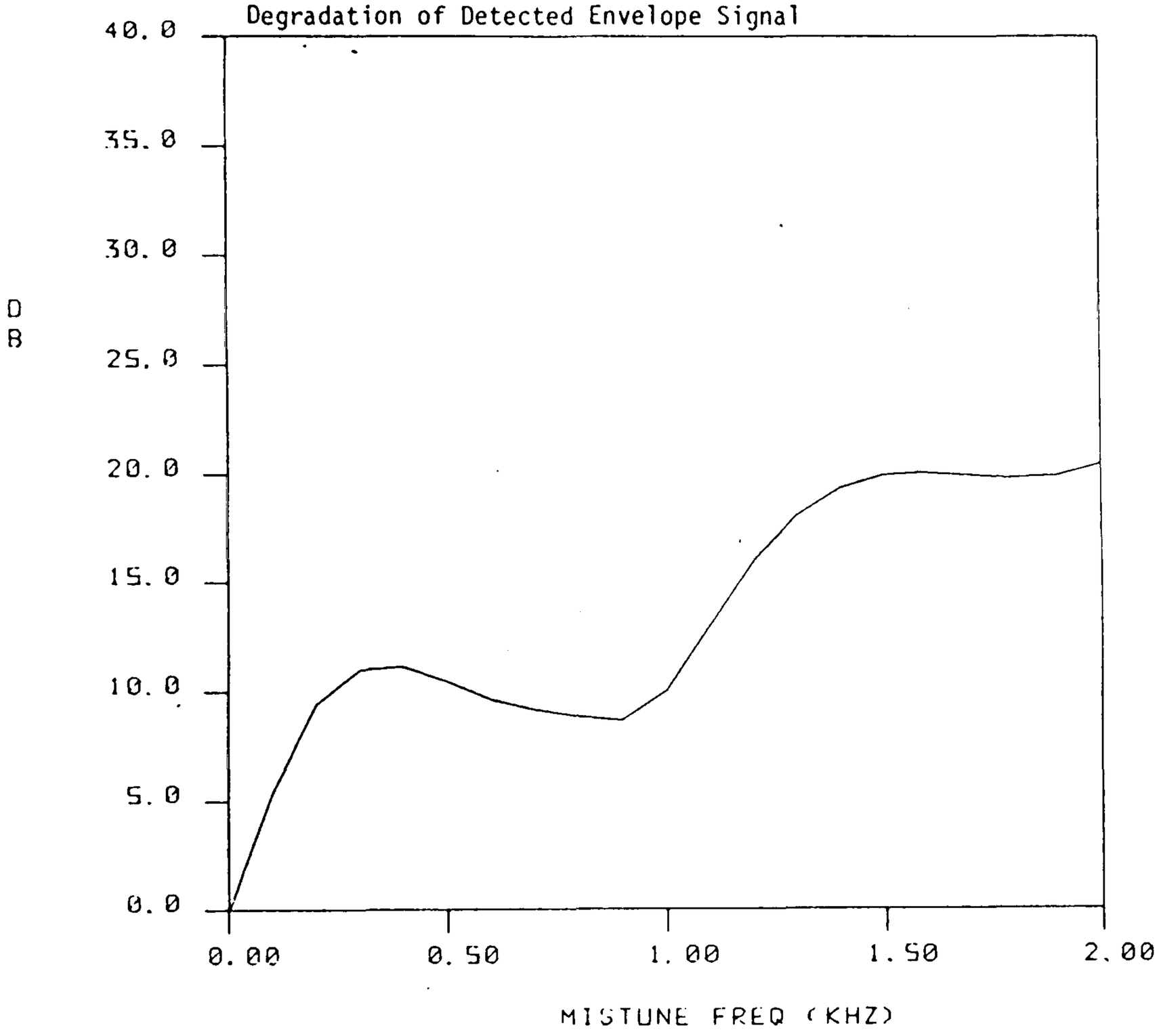

Fig. 5.27 Degradation of detected envelope for 50% modulation.

propagating upwards being bent by an electrically charged layer in the upper atmosphere (ionosphere) and reflected back towards the earth. During the day time, l.f. and m.f. sky-waves are absorbed by the ionosphere and are therefore unable to propagate further. During the night, however, the D layer of the ionosphere, which absorbs the sky-waves during the day, decays and waves are reflected from the higher E and F layers (33). Interference fading results from this diurnal fluctuation in the ionosphere causing the received signal to be the sum of a number of components with different path lengths. It is therefore important to consider the effect of sky-wave fading on the performance of ZSFM, since it has potential application to the m.f. band broadcast services. At night the strength of the reflected sky-wave from the ionosphere may be sufficient to cause a noticeable deterioration of the quality of detected ZSFM signals.

In order to simulate a two-path fading condition of ZSFM, a direct ZSFM signal must be added to the reflected delayed version multiplied by a constant smaller than one. If r(t) is the received signal, and c(t) is the ZSFM complex signal then:

$$r(t) = c(t) + k\, c(t - \tau) \qquad (5.19)$$

where $k \leq 1$, and τ is the time difference between the two paths. Substituting for c(t) in eqn. (5.19) gives:

$$r(t) = s(t)e^{j\theta(t)}e^{j\omega_o t} + ks(t-\tau)\, e^{j\theta(t-\tau)}\, e^{j\omega_o(t-\tau)}$$
$$= e^{j\omega_o t}\{s(t)\, e^{j\theta(t)} + k\, e^{-j\omega_o\tau}\, s(t-\tau)\, e^{j\theta(t-\tau)}\}$$

where s(t) is the envelope, $\theta(t)$ is the phase modulation, and ω_o is the carrier frequency. Neglecting the translation

operator $e^{j\omega_o t}$, the baseband version of r(t) is:

$$r'(t) = s(t)e^{j\theta(t)} + k\, e^{-j\omega_o \tau}\, s(t-\tau)\, e^{j\theta(t-\tau)}$$

Letting $z(t) = s(t)e^{j\theta(t)}$, the above becomes:

$$r'(t) = z(t) + k\, e^{-j\omega_o \tau}\, z(t-\tau)$$

Taking Fourier transform of r'(t) gives:

$$\begin{aligned} R'(f) &= Z(f) + k\, e^{-j\omega_o \tau}\, Z(f)\, e^{-j2\pi f\tau} \\ &= Z(f)\, \{1 + k\, e^{-j2\pi(f+f_o)\tau}\} \\ &= Z(f)\, X(f) \end{aligned} \qquad (5.20)$$

where X(f) is the channel transfer function with two-path fading. The magnitude response of this fading channel is:

$$\begin{aligned} |X(f)| &= |1 + k\, e^{-j2\pi(f+f_o)\tau}| \\ &= \sqrt{1 + k^2 + 2k \cos 2\pi(f+f_o)\tau} \end{aligned} \qquad (5.21)$$

The first trough of $|X(f)|$ occurs at:

$$2\pi(f+f_o)\tau = \pi$$

$$\therefore\ f = \frac{1}{2\tau} - f_o$$

The worst fading occurs when k = 1, in which case the trough attains zero as shown in Figure 5.28.

By considering X(f) as a function of τ, it is possible to show that R'(f) will be minimum at the trough of X(f). The carrier will be minimum when $\tau = \frac{1}{2f_o}, \frac{3}{2f_o}, \frac{5}{2f_o}, \ldots$ If f_o = 1 MHz then this first occurs at τ = 0.5 μ sec and repeats at 1 μ sec intervals. The distortion introduced will depend on

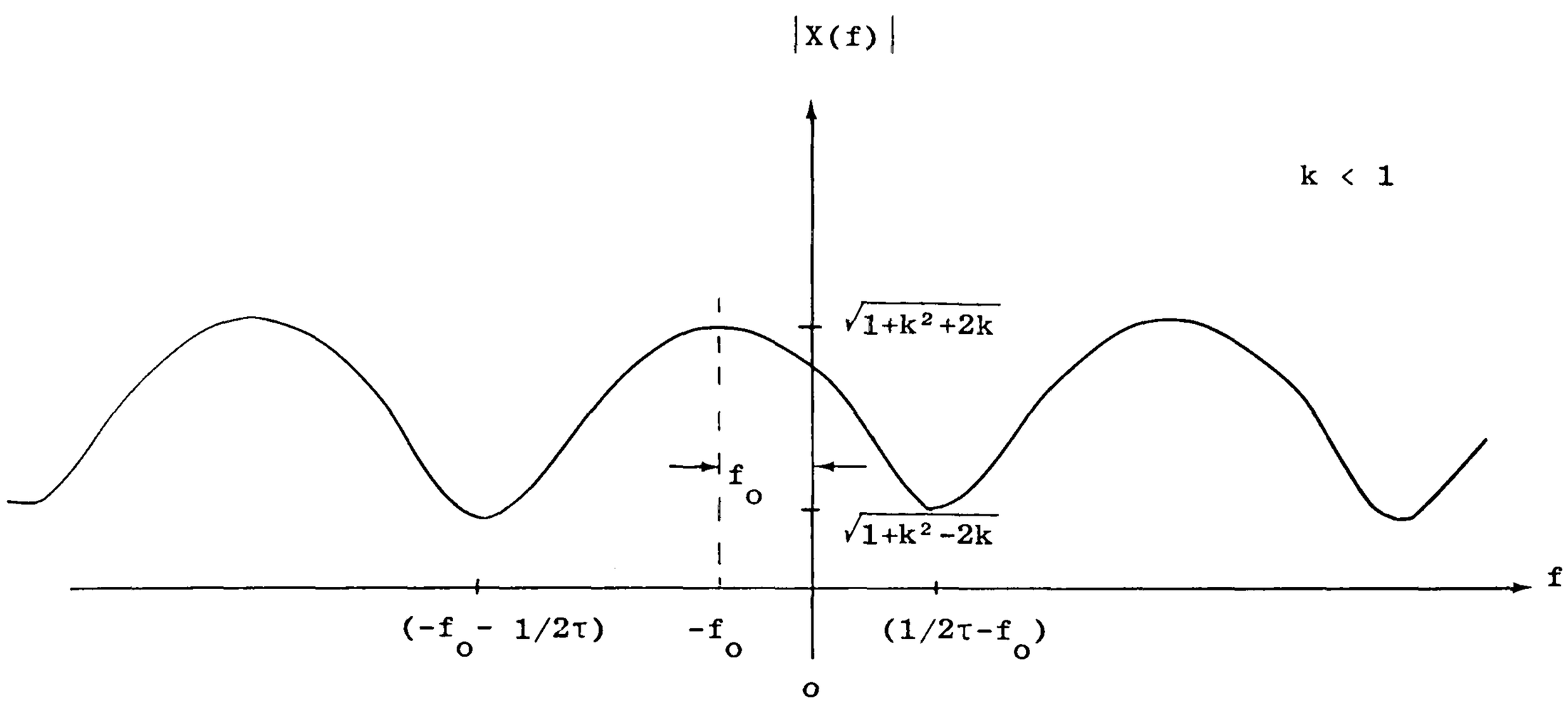

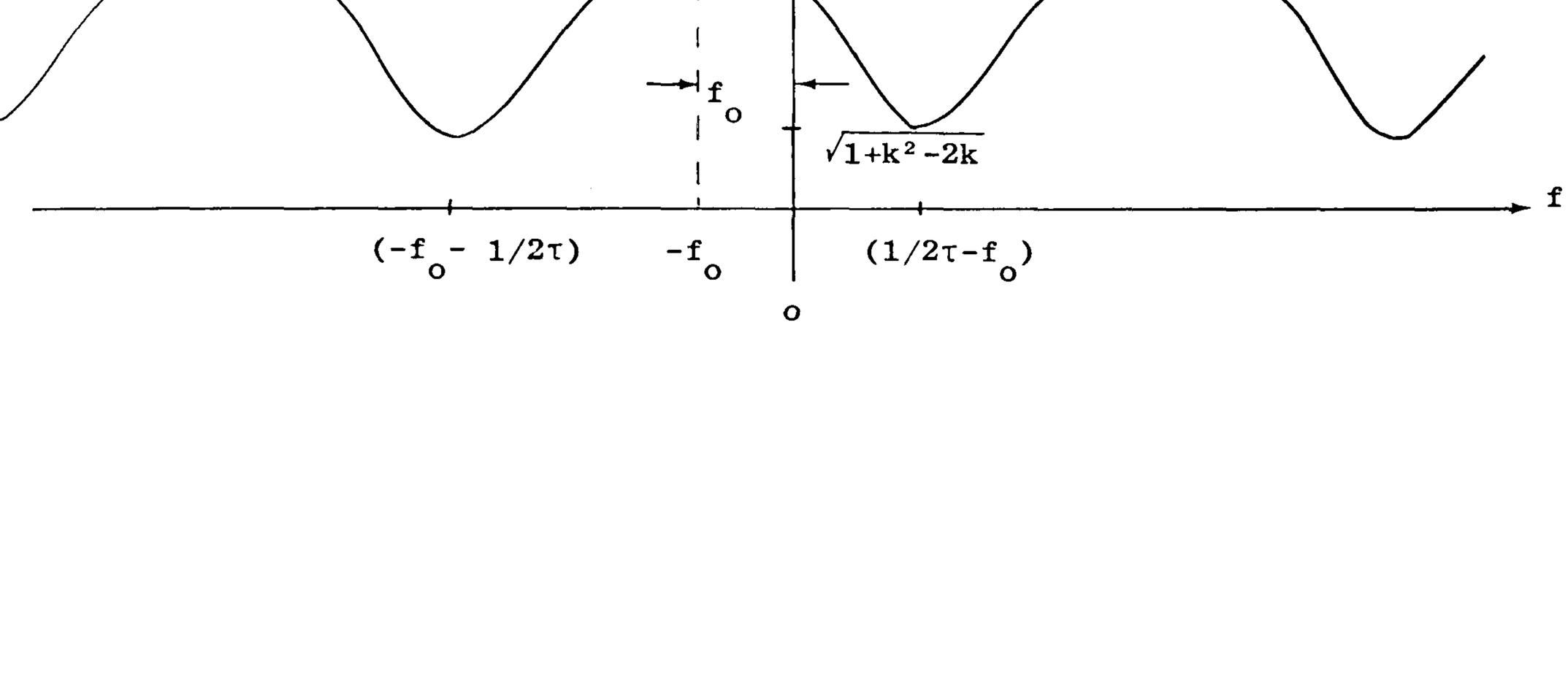

Characteristic of a two-path fade

Fig. 5.28

where the carrier frequency of the signal falls, and the worst distortion occurs when k = 1 and the carrier falls on the channel trough. Assuming that the carrier lies at equidistance from any two successive troughs, then for a 10 kHz broadcast channel the lowest fade occurs if:

$$\frac{1}{\tau} \geq 10 \text{ kHz}$$

$$\therefore \tau \leq 0.1 \text{ msec}$$

However, in practice the path time difference (τ) might be greater than 0.1 msec. It is reasonable to assume that the maximum path difference between the direct and reflected waves is around 100 km for a single-hop propagation. This implies a time difference (τ) of 0.3 msecond.

Experiment 13

In this experiment the signal-to-distortion ratio of the detected envelope signal of ZSFM during a two-path fading condition is measured. The baseband version of the received signal in a two-path fade is as given above:

$$r'(t) = s(t)\, e^{j\theta(t)} + k\, e^{-j\omega_o\tau}\, s(t-\tau)\, e^{j\theta(t-\tau)},\ k \leq 1$$

It is apparent that the worst case occurs when k = 1 and $\omega_o\tau = \pi, 3\pi, 5\pi, \ldots$, where the carrier term is cancelled as explained above. For DSB-AM signals, it has been found that satisfactory sound reception in a multipath

fade is not possible where k > 0.5 (8).

The ZSFM considered is the same as in Section 5.6, where the data signal is alternate positive and negative conjugation applied to 6 zero pairs, giving a data rate of $\frac{6}{40960 \times 10^{-6}} = 146.5$ bit/sec. The same practical IF stage with 5 kHz 3-dB bandwidth is used. The modulation depth is maintained at 50%, while a carrier frequency of $\frac{\omega_o}{2\pi}$ = 1 MHz was chosen to represent a possible medium-wave radio frequency. This implies that the distorting effect of the sky-wave on the envelope will be maximised due to partial carrier cancellation when τ = 0.5, 0.15, 0.25, ... μsec as discussed before in this section. The path time difference (τ) is varied between 0.5 μsec and 0.3 msec in steps of 0.5 μsec, while the S/D ratio is measured for k values of 0.3 and 0.5 respectively. Since partial carrier cancellation occurs when $\tau = \frac{1}{2f_o}, \frac{3}{2f_o}, \frac{5}{2f_o}, \ldots,$ the p.m./a.m. conversion will fluctuate at this rate with increasing delay. Figure 5.29(a) shows the variation of the S/D for k = 0.3, and the curve has been expanded over the range of 0 → 0.075 msec to show the behaviour of the S/D fluctuations, where there are 10 minima points every 10 μsec. Figure 5.29(b) shows the result for k = 0.3 and over the whole range of τ considered, where the two curves describe the upper and lower limits of this fluctuation. It is apparent that the detected envelope quality deteriorates significantly

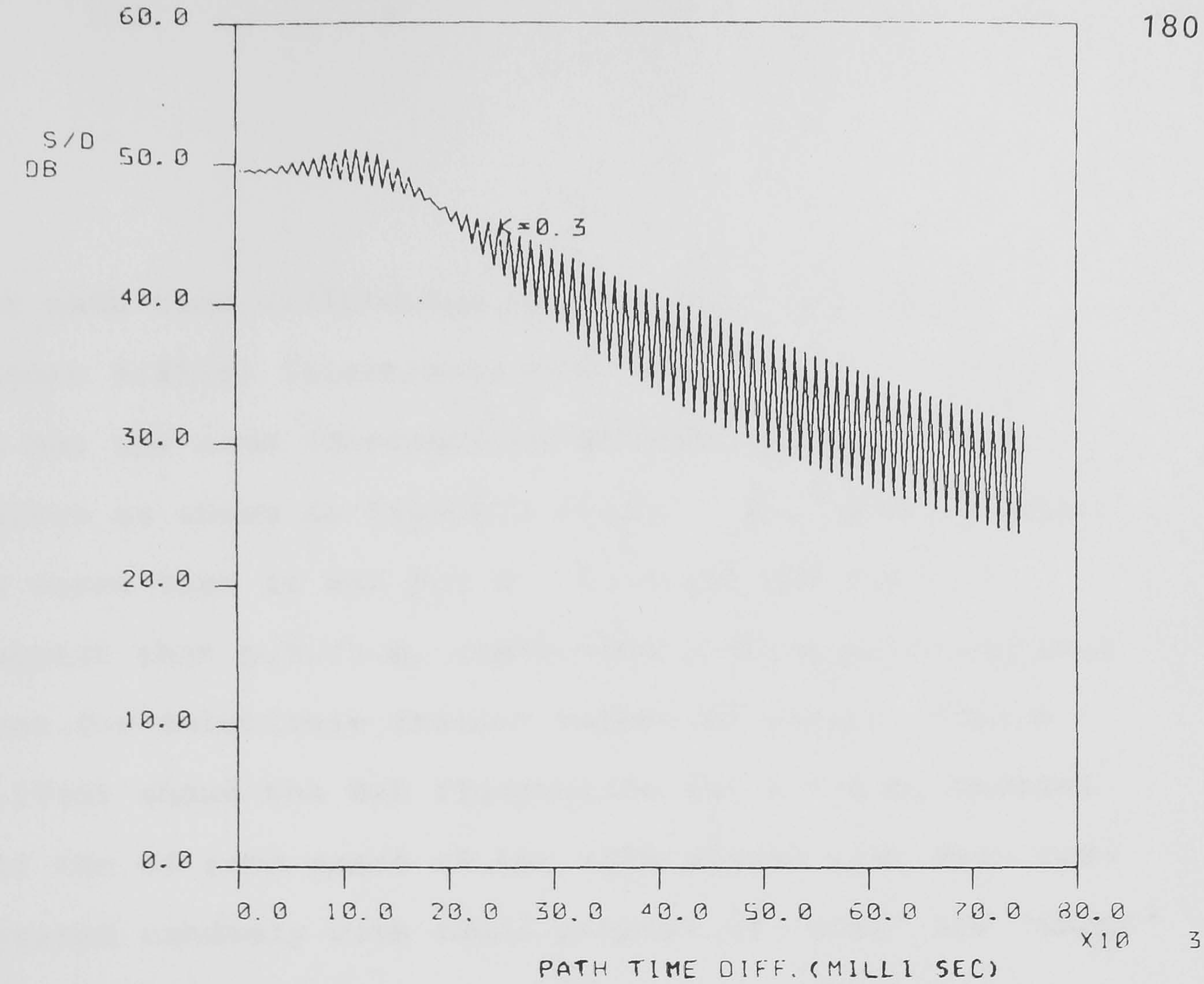

Fig. 5.29(a) Signal/distortion variation for k = 0.3, 50% modulation depth.

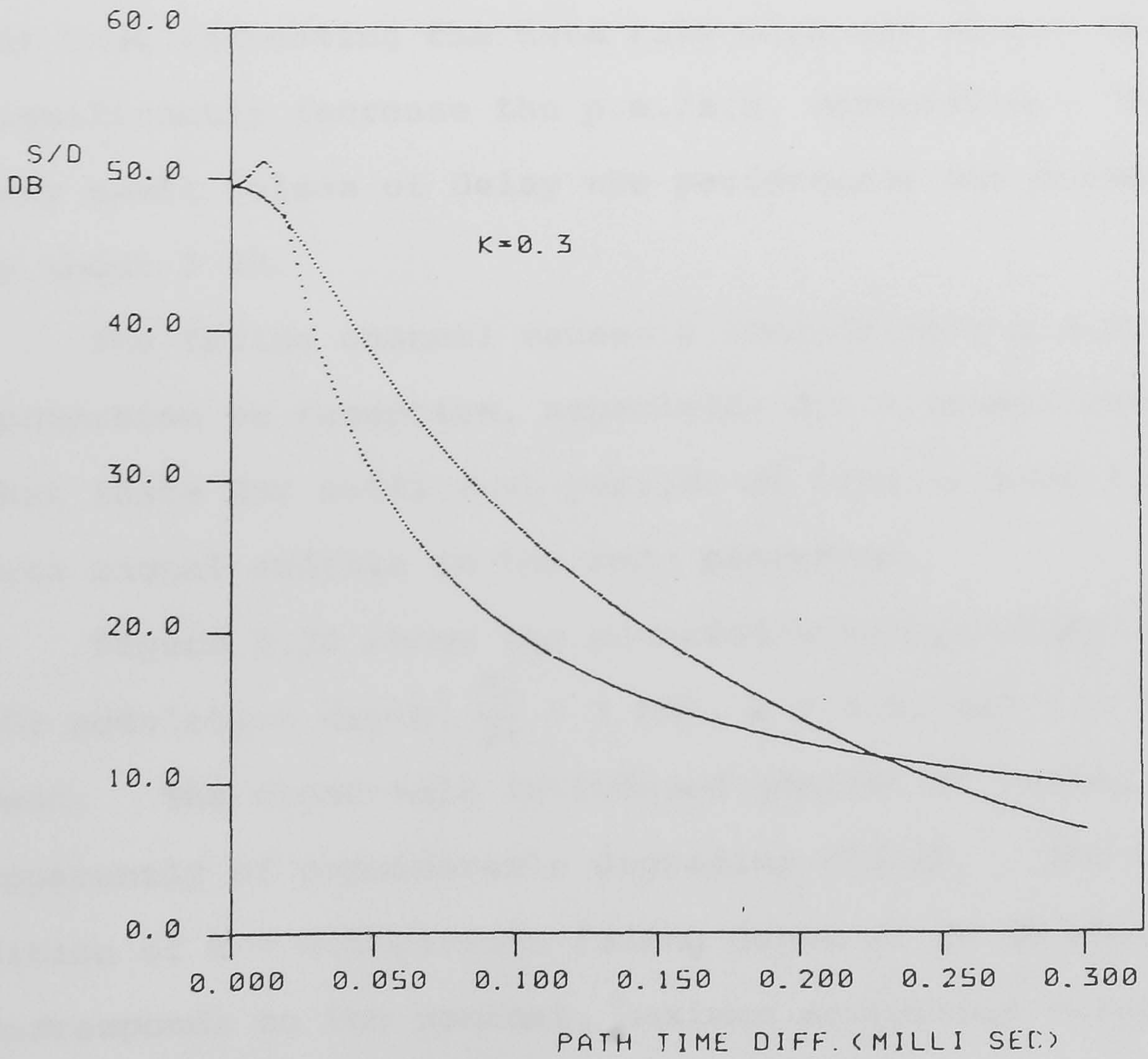

Fig. 5.29(b) Signal/distortion variation for k = 0.3, 50% modulation depth.

for path time differences greater than 0.15 msec. Figure 5.29(c) illustrates the result for k = 0.5 and it has the same fluctuations between upper and lower curves as shown in Figure 5.29(a). The deterioration is worse than it was for k = 0.3, and the results suggest that p.m./a.m. conversion will be problematical even for relatively smaller values of delay. Figure 5.29(d) shows the S/D fluctuation for k = 0.5, whereas all the 64 zero pairs of the ZSFM signal have been conjugated randomly with equal numbers of "ones" and "zeros" giving a data rate of $\frac{64}{40960 \times 10^{-6}}$ = 1562.5 bit/sec. It can be noticed by comparing Figures 5.29(c) and 5.29 (d) that increasing the data rate does not appear to significantly increase the p.m./a.m. conversion. For very small values of delay the performance has worsened by about 3 dB.

The fading channel causes a considerable p.m./a.m. conversion on reception, especially for a severe fade that lasts for sufficient periods of time to make the data signal audible in the main programme.

Figure 5.30 shows the detected envelope signal for 50% modulation depth, $\frac{\omega_o}{2\pi}$ = 1 MHz, k = 0.5, and τ = 0.2 msec. The cross-talk introduced because of fading is apparently of considerable degrading effect. The condition of k = 0.5 gives a fading depth of 10 dB which corresponds to the nominal, maximum acceptable value (8).

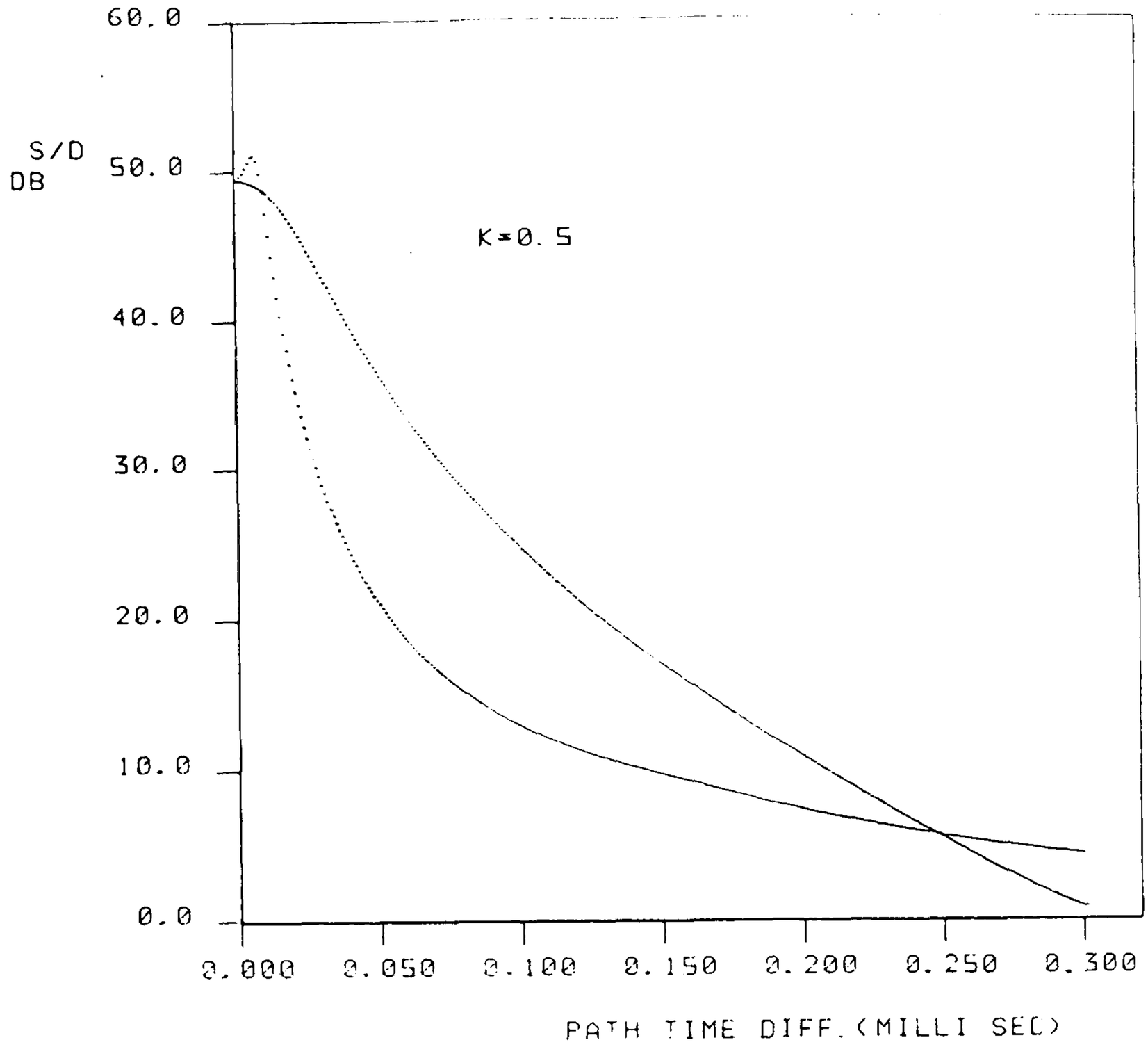

Fig. 5.29(c) Signal/distortion variation for k = 0.5, 50% modulation depth.

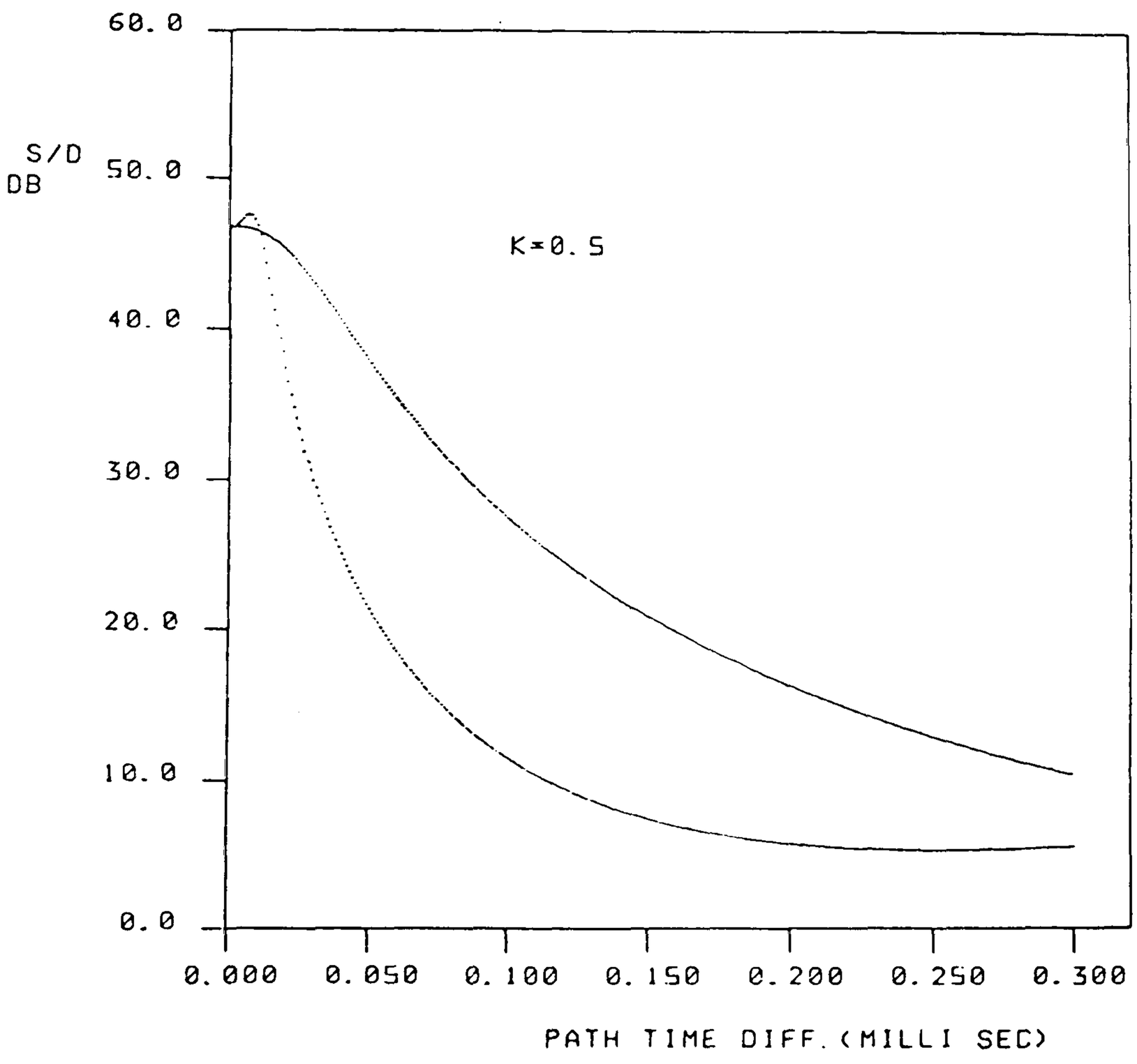

Fig. 5.29(d) Signal/distortion variation for k = 0.5, 50% modulation depth.

However, smaller values of k (due to different path losses) might give a tolerable degrading effect. Figure 5.31 shows the detected binary code (101010) for the same conditions; apparently the data signal is not so badly affected by fading as the envelope signal.

The p.m./a.m. conversion caused by multipath propagation conditions is, therefore, expected to be a major limiting factor. However, in a severe fading condition the envelope signal will be impaired significantly even without the interference imposed by the data signal.

An experimental ZSFM system will be needed to assess basic performance under realistic operating conditions.

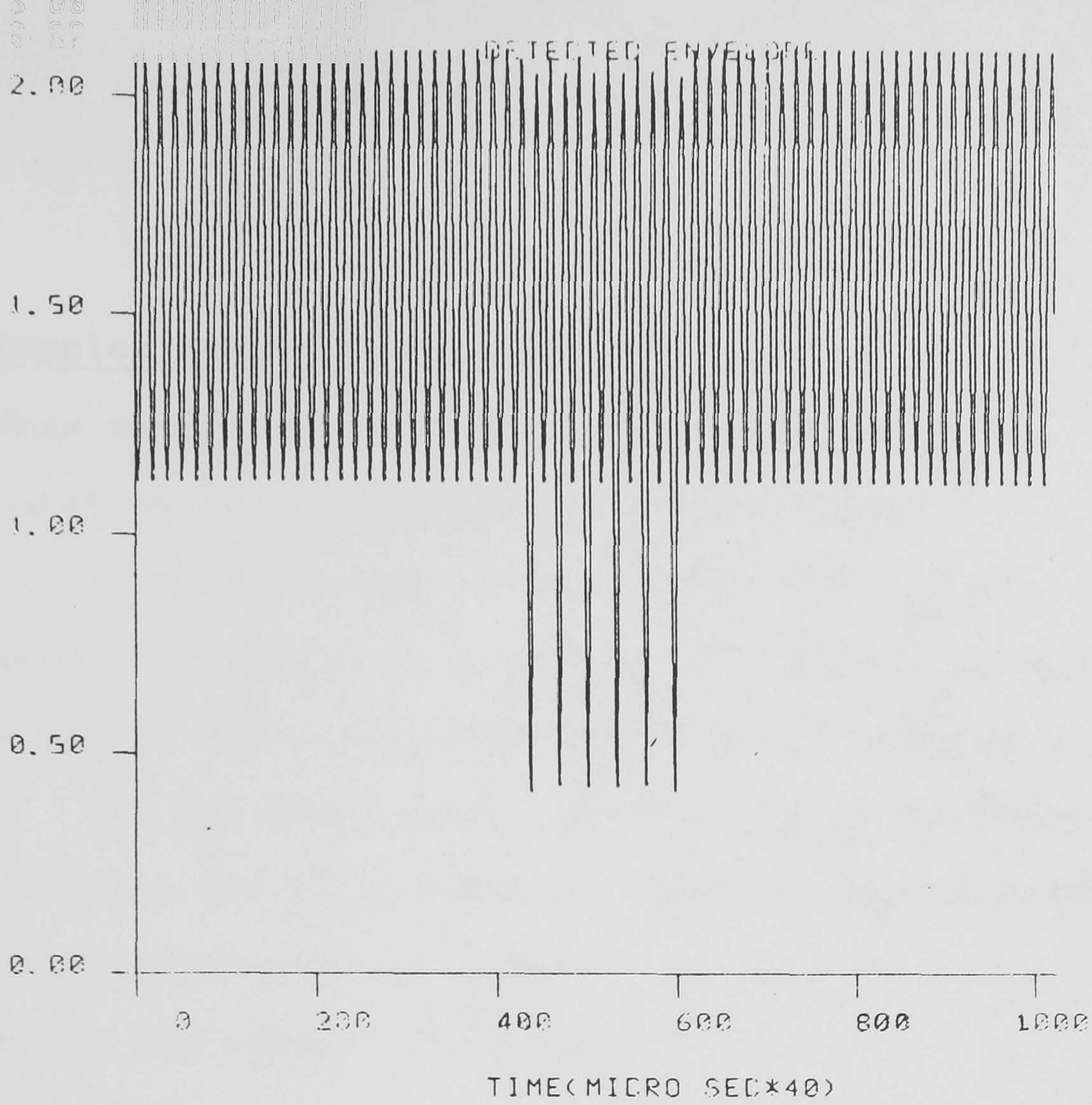

Fig. 5.30 Detected envelope signal for 50% modulation depth, $\frac{\omega_o}{2\pi}$ = 1 MHz, k = 0.5, and τ = 0.2 m/sec.

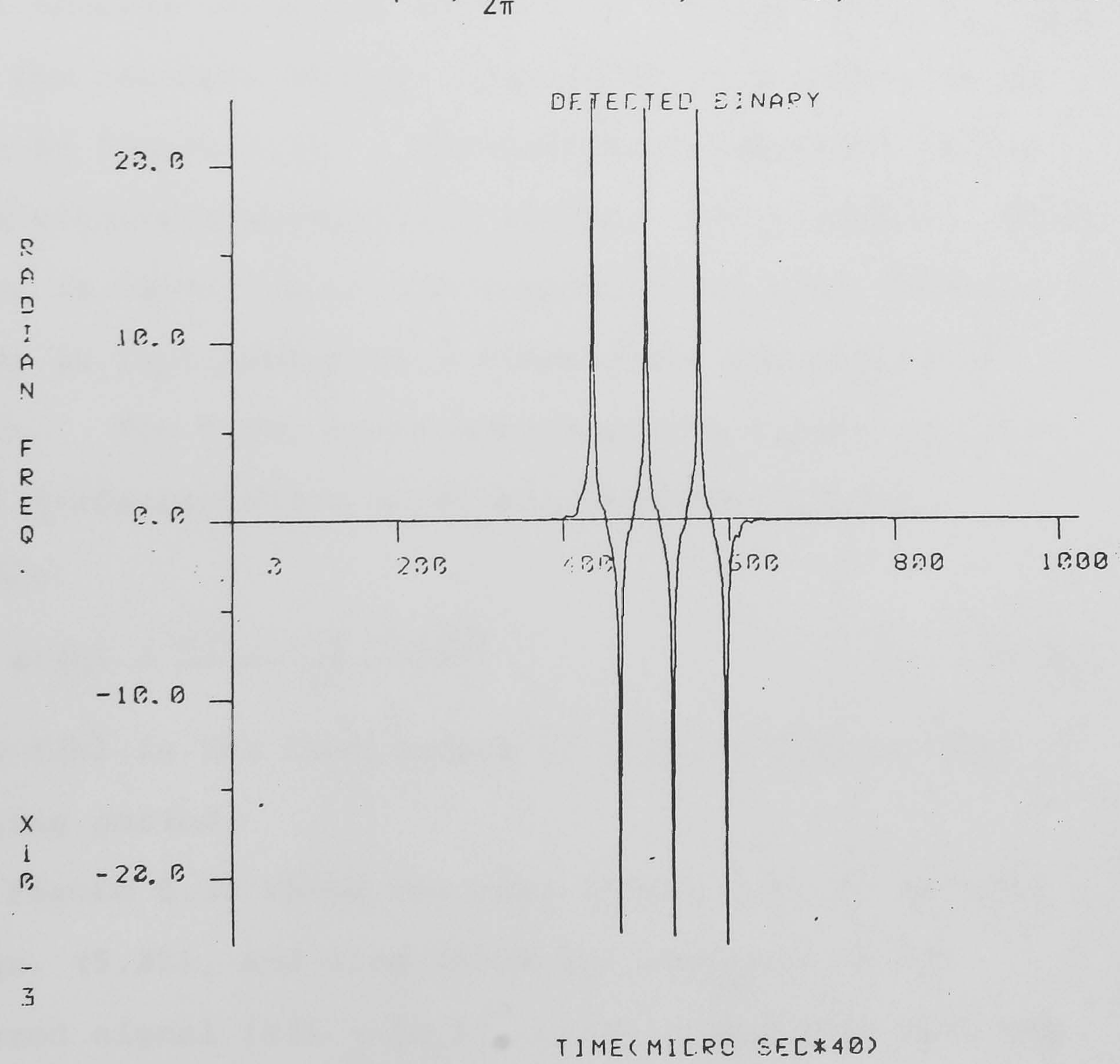

Fig. 5.31 Detected data signal for the same conditions.

5.9 Complex Filter Implementation

This section is devoted to a discussion of the implementation of complex filters on the computer. Two possible realisations of the complex filter are considered; the first as a cascade of differentiators in time domain and the second by FFT in the frequency domain. It has been explained (Section 4.5.b) that a complex filter can be realised by cascaded differentiators, weighting resistors and a summer.

Considering the simple real signal:

$$s(t) = 1 + a^2 t^2 \qquad (5.22)$$

whose complex zeros are given by $X = \pm j\frac{1}{a}$, i.e. $\sigma_r = \frac{1}{a}$, then the required complex filter for this signal is as shown by Figure 4.17. The filter is comprised of two differentiators, multiplying weights, and a summer. This filter is simulated on the computer, and each differentiator is implemented as a first order non-recursive filter. The first order non-recursive filter approximates differentiation using the forward-difference formula:

$$s'(k) = \frac{s(k + 1) - s(k)}{TD} \qquad (5.23)$$

where s(k) is the time sample of s(t), and TD is the sampling period.

Figure 5.32 shows the real signal s(t) as defined by eqn. (5.22), and also shows the envelope of the filtered signal $|s(t - j\sigma_r)|$. It is apparent that the

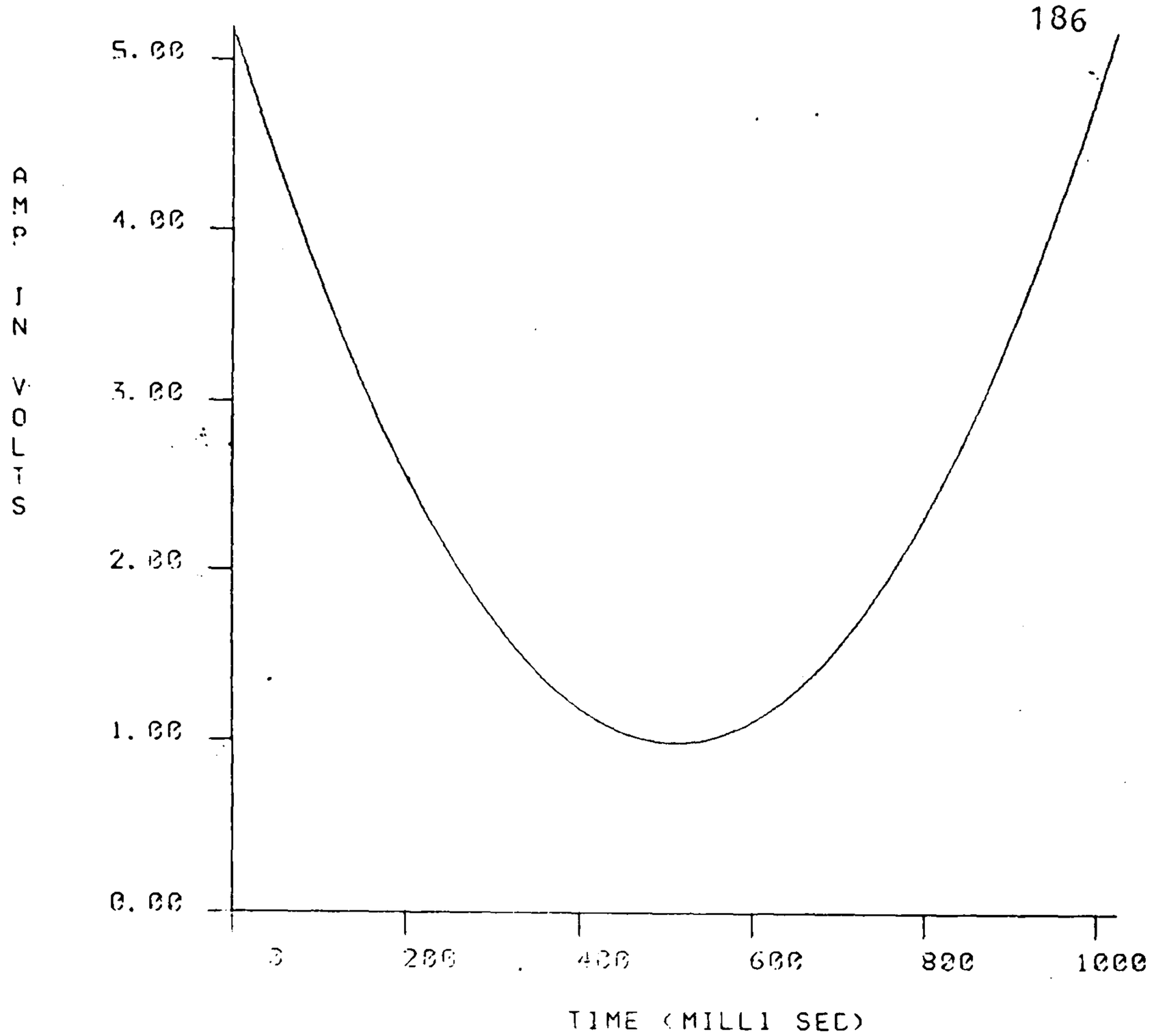

Fig. 5.32 Real signal $s(t) = 1 + a^2t^2$

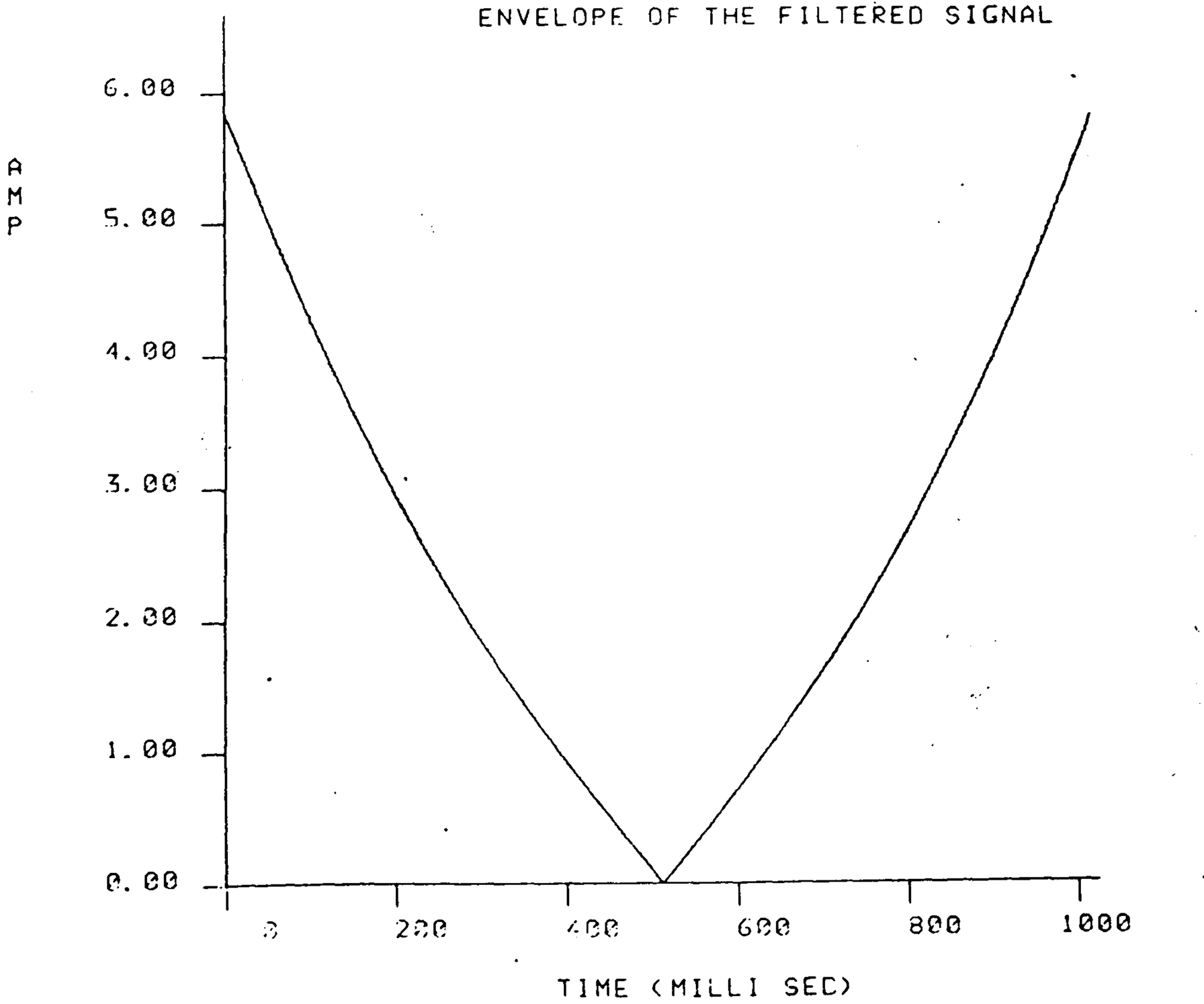

Fig. 5.32 Envelope of filtered signal $|s(t-j\sigma_r)|$.

complex zero of s(t) has been converted into an easily detected real zero at the same instant of time.

Another possible way of realising the complex filter is by processing the signal in the frequency domain. The real signal s(t) is processed by the computer in blocks by an FFT subroutine that gives the frequency domain samples of the signal. These frequency samples are digitally weighted by the respective filter frequency responses (i.e. by values of $H_{\sigma_r}(f) = e^{2\pi f\sigma_r}$). The resulting product corresponds to the frequency samples of the complex filtered signal. Using the FFT subroutine in the inverse direction produces the time samples of the filtered signal. The envelope of this filtered signal is observed, and any detected real zero of this envelope signifies a complex zero detection. This has been simulated on the computer with two real positive signals for complex zero detection.

The first signal is the familiar single-tone defined as:

$$s(t) = 1 + a^2 - 2a\cos\Omega t \qquad (5.24)$$

A block of 10 cycles at $\frac{\Omega}{2\pi}$ = 1 kHz is generated, and then it is processed in the computer as above. The imaginary value of the complex zeros of s(t) can be theoretically obtained as:

$\sigma_r = \pm \frac{\ln a}{\Omega}$, as discussed previously (Section 3.4).

The complex filter response is bandlimited to $\pm f_c = \pm 3$kHz (Section 4.4).

Figure 5.33 shows 10 cycles of the real signal s(t) for a = 0.3, and also it shows the envelope of the filtered signal $|s(t - j\sigma_r)|$. It is apparent that the complex zeros of s(t) that lie at the troughs have been changed into real zeros of $|s(t - j\sigma_r)|$ at the same instants of time. The condition of filter imperfection was also simulated, where each complex filter in the bank (see Figure 3.15) corresponds to a small range of σ_r values. This can be simulated by generating the following response:

$$H_{\sigma_r}(f) = e^{2\pi f(\sigma_r + \Delta\sigma_r)} \tag{5.25}$$

where $\Delta\sigma_r$ is the error in σ_r value.

Figure 5.34 shows the envelope of the detected signals as in Figure 5.33, but the errors in σ_r value are 2 μ sec, 10 μ sec respectively. It can be observed that for 2 μ sec error the real zeros are approximately the same as the perfect case ($\Delta\sigma_r = 0$). For $\Delta\sigma_r$ = 10 μ sec the envelope of the filtered signal has a trough value slightly larger than zero.

The second signal considered for complex zero detection is a positive pseudo-random real signal with Gaussian distribution. This random signal is bandlimited by multiplying its spectrum with that of a low-pass filter having cut-off frequency at ± 3 kHz, and then the zeros of the bandlimited random signal are found

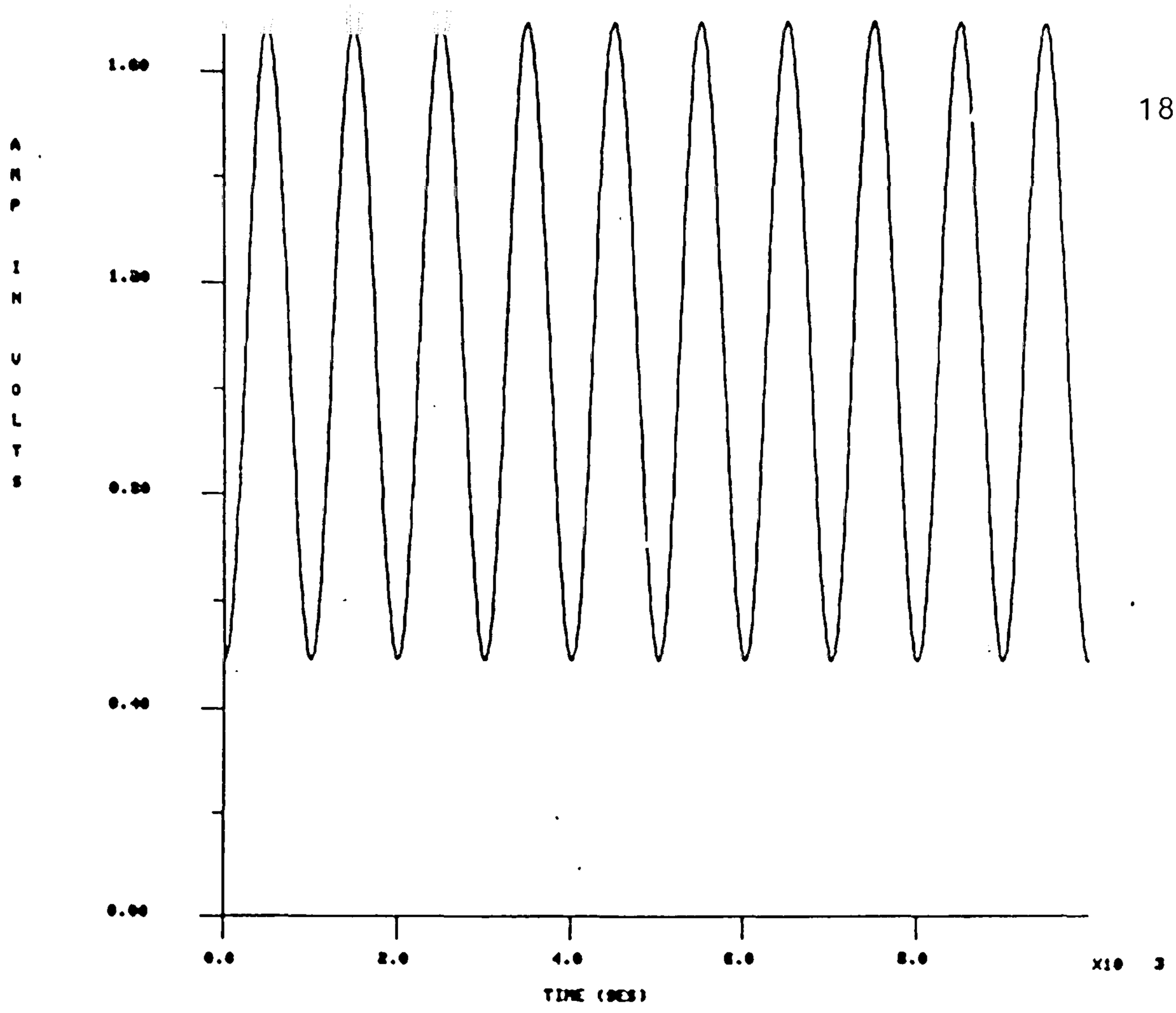

Fig. 5.33 Real signal $s(t) = 1 + a^2 - 2a\cos\Omega t$.

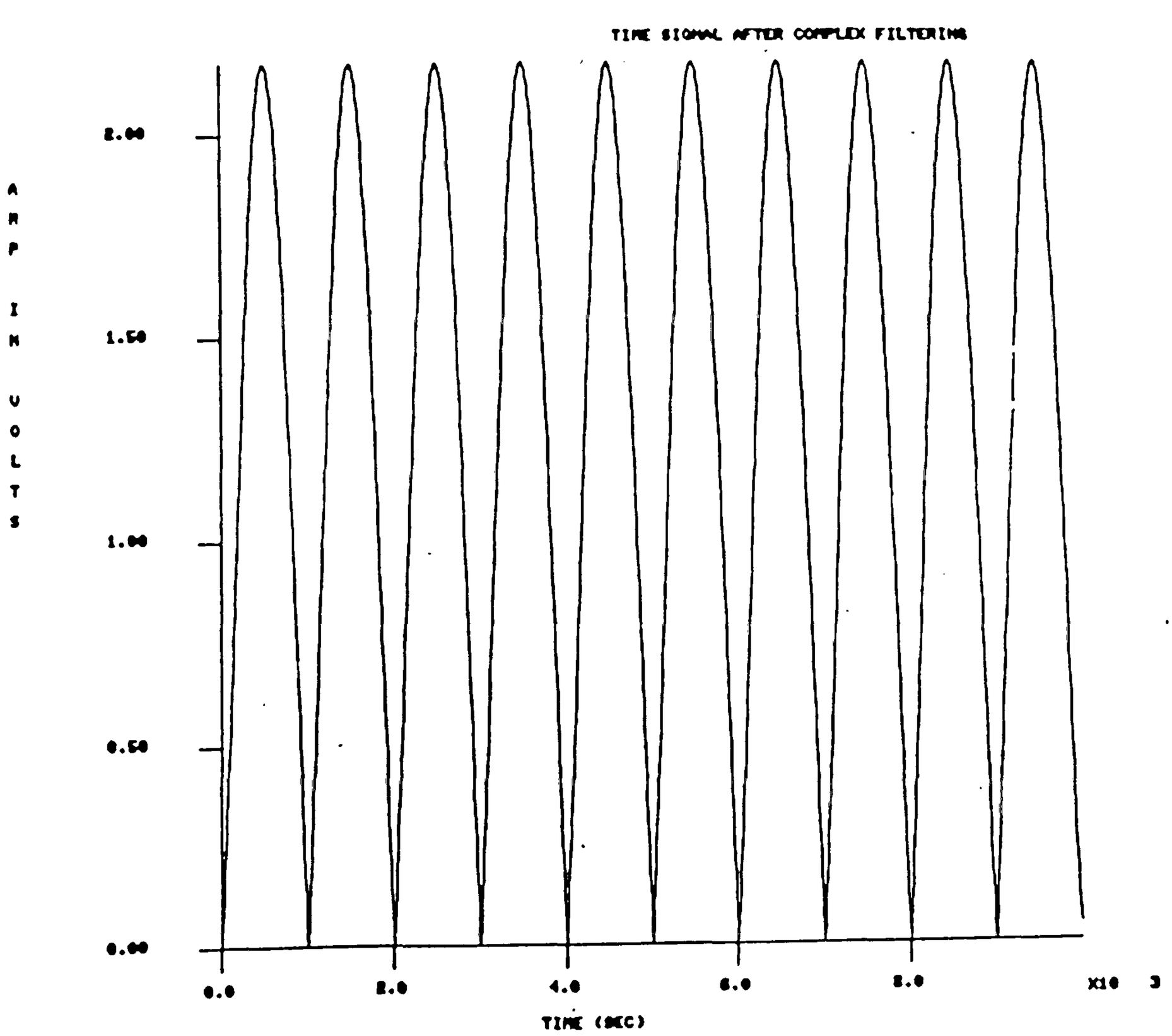

Fig. 5.33 Envelope of filtered signal $|s(t - j\sigma_r)|$.

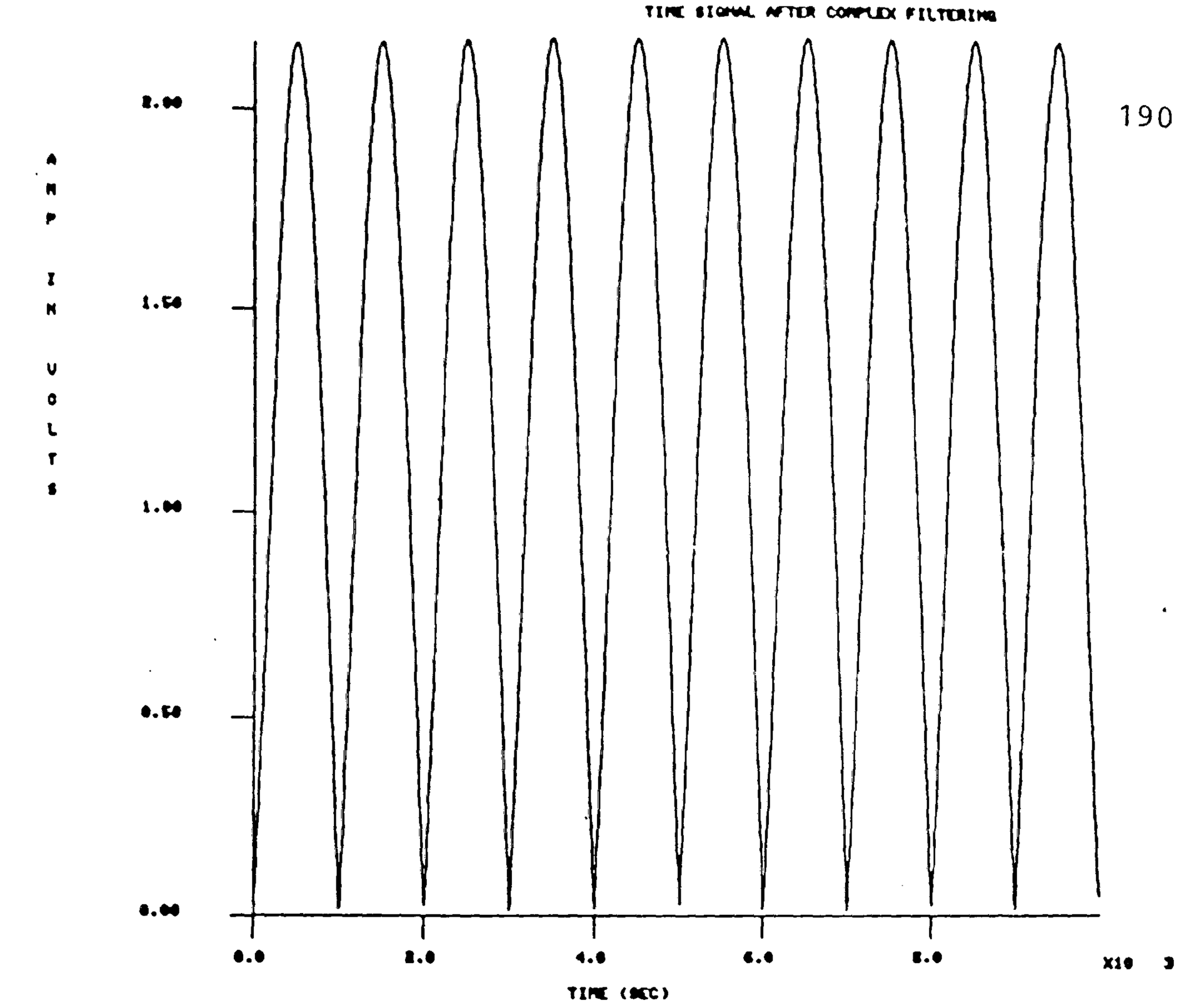

Fig. 5.34 Envelope of filtered signal with $\Delta\sigma_r$ = 2 μsec.

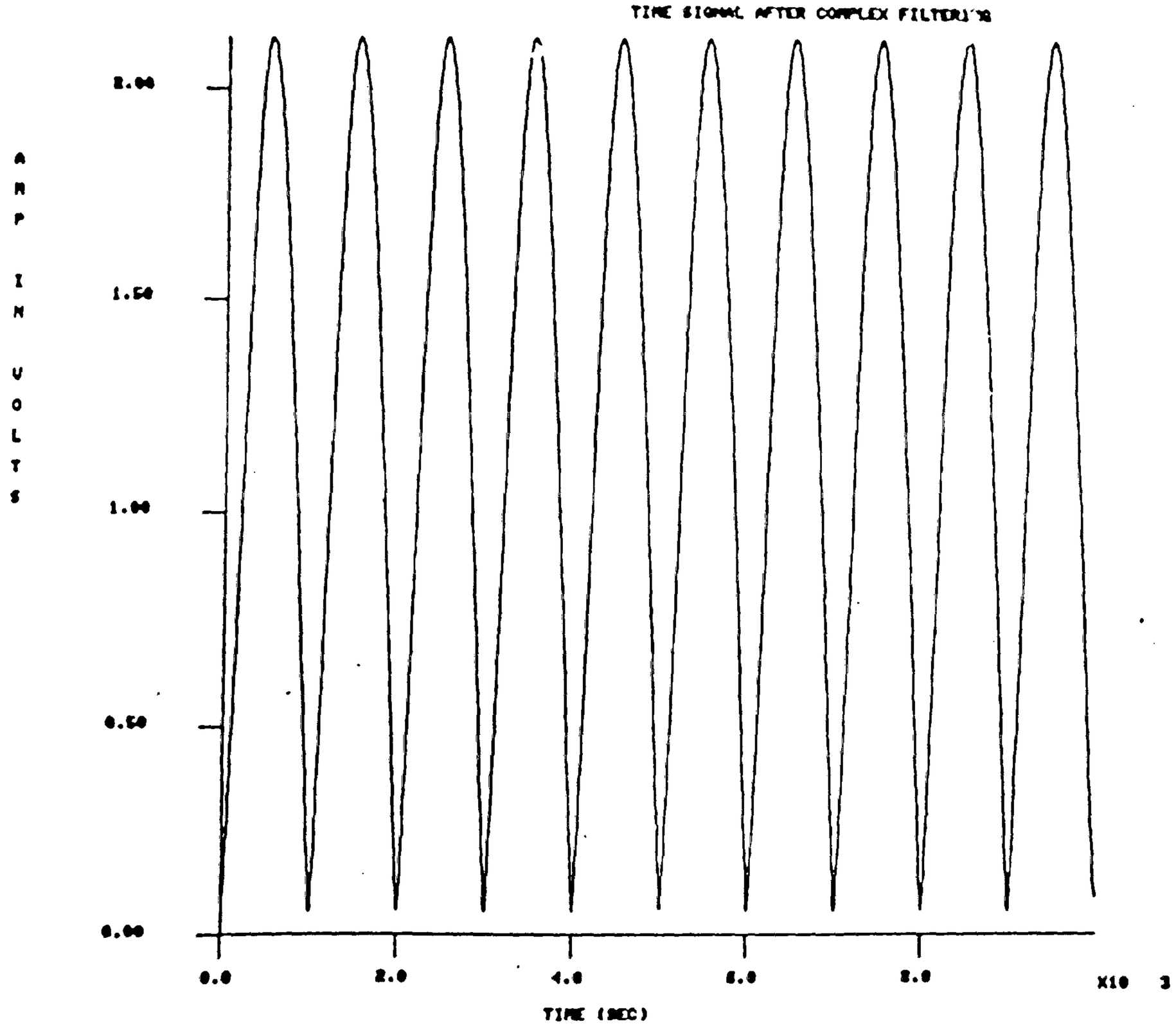

Fig. 5.34 Envelope of filtered signal with $\Delta\sigma_r$ = 10 μsec.

using its Fourier coefficients. This approach is discussed in detail in Section 6.3. Complex filtering is then accomplished in the same way as the last single-tone signal, i.e. by multiplying the frequency samples of the bandlimited random signal by the respective filter frequency responses using different σ_r values that correspond to the complex zeros of the random signal. Investigation of the envelope of time samples of the filtered signal gives the detected real zeros that correspond to complex zeros of the random signal.

Figure 5.35(a) shows the bandlimited positive real random signal that has a mean value of 5 and standard deviation value of 8. Figure 5.35(b) shows the envelope of the filtered signal, and the real zero at t_r = 9148 μ sec corresponds to a complex zero with σ_r = 151.9 μ sec and t_r = 9148 μ sec. It is apparent from the figure that there is another real zero at t_r = 2990 μ sec, and this corresponds to a complex zero with σ_r = 153 μ sec and t_r = 2990 μ sec. These two complex zeros detected by the same filter are separated by $\Delta\sigma_r$ = 1.1 μ sec. Figure 5.35(c) shows a real zero corresponding to a complex zero with σ_r = 351.1 μ sec and t_r = 7895 μ sec. Figure 5.35(d) shows another complex zero detected at t_r = 2397 μ sec and the complex zero lies at σ_r = 427.1 μ sec and t_r = 2397 μ sec. Figure 5.35(e) shows another real zero corresponding to a complex zero at σ_r = 138.8 μ sec and t_r = 9871 μ sec. Figure 5.35(f) shows two real zeros corresponding to two complex zeros at

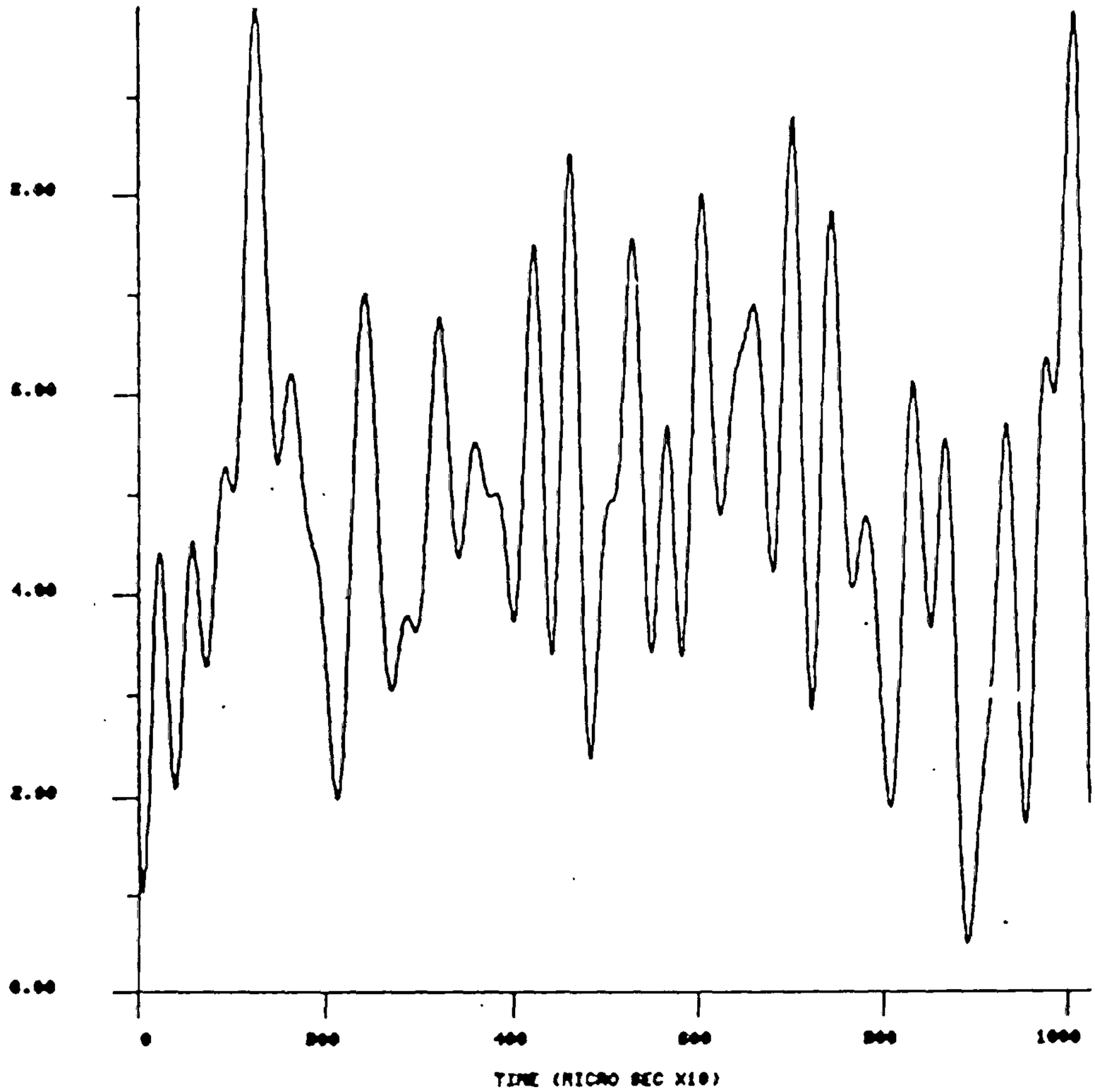

Fig. 5.35(a) Bandlimited real positive random signal.

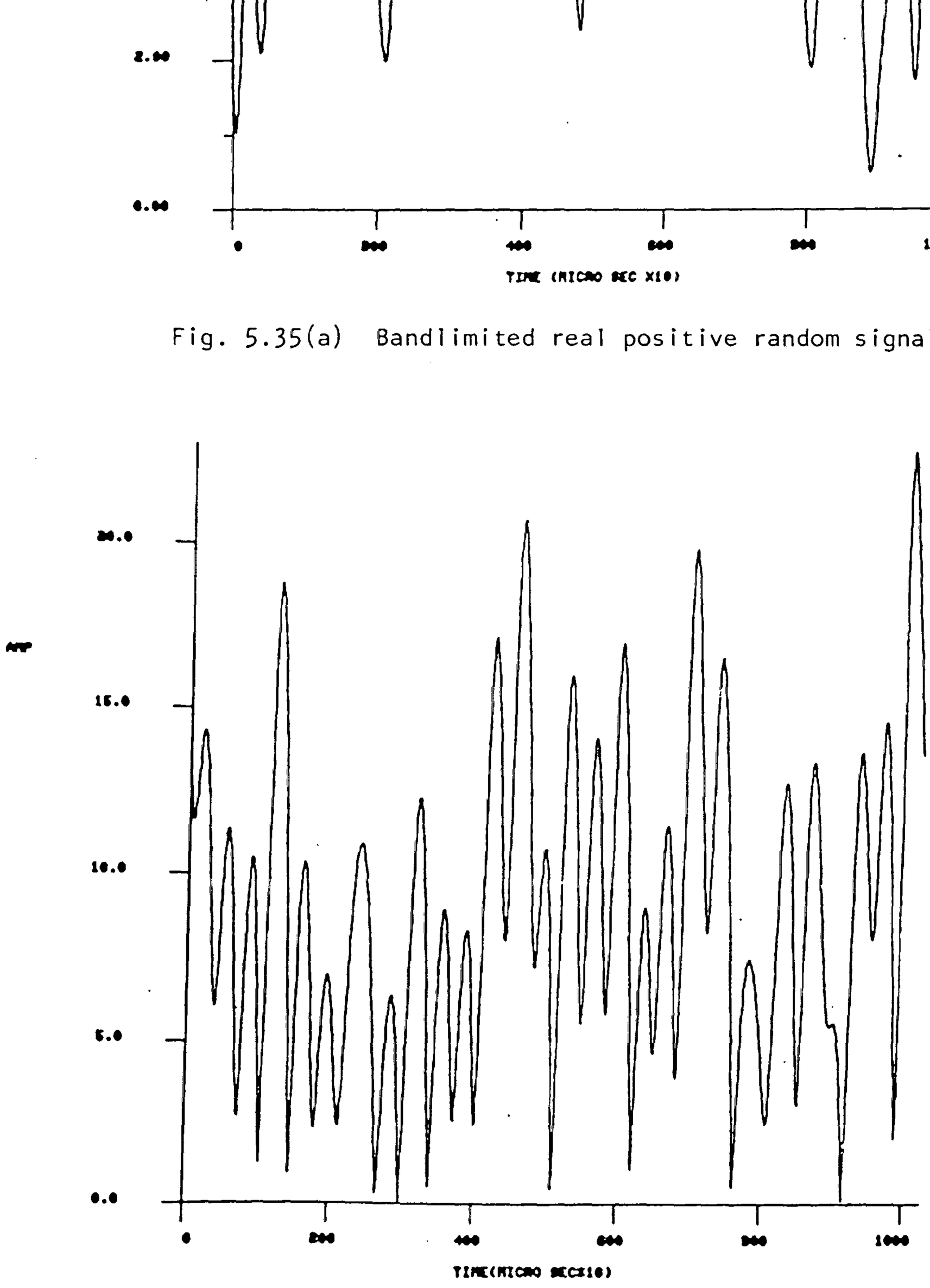

Fig. 5.35(b) Envelope of filtered signal.

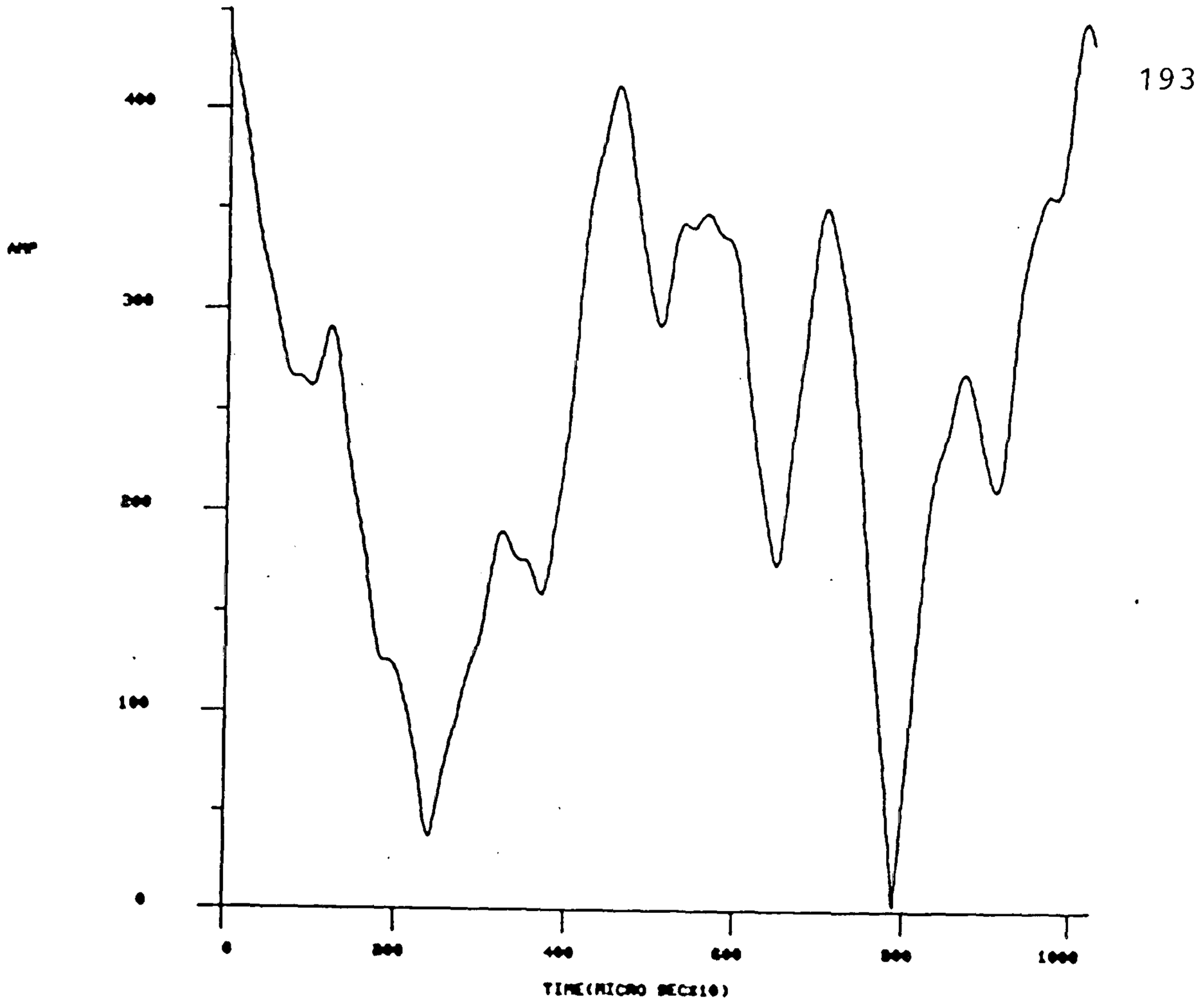

Fig. 5.35(c) Envelope of filtered signal.

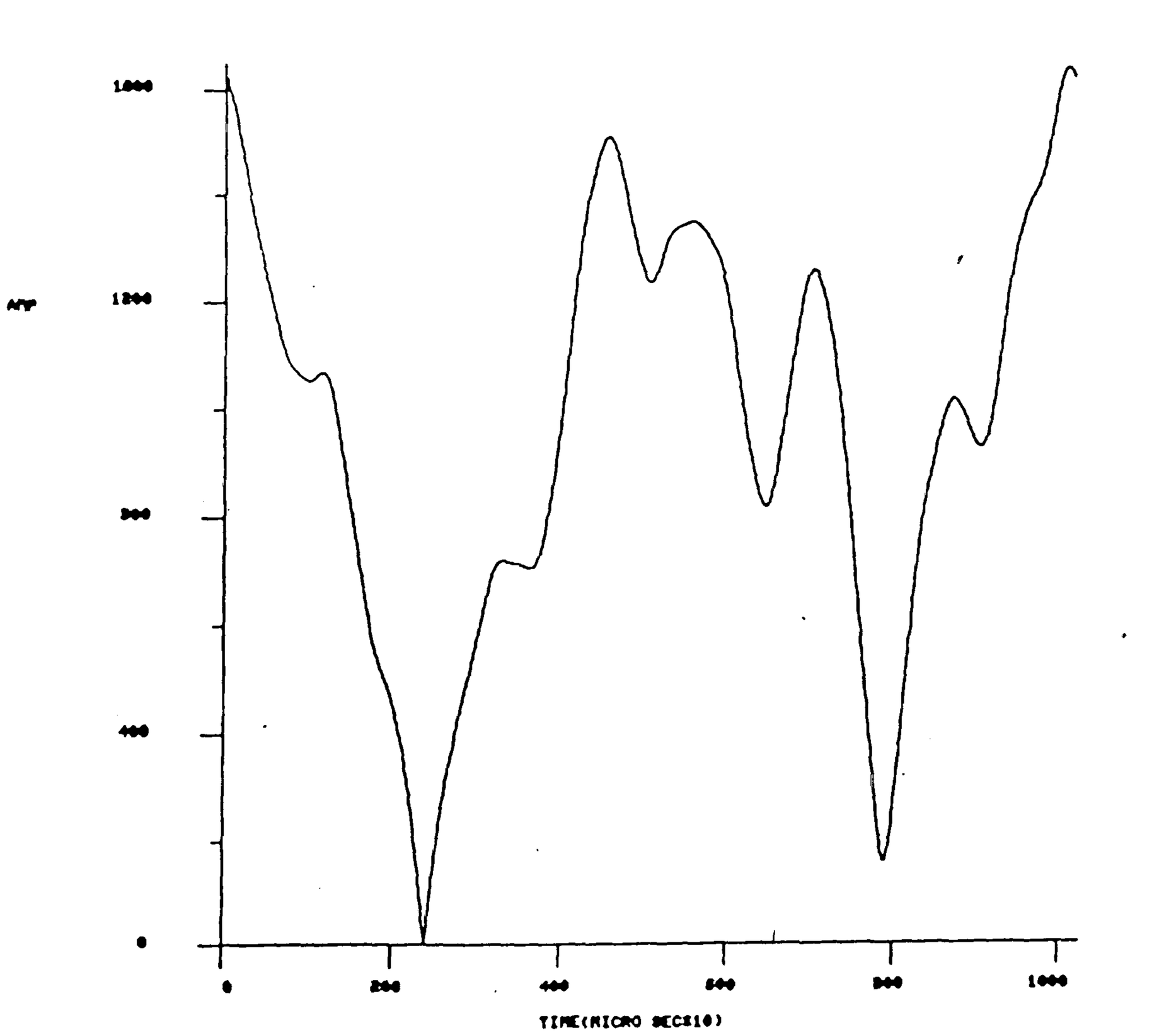

Fig. 5.35(d) Envelope of filtered signal.

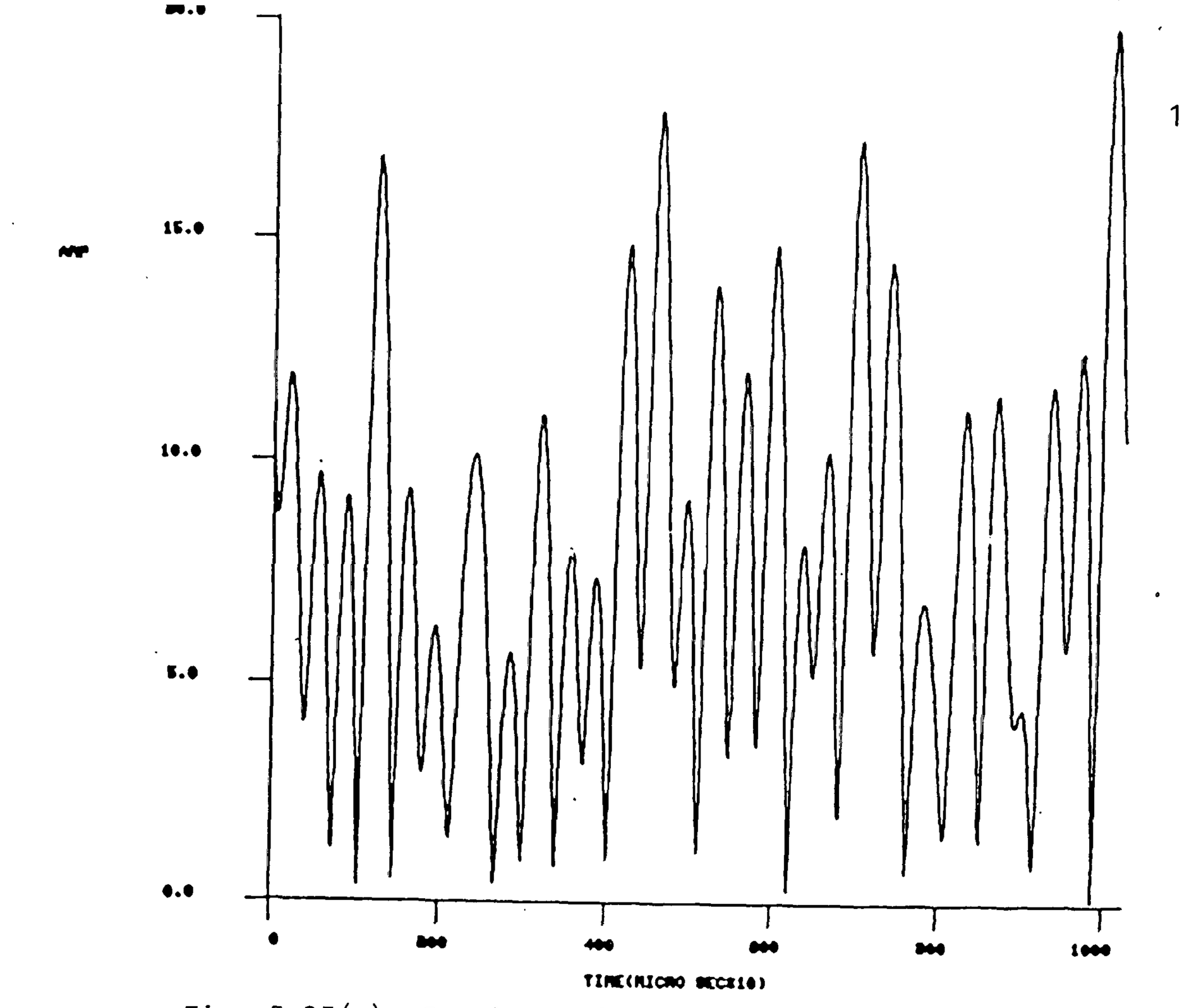

Fig. 5.35(e) Envelope of filtered signal.

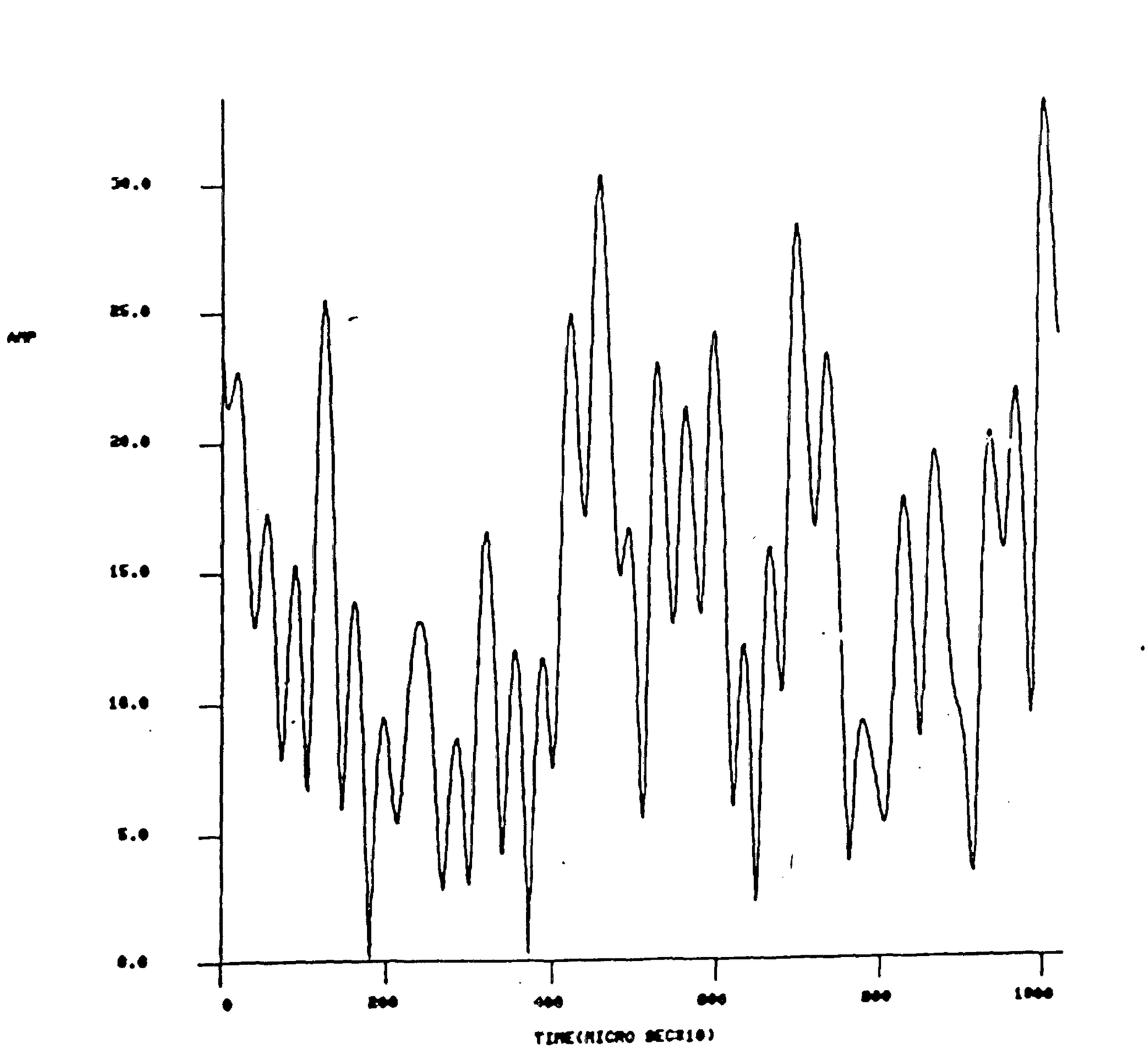

Fig. 5.35(f) Envelope of filtered signal.

σ_r = 182.7 μ sec, 182.8 μ sec and t_r = 1789 μ sec, 3717 μ sec respectively. Figure 5.35(g) shows a real zero at t_r = 7211 μ sec that corresponds to a complex zero with σ_r = 89.27 μ sec and t_r = 7211 μ sec. It can be noticed from the figure also that there is a trough very close to zero at t_r = 381 μ sec, and this corresponds to a complex zero at σ_r = 92.24 μ sec and t_r = 381 μ sec. These two complex zeros are separated by $\Delta\sigma_r$ = 3.13 μ sec. It is considered therefore, that the different complex filters in the bank (see Figure 3.15) can be designed so that for any two successive filters $\Delta\sigma_r$ = 2 μ sec. The logic circuit at the bank output can decide whether the envelope trough is closer to zero for the filter with σ_{r_1} or for the filter with σ_{r_2}, where $\sigma_{r_2} - \sigma_{r_1} = \Delta\sigma_r$. The number of filters required in the bank can be decreased if $\Delta\sigma_r$ is made larger or also if the range of σ_r values of interest is made smaller. A possible number of complex filters is considered in Section 6.5.

5.10 Effects of Truncating the FM Function

The FM function, imposed in order to achieve complex zero conjugation, has to be truncated within a finite time interval of length P seconds (see Section 3.8). This section investigates the effects of this truncation on the performance of ZSFM, and it also describes how this situation can be simulated.

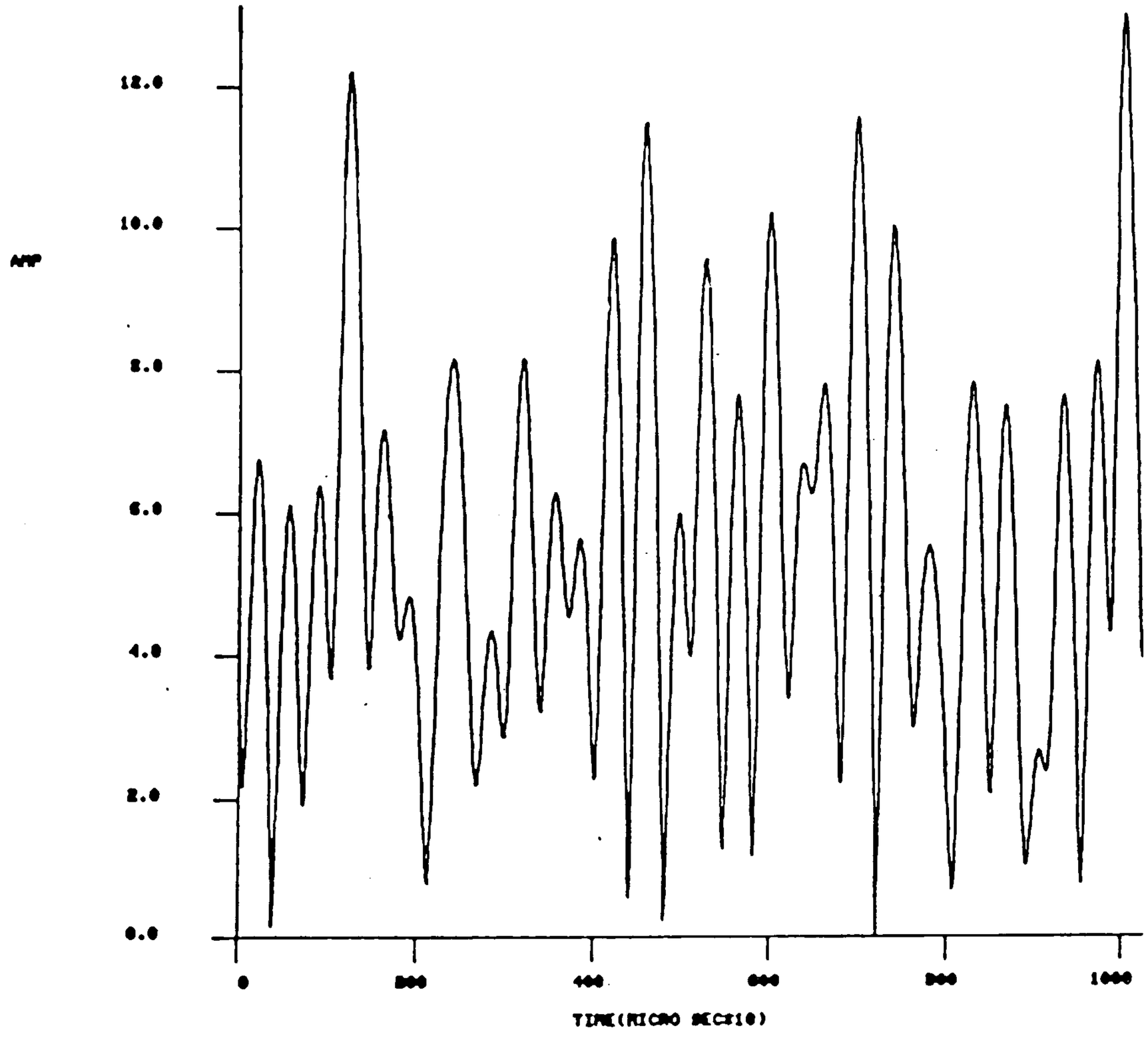

Fig. 5.35(g) Envelope of filtered signal.

Consider a block of a signal x(t) representing a DSB-AM signal with only one complex zero pair conjugated at the middle, where the FM function is applied through a window of width P seconds only. The signal x(t) is assumed to be bandlimited. Figure 5.36 illustrates such a modulated signal having 5 zero pairs, and the carrier frequency has been made unrealistically low in order to distinguish individual carrier cycles. The FM function has been impressed so that the complex zero pair at t = 0 is conjugated in the positive sense. The resulting increase in the instantaneous frequency and carrier phase inversion is evident in the vicinity of t = 0.

$x_1(t)$ is the conjugated part of x(t) that lies through the window P seconds long.

The signal outside the P seconds window can be expressed as:

$$x(t) \quad [1 - \text{rect } (\frac{t}{P})]$$

$$\text{where} \qquad \text{rect } (\frac{t}{P}) \quad = \quad \begin{cases} 1, & |t| \leq P/2 \\ 0, & \text{otherwise} \end{cases}$$

as shown in Figure 5.37.

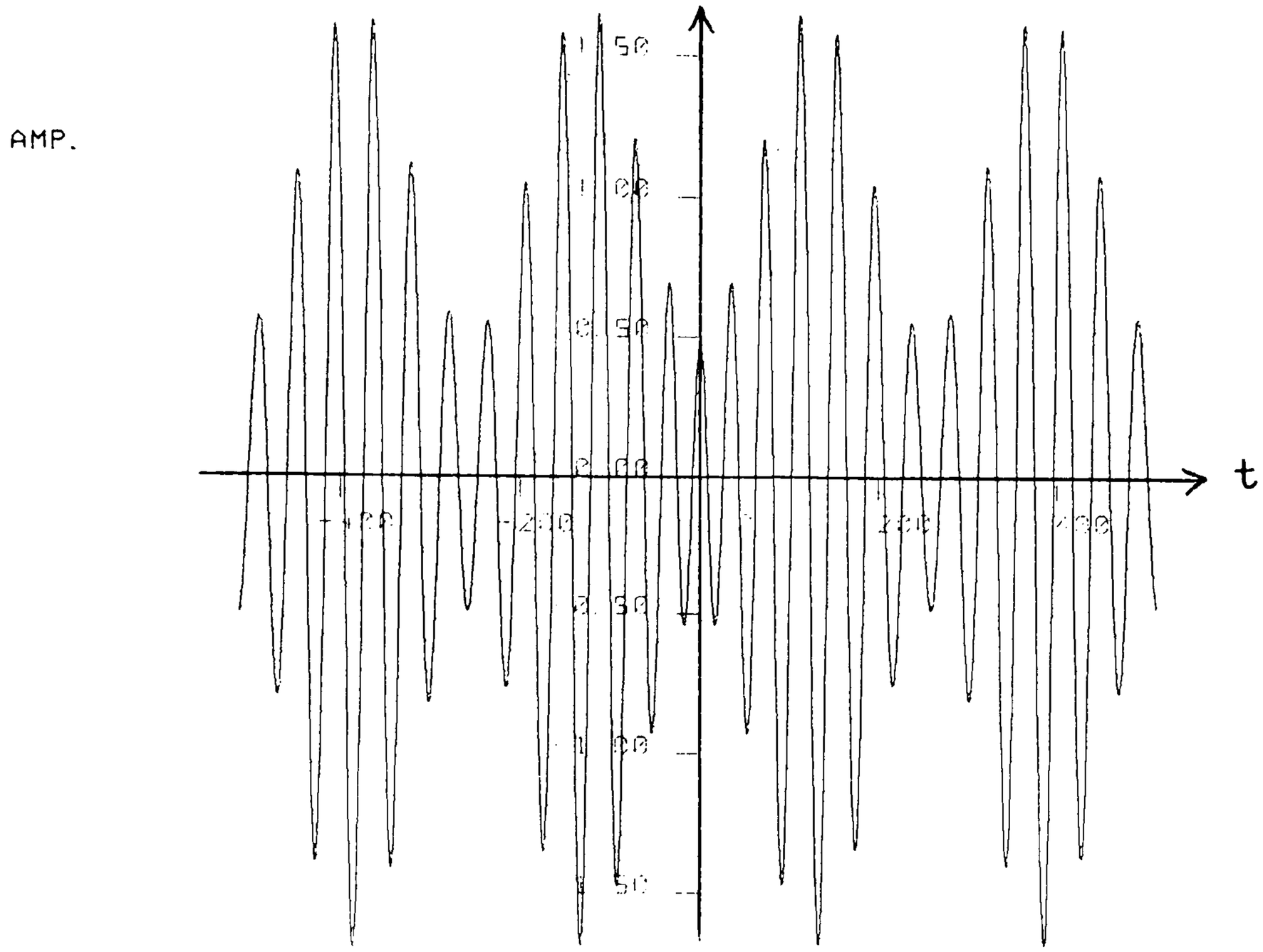

Fig. 5.36 The signal x(t) having one zero conjugated at t = 0

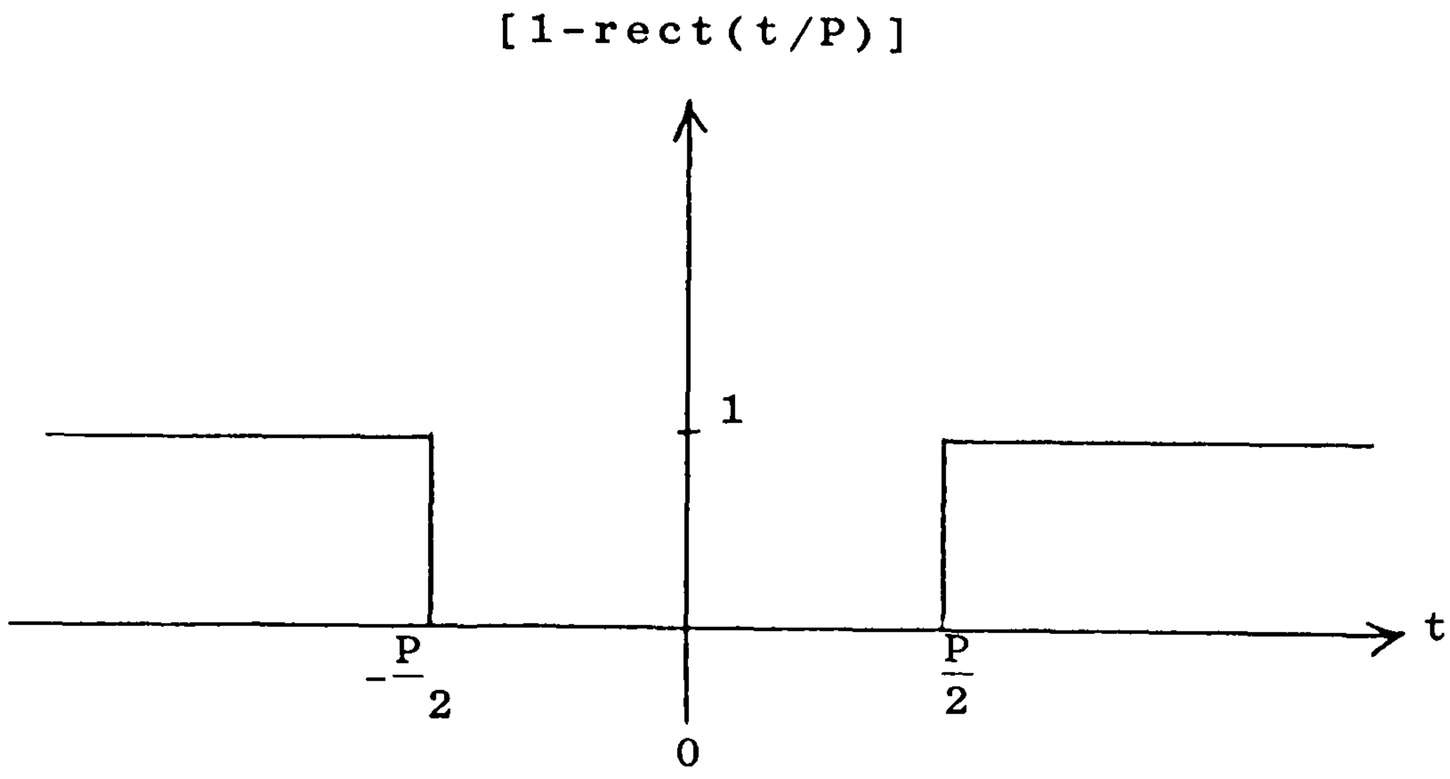

Fig. 5.37

The conjugated signal can be written in the form:

$$y(t) = x(t)\ [1-\text{rect}(\tfrac{t}{P})] + x_1(t)\ \text{rect}(\tfrac{t}{P})$$

$$= x(t) + \text{rect}(\tfrac{t}{P})\ [x_1(t) - x(t)] \qquad (5.26)$$

The signal inside the P seconds window, $x_1(t)$, can be written in the form given by eqn. (5.3):

$$x_1(t) = x(t)\ e^{j\theta(t)}$$

$$= x(t)\ e^{j2\tan^{-1}(t/\sigma_r)}$$

$$= x(t)\ \left\{\frac{1 + j\ t/\sigma_r}{1 - j\ t/\sigma_r}\right\}$$

$$= x(t)\ \left\{\frac{\sigma_r + jt}{\sigma_r - jt}\right\} \qquad (5.27)$$

Substituting for $x_1(t)$ in eqn. (5.26) gives:

$$y(t) = x(t) + \text{rect}(\tfrac{t}{P})\,[x(t)\ \left\{\frac{\sigma_r + jt}{\sigma_r - jt}\right\} - x(t)]$$

$$= x(t) + \text{rect}(\tfrac{t}{P})\ x(t)\,[\ \left\{\frac{\sigma_r + jt}{\sigma_r - jt}\right\} - 1]$$

$$= x(t) + \text{rect}(\tfrac{t}{P})\ x(t)\ \left[\frac{j2t}{\sigma_r - jt}\right]$$

$$= x(t) + \text{rect}(\tfrac{t}{P})\ q(t) \qquad (5.28)$$

where $q(t) = x(t)\left(\frac{j2t}{\sigma_r - jt}\right) = x_1(t) - x(t)$

$q(t)$ is bandlimited as both $x_1(t)$ and $x(t)$ are theoretically bandlimited signals. The signal $x_1(t)$ is bandlimited as it is derived from a bandlimited signal ($x(t)$) by conjugating only one zero pair, and the process of zero conjugation does not increase the bandwidth (Section 3.8).

If $Y(f)$, $X(f)$, and $Q(f)$ are the Fourier transforms of $y(t)$, $x(t)$, and $q(t)$ respectively, then taking the Fourier transform of eqn. (5.28) gives:

$$Y(f) = X(f) + P\ \text{sinc}\ (Pf) * Q(f) \qquad (5.29)$$

where * denotes convolution and

$$P\ \text{sinc}(Pf) = P\ \frac{\sin(\pi Pf)}{\pi Pf}$$

The sinc function has zero crossings at

$$f = \pm \frac{k}{P},\quad k = 1, 2, 3, \ldots$$

The spectrum of $y(t)$ is non-bandlimited, and the out-of-band components are due to the convolution of the sinc with $Q(f)$. The bigger P is, the smaller the out-of-band components are. In the limit when P becomes infinitely large, the spectrum of $y(t)$ will be bandlimited as the sinc function will become a dirac-delta giving the same bandlimited spectrum when convolved with $Q(f)$.

Therefore the ZSFM signal is not strictly bandlimited when the FM function is truncated in practice. This effect can be studied through imposing the truncation effect on the PM function $\theta(t)$. Consider the truncated

version of the FM function given as:

$$\theta'(t) = \frac{2\sigma_r}{\sigma_r^2 + t^2} \text{ rect}(\frac{t}{P}) \qquad (5.30)$$

$$\text{where} \quad \text{rect}(\frac{t}{P}) = \begin{cases} 1, & |t| \leq P/2 \\ 0, & \text{otherwise} \end{cases}$$

Figure 5.38 shows this truncated FM function.

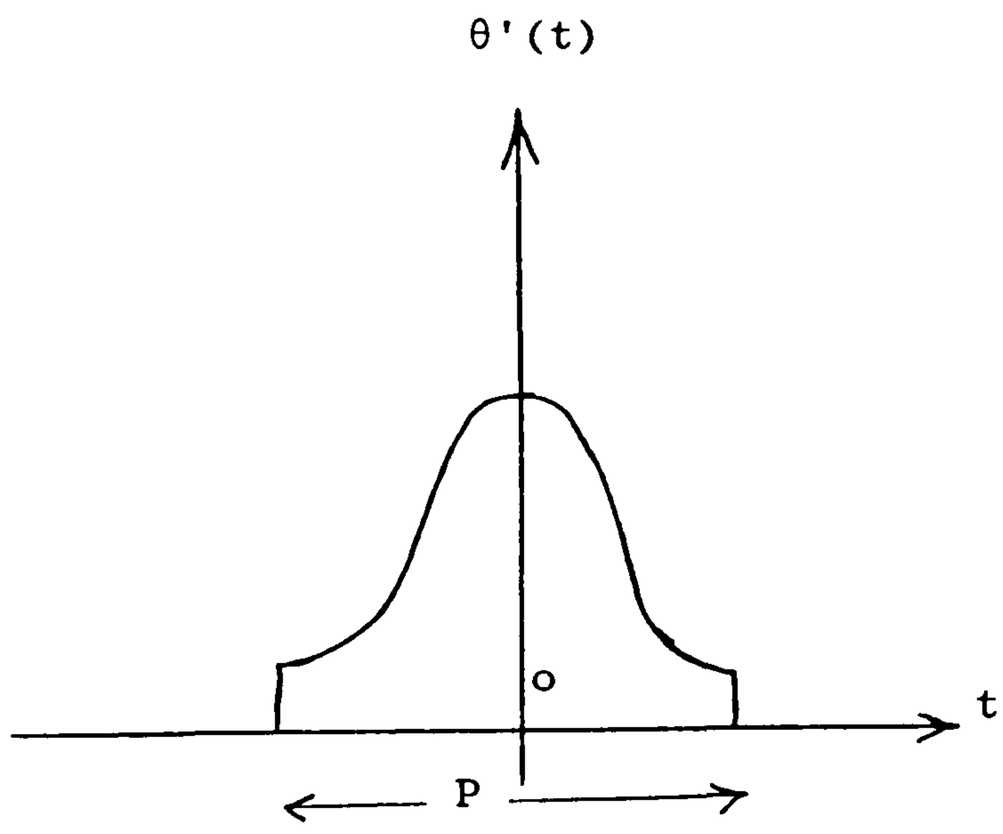

Fig. 5.38

The PM function can be obtained analytically by integrating $\theta'(t)$:

For $t < -P/2$, $\theta(t) = 0$

For $-P/2 \leq t \leq P/2$

$$\theta(t) = \int_{-P/2}^{t} \frac{2\sigma_r}{\sigma_r^2 + \tau^2} d\tau = [2 \tan^{-1}(\frac{\tau}{\sigma_r})]_{-P/2}^{t}$$

$$= 2 \tan^{-1}(\frac{t}{\sigma_r}) + 2 \tan^{-1}(\frac{P}{2\sigma_r}) \qquad (5.31)$$

at $t = -P/2$, $\theta(t) = 0$

at $t = 0$, $\theta(t) = 2 \tan^{-1} (P/2\sigma_r)$

at $t = +P/2$, $\theta(t) = 4 \tan^{-1}(P/2\sigma_r)$

If $|\sigma_r| = |\frac{\ln a}{\Omega}|$, $\frac{\Omega}{2\pi} = 1.5625$ kHz , a = 0.3, then

$|\sigma_r| = 1.23 \times 10^{-4}$ sec, and the following table shows the range of $\theta(t)$ for different P values:

P(μ sec)	P/σ_r	$\theta(t)$ range
800	6.5	0 → 291.6°
1600	13	0 → 325°
3200	26	0 → 342.4°
6400	52	0 → 351.2°
12800	104	0 → 355.6°
25600	208	0 → 357.8°
51200	416	0 → 358.9°

The results show that as the width (P) of the window increases, then $\theta(t)$ varies through ranges approaching 2π radians.

In the computer simulation, a block of 64 cycles of:

$$s(t) = 1 + a^2 - 2a\cos\Omega t$$

is generated, and only two complex zero pairs at the middle (27th and 37th pairs) are conjugated using the truncated FM function:

$$\theta'(t) = \frac{2\sigma_r}{\sigma_r^2 + (t-t_r)^2} \text{rect}(\frac{t-t_r}{P}) - \frac{2\sigma_r}{\sigma_r^2+(t-t_s)^2}\text{rect}(\frac{t-t_s}{P}) \qquad (5.32)$$

This truncated FM function represents the binary code

code (10), and is shown in Figure 5.39.

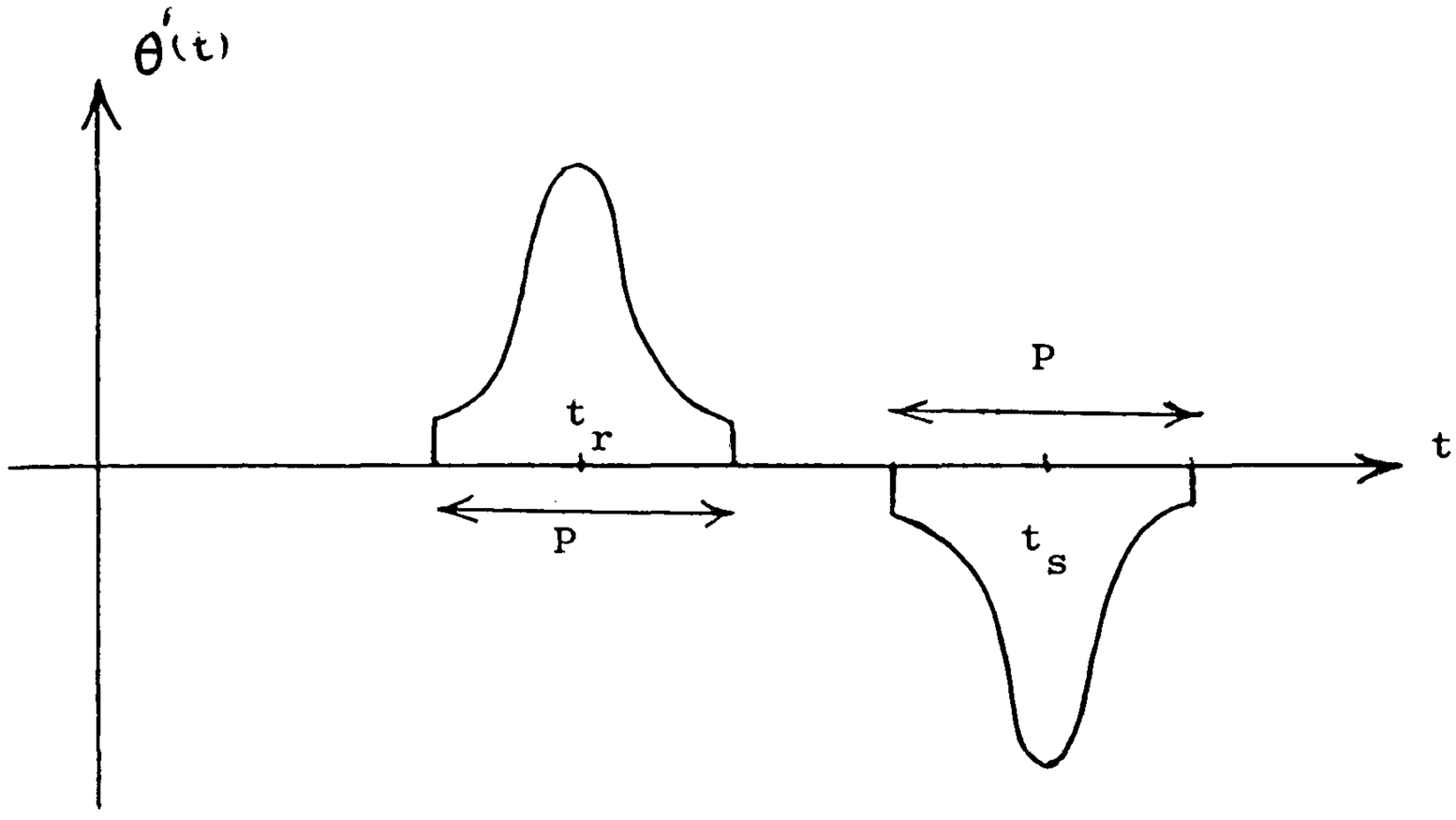

Fig. 5.39

The corresponding truncated PM function can be obtained by integration.

For $t < t_r - \frac{P}{2}$, $\theta(t) = 0$

For $t_r - \frac{P}{2} \leq t \leq t_r + \frac{P}{2}$, $\theta(t) = 2 \tan^{-1}\left(\frac{t-t_r}{\sigma_r}\right) + 2 \tan^{-1}\left(\frac{P}{2\sigma_r}\right)$

For $t_r + \frac{P}{2} \leq t \leq t_s - \frac{P}{2}$, $\theta(t) = 4 \tan^{-1}\left(\frac{P}{2\sigma_r}\right)$

For $t_s - \frac{P}{2} \leq t \leq t_s + \frac{P}{2}$, $\theta(t)$ is obtained by integrating over the negative area and adding the result to the previous $\theta(t)$ value, i.e.

$$\theta(t) = 4 \tan^{-1}\left(\frac{P}{2\sigma_r}\right) + \int_{t_s - P/2}^{t} \frac{-2\sigma_r}{\sigma_r^2 + (\tau - t_s)^2} \, d\tau$$

$$= 4 \tan^{-1}\left(\frac{P}{2\sigma_r}\right) - \left[2 \tan^{-1}\left(\frac{\tau - t_s}{\sigma}\right)\right]_{t_s - P/2}^{t}$$

$$= 2 \tan^{-1}\left(\frac{P}{2\sigma_r}\right) - 2 \tan^{-1}\left(\frac{t - t_s}{\sigma_r}\right)$$

$$\text{At } t = t_s - \frac{P}{2}\ ,\ \theta(t) = 4 \tan^{-1}\left(\frac{P}{2\sigma_r}\right)$$

$$\text{At } t = t_s + \frac{P}{2}\ ,\ \theta(t) = 0$$

The following table summarises the analytical expressions of $\theta(t)$ for the respective intervals.

Interval	$\theta(t)$
$t < t_r - P/2$	0
$t_r - P/2 < t < t_r + P/2$	$2 \tan^{-1}\left(\frac{t-t_r}{\sigma_r}\right) - 2 \tan^{-1}\left(\frac{P}{2\sigma_r}\right)$
$t_r + P/2 < t < t_s - P/2$	$4 \tan^{-1}\left(\frac{P}{2\sigma_r}\right)$
$t_s - P/2 < t < t_s + P/2$	$2 \tan^{-1}\left(\frac{P}{2\sigma_r}\right) - 2 \tan^{-1}\left(\frac{t-t_s}{\sigma_r}\right)$
$t > t_s + P/2$	0

Figure 5.40 shows the truncated phase function for the binary code (1 0).

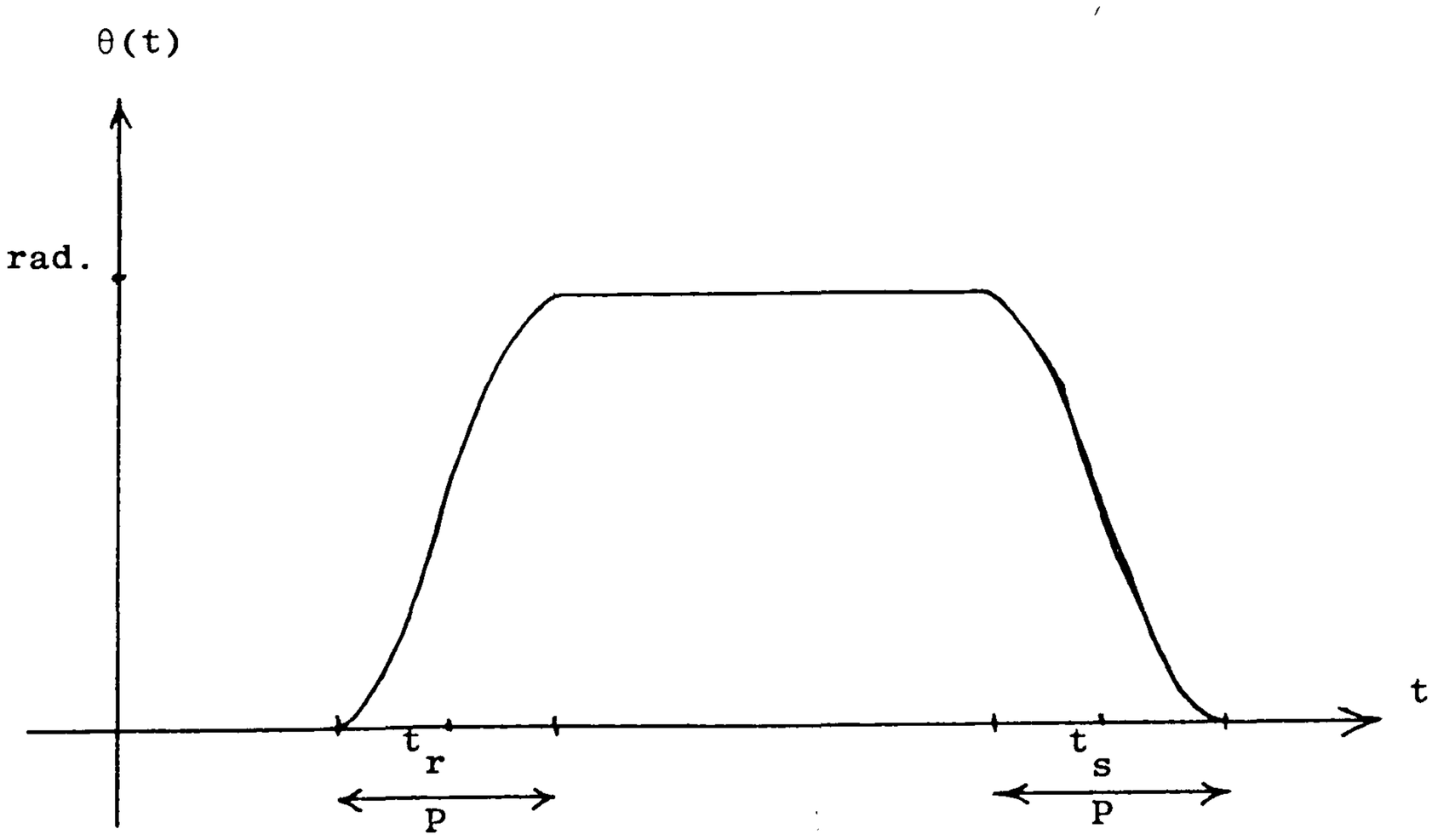

Fig. 5.40

It is apparent that the width of window (P) is not to exceed the upper value of:

$$P \leq (t_s - t_r)$$

i.e. the time slot between two successive conjugated zero pairs. If P exceeds this value, then a discontinuity (jump) will occur in $\theta(t)$ corresponding to an infinite $\theta'(t)$ at the corresponding instant of time. The shorter P is, the data rate of ZSFM is more as more zero pairs can be conjugated within a finite time slot.

Experiment 14

The above situation was studied through computer simulation, with two zero pairs conjugated according to the binary code (10) using the truncated PM function as given analytically in the previous Table. The value of $(t_s - t_r)$ is 6400 μ sec, and therefore the window width cannot exceed this value. P is varied to find the truncation effect on the bandwidth of the ZSFM signal, while the modulation depth is kept constant.

The experiment calculates the suppression (in dB) of the biggest out-of-band component compared to the single-tone component at $\frac{\Omega}{2\pi}$ = 1.56 kHz. It is known from a previous result (Section 3.8) that the FM function $\theta'(t)$ is symmetrical about $t = t_r$ and falls asymptotically to zero with t^2. However, when $\theta'(t)$ is truncated within P seconds interval, the approximation error introduced because of truncation is larger for high σ_r

values than for small σ_r values. Thus it is beneficial to evaluate the ZSFM performance for the worst extreme case, i.e. for high σ_r values. Choosing a modulation depth of m = 30% gives σ_r value of approximately 194 μ sec ($\sigma_r = \pm \frac{1na}{\Omega}$) and this might represent an extreme σ_r value suitable for conjugation (see Section 5.4 and Chapter 6).

Figure 5.41 shows the suppression against the window width for modulation depths of 30% and 70%. For 70% modulation the value of σ_r is 91 μ sec and as expected the truncation effect is smaller than for the 30% modulation case. It must be mentioned that the out-of-band components decrease significantly and quickly in magnitude as the difference in frequency from the single-tone at $\frac{\Omega}{2\pi}$ increases. The suppression obtained for 70% modulation is improved by 6-7 dB over the case for 30% modulation for the same P value. The case when P = 640 μ sec allows all the complex zero pairs of the signal to be conjugated as it is the time slot between any two successive zero pairs. On the other hand for this P value the out-of-band components might not be tolerable. If the window width is made equal to 1280 μ sec, then for the worst case the suppression is more than 17 dB, but this means that the data rate will be halved, and for a 10 kHz channel the rate is 2.5 k bit/sec rather than 5 k bit/sec.

It is considered that if more than one conjugating function generator is used, then the truncation effect

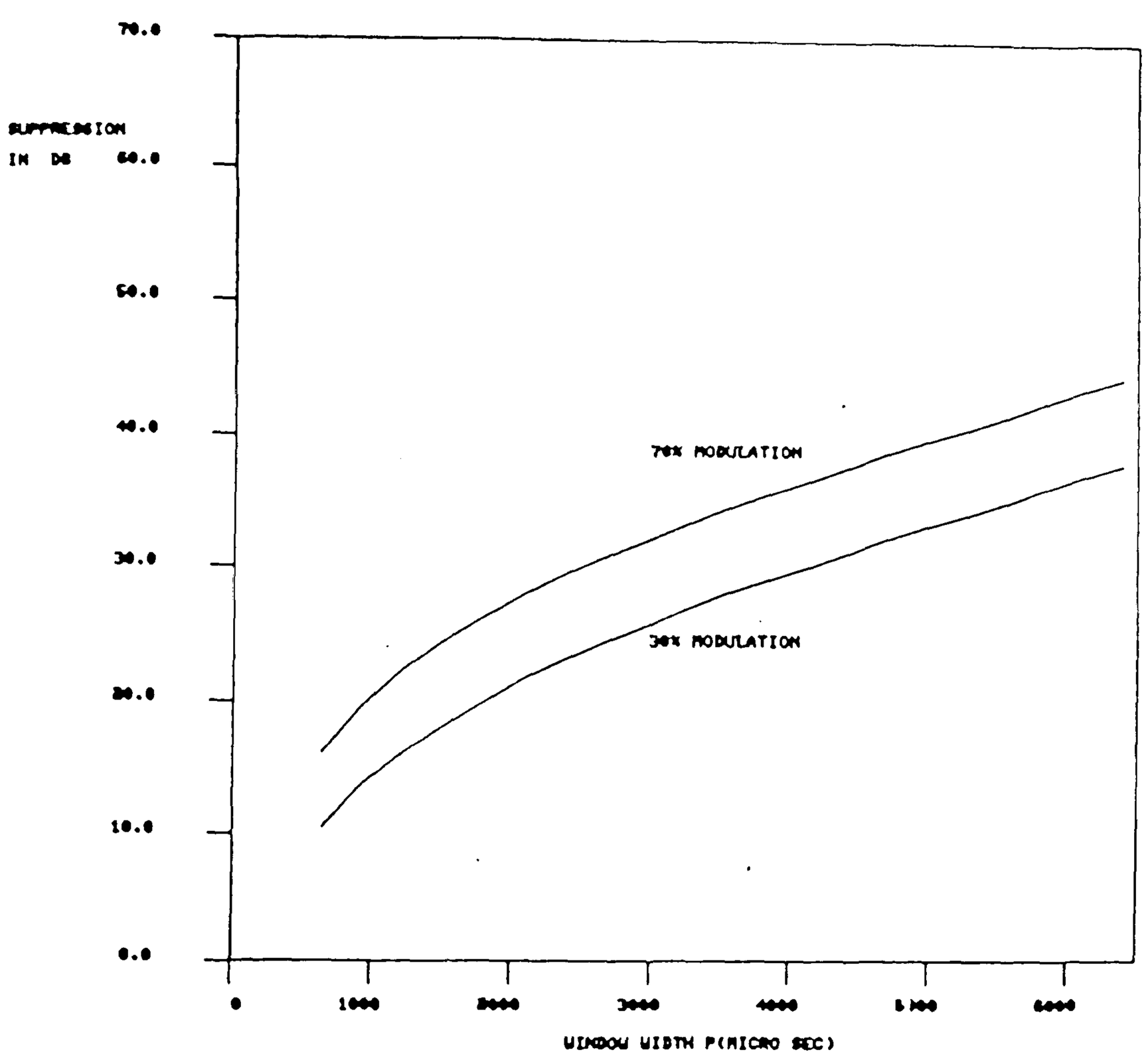

Fig. 5.41 Out-of-band suppression against window width P.

will be less pronounced. For example, two conjugating function generators can be interlaced each one for different range of σ_r values. In this case the generator for high σ_r values can be given larger P to minimise the approximation error, while the other generator for small σ_r values functions through shorter P.

Figure 5.42 shows the ZSFM signal spectrum for 70% modulation and 4000 μ sec window width.

Experiment 15

In this experiment the effect of truncated FM function $\theta'(t)$ on the detected envelope signal of ZSFM is studied. The same ZSFM signal as in the last experimen is used. In the receiver the same practical IF stage with phase non-linearity is used. The modulation depth is kept at 50%, while the window width is varied. The signal-to-distortion ratio of the detected envelope signal is calculated in the same way given in Section 5.7. The σ_r value corresponding to 50% modulation is $\sigma_r = 1.34 \times 10^{-4}$ sec ($\sigma_r = \pm \frac{\ln a}{\Omega}$). Figure 5.43 shows the calculated S/D ratio against different values of $\frac{P}{\sigma_r}$ where σ_r is kept unchanged. The window width is changed between (100-6400) μ sec. It is apparent that the detected envelope quality is nearly independent of the window width for $P \geq 800$ μ sec. Even for $P < 640$ μ sec the S/D ratio is more than 45 dB. Figure 5.44 shows the detected envelope and data (10) signals for 50% modulation and window width of 640 μ sec. It can be

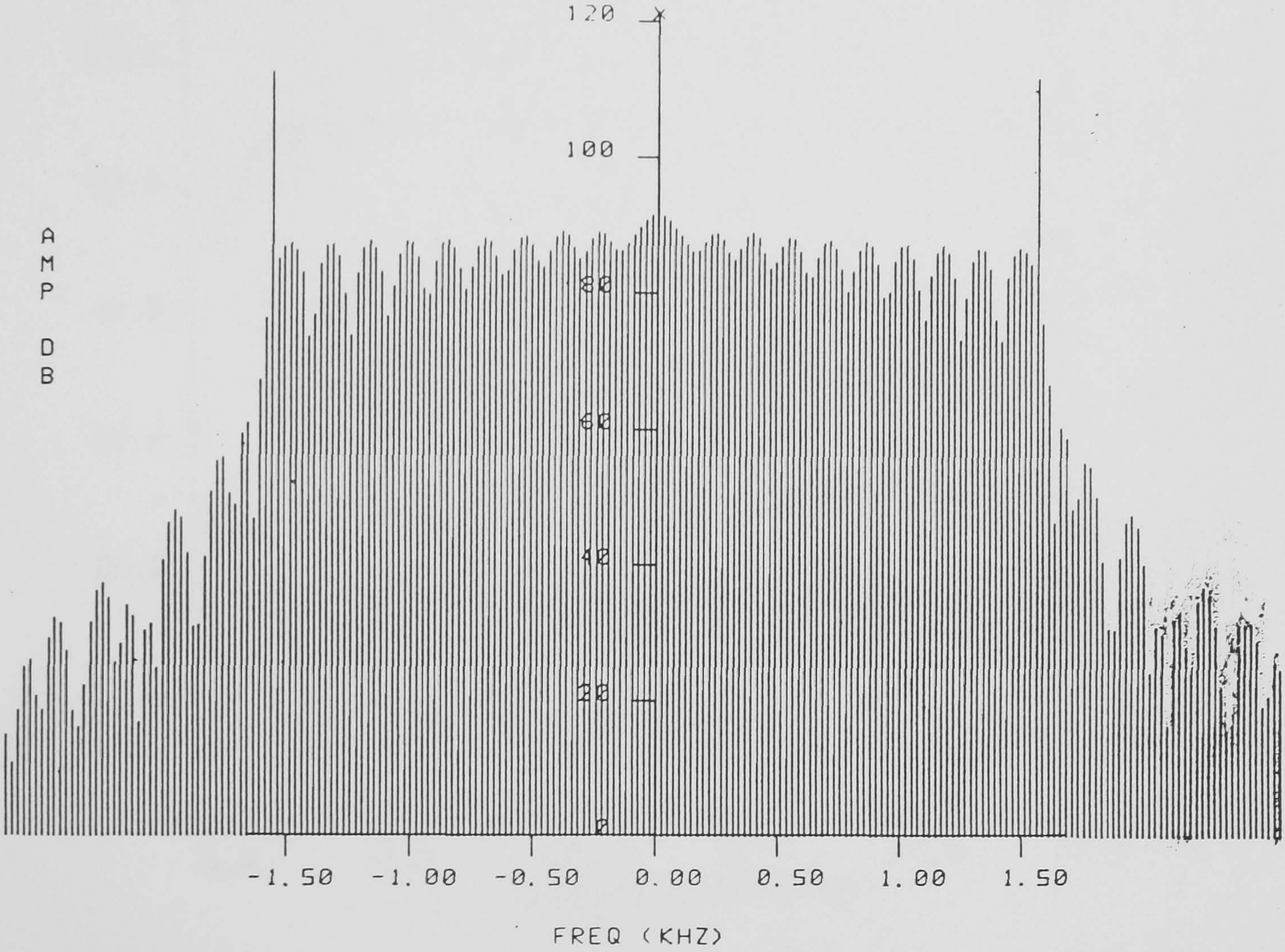

Fig. 5.42 Spectrum of ZSFM signal for 70% modulation and 4000 μ sec window width.

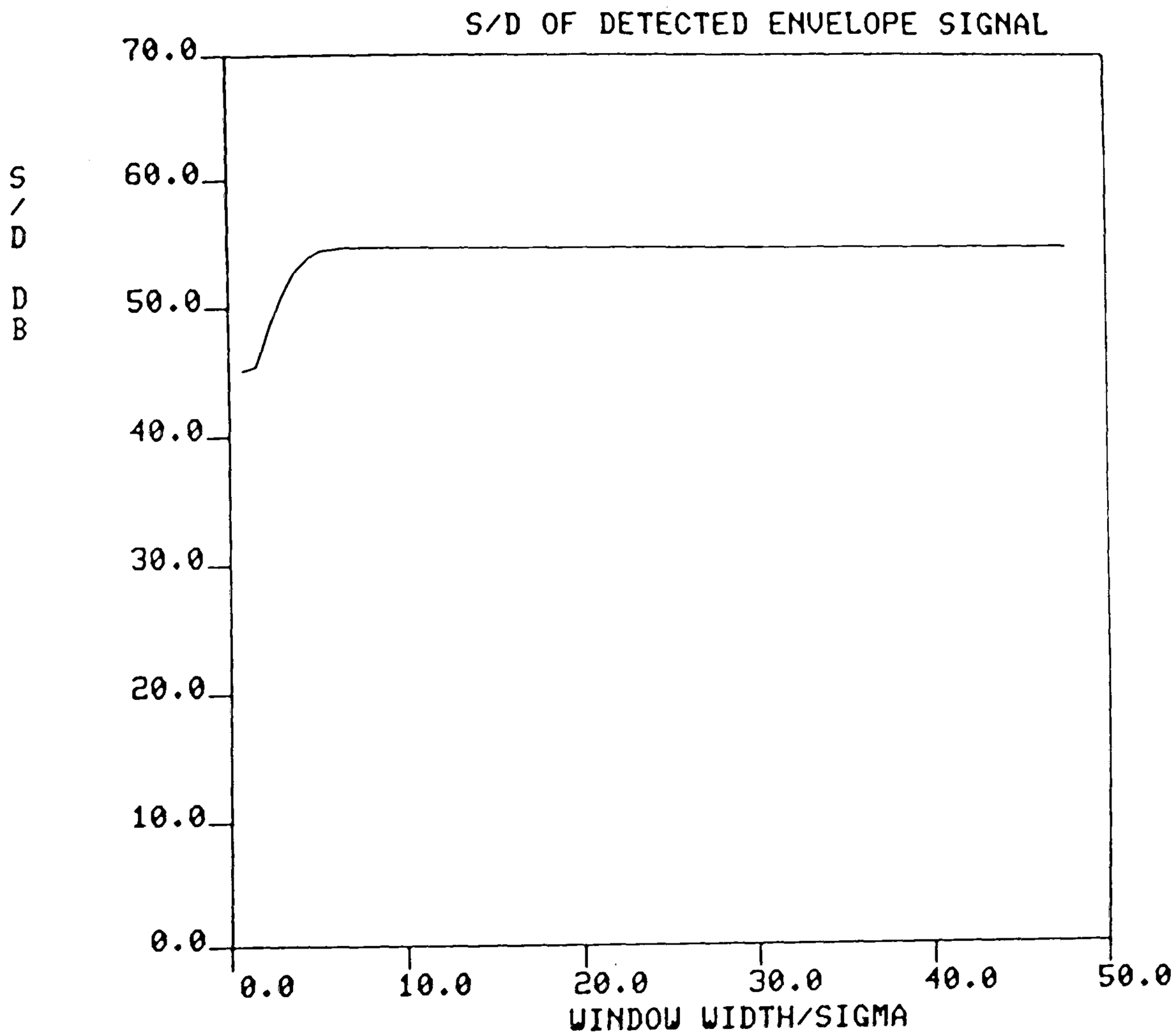

Fig. 5.43 Signal/distortion power ratio for 50% modulation depth.

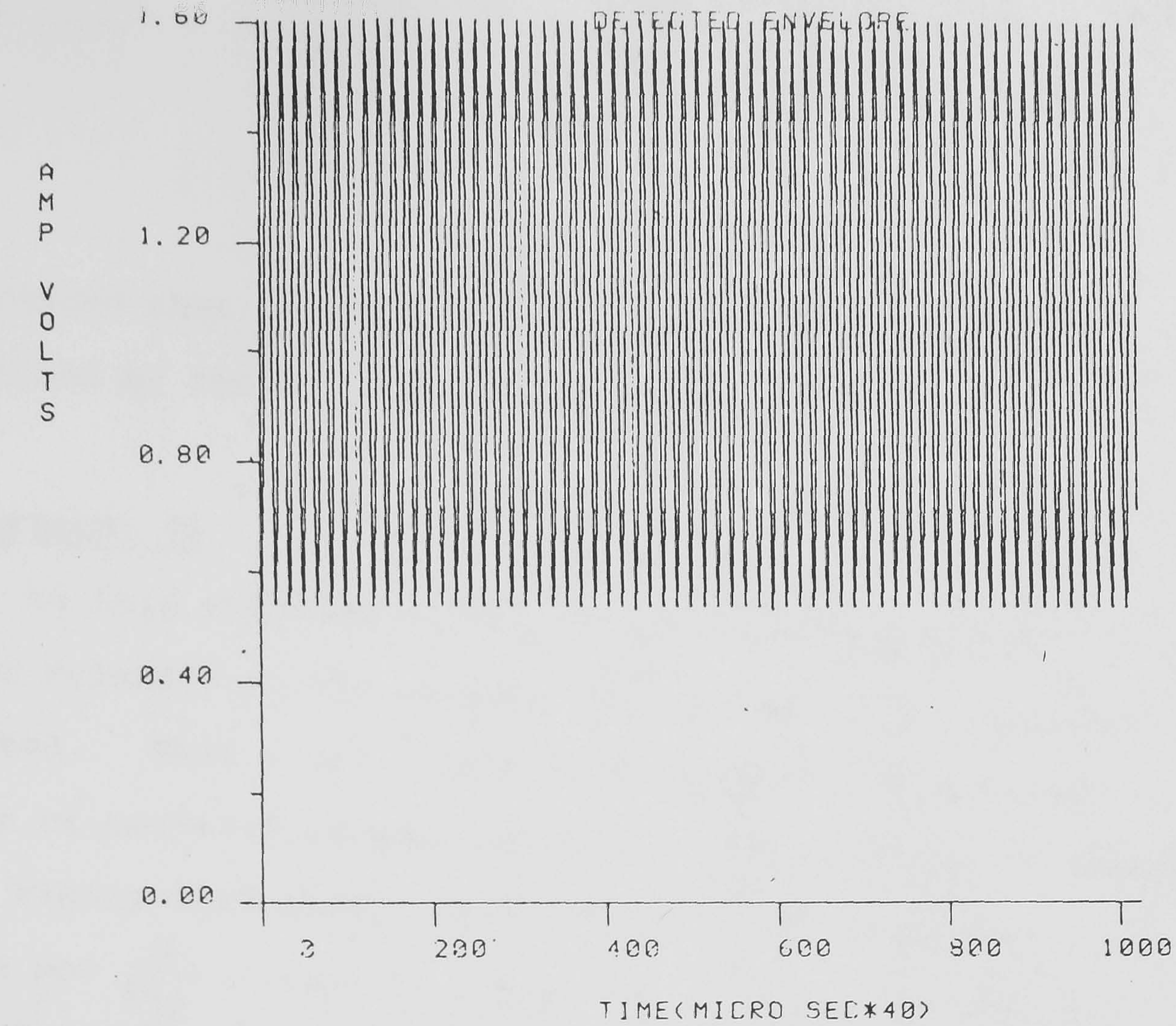

Fig. 5.44 Detected envelope signal for 50% modulation depth and P = 640 μ sec.

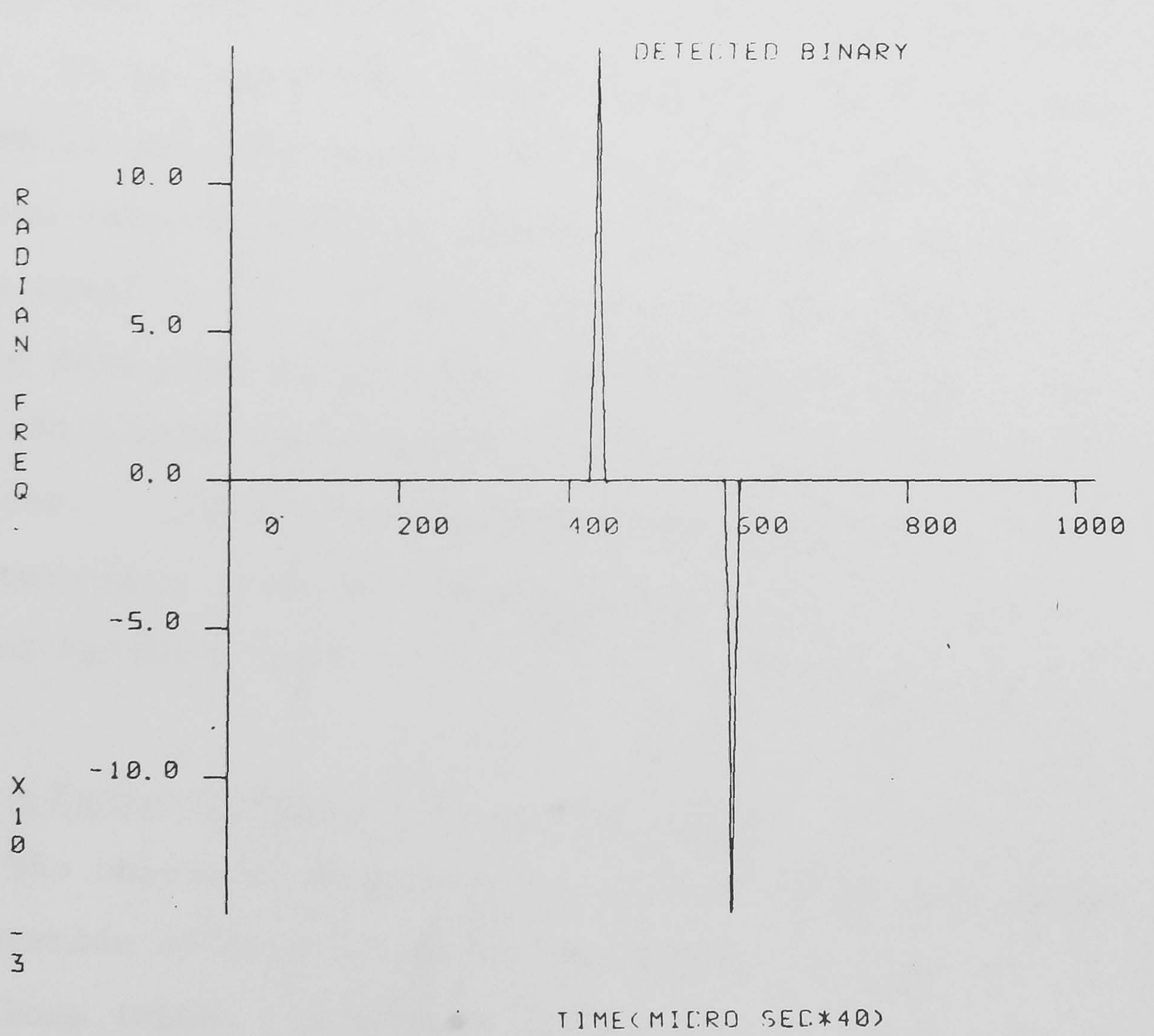

Fig. 5.44 Detected data signal for the same conditions.

concluded that the detected signals of ZSFM are not impaired by the FM function truncation.

Experiment 16

In this experiment, the out-of-band components power relative to the average ZSFM signal power is calculated. This gives a better estimate of the significance of out-of-band components due to the truncation effect.

Figure 5.45 shows the result of 50% modulation depth and $(\frac{P}{\sigma_r})$ ratios of 3 and 25. It is apparent that even for the case of $\frac{P}{\sigma_r} = 3$ the highest out-of-band component is about 25 dB below the signal average power, knowing that zero frequency corresponds to the band edge $(\frac{\Omega}{2\pi})$. It is, therefore, thought that the bandlimitation of ZSFM is not affected considerably due to truncation. The data rate of ZSFM will depend on the window width P and is equal to $\frac{1}{P}$. Hence if P is taken as equal to $3\sigma_r$ the data rate is $\frac{1}{3\sigma_r}$ and for the extreme case ($\sigma_r = 200$ μ sec) the data rate is approximately 1.667 k bit/sec. Using interlaced conjugating function generators will increase the data rate, but at the expense of hardware costs.

5.11 A Demonstration of Data Demodulation

The object of this section is to provide a practical demonstration of data detection in ZSFM using a phase-locked loop (PLL). A general ZSFM signal is expressed as:

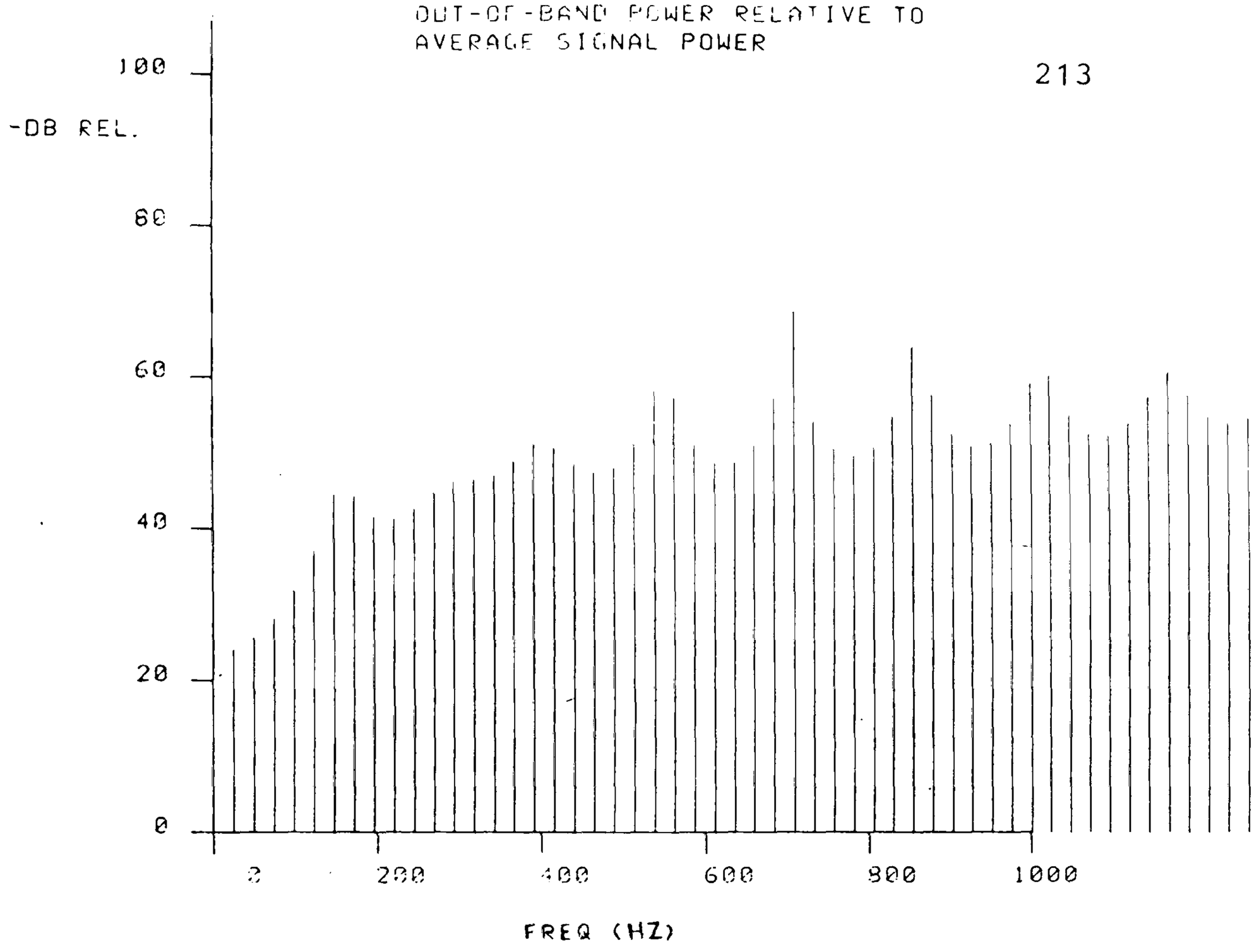

Fig. 5.45 Out-of-band power relative to average ZSFM signal power for $\frac{P}{\sigma_r} = 3.$

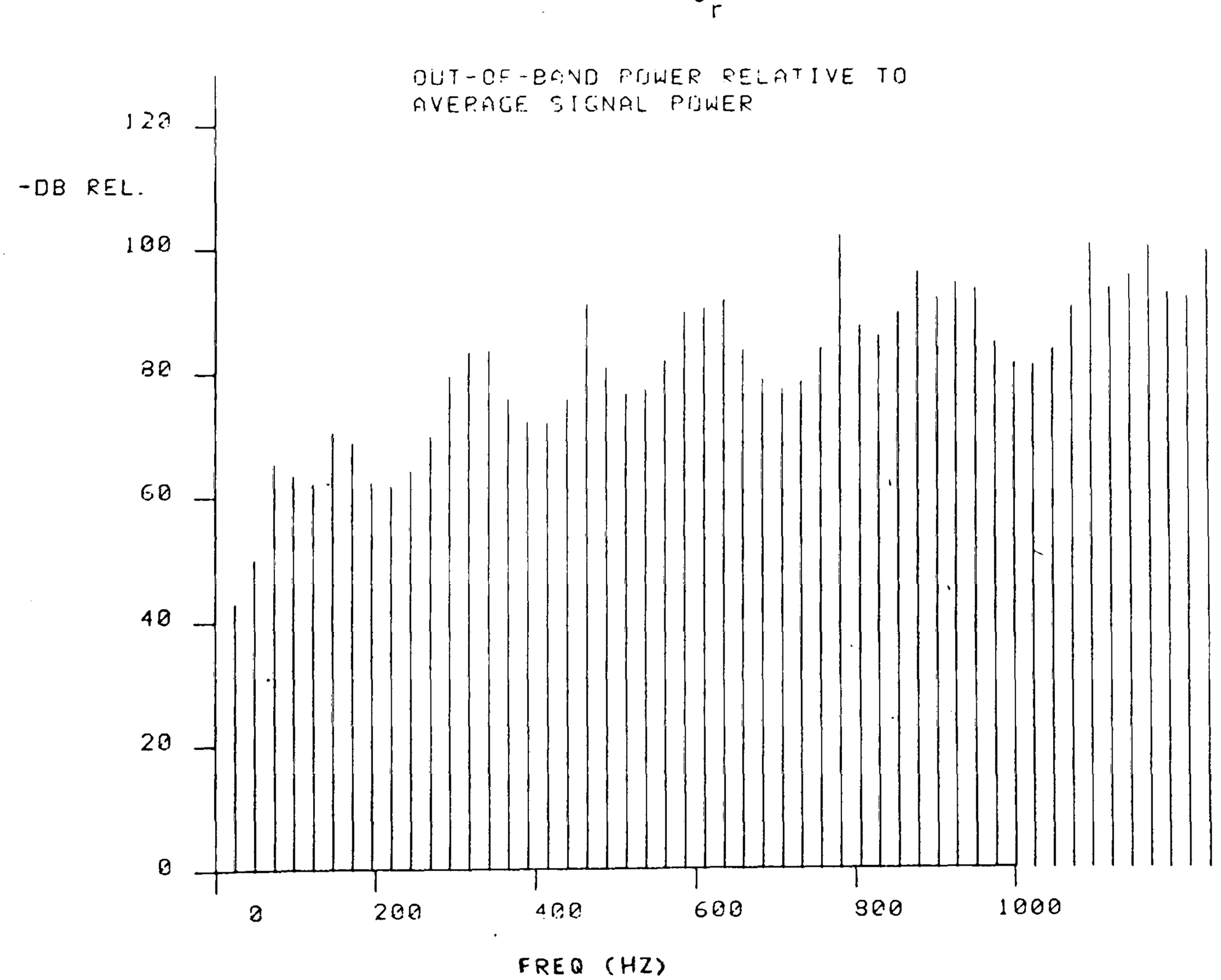

Fig. 5.45 Out-of-band power relative to average ZSFM signal power for $\frac{P}{\sigma_r} = 25$

$$x(t) = s(t) \cos(\omega_o t + \theta(t)) \qquad (5.33)$$

where ω_o is the carrier frequency and $\theta(t)$ is the phase information that conveys the binary data signal. A phase-locked loop should give an output voltage linearly related to the instantaneous frequency $\theta'(t)$ of ZSFM. A phase step produces a large frequency spike (click) when applied to a PLL, and it is this instantaneous frequency click that should be detected in ZSFM. The polarity of this instantaneous frequency click determines whether a "one" or a "zero" has been transmitted.

To investigate experimentally the response of a phase-locked loop to ZSFM signals, two sine waves of different frequencies were added. Consider the signal:

$$m(t) = 1 + a\, e^{j\Omega t}$$

$$= |m(t)|\, e^{j\theta_m(t)}$$

where $\theta_m(t) = \arctan\left(\frac{a \sin\Omega t}{1 + a \cos\Omega t}\right)$

then two added sine wave can be represented as:

$$\mathrm{Re}\left[(1 + a\, e^{j\Omega t})\, e^{j\omega_o t}\right] = \cos\omega_o t + a \cos(\omega_o + \Omega)t$$

where Re denotes real part.

The sum of these two sinusoids should, therefore, give $\theta'_m(t)$ when applied to a PLL. A simple circuit incorporating an adder and a PLL has been built for this purpose. Figure 5.46 shows the added signal and the output of the PLL for $a = 0.5$, $\Omega = 4\pi$ k rad/sec, and $\omega_o = 80\pi$ k rad/sec. It can be seen that the spikes corresponding to maximum values of $\theta'_m(t)$ occur at the

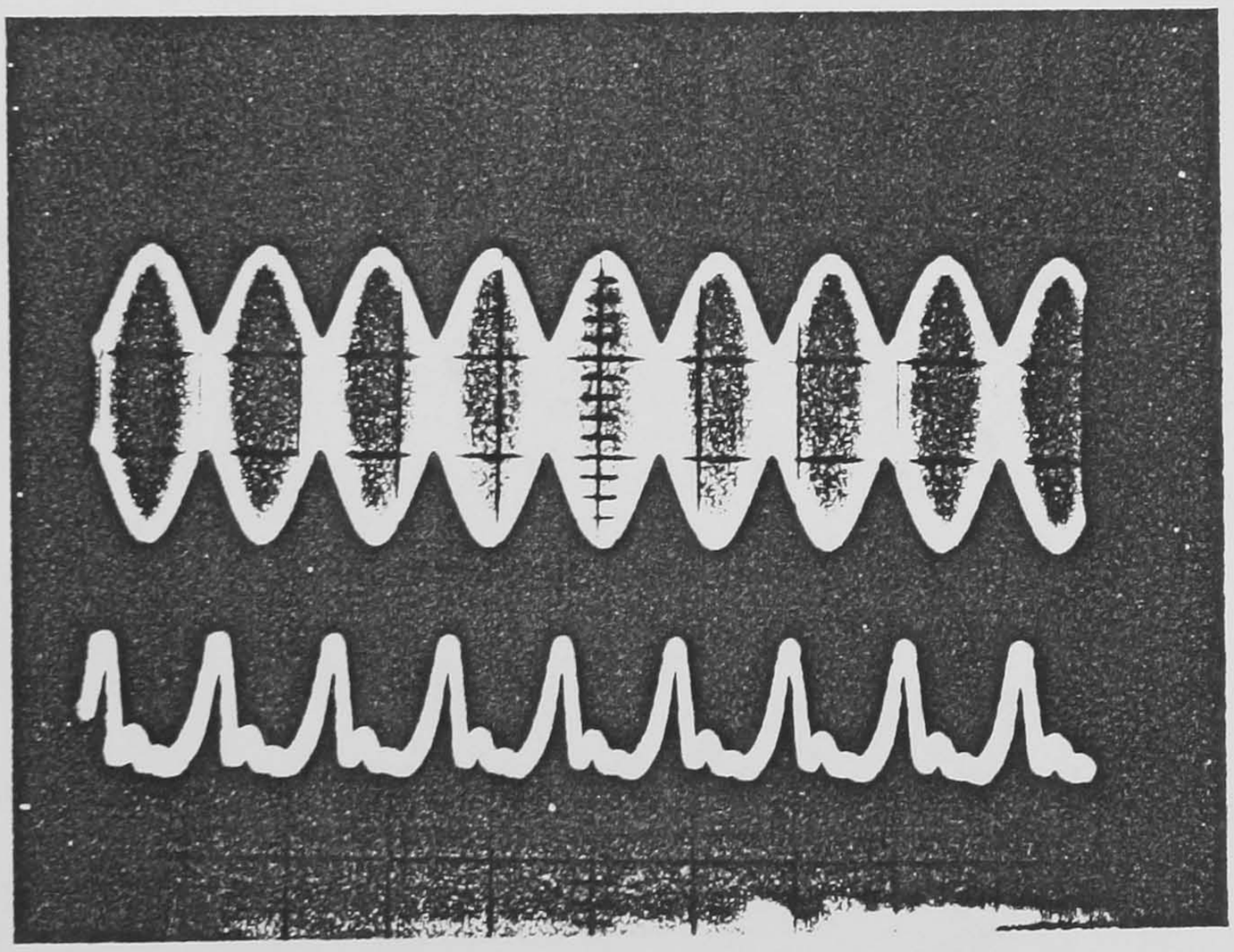

Data detection by a phase-locked loop for a = 0.5, $\Omega = 4\pi$ k rad/sec, and $\omega_o = 80\pi$ k rad/sec.

Fig. 5.46

envelope troughs of the signal. This demonstrates that the phase-locked loop can be used to detect the data signal of ZSFM. However, other frequency discriminators should also be suitable for this purpose.

5.12 Final Remarks

A number of different aspects of the performance of ZSFM has been studied under different circumstances. It was shown that ZSFM preserves the bandwidth and does not distort the envelope of DSB-AM signal, when super-imposing data. It has been verified by computer simulation that cross-talk between the two channels might be problematical only under conditions of severe multipath fading. However, the envelope distortion of conventional DSB-AM will also be significant under the same conditions.

Computer simulation of complex filtering has demonstrated the efficiency of a novel technique for detecting complex zeros of real signals.

The effect of truncating the FM function required for zero conjugation is expected to reduce the maximum theoretical data rate of ZSFM (5 k bits/sec for 10 k Hz channel). Data rates of 1.67* k bits/sec may be feasible, which compares favourably with BBC radio-data at 25 bits/sec (7).

* N.B. Assuming the out-of-band radiation levels of 20 dB are acceptable in practice.

CHAPTER 6

COMPLEX ZEROS OF POSITIVE BANDLIMITED SIGNALS

6.1 Introduction

The expression of bandlimited signals in terms of their real and complex zeros (Chapters 2 and 3) leads us to regard these zeros as informational bearing attributes.

This chapter presents theoretical and experimental studies of the distribution of the complex zeros of positive bandlimited signals. As complex zero conjugation is the basis of data superposition in ZSFM, a knowledge of the zero distribution is required for a determination of realistic data rates. The complex zero distribution of entire signals is discussed revealing the zero distribution characteristic of any bandlimited signal. An experimental study is carried out to estimate the probability - density function (p.d.f.) of the complex zero distribution of a positive bandlimited random signal with Gaussian distribution. The achievable bit-rate of ZSFM is then discussed, as it partly depends on the number of complex zeros available in a given range of σ_r.

6.2 Entire Functions

A description of the complex zero distribution of entire functions, that are generalisation of bandlimited

signals , is presented in this section.

Any bandlimited signal is an entire function (EF), as it is analytic in the finite x-plane (see Section 2.3). Entire functions should be continuous and differentiable any number of times in the finite x-plane (11). An entire function is a generalisation of polynomials of infinite degree, and hence usually an EF has an infinite number of aperiodic zeros in the complex x-plane ($x = t + j\sigma$). The Taylor series of an EF is (18):

$$f(x) = \sum_{n=o}^{\infty} a_n x^n \qquad (6.1)$$

which converges for all finite x.

As a polynomial of degree n admits a product expansion in terms of its n roots, an EF can also be expressed in terms of its zeros. If the above EF is expressed as a product expansion of the x-plane zeros as $\pi(1 - \frac{x}{x_n})$, then the infinite product may not converge. An entire function of finite order δ can be expanded as (18):

$$f(x) = x^m e^{Q(x)} \prod_{n=1}^{\alpha} (1 - \frac{x}{x_n}) e^{\left(x/x_n + \frac{(x/x_n)^2}{2} + \ldots + \frac{(x/x_n)^P}{P}\right)}$$

$$\alpha \leq \infty \qquad (6.2)$$

where x_n are the non-zero roots of f(x), $P \leq \rho$, Q(x) is a polynomial of degree $q < \rho$, and m is the number of zeros at the origin. If the complex x-plane can be divided into three sections as shown in Figure 6.1,

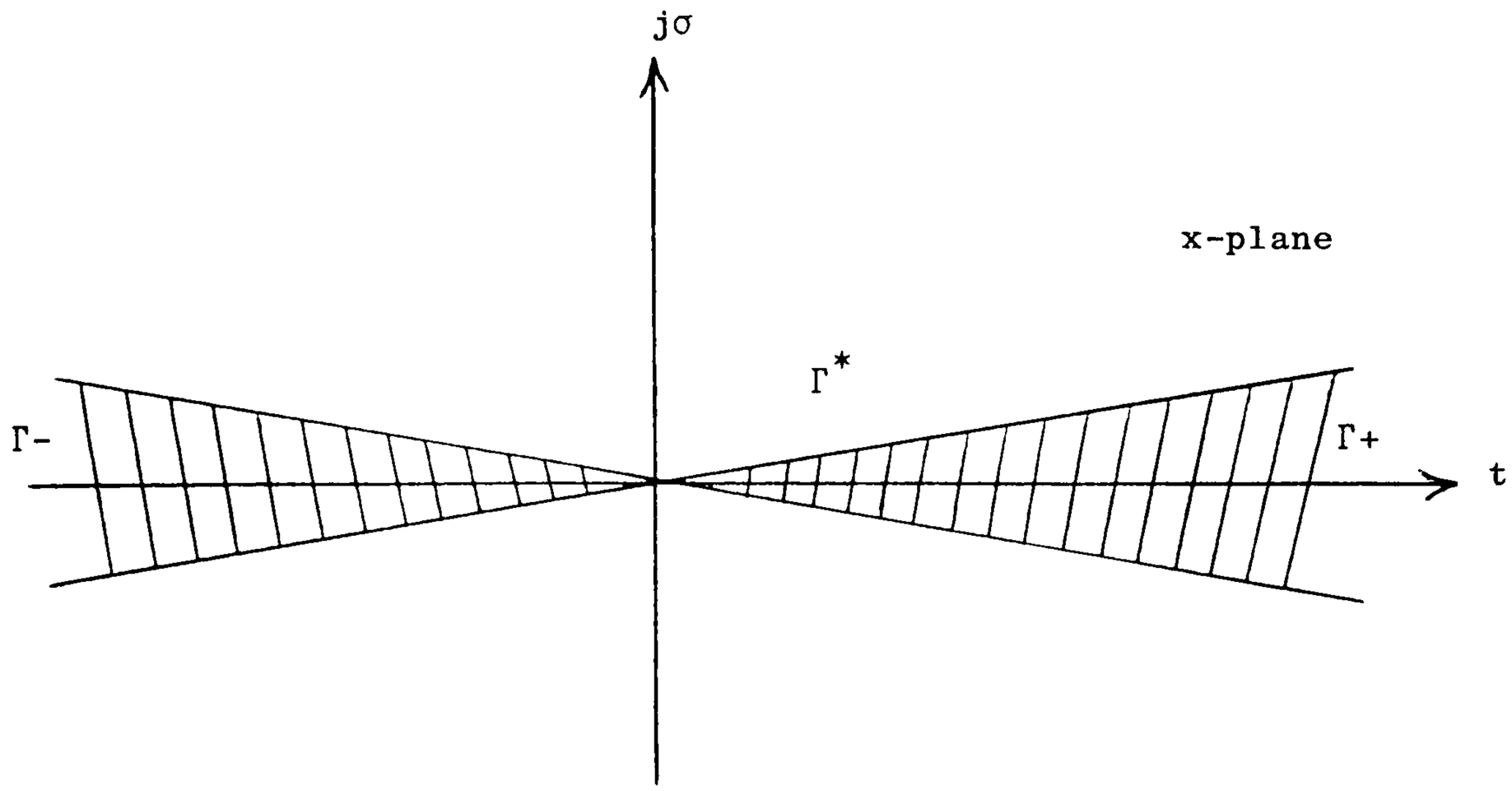

Fig. 6.1

and also if it can be assumed that the number of zeros with modulii less than r which lie in Γ^*, Γ^+, and Γ^- are $n^*(r)$, $n^+(r)$, and $n^-(r)$ respectively, then an EF has zeros close to the real axis if its zeros satisfy:

$$\sum_{n=1}^{\infty} \left| \mathrm{Im} \left(\frac{1}{x_n}\right) \right| < \infty$$

$$\text{or} \quad \lim_{r\to\infty} \frac{n^*(r)}{r} = 0 \tag{6.3}$$

where Im denotes imaginary part.

The above implies that there are not too many zeros in the region Γ^*, i.e. with high σ values.

Define the density of zeros in the three sections as:

$$\Delta^+ = \lim_{r\to\infty} \frac{n^+(r)}{r}, \quad \Delta^- = \lim_{r\to\infty} \frac{n^-(r)}{r}, \quad \Delta^* = \lim_{r\to\infty} \frac{n^*(r)}{r}$$

An EF satisfying eqn. (6.3) and having $\Delta^+ = \Delta^-$, $\Delta^* = 0$ is called a B-function. The complex zeros of a B-function are close to the real axis, i.e. they have small σ_r values.

Any bandlimited signal in the usual sense is a B-function, and trigonometric polynomials are a class of periodic B-function. For trigonometric polynomial the bandwidth is proportional to the number of zeros per period (zero count), while for B-function the bandwidth is proportional to the zero density as defined above.

The zero distribution characteristic of a B-function simplifies the task of detecting complex zeros in ZSFM, as it implies that the majority of complex zeros are distributed within a finite range of σ_r values. This zero distribution is estimated experimentally by computer simulation in the following section.

6.3 Factorisation of Fourier Coefficients

It is explained in this section how the Fourier coefficient can be used to find the complex zeros of a real, positive, bandlimited random signal, in the computer simulation. This approach is used in a following section to determine zero distribution.

The signal used in the computer simulation is a pseudo-random positive real signal with Gaussian distribution. This random signal is bandlimited to $\pm f_c$ Hz by an ideal filter in the frequency domain. The discrete Fourier transform (DFT) and the inverse DFT can be expressed (22) as:

$$X(n) = \frac{1}{N} \sum_{k=0}^{N-1} x(k)\ e^{-j2\pi n\frac{k}{N}}$$

$$x(k) = \sum_{k=0}^{N-1} X(n)\ e^{j2\pi n\frac{k}{N}} \qquad (6.4)$$

where N is the number of samples.

Now if x(t) represents a bandlimited ($\pm f_c = \pm$ 3 k Hz) random real signal, and if the number of samples is N = 1024, then a sampling interval of TD = 10 μ sec would imply that the time duration of the signal is:

$$(N-1)\ TD = 1023 \times 10 \times 10^{-6} = 0.01023 \text{ sec} = 10230\ \mu \text{ sec.}$$

The sampling frequency is $FMAX = \frac{1}{2TD} = 50$ kHz, while the frequency increment between any two successive frequency samples is:

$$FINC = 2\ FMAX/N = 97.66 \text{ Hz}$$

Taking the FFT of x(t) gives its frequency samples X(n), which are the Fourier coefficients of the signal x(t). These, generally complex, Fourier coefficients are used to find the complex zeros of x(t) by utilising a NAG Library subroutine(14) that calculates roots of a polynomial with complex coefficients. As a result of bandlimitation, it is not required to use N = 1024 frequency samples of X(n). For $\pm f_c = \pm$ 3 k Hz bandlimitation, it is necessary to consider only:

$$2\ (\frac{f_c}{FMAX})\ (\frac{N}{2}) = 2\ (\frac{3}{50}\ \frac{1024}{2}) = 61 \text{ frequency samples}$$

This implies that the number of zeros is equal to 60.

It can be deduced that the dimensionality of the signal is also equal to the number of zeros as:

$$\text{dimensionality} = 2 \times \text{time duration} \times \text{bandwidth}$$

$$= 2 \times 10230 \times 10^{-6} \times 3000$$

$$= 60 = \text{number of zeros}$$

The Fourier coefficients X(n) are ordered in the form:

$$X(1)+X(2)z+X(3)z^{2} + \ldots + X(31)z^{30} + X(995)z^{-30} + \ldots + X(1023)z^{-2} + X(1024)z^{-1}$$

where $z = e^{j2\pi\ \mathrm{FINC}\ t}$

After locating the zeros in z as defined above, then the corresponding zeros in complex time are required. For (M+1) Fourier coefficients there are M zeros in z. If z_m is the generally complex zero given by:

$$z_m = |z_m|\ e^{j\ \arg\ z_m}$$

then the corresponding time domain zero is obtained by equating $e^{j2\pi\ \mathrm{FINC}\ t}$ to z_m and solving for t, i.e.

$$e^{j2\pi\ \mathrm{FINC}\ t} = |z_m|\ e^{j\ \arg\ z_m} \qquad (6.5)$$

Taking natural logarithm of the above yields:

$$j2\pi\ \mathrm{FINC}\ t = \ln\ |z_m| + j\ \arg\ z_m$$

$$\therefore\ t = \frac{\arg\ z_m}{2\pi\ \mathrm{FINC}} - j\ \frac{\ln\ |z_m|}{2\pi\ \mathrm{FINC}} \qquad (6.6)$$

where FINC = 97.66 Hz = frequency resolution.

Therefore ordinate values of complex zeros are given by:

$$\sigma_r = -\ \frac{\ln\ |z_m|}{2\pi\ \mathrm{FINC}}$$

The above method was used in the simulation to determine the complex zeros of a positive real bandlimited signal.

Example

Consider the output of the FFT whose frequency samples are given by the array X(1024). Assuming for 3 kHz bandwidth there are 30 non-zero samples for positive frequency, and 30 non-zero samples for negative frequency as shown in Figure 6.2.

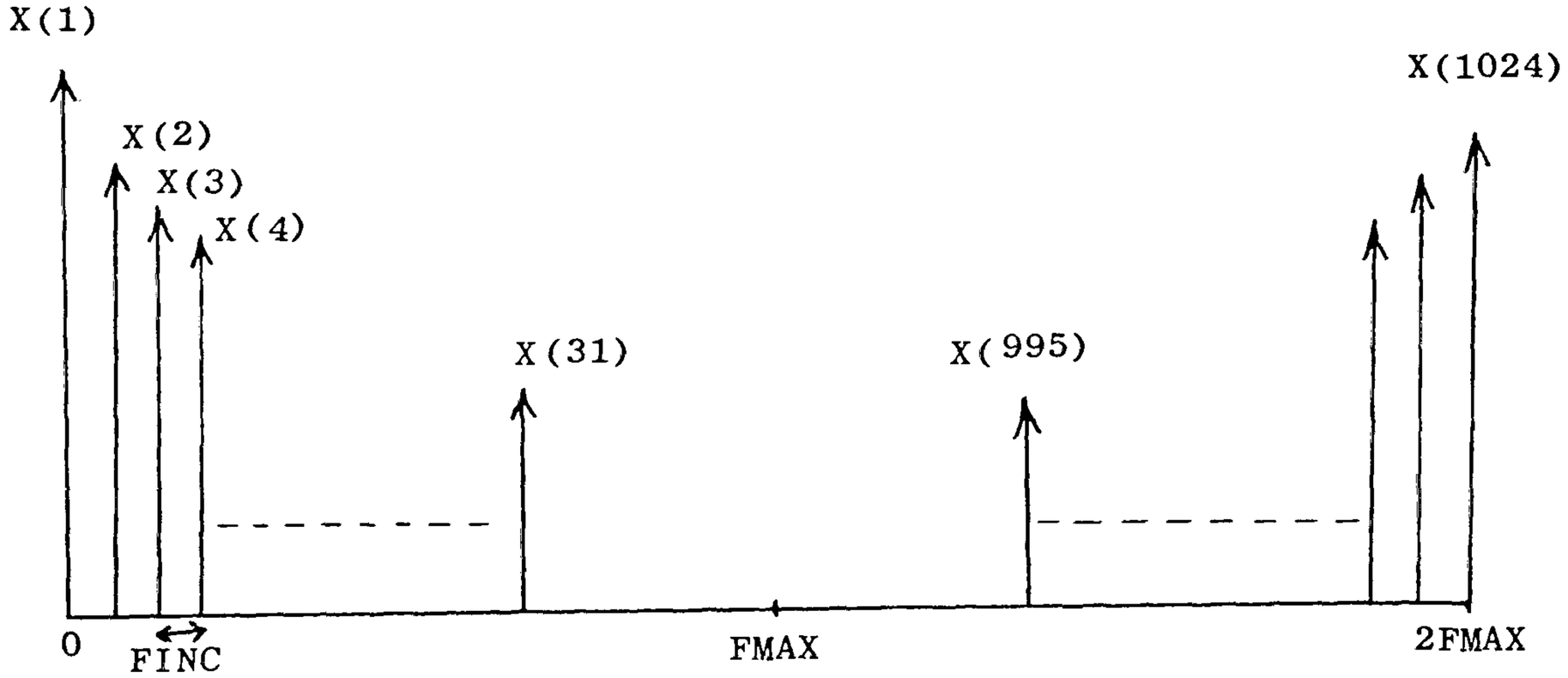

Frequency samples of X(n)

Fig. 6.2

The polynomial in z can be written as:

$$P(z) = X(1) + X(2)z + \ldots + X(31)z^{30} + X(995)z^{-30} + \ldots X(1024)z^{-1}$$

where $z = e^{j2\pi \text{ FINC } t}$

Rewriting P(z) as:

$$P(z)=X(31)z^{30}+\ldots+X(2)z+X(1)+X(1024)z^{-1}+\ldots+X(995)z^{-30}$$
$$= z^{-30}[X(31)z^{60}+\ldots+X(2)z^{31}+X(1)z^{30}+X(1024)z^{29}+\ldots+X(995)]$$

(6.8)

The above represents a polynomial in z of degree M = 60, and with 61 coefficients. Solving for the roots gives 60 zeros in z, and the corresponding time domain zeros are obtained via eqn. (6.6). Figure 6.3 shows the bandlimited version of a real positive pseudo-random signal with mean-value of 5 and standard deviation of 8. It is bandlimited to ± 3 kHz and hence as discussed above is expected to have 60 complex zeros, which lie in complex conjugate pairs as the signal is positive and real. Figure 6.4 shows the complex zeros of the bandlimited positive, real signal. It can be seen by comparing Figures 6.3 and 6.4 that most of the complex zeros occur in the vicinity of signal troughs. It is also clear that very few complex zeros have high σ_r values, and thus they are consistent with the B-function zero distribution characteristic explained in Section 6.2

6.4 Distribution of Complex Zeros

The theoretical background, necessary for determining the probability-density function (p.d.f.) of the complex zero distribution of a positive real random signal, is presented in this section. In order to determine the p.d.f. of a random variable by an empirical method, consider a waveform x(t) available over a very large time interval as shown in Figure 6.5.

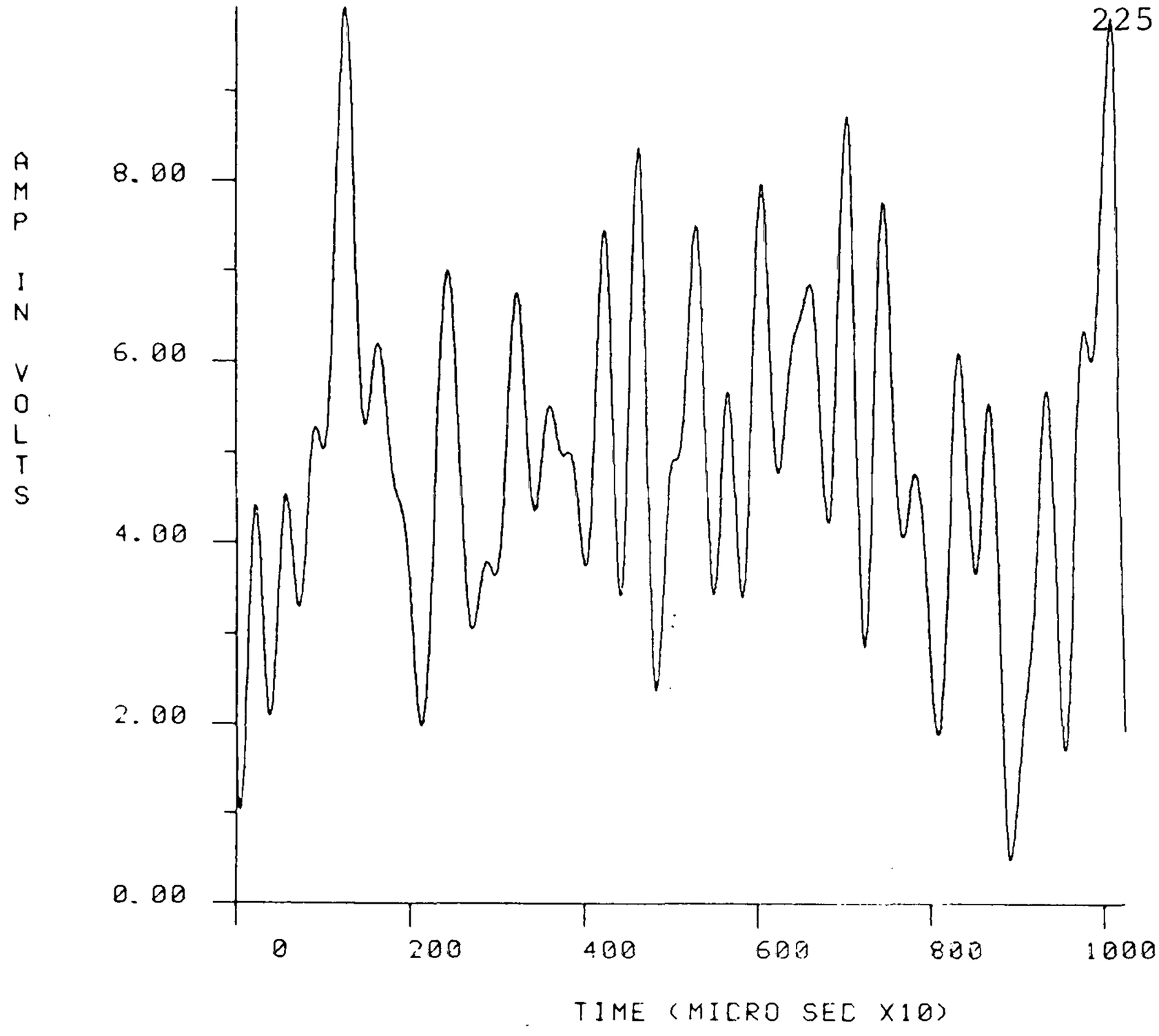

Fig. 6.3 Bandlimited positive real random signal.

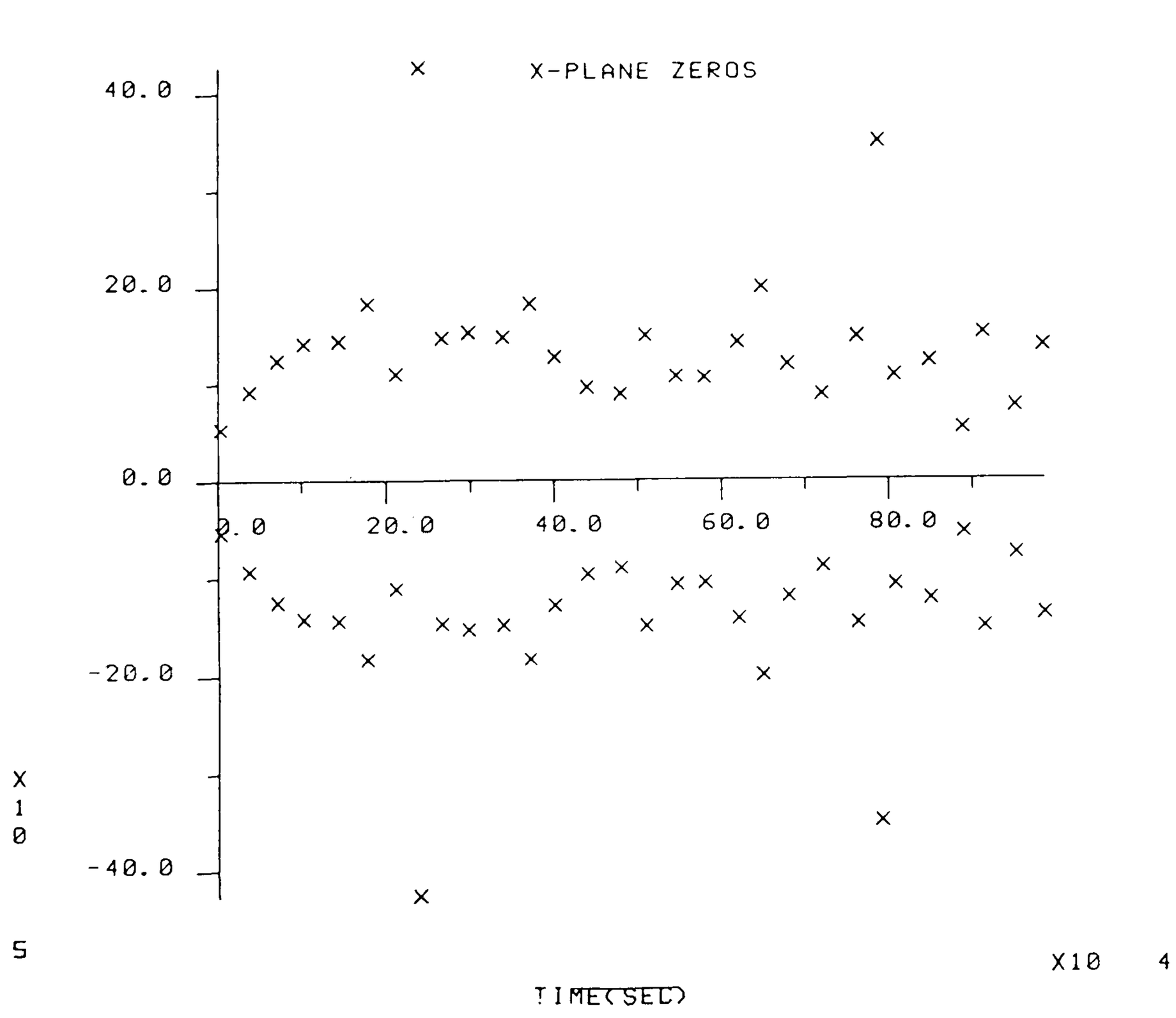

Fig. 6.4 Complex zeros of the random signal.

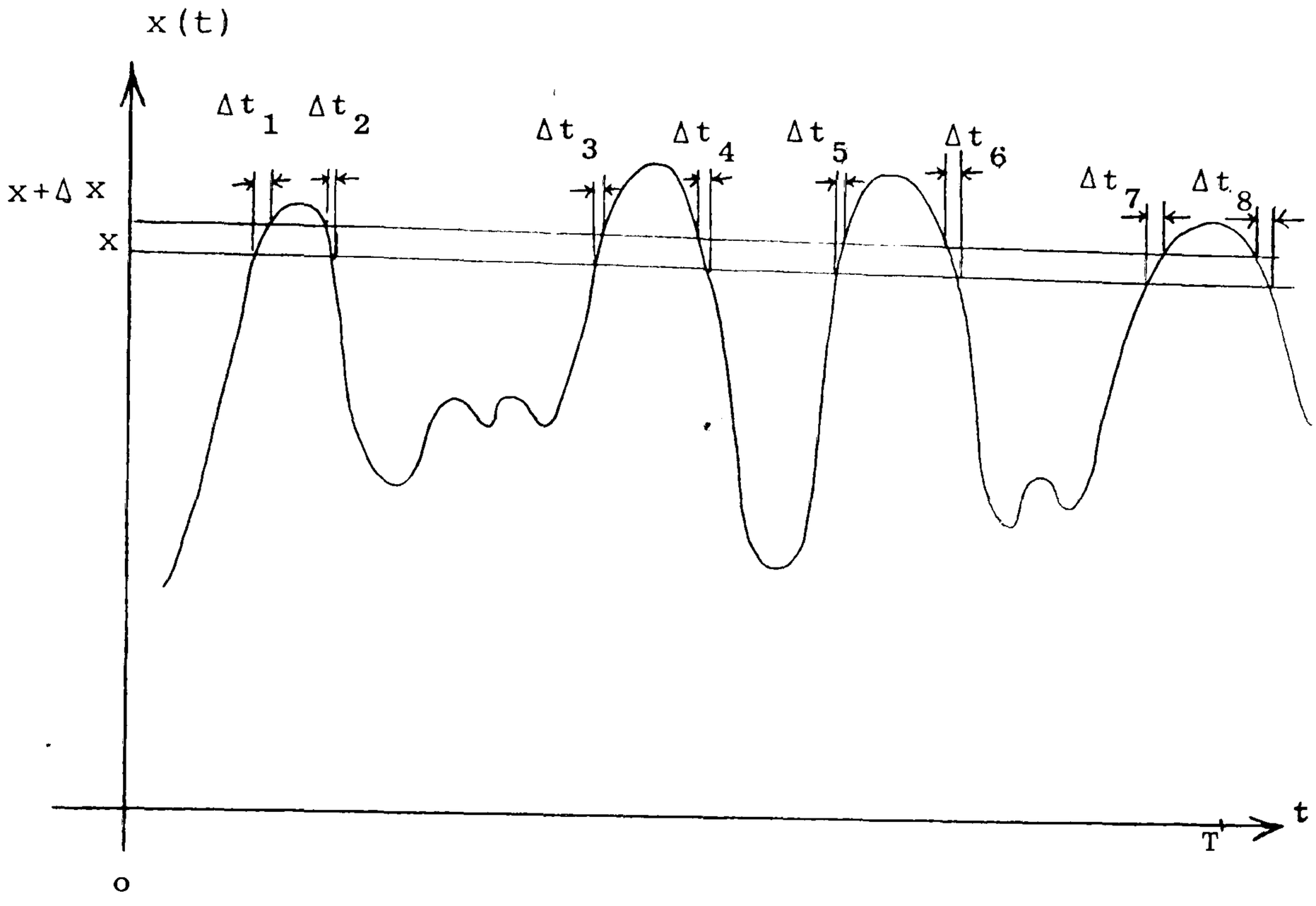

Fig. 6.5

The amplitude of x(t) varies randomly, i.e. it can be considered as a random variable x. The p.d.f., p(x), based upon the relative-frequency interpretation of probability (34) is required.

$$\lim_{\Delta x \to 0} p(x)\ \Delta x = \text{probability}\ (x < x(t) \leq x + \Delta x)$$

According to the relative-frequency interpretation, the probability that x(t) assumes a value between x and $x + \Delta x$ is the ratio $\frac{T_x}{T}$, where T_x is the total amount of time that x(t) falls inside the range $(x, x + \Delta x)$ during the observation time T $(T \to \infty)$. Thus:

$$\lim_{\Delta x \to 0} p(x) = \lim_{T \to \infty} \frac{T_x}{T} \tag{6.9}$$

$$\therefore\ p(x) = \lim_{\substack{T \to \infty \\ \Delta x \to 0}} \frac{T_x}{T\ \Delta x} = \lim_{\substack{T \to \infty \\ \Delta x \to 0}} \frac{\Sigma \Delta t_1}{T\ \Delta x} \tag{6.10}$$

Similarly in order to determine the p.d.f. of the complex zero distribution of a positive, real random signal by an empirical method, the same procedure can be followed. Consider the zero pattern shown in Figure 6.6.

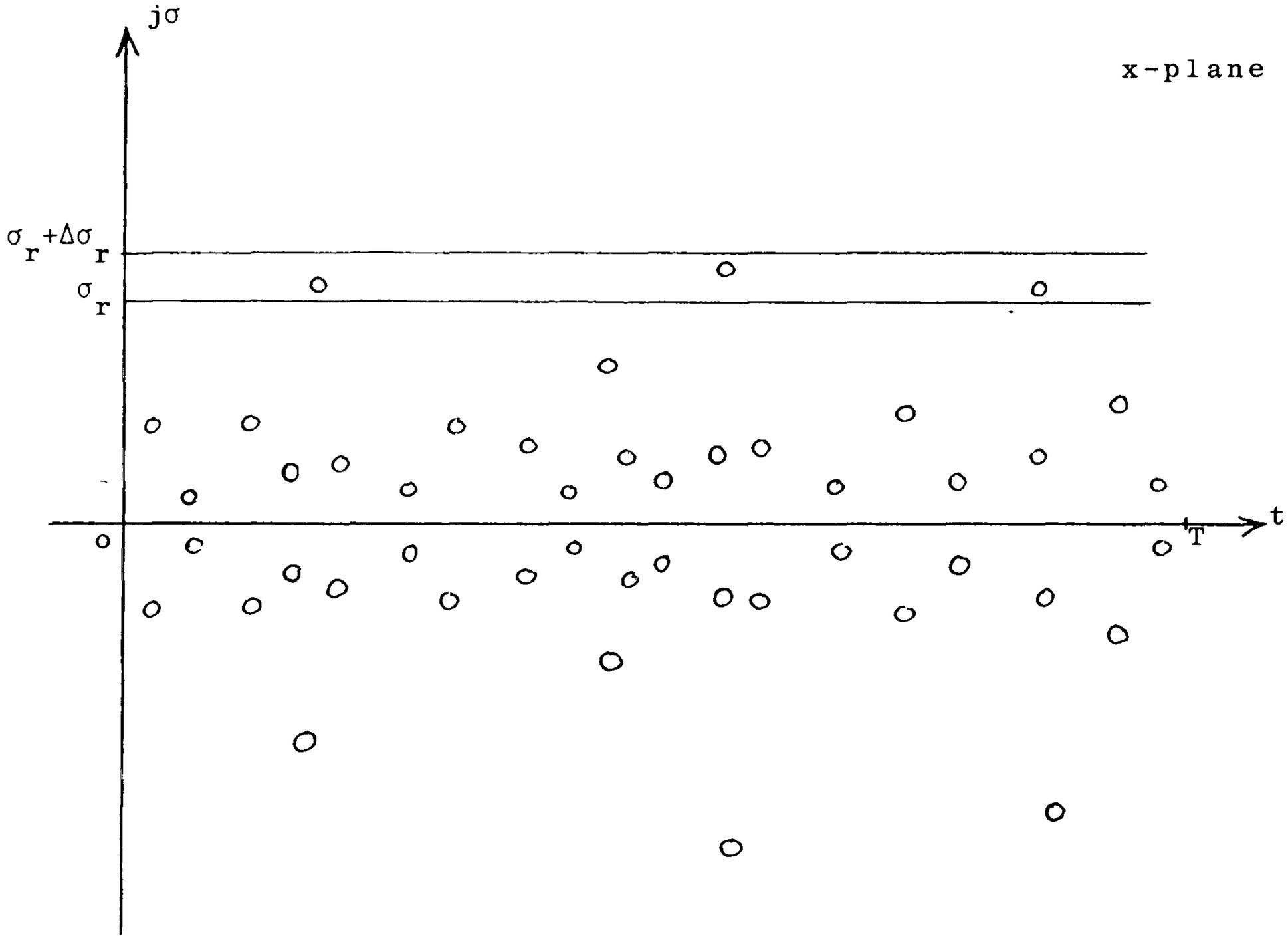

Fig. 6.6.

The ordinate value σ of a complex zero takes different values randomly, i.e. σ is a random variable. The probability-density function, p(σ), can be found by using the relative-frequency interpretation of probability, i.e.

$$\lim_{\Delta\sigma_r \to 0} \; p(\sigma_r)\, \Delta\sigma_r = \text{probability}\ (\sigma_r < \sigma \leq \sigma_r + \Delta\sigma_r)$$

i.e. the probability that at any given instant of time t, the ordinate value of a complex zero falls in the range $(\sigma_r\ ,\ \sigma_r + \Delta\sigma_r)$.

According to relative-frequency interpretation, the probability that σ assumes a value between σ_r and $\sigma_r+\Delta\sigma_r$ is the ratio $(\frac{v}{n})$, where n is the total number of complex zeros having positive ordinate values during the observation time T $(T \to \infty)$, and v is the number of complex zeros with σ values in the range $(\sigma_r , \sigma_r + \Delta\sigma_r)$.

Therefore we have:

$$\lim_{\Delta\sigma_r \to 0} p(\sigma_r)\ \Delta\sigma_r = \lim_{n\to\infty} \frac{v}{n}$$

$$\therefore\ p(\sigma_r) = \lim_{\substack{n\to\infty \\ \Delta\sigma_r \to 0}} \frac{v}{n\ \Delta\sigma_r} \qquad (6.11)$$

It is clear that $\lim_{n\to\infty}$ implies $\lim_{T\to\infty}$

In practice n will be taken as a finite number, and also $\Delta\sigma_r$ will be taken as a positive small number different from zero. Thus an approximate p.d.f. should be expected.

$$p(\sigma_r) \simeq \frac{v}{n\ \Delta\sigma_r} \qquad (6.12)$$

The empirical method, outlined in this section, is used in the following section to estimate the p.d.f. of the complex zero distribution of a positive, real, bandlimited random signal.

6.5 An Experimental Study of Complex-Zero Probability Distribution

This section summarises the experimental procedure followed in obtaining the probability-density function

(p.d.f.) of the complex zero distribution of a positive, real, bandlimited random signal. The study is confined to the experimental estimation of the p.d.f. of complex zero distribution using the empirical method explained in Section 6.4.

For positive real signals the zeros occur as complex conjugate pairs. Because of the symmetry of the complex zero distribution around the real time axis ($\sigma = 0$), the p.d.f. of complex zero distribution is expected to have an even symmetry about $\sigma = 0$, i.e. .

$$p(\sigma) = p(-\sigma)$$

A positive, real, bandlimited random signal with Gaussian distribution is considered, whose complex zero's p.d.f. will be estimated experimentally. Different positive random signals having different modulation depths are considered. The range of σ_r values considered is $0 \rightarrow 500$ μ sec, which is sufficient to cover all the possible complex zeros expected. If $\Delta\sigma_r$ is chosen to be 5 μ sec, then the total σ_r range under consideration is divided into 100 narrow strips, each of $\Delta\sigma_r = 5$ μ sec width. To prevent repeated counting of complex zeros in two successive strips, the number of complex zeros falling in each strip will be considered such that:

$$(k - 1)\ \Delta\sigma_r \leq \sigma < k\ \Delta\sigma_r$$

where k is the strip number.

The random signal considered has 30 complex zero pairs on bandlimitation to ± 3 kHz (see Section 6.3).

Therefore if the computer programme is run 100 times (varying the modulation depth of the positive random signal) the total number of complex zeros having positive ordinate value is:

$$n = 30 \times 100 = 3000 \text{ complex zeros}$$

$$\therefore\ n\ \Delta\sigma_r = 3000 \times 5 \times 10^{-6} = 0.015$$

Using the empirical formula of the p.d.f. given by eqn. (6.12):

$$p(\sigma_r) \simeq \frac{v}{n\ \Delta\sigma_r}$$

$$\simeq \frac{v}{0.015} \qquad (6.13)$$

where v is the total number of complex zeros that lies within any strip of σ during the 100 different runs.

The approximate relation given in eqn. (6.13) becomes exact in the limit when an infinite number of complex zeros is considered in the measurement interval, and when $\Delta\sigma_r \to 0$.

Finally, the histogram of the complex-zero p.d.f. corresponding to the positive real random signal can be obtained.

Experiment 1

In this experiment the p.d.f. of the complex zero distribution is measured for a positive, real bandlimited (± 3 kHz) random signal with Gaussian distribution. The computer programme was run 100 times using a mean value of 6 while the standard deviation was varied between 0.7 and

10.5. This corresponds to varying the modulation depth of the random signal between 6% and 98%. The number of complex zeros corresponding to the 100 different strips of σ is given in Table 6.1.

σ strips	Number of complex zeros									
1-10	0	0	0	0	0	1	1	2	3	6
11-20	6	6	7	8	12	12	18	30	37	39
21-30	56	56	58	66	76	78	73	92	120	139
31-40	140	123	118	100	100	91	102	96	86	90
41-50	81	79	70	62	59	51	45	40	37	38
51-60	31	27	23	24	18	12	12	10	8	7
61-70	6	5	3	1	2	0	1	0	0	0
71-80	47	21	11	6	5	3	3	1	2	1
81-90	0	0	0	0	0	58	24	9	5	2
91-100	2	0	0	0	0	0	0	0	0	0

TABLE 6.1

It is apparent that the total number of complex zeros is 3000, which is the total outcome of the process for 100 trials. Also, 88% of the complex zeros have σ_r value less or equal to 200 μ sec. The p.d.f. is calculated by the relation given in eqn. (6.13) and Figure 6.7 shows the p.d.f. histogram. The distribution is Gaussian in nature in the σ_r range (50 - 350) μ sec, while the two spike-shaped parts of the distribution are attributed to the estimation error given the very few complex zeros with high σ_r values. This is consistent with the zero distribution characteristic of a B-function discussed previously in Section 6.2.

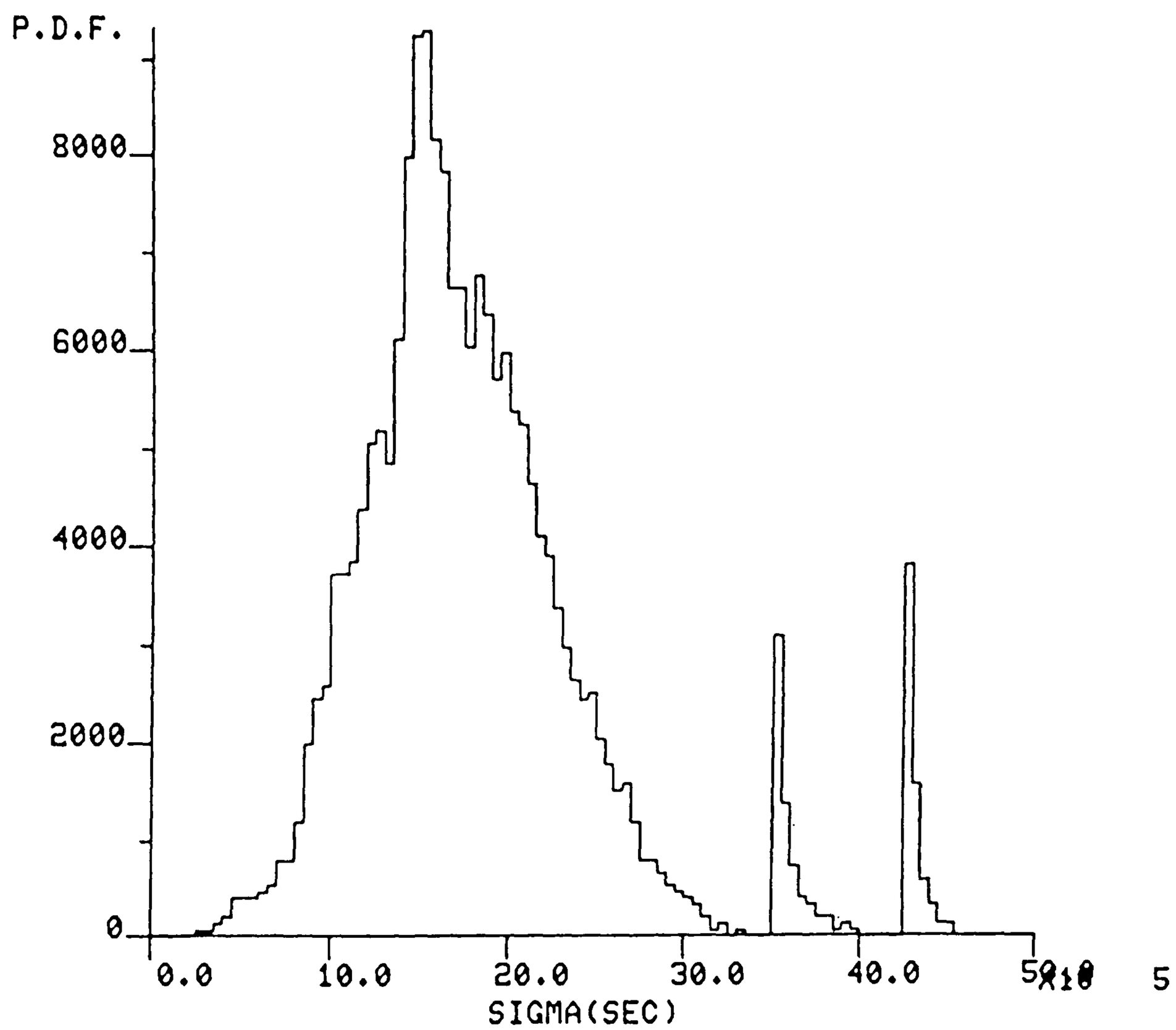

Fig. 6.7 p.d.f. histogram (Experiment 1).

Experiment 2

In this experiment, the same positive, real, band-limited (± 3 kHz) random is used similar to Experiment 1. The same procedure to find the p.d.f. is followed, but the modulation depth was varied between 29% and 80%. The mean value of the random signal was kept at 6, while its standard deviation was varied between 3.15 and 8.54. Table 6.2 below shows the number of complex zeros that correspond to the 100 different strips of σ.

σ strips	Number of complex zeros									
1-10	0	0	0	0	0	0	0	0	0	0
11-20	0	0	0	5	8	9	13	16	23	30
21-30	48	64	64	81	80	95	113	123	124	139
31-40	160	199	196	169	150	126	114	107	109	87
41-50	71	80	60	43	33	30	21	10	0	0
51-60	0	0	0	0	0	0	0	0	0	0
61-70	0	0	0	0	0	0	0	0	0	0
71-80	49	38	13	0	0	0	0	0	0	0
81-90	0	0	0	0	0	69	31	0	0	0
91-100	0	0	0	0	0	0	0	0	0	0

TABLE 6.2

It can be calculated from Table 6.2 that 82% of the complex zeros lie between σ_r values of 70 and 200 μ sec. Figure 6.8 shows the corresponding p.d.f. histogram, and it is apparent that the distribution is restrained to a narrower width of σ_r values than Figure 6.7 showed. This is attributed to the fact that modulation depths of very small or very high values are not considered in this

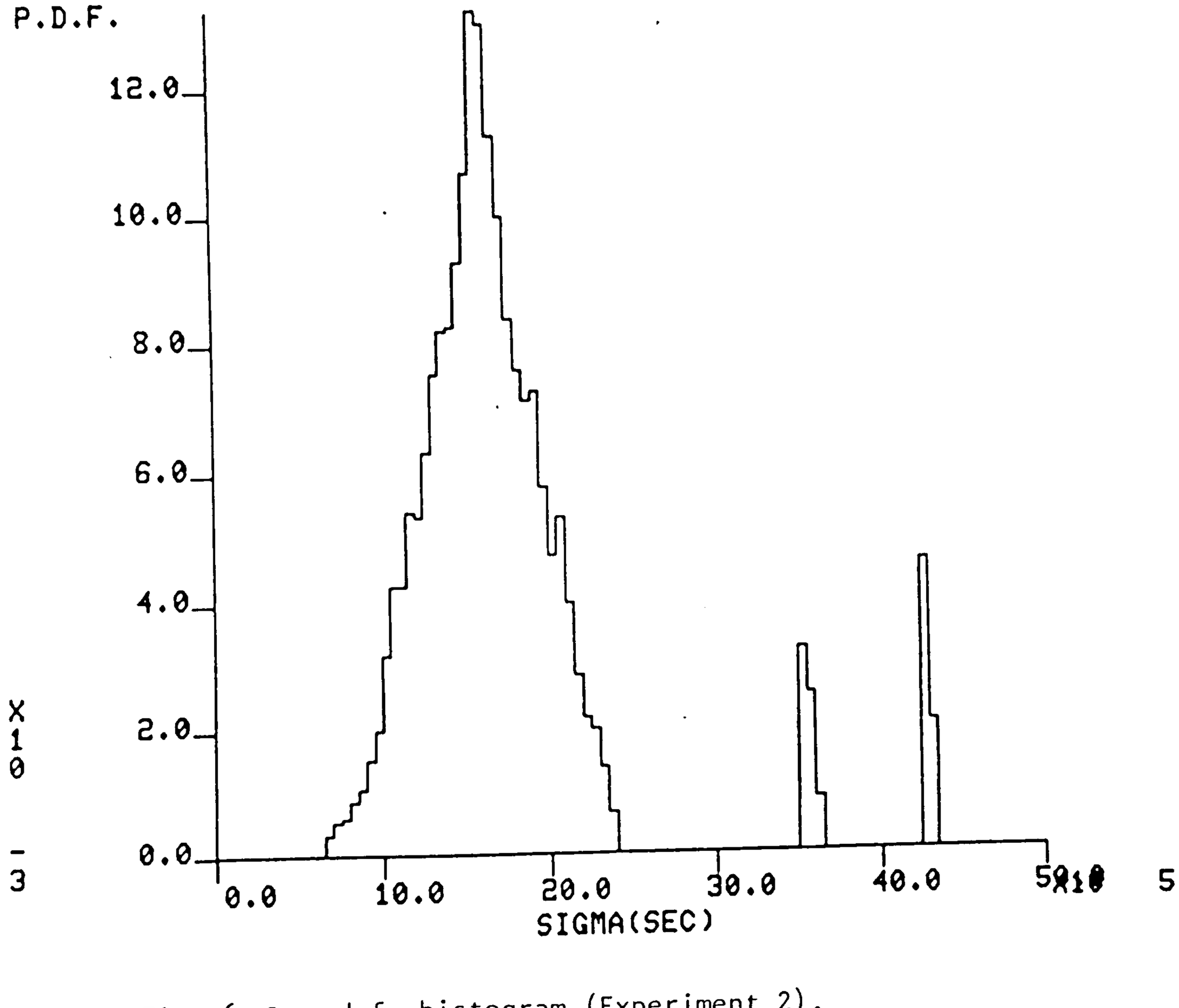

Fig. 6.8 p.d.f. histogram (Experiment 2).

experiment. This corresponds to excluding complex zeros of very small or very high σ_r values. The two spike-shaped parts of the distribution at high σ_r values are narrower than in the last experiment, implying less contribution to the distribution function. The main part of the p.d.f. has similarly a Gaussian shape.

Experiment 3

The same random signal is used, and the same procedure is followed in finding the p.d.f. as in the last two experiments. The computer programme was run 100 times, but both the mean value and standard deviation of the random signal were varied. Five different mean values of 5, 6, 7, 8, and 9 were used respectively for each 20 runs, while the standard deviation was varied such that for every 20 runs the modulation depth ranges approximately between 25% and 85%. Table 6.3 below gives the number of different complex zeros.

σ strips	Number of complex zeros									
1-10	0	0	0	0	0	0	0	0	0	0
11-20	0	2	3	10	5	10	14	14	26	33
21-30	51	53	66	72	87	91	104	109	117	143
31-40	169	189	169	167	141	131	118	118	105	84
41-50	84	84	61	46	39	33	27	14	4	4
51-60	3	0	0	0	0	0	0	0	0	0
61-70	0	0	0	0	0	0	0	0	0	0
71-80	47	36	15	2	0	0	0	0	0	0
81-90	0	0	0	0	0	66	33	1	0	0
91-100	0	0	0	0	0	0	0	0	0	0

TABLE 6.3

It can similarly be calculated from the above table that 80% of the complex zeros lie in the σ_r range of (70 - 200) μ sec. Figure 6.9 shows the corresponding p.d.f. histogram, which is similar to the p.d.f. obtained in Experiment 2.

The cumulative distribution function can be found by calculating areas under the p.d.f. curve. The p.d.f. shown in Figure 6.9 is numerically integrated and Figure 6.10 shows the cumulative distribution function, which is a non-decreasing function of σ.

The measurements made during this study showed that the complex-zero distribution's p.d.f. are similar in nature for the last three experiments. When the bandwidth of the positive random signal is changed from ± 3 kHz, the p.d.f. of complex-zero distribution shows a very similar nature and the majority of the complex zeros are again found to lie in the σ_r range (70 - 250) μ sec. This verifies the complex-zero distribution that characterises a B-function (Section 6.2).

The experimental study introduced in this section has revealed that more than 80% of the complex zeros are located in the σ_r range (70 - 200) μ sec. If only these complex zeros are to be considered for conjugation in ZSFM, then the bank of complex filters (Section 5.9) will have to cover this range of σ_r values. Given that the value $\Delta\sigma_r = \sigma_{r_2} - \sigma_{r_1}$ in the bank of complex filters may be taken as 2 μ sec (Section 5.9), then it is possible to cover the required range with $\frac{200 - 70}{2}$ = 65 filters.

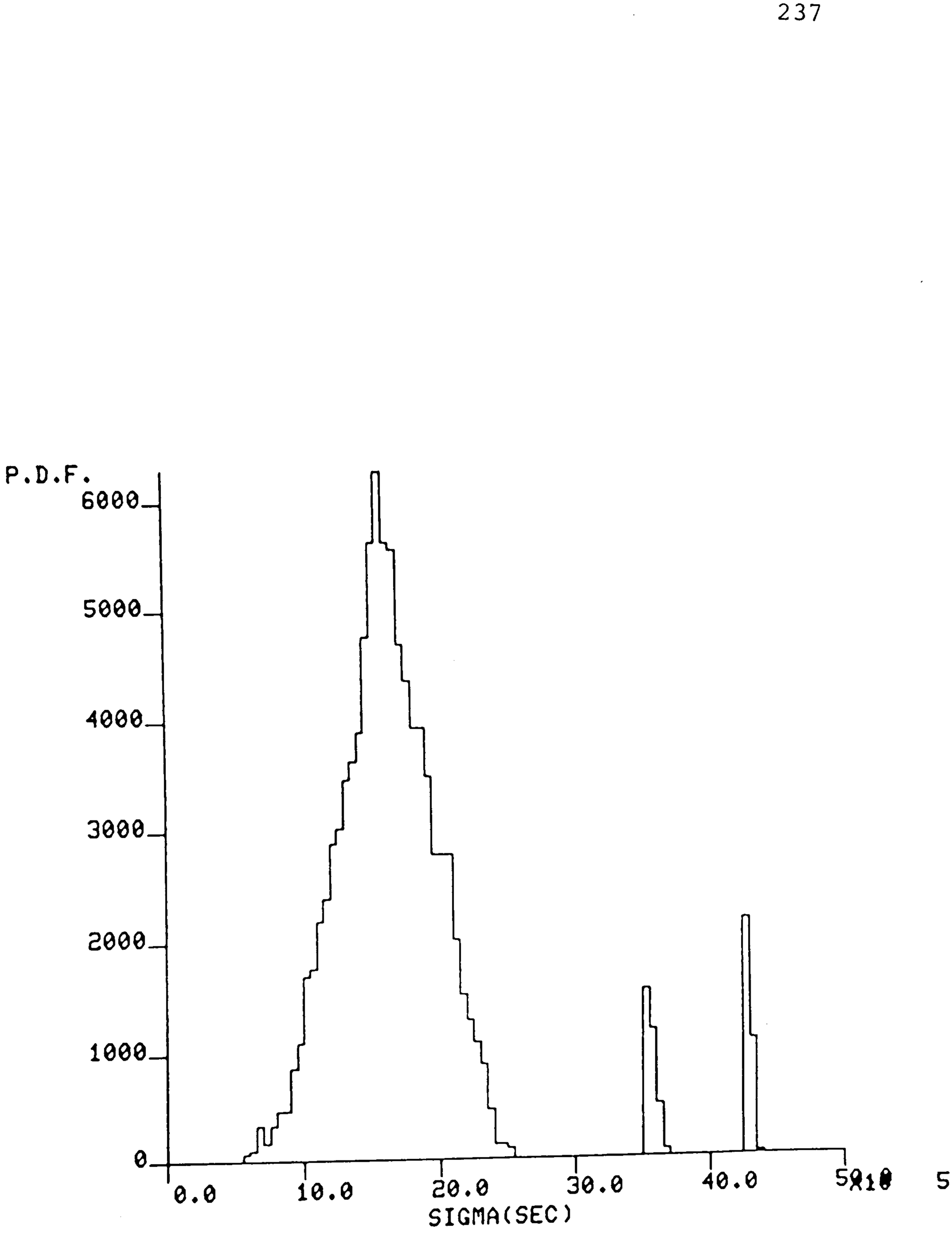

Fig. 6. 9 p.d.f. histogram (Experiment 3).

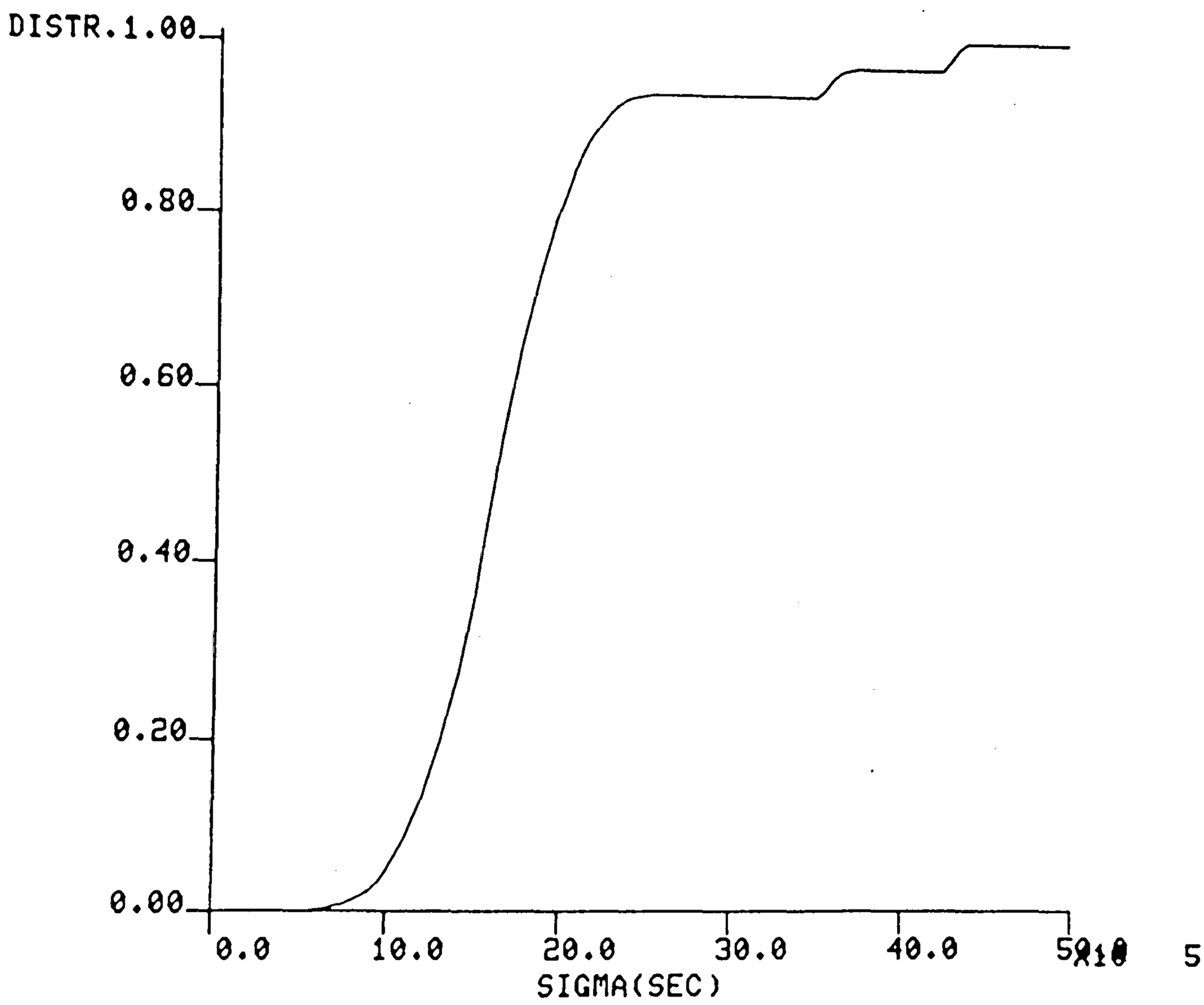

Fig. 6.10 Distribution function (Experiment 3).

6.6 Achievable Bit Rate

The maximum theoretical data rate of ZSFM was shown (Section 3.9) to be 5 kbit/sec for a 10 kHz broadcast channel. However, in practice, this rate is not expected to be reached for different reasons. The truncation effect of the FM function $\theta'(t)$ (Section 5.10), with one conjugating function generator, reduces the data rate to $\frac{1}{P}$ and if the window width P is made equal to $3\sigma_r$, then the data rate becomes $\frac{1}{3\sigma_r}$. The FM function, $\theta'(t)$, used in ZSFM is expressed as:

$$\theta'(t) = \pm \frac{2\ \sigma_r}{\sigma_r^2 + (t-t_r)^2}$$

and it diminishes to its half maximum value ($\pm \frac{2}{\sigma_r}$) at $(t-t_r) = \sigma_r$, i.e.

$$\theta'(t)\Big|_{t-t_r=\sigma_r} = \pm \frac{2\ \sigma_r}{\sigma_r^2 + \sigma_r^2}$$

$$= \pm \frac{1}{\sigma_r} \qquad (6.14)$$

Therefore the larger is σ_r, the longer time $\theta'(t)$ takes to attain half the maximum value, and in general the truncated FM function will require a longer P window for large σ_r than for small σ_r to give the same performance. Figure 6.11 shows the FM function $\theta'(t)$ for small σ_r and large σ_r values.

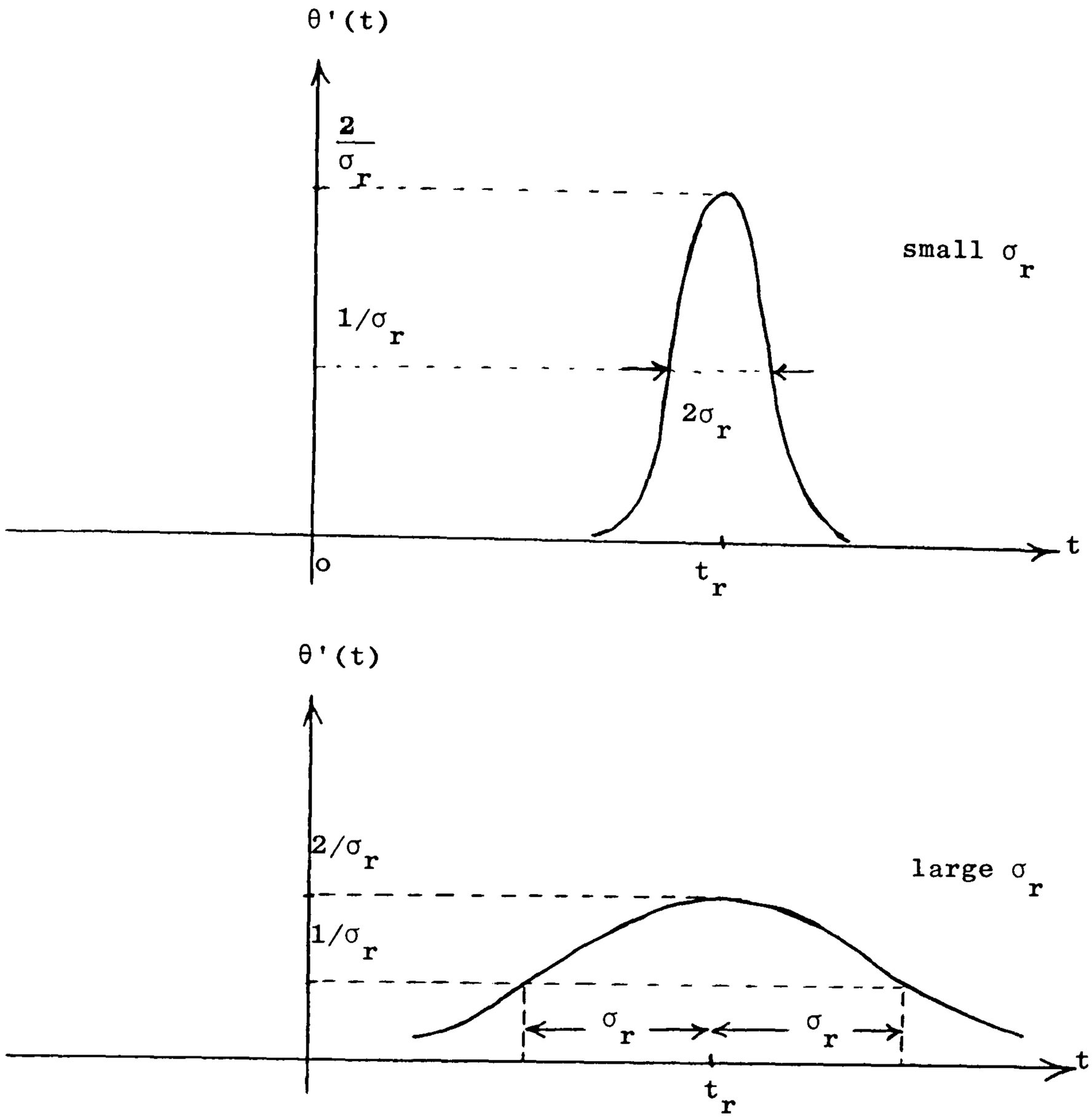

FM function

Fig. 6.11

The other factor affecting the practical data rate of ZSFM is the value of σ_r used in complex zero conjugation. It was previously discussed (Section 3.9) that complex zeros having very large σ_r values are unsuitable for conjugation as the frequency deviation $\theta'(t)$ becomes insufficient for detection. Also for complex zeros with high σ_r, the window width P through which the FM function $\theta'(t)$ is imposed on the carrier needs to be very long. However, it was found experimentally in Section 6.5 that most of the complex zeros of a positive bandlimited signal are distributed in a finite range of σ_r. More than 80% of

the available complex zeros were found to have σ_r values ranging between 70 μ sec and 200 μ sec. Hence the value of σ_r = 200 μ sec can be taken as an upper bound for usable σ_r values, and yet more than 80% of the available complex zeros are covered. If only one conjugating function generator is used, then the data rate $(\frac{1}{3\sigma_r})$ is equal to 1.67 kbit/sec for an upper bound of σ_r = 200 μ sec. However, if two conjugating function generators can be interlaced, the data rate of ZSFM will double to 3.34 kbit/sec at the expense of additional hardware.

Confining the usable σ_r values to the range (70 - 200) μ sec will mitigate the task of complex zero filtering (Chapter 4), and consequently the number of complex filters in the bank is reduced.

The maximum and minimum frequency deviations θ'(t) that correspond to minimum and maximum usable σ_r value respectively are:

$$\theta'(t)_{max} = \pm \frac{2}{\sigma_r} = \frac{2}{70 \times 10^{-6}} = \pm 28571.428 \text{ rad/sec}$$

$$= \pm 4.5 \text{ kHz}$$

$$\theta'(t)_{min} = \pm \frac{2}{\sigma_r} = \pm \frac{2}{200 \times 10^{-6}} = \pm 10000 \text{ rad/sec}$$

$$= \pm 1.5 \text{ kHz}$$

In practice, the above frequency deviations can easily be detected by a phase-locked loop. Determining the lower bound of the frequency deviation, $\theta'(t)_{min}$, helps to give a threshold value for noise clicks on detection. Every frequency spike at the output of a ZSFM frequency de-

modulator, having a value less than 10^4 rad/sec is regarded as a noise frequency click and therefore discarded. If a threshold value of 10^4 rad/sec is assigned, then noise clicks larger than this value will give an error.

6.7 Final Remarks

The complex-zero distribution of positive bandlimited signals has been studied theoretically and experimentally. Entire functions representing generally bandlimited signals were introduced with their characteristic zero distributions. Factorisation of Fourier coefficients of the random bandlimited signal was used to locate the zeros in the computer simulation. The results obtained verify the theoretical zero distribution characteristic of entire functions. The p.d.f. of the complex zeros of a positive bandlimited random signal has been estimated using a computer simulation. More than 80% of the available complex zeros were found to lie in the σ_r range (70 - 200) μ sec. Possible data rates for ZSFM were also discussed, and it was concluded that the bit rate is not expected to be less than 1.67 kbit/sec. The data rate can be increased but at the expense of cost. It should finally be noted that data rates of ZSFM compares favourably with that of BBC system for MW broadcast that handles 25 bit/sec (8).

CHAPTER 7

CONCLUSIONS

A new modulation technique has been considered and developed that may be applied to the provision of radio-data services for l.f. and m.f. sound broadcasting using DSB-AM. It has been shown that this technique, ZSFM, allows a DSB-AM carrier to be frequency or phase modulated without increasing the bandwidth of the transmitted signal or disturbing its envelope.

Radio-data systems for v.h.f./f.m. have been implemented and tested in several European countries and some progress has been made towards standardisation (16). Development of radio-data systems is, however, considerably less advanced for l.f. and m.f. broadcasting where AM predominates and the inherent redundancy of the DSB-AM signal is more difficult to exploit.

It has been shown that provided certain frequency modulating functions are impressed on a DSB-AM carrier in synchronism with the complex zeros of the amplitude modulating signal, then the transmitted signal will remain strictly bandlimited. It was shown that the principle of ZSFM derives from the concept of the "common envelope set" of signals, each of which possesses an identical envelope, occupies the same bandwidth but differs in phase modulation. The process of complex zero conjugation of a signal leads to the generation

of other signals of the same "common envelope set". The symmetrical zero pattern of a conventional DSB-AM signal has been studied, and it has been shown how a process of conjugating the complex zeros of a DSB-AM signal preserves the bandwidth and does not distort the envelope of the transmitted signal. Frequency modulating functions appropriate to the conjugation of isolated complex zero pairs of aperiodic signals have been derived. Provided the number of zeros conjugated in one sense equals the number of zeros conjugated in the other sense, then for all practical purposes, there will be no shift in the carrier frequency of the DSB-AM signal.

The data rate of ZSFM depends on the rate at which zero pairs can be satisfactorily detected and conjugated, and it has been shown that for a W Hz channel the data rate is upper-bounded by $\frac{W}{2}$ bit/sec. This implies an upper theoretical data rate of 5 kbit/sec over a 10 kHz broadcast channel. In practice, however, this data rate is not expected to be achieved for various reasons. If one FM function generator is used, the average data rate will be limited to $\frac{1}{P}$ bit/sec where P is the window over which the FM function is impressed on the carrier, assuming that at least one zero pair is detected every P second interval. A data rate of 1.67^{*} kbit/sec is considered feasible for ZSFM, although this could be increased at the expense of more hardware.

The BBC radio-data system for l.f. and m.f. broadcast, using linear phase modulation of the carrier by the shaped data signal, can provide 25 bit/sec data rate (7). The data rate of ZSFM has been shown to compare favourably with that of the BBC.

The performance of Zero Synchronous Frequency Modulation (ZSFM) has been studied using digital computer simulation. Some practical aspects of ZSFM have been investigated such as the bandwidth of the ZSFM signal, and the detection performance under noisy conditions. It has been verified that the ZSFM signal is strictly bandlimited to the same bandwidth of a DSB-AM signal, and this confirms that theoretically there will be no co-channel interference. However, when the FM function generator is truncated within a finite time interval of length P seconds, the spectrum of ZSFM signal will be non-bandlimited due to the truncation effect. Nevertheless, it has been shown that the out-of-band components relative to the average ZSFM signal power are of insignificant importance, and therefore it is considered that the out-of-band components have negligible effect on co-channel interference. The detection performance of ZSFM signals has proved to be satisfactory for all carrier-to-noise ratios (CNR) greater than 30 dB. The results of the experiments described have shown that the detection of the data channel of ZSFM is most affected at high modulation

depths, when the instantaneous signal-to-noise ratio (SNR) is low during envelope troughs.

Characteristics such as p.m./a.m. and a.m./p.m. conversions due to practical IF filtering at the receiver and other mismatches have been studied, and their degrading effects on ZSFM performance have been evaluated. The cross-talk caused by IF filters, having non-linear characteristics, was found to be of negligible importance. It has been shown that there will be some distortion introduced to the detected data signal due to the a.m./p.m. conversion in the case of a receiver mistune. However, the results of the experiments described in Chapter 5 suggest that the cross-talk caused by IF filtering does not appear to significantly impair the detected envelope and data signals, even under conditions of receiver mistune.

It has become apparent that, of all mechanisms likely to cause cross-talk from the data channel to the AM sound channel, the dominant effect is that of multi-path propagation. Computer simulation results have confirmed that p.m./a.m. conversion as a result of multipath propagation conditions is expected to be a major limiting factor. However, the envelope signal will be impaired significantly in a severe fading condition even without the interference imposed by the data signal. The simulation results have shown that the p.m./a.m. conversion, in multipath propagation conditions, does not significantly increase when the

data rate of ZSFM was increased from 146.5 bit/sec to 1562.5 bit/sec. An experimental ZSFM system is required to assess the performance under realistic fading conditions, in which case subjective tests can be carried out.

The effects of truncating the FM function generator on the performance of ZSFM have been considered. It has been shown that the approximation error introduced because of truncation is larger for high σ_r values than for small σ_r values. A window width of $P = 3\ \sigma_r$, giving $\frac{P}{\sigma_r}$ ratio of 3, is considered to be feasible for satisfactory performance. The simulation results suggest that the effect of a truncated FM function on the IF filtered and detected envelope signal is almost negligible, even for very small values of the window length (P). It has also been shown that the out-of-band components, due to the truncation effect, have negligible contribution to the average ZSFM signal power. It is, therefore, considered that the band-limitation of ZSFM is not affected significantly by truncation. However, the data rate of ZSFM will be reduced because of truncation, and it has been shown that a data rate of 1.67* kbit/sec is feasible when using one FM function generator only. This data rate compares favourably with the BBC radio-data system that handles 25 bit/sec (8). The data rate of ZSFM would be increased if more than one FM function generator

could be interlaced, but at the expense of hardware costs.

The theoretical foundation of complex filtering has been developed, and it has been shown how complex filters could detect the complex zeros of real signals. Practical realisations of the complex filter have been described in three different ways. The simulation results have shown that the complex filters in the bank can be designed so that for any two successive filters $\Delta\sigma_r = 2$ μ sec. The computer simulation has demonstrated the efficiency of the novel technique for detecting complex zeros of real signals.

The distribution of the complex zeros of positive bandlimited random signals has been investigated. An experimental study has been carried out to estimate the probability-density function (p.d.f.) of the complex zero distribution of a positive bandlimited random signal. The results have shown that the main part of the distribution is Gaussian in nature, and it has also been shown that more than 80% of the available complex zeros are located in the σ_r range (70 - 200) μ sec. In order to detect the majority of complex zeros contained in the above range only, the bank of filters should contain at least 65 complex filters.

ZSFM requires no modifications at the transmitter other than provision for carrier frequency modulation, and complex zero detection by a bank of filters. At the

receiver, envelope detection is carried out in the usual way to recover the amplitude modulating signal. The data signal can be recovered simply by any frequency demodulator, such as a phase-locked loop which detects positive or negative frequency deviations from the carrier. This favours applications such as broadcasting where one transmitter serves a large number of receivers and expensive modifications of receivers is uneconomic.

* N.B. Assuming the out-of-band radiation levels of 20 dB are acceptable in practice.

APPENDICES

APPENDIX 1

$$h(t) = \frac{1}{\pi t}$$

Consider the integral:

$$\int_{\Gamma} \frac{e^{jzt}}{z}\, dz, \quad t > 0$$

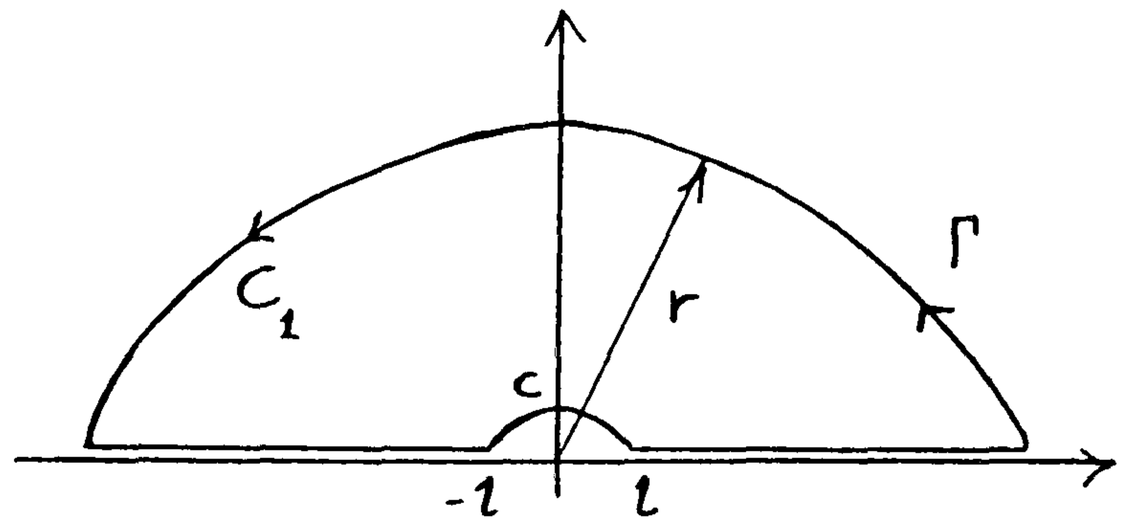

where z is a complex variable and Γ is a closed contour as shown nearby.

As $\frac{1}{z} \to 0$ when $z \to \infty$, then

$\int_{C_1} \frac{e^{jzt}}{z}\, dz \to 0$ as $r \to \infty$ according to one of the Jordon's Lemmas

$$\therefore \int_{\Gamma} \frac{e^{jzt}}{z}\, dz = 0 \text{ as } \frac{e^{jzt}}{z} \text{ has no singularities on } \Gamma.$$

$$\therefore \int_{C_1} \frac{e^{jzt}}{z}\, dz + \int_{-r}^{-1} \frac{e^{j\omega t}}{\omega}\, d\omega + \int_{1}^{r} \frac{e^{j\omega t}}{\omega}\, d\omega + \int_{c} \frac{e^{jzt}}{z}\, dz = 0$$

as $r \to \infty$

$$\int_{-\infty}^{-1} \frac{e^{j\omega t}}{\omega}\, d\omega + \int_{1}^{\infty} \frac{e^{j\omega t}}{\omega}\, d\omega = -\int_{\pi}^{0} \frac{e^{jtle^{j\theta}}}{le^{j\theta}}\, lje^{j\theta}\, d\theta$$

as $l \to 0$

$$\int_{-\infty}^{\infty} \frac{e^{j\omega t}}{\omega}\, d\omega = j\pi$$

$$\therefore \frac{1}{2\pi} \int_{-\infty}^{\infty} \frac{e^{j\omega t}}{j\omega}\, d\omega = \frac{1}{2}, \quad t > 0$$

Consider the integral:

$$\int_{\Gamma} \frac{e^{-jzt}}{z}\, dz \;,\; t < 0$$

where Γ is a closed contour as shown nearby.

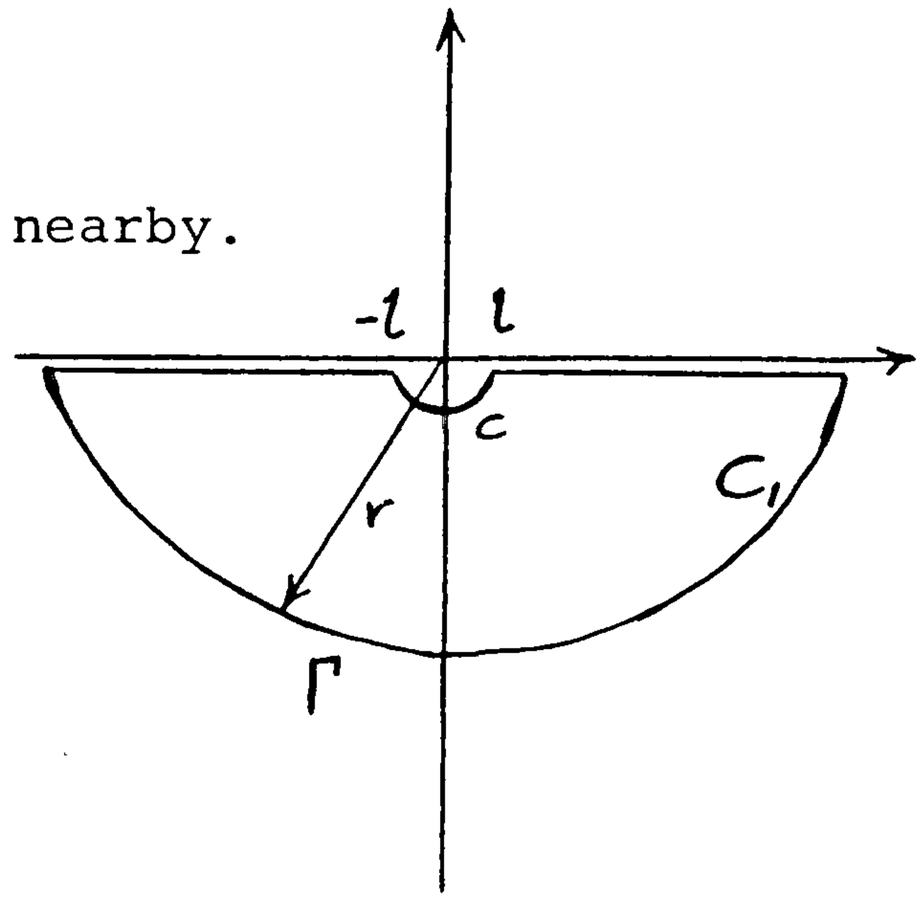

Similarly it can be shown that:

$$\frac{1}{2\pi} \int_{-\infty}^{\infty} \frac{e^{j\omega t}}{j\omega}\, d\omega = -\frac{1}{2} \;,\; t < 0$$

$$\therefore \; \mathrm{sgn}(t) \leftrightarrow \frac{2}{j\omega} = \frac{2}{j2\pi f} = \frac{1}{j\pi f}$$

$$\therefore \; \mathrm{sgn}(t) \leftrightarrow -j\frac{1}{\pi f}$$

Or in other words:

$$\frac{1}{\pi t} \leftrightarrow -\, j\mathrm{sgn}(f)\,.$$

APPENDIX 2

$$I_1 = \oint_C \frac{g(x)}{x - t_1}\, dx$$

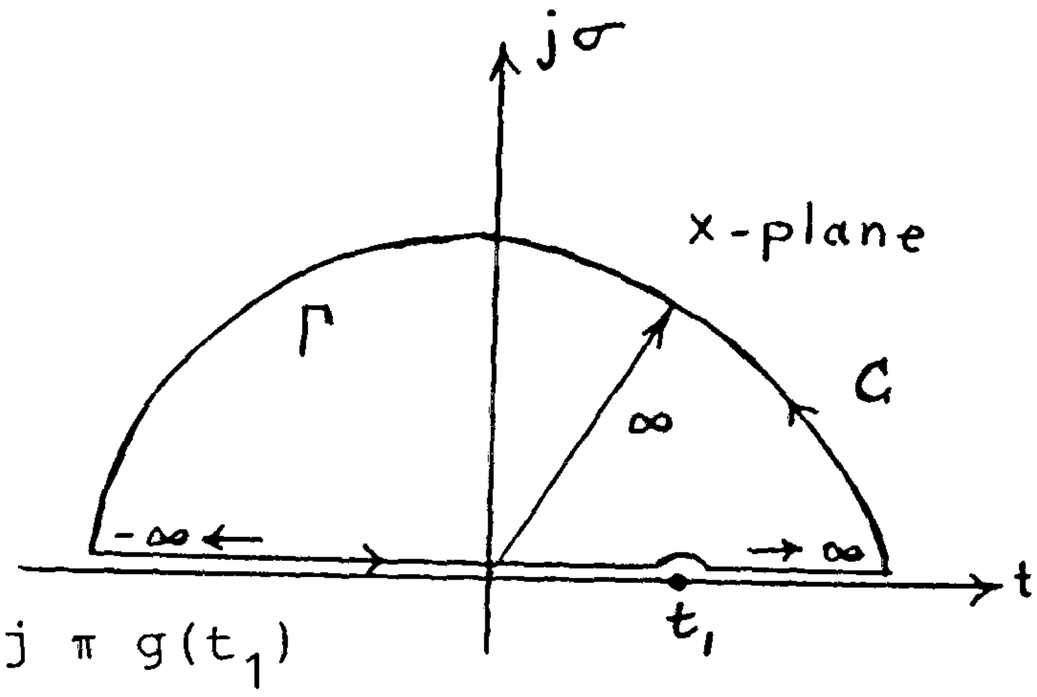

$$= \int_{-\infty}^{\infty} \frac{g(t)}{t - t_1}\, dt + \int_{\Gamma} \frac{g(x)}{x - t_1}\, dx - j\,\pi\, g(t_1)$$

I_1 must vanish as g(x) is analytic on C

$$\therefore \int_{-\infty}^{\infty} \frac{g(t)}{t - t_1}\, dt + \int_{\Gamma} \frac{g(x)}{x - t_1}\, dx - j\,\pi\, g(t_1) = 0$$

If g(x) vanishes on Γ for being square-integrable on real time axis then:

$$\int_{-\infty}^{\infty} \frac{g(t)}{t - t_1}\, dt = j\,\pi\, g(t_1)$$

Let $t = \tau$, $t_1 = t$

$$\therefore \int_{-\infty}^{\infty} \frac{g(\tau)}{\tau - t}\, d\tau = j\,\pi\, g(t)$$

$$\therefore \frac{1}{\pi} \int_{-\infty}^{\infty} \frac{g(\tau)}{t - \tau}\, d\tau = -\,j\, g(t)$$

$$\frac{1}{\pi} \int_{-\infty}^{\infty} \left\{ \frac{Re(g(\tau)) + jIm(g(\tau))}{t - \tau} \right\} d\tau = -j[Re(g(t)) + j\ Im(g(t))]$$

$$\therefore Im[g(t)] = H\{Re[g(t)]\}$$

$$\therefore Re[g(t)] = -H\{Im[g(t)]\}$$

APPENDIX 3

The equivalent circuit diagram for the double-tuned transformer with mutual inductance coupling is shown below:

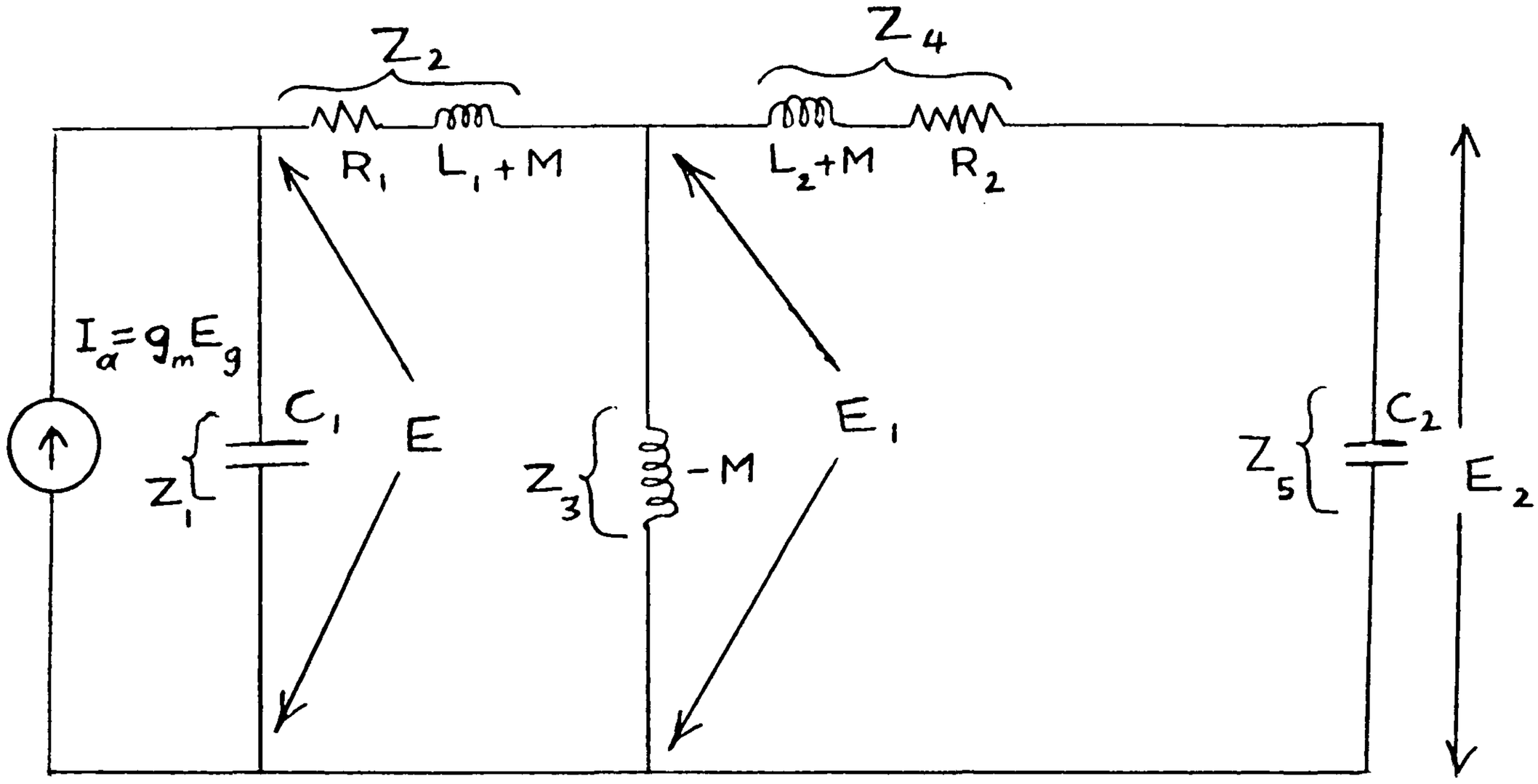

Equivalent circuit for a
double-tuned IF transformer.

The transfer impedance ($Z_T = \frac{E_2}{I_a}$) can be calculated as:

$$\frac{E_2}{E_1} = \frac{Z_5}{Z_4 + Z_5}$$

$$\frac{E_1}{E} = \frac{\frac{Z_3 \ (Z_4 + Z_5)}{Z_3 + Z_4 + Z_5}}{\frac{Z_3 \ (Z_4 + Z_5)}{Z_3 + Z_4 + Z_5} + Z_2}$$

$$\frac{E_2}{E} = \frac{E_2}{E_1}\,\frac{E_1}{E} = \frac{Z_3 Z_5}{Z_3(Z_4 + Z_5) + Z_2(Z_3 + Z_4 + Z_5)}$$

$$\text{But } E = I_a Z_1 \frac{Z_2 + \dfrac{Z_3\,(Z_4 + Z_5)}{Z_3 + Z_4 + Z_5}}{Z_1 + Z_2 + \dfrac{Z_3\,(Z_4 + Z_5)}{Z_3 + Z_4 + Z_5}}$$

$$\therefore\ Z_T = \frac{E_2}{I_a} = \frac{Z_1 Z_3 Z_5}{(Z_1 + Z_2 + Z_3)(Z_3 + Z_4 + Z_5) - Z_3^2}$$

$Q_1 = \dfrac{\omega_o L_1}{R_1}$, $F = \dfrac{2\Delta f}{f_o}$, f_o = central or mid-band frequency

$$Q_2 = \frac{\omega_o L_2}{R_2}$$

$$f_o = \frac{1}{2\pi\sqrt{L_1 C_1}} = \frac{1}{2\pi\sqrt{L_2 C_2}}$$

$$Z_T = \frac{j\ R_{D_1}\ Q_2\ k\ \sqrt{L_2/L_1}}{(1 + j\ Q_1 F)(1 + j\ Q_2\ F) + Q_1 Q_2 k^2}$$

where R_{D_1} is the dynamic resistance of the primary when not coupled to the secondary circuit.

k is the coupling coefficients, ($k \ll 1$).

When the two circuits are identical,

$L_1 = L_2$, $C_1 = C_2$, $Q_1 = Q_2 = Q$

$\therefore$ Z_T becomes:

$$Z_T = \frac{j\ R_D\ Q\ k}{(1 + j\ Q\ F)^2 + Q^2 k^2}$$

$$= \frac{j\ R_D\ Q\ k}{1 + Q^2(k^2 - F^2) + j2\ Q\ F}$$

$$\therefore \quad |Z_T| = \frac{R_D \; Q \; k}{\sqrt{[1 + Q^2(k^2 - F^2)]^2 + 4 \; Q^2 F^2}}$$

The conditions for maximum $|Z_T|$, the peaks of the frequency response curves, can be found by differentiating the above with respect to F and equating to zero. This gives:

$$F\Big|_{\max Z_T} = \pm\sqrt{k^2 - \frac{1}{Q^2}}$$

Three conditions: $k < \frac{1}{Q}$, $k = \frac{1}{Q}$, $k > \frac{1}{Q}$

When $k < \frac{1}{Q}$, $F\Big|_{\max ZT}$ is imaginary and max value of Z_T occurs at F = 0, $|Z_T|_{\max} = \frac{R_D Q k}{1+Q^2k^2}$

When $k = \frac{1}{Q}$, $|Z_T|_{\max}$ occurs at F = 0 and $|Z_T|_{\max} = \frac{R_D}{2}$.

When $k > \frac{1}{Q}$, $F\Big|_{\max Z_T} = \pm\sqrt{k^2 - \frac{1}{Q^2}}$, i.e. double peaked response is produced and also $|Z_T|_{\max} = \frac{R_D}{2}$.

The maximum value of $|Z_T|$ never exceeds $\frac{R_D}{2}$.

In order to calculate the magnitude frequency response of the IF transformer, it is only required to find $\frac{|Z_T|}{|Z_T|_{\max}}$

and taking into consideration that:

$$|Z_T|_{\max} = \frac{R_D}{2}$$

$$\therefore \quad |H(F)| = \frac{|Z_T|}{|Z_T|_{\max}} = \frac{2 \; Qk}{\sqrt{[1 + Q^2(k^2 - F^2)]^2 + 4Q^2F^2}}$$

The phase response of the IF transformer can be obtained from the transfer impedance Z_T since it represents phase change from primary input to secondary output.

Using the expression for Z_T and rationalising it, yields:

$$Z_T = \frac{R_D \; Q \; k[2 \; QF + j(1 + Q^2(k^2 - F^2))]}{[1 + Q^2(k^2 - F^2)]^2 + 4 \; Q^2F^2}$$

From the above, the phase angle ϕ can be obtained:

$$\phi = \arg[H(F)] = \arg(Z_T) = \text{arc tan} \frac{1 + Q^2(k^2 - F^2)}{2 \; QF}$$

REFERENCES

1. SVIRIDEN, S., "Some technical aspects of spectrum utilisation", Telecommunication Journal, Vol.43, 1976, pp.683-687.

2. RATCLIFF, P.A., "Modern television bandwidth compression techniques", IEEE Conference on: Radio spectrum conservation techniques, London, England, July 1980.

3. ELY, S.R., "The impact of radio-data on broadcast receivers", IERE Conference on: Radio receivers and associated systems, Leeds, England, July 1981, pp.349-362.

4. ELY, S.R., and WRIGHT, D.T., "Data and identification signalling for future radio receivers", SERT Conference on Consumer Electronics, July 1979, pp.67-75.

5. WHYTHE, D.J., and ELY, S.R., "Data and identification signalling for future radio receivers", IEE Conference Publication No. 166, International Broadcasting Convention, 1978, pp.324-326.

6. LOCKHART, G.B., "A spectral theory for hybrid modulation", IEEE Trans., COM-21, July 1973, pp.790-800.

7. ELY, S.R., and WRIGHT, D.T., "L.F. radio-data: specification of BBC experimental transmissions 1982", BBC Research Report, RD 1982/2.

8. LYNER, A.G., "L.F./M.F. radio-data: compatibility tests", BBC Research Report, RD 1982/15.

9. VOELCKER, H.B., "Toward a unified theory of modulation, part I: phase envelope relationships", Proc. IEEE, Vol.54, March 1966, pp.340-353.

10. VOELCKER, H.B., "Toward a unified theory of modulation, part II: zero manipulation", Proc. IEEE, Vol.54, May 1966, pp.735-755.

11. TITCHMARSH, E.C., "The theory of functions", London, England, Oxford Univ. Press, 2nd edition, 1939.

12. BEDROSIAN, E., "The analytic signal representation of modulated waveforms", Proc. IRE, Vol.50, 1962, pp.2071-2076.

13. LOCKHART, G.B., and AL-JALILI, Y.O., "A method for superimposing data on amplitude-modulated signals", Electronics Letters, Vol.18, No.9, 29th April 1982, pp.379-381.

14. Numerical Algorithms Group (NAG), FORTRAN Library Manual, Mark 9, Volumes (1 - 6).

15. SPIEGEL, M.R., "Mathematical handbook of formulas and tables", McGraw-Hill Inc., 1968.

16. ELY, S.R., "The impact of radio-data on broadcast receivers", Radio and Electronic Engineer, Vol.52, No.5, June 1982, pp.291-296.

17. AL-JALILI, Y.O., and LOCKHART, G.B., "Zero synchronous frequency modulation", International Broadcasting Convention, Brighton, England, September 1982, pp.289-292.

18. REQUICHA, A.A., "The zeros of entire functions: theory and engineering applications", Proc. IEEE, Vol.68, No.3, March 1980, pp.308-328.

19. CRYSTAL, T.H., and EHRMAN, L., "The design and applications of filters with complex coefficients", IEEE Trans., AU-16, 1968, pp.315-320.

20. THOMAS, G.B., "Calculus and analytic geometry", Addison-Wesley Publishing Company, 4th edition, 1973.

21. PAPOULIS, A., "Circuits and systems: a modern approach", Holt-Saunders, 1980.

22. BOGNER, R.E., and CONSTANTINIDES, A.G., "Introduction to digital filters", Wiley, 1977.

23. McLELLAN, J.H., and PARKS, T.W., "A unified approach to the design of optimum FIR linear-phase digital filters", IEEE Trans., Vol.CT-20, No.6, November 1973, pp.697-701.

24. ACKROYD, M.H., "Digital filters", London, Butterworth, 1973.

25. BOND, F.E., and CAHN, C.R., "On sampling the zeros of bandwidth limited signals", IRE Trans., Vol. IT-4, 1958, pp.110-113.

26. CARLSON, A.B., "Communication systems", McGraw-Hill, 2nd edition, 1975.

27. COOK, A.B., and LIFF, A.A., "Frequency modulation receivers", Prentice-Hall Inc., 1968.

28. KING, G.J., "Radio circuits explained", Butterworth & Co. Ltd., 1977.

29. Radio Society of Great Britain, "The radio communication handbook", 4th edition, September 1968.

30. STURLEY, K.R., "Radio receiver design", Chapman & Hall Limited, 2nd edition, 1953.

31. HENDERSON, H. "Radio reception", Focal Press Limited, 1963.

32. HILLS, M.T., and EVANS, B.G., "Telecommunications systems design, volume 1: transmission systems", George Allen & Unwin Ltd., London, 1973.

33. KNIGHT, P., "L.F. and m.f. propagation: sky-wave field-strength prediction", BBC Research Report, RD 1974/3.

34. LATHI, B.P., "An introduction to random signals and communication theory", Intertext Books, London, 1970.